SPIN-1 DROPLETS STABILIZED BY SPIN FLUCTUATIONS

A THESIS SUBMITTED TO
THE GRADUATE SCHOOL OF NATURAL AND APPLIED SCIENCES
OF
MIDDLE EAST TECHNICAL UNIVERSITY

BY

TAHA ALPER YOĞURT

IN PARTIAL FULFILLMENT OF THE REQUIREMENTS
FOR
THE DEGREE OF DOCTOR OF PHILOSOPHY
IN
PHYSICS

SEPTEMBER 2023

Approval of the thesis:

SPIN-1 DROPLETS STABILIZED BY SPIN FLUCTUATIONS

submitted by **TAHA ALPER YOĞURT** in partial fulfillment of the requirements for the degree of **Doctor of Philosophy in Physics Department, Middle East Technical University** by,

Prof. Dr. Halil KALIPÇILAR
Dean, Graduate School of **Natural and Applied Sciences** _____

Prof. Dr. Seçkin KÜRKÇÜOĞLU
Head of Department, **Physics** _____

Assist. Prof. Dr. Ahmet KELEŞ
Supervisor, **Physics, Middle East Technical University** _____

Prof. Dr. Mehmet Özgür OKTEL
Co-supervisor, **Physics, Bilkent University** _____

Examining Committee Members:

Prof. Dr. Mehmet Emre TASGIN
Physics, Hacettepe University _____

Assist. Prof. Dr. Ahmet KELEŞ
Physics, METU _____

Prof. Dr. Sadi TURGUT
Physics, METU _____

Prof. Dr. Bayram TEKİN
Physics, METU _____

Prof. Dr. Rıfat Onur UMUCALILAR
Physics, Mimar Sinan Fine Arts University _____

Date: 08.09.2023

I hereby declare that all information in this document has been obtained and presented in accordance with academic rules and ethical conduct. I also declare that, as required by these rules and conduct, I have fully cited and referenced all material and results that are not original to this work.

Name, Surname: Taha Alper Yoğurt

Signature :

ABSTRACT

SPIN-1 DROPLETS STABILIZED BY SPIN FLUCTUATIONS

Yoğurt, Taha Alper
Ph.D., Department of Physics
Supervisor: Assist. Prof. Dr. Ahmet KELEŞ
Co-Supervisor: Prof. Dr. Mehmet Özgür OKTEL

September 2023, 176 pages

The interacting Bose-Einstein condensates are mechanically stabilized by an external confinement such as magnetic, or optical traps. When the confinement is removed, they exhibit an expansion or collapse behavior depending on the interaction being repulsive, or attractive, respectively. The Gross-Pitaevskii mean-field theories are generally sufficient to provide a qualitative understanding of the condensate equilibrium properties and dynamics, therefore, beyond mean-field fluctuations are considered as minor quantitative corrections. The quantum droplet phases are self-stabilized phases of the condensate, in which the attractive mean-field interaction is stabilized by the repulsive Lee-Huang-Yang fluctuations without any external trap. The droplets are studied theoretically for binary Bose mixture and dipolar condensates, and both are recently realized in the ultracold atomic gas experiments. Here we propose the spin-1 condensate as another candidate to exhibit a quantum droplet phase. We argue that the spin-1 condensates in the polar and anti-ferromagnetic order parameters can exhibit a similar self-stabilizing mechanism.

We also realize an analogy between the polarized spin-1 and Rabi-coupled binary

mixture condensates. The Rabi frequency ω_R and quadratic Zeeman energy q can tune the Lee-Huang-Yang energy for the Rabi-coupled mixture and spin-1 gas, respectively. Furthermore, the detuning δ and linear Zeeman energy p are external parameters to tune the polarization in Rabi-coupled mixture, and spin-1 gas, respectively, which can significantly change the mean-field energy. We create the phase diagram for the mechanical stability of the Rabi-coupled mixture and spin-1 gas on the parameter planes of $\omega_R - \delta$ and $q - p$, respectively.

We finally address how the Bose mixture quantum droplets respond to the rotation. We find that the strongly confined quantum droplets exhibit triangular vortex lattices under rapid rotation. The properties of the vortex lattices differ from the repulsive condensates in three points. First, the change in the droplet size is only fractional at the rapid rotation limit, unlike the diverging radius of the repulsive condensate. This property can lead the way to realizing the lowest Landau level states and strongly correlated phases in the rotating ultracold gases. Secondly, the change in the core size throughout the vortex lattice is more tractable due to the finite density at the edge of the condensate. Finally, the vortex lattices are slightly distorted, which agrees with the expected vortex density profile due to the nonuniform superfluid density. In the rapid rotation limit, the droplet approaches the flat-top density profile, in which the vortex lattice is closest to a perfect periodicity.

Keywords: Bose Condensation, Quantum Droplet, Beyond Mean-Field, Vortex Lattice, Spin-1 Condensate

ÖZ

SPİN ÇALKANTILARIYLA KARARLILAŞTIRILMIŞ SPİN-1 DAMLACIKLARI

Yoğurt, Taha Alper
Doktora, Fizik Bölümü
Tez Yöneticisi: Dr. Öğr. Üyesi. Ahmet KELEŞ
Ortak Tez Yöneticisi: Prof. Dr. Mehmet Özgür OKTEL

Eylül 2023 , 176 sayfa

Etkileşen Bose-Einstein yoğunlaşmaları, manyetik veya optik tuzaklar gibi harici bir sınırlamayla mekanik olarak stabilize edilir. Sınırlandırma kaldırıldığında etkileşimin itici veya çekici olmasına bağlı olarak genişleme veya çökme davranışı sergilerler. Gross-Pitaevskii ortalama alan teorileri genellikle yoğuşma denge özellikleri ve dinamiklerinin niteliksel olarak anlaşılmasını sağlamak için yeterlidir, bu nedenle ortalama alan dalgalanmalarının ötesindeki dalgalanmalar küçük niceliksel düzeltmeler olarak kabul edilir. Kuantum damlacık fazları, çekici ortalama alan etkileşiminin, herhangi bir dış tuzak olmaksızın itici Lee-Huang-Yang dalgalanmaları tarafından dengelendiği, yoğunlaşmanın kendi kendini dengeleyen fazlarıdı. Damlacıklar teorik olarak ikili Bose karışımı ve dipolar yoğunlaşmalar için incelendi ve her ikisi de son zamanlarda ultra soğuk atomik gaz deneylerinde gerçekleştirildi. Burada spin-1 yoğunlaşmasını kuantum damlacık fazı sergileyen başka bir aday olarak öneriyoruz. Polar ve anti-ferromanyetik düzen parametrelerindeki spin-1 yoğunlaşmalarının benzer bir kendi kendini dengeleme mekanizması sergileyebileceğini savunuyoruz.

Ayrıca polarize spin-1 ile Rabi-bağlı ikili karışım yoğunlaşmaları arasında bir benzetimin farkına varıyoruz. Rabi frekansı ω_R ve ikinci dereceden Zeeman enerjisi q, sırasıyla Rabi-bağlantılı karışım ve spin-1 gazı için Lee-Huang-Yang enerjisini ayarlayabilir. Ayrıca, ayar bozucu δ ve doğrusal Zeeman enerjisi p, ortalama alan enerjisini önemli ölçüde değiştirebilen sırasıyla Rabi-bağlı karışım ve spin-1 gazındaki polarizasyonu ayarlamak için harici parametrelerdir. Sırasıyla $\omega_R - \delta$ ve $q - p$ parametre düzlemlerinde Rabi-bağlı karışımın ve spin-1 gazının mekanik stabilitesi için faz diyagramını oluşturuyoruz.

Son olarak Bose karışımı kuantum damlacıklarının döndürmeye nasıl tepki verdiğini ele alıyoruz. Güçlü bir şekilde sınırlanmış kuantum damlacıklarının hızlı dönüş altında üçgen girdap örgüleri sergilediğini bulduk. Girdap örgülerinin özellikleri itici yoğunlaşmalardan üç noktada farklılık gösterir. İlk olarak, damlacık boyutundaki değişiklik, itici yoğunlaşmanın uzaklaşma yarıçapının aksine, hızlı dönüş sınırında yalnızca kesirlidir. Bu özellik, dönen ultra soğuk gazlarda en düşük Landau seviyesi durumlarının ve güçlü bir şekilde ilintili fazların gerçekleştirilmesine yol açabilir. İkinci olarak, girdap örgüsü boyunca çekirdek boyutundaki değişiklik, yoğunlaşmanın kenarındaki sonlu yoğunluk nedeniyle daha kolay takip edilebilir. Son olarak, girdap örgüleri hafifçe bozulmuştur; bu bozulmanın miktarı, düzgün olmayan süperakışkan yoğunluğundan dolayı beklenen girdap yoğunluğu profiline uygundur. Hızlı dönüş sınırında damlacık, girdap örgüsünün mükemmel periyodikliğe en yakın olduğu düz tepe yoğunluk profiline yaklaşır.

Anahtar Kelimeler: Bose Yoğuşması, Kuantum Damlacıklar, Orta-Alan Ötesi, Girdap Örgüleri, Spin-1 Yoğuşması

To my beloved family

ACKNOWLEDGMENTS

I want to express my deepest gratitude to my supervisors Prof. Mehmet Özgür OKTEL, and Prof. Ahmet KELEŞ, for their constant support and guidance during my Ph.D. journey. I believe the ultimate aim of mastering a science is to feel the joy of learning and understanding, that I had in each of every discussion we had during the Ph.D. course. Not only that I learn from them the professional attitude of a great researcher and educator, but I also enjoyed accompanying great personalities.

I am also grateful to Prof. Bayram TEKİN and Prof. Sadi TURGUT for their great lectures, support, and inspiration as a theoretical physicist. Their unique ways of thinking have always motivated me towards becoming a physicist, and I owe a great deal of my physics knowledge to them.

I extend my sincere thanks to Prof. Mehmet Emre TAŞGIN, and Prof. Rıfat Onur UMUCALILAR for their help and advice during my Ph.D. course. Special thanks to my colleague Umut TANYERİ for his contributions and valuable discussions.

I also want to express my deepest appreciation to my beloved parents, Birgül and Necati YOĞURT for their great support during my whole life. Even though they were at first skeptical when I decided to study physics by quitting engineering, they always respected my choices and encouraged me for further progress. I also want to thank in advance to my brother Batuhan YOĞURT, for being a great brother and uncle.

Finally, I acknowledge my great thanks to my lovely wife, Şeymanur TAŞKOPARAN YOĞURT for bringing inspiration and joy into my life. I also owe her another thanks for being patient and parenting our son alone during my long hours in the office. Finishing this work would be much harder without her love and support. Last words for my son, İbrahim Agah YOĞURT, with the hope that he may read these words when he can: Your laughter and joy always brightened my day and inspired my heart with a great feeling of love.

TABLE OF CONTENTS

ABSTRACT v

ÖZ vii

ACKNOWLEDGMENTS x

TABLE OF CONTENTS xi

LIST OF TABLES xv

LIST OF FIGURES xvi

LIST OF ABBREVIATIONS xxii

CHAPTERS

1 WEAKLY INTERACTING BOSE CONDENSATES 1

1.1 Ideal and Weakly Interacting Bose Condensates 2

1.1.1 Non-interacting BEC under the Harmonic Trap 4

1.1.2 Interacting BEC: General Approach 6

1.1.3 Interacting BEC: Mechanical Stability of BEC 11

1.1.4 Interacting BEC: Bogoliubov Microscopic Theory 14

1.2 Two-Component Mixture Bose Condensates 24

1.2.1 Gross-Pitaevskii Mean-Field Theory of Bose Mixture 24

1.2.2 Bogoliubov Theory of Bose Mixture 28

1.3 Spin-1 Bose Condensates 41

1.3.1 Spin-1 Bose Gas Hamiltonian 42
1.3.2 MF Theory of Spin-1 Condensate 49
1.3.3 Bogoliubov Theory of Spin-1 Condensate 55
1.3.3.1 Ferromagnetic Order 58
1.3.3.2 Polar Order 61
1.3.3.3 Anti-ferromagnetic Order 64
1.4 Vortex Lattices in the Interacting Bose Condensates 66
1.4.1 Single Particle Hamiltonian under Rotation and Landau Levels 68
1.4.2 Infinite Perfect Lattices in the Lowest Landau Level: Single Vortex per Unit Cell 71
1.4.3 Infinite Perfect Lattices in the Lowest Landau Level: Two Vortices per Unit Cell 78
2 BOSE MIXTURE DROPLETS 81
2.1 Theory of Bose Mixture Droplet 81
2.1.1 Infinite Bose Mixture Droplet 83
2.1.2 Finite Bose Mixture Droplet 85
2.2 Bose Mixture Droplet Experiments 90
2.2.1 ICFO Group 91
2.2.2 LENS Group 92
2.2.3 Beijing Group 92
3 SPIN-1 AND RABI-COUPLED DROPLETS 95
3.1 Spin-1 Droplets 95
3.1.1 Polar Spin-1 Droplets 102
3.1.2 AF Spin-1 Droplets 105

3.1.3 Discussion of experimental realization and Conclusion 107
3.2 Rabi-coupled Bose Mixture Droplets 109
3.2.1 Introduction 109
3.2.2 Rabi-Coupled Bose Mixtures: Bogoliubov Theory 112
3.2.3 The Bogoliubov Theory of Rabi-coupled Mixture 115
3.2.4 Rabi-Coupled Bose Mixture Droplet 118
3.3 Polarized Spin-1 Droplet 122
3.3.1 Polarized Spin-1 Gases: Bogoliubov Theory 122
3.3.2 Bogoliubov Theory of Spin-1 Gas 126
3.3.3 Analytical approximation for $I_0(\tilde{q}, \beta)$ 128
3.3.4 Polarized AF Spin-1 Droplet 128
3.3.5 Discussion of experimental realization and Conclusion 130
4 VORTEX LATTICES IN BOSE MIXTURE DROPLETS 133
4.1 Introduction 134
4.2 Length scales and parameter regimes 137
4.3 Strongly Confined Thomas-Fermi Regime 141
4.4 Analytical Solution of the Cubic TF Equation 146
4.5 Properties of the Vortex Lattice 147
4.6 Vortex Lattices with Low Filling Factors 152
4.7 Discussion of experimental realization and Conclusion 155
5 JACOBI-THETA FORMALISM OF BOSE MIXTURE DROPLET 157
5.1 Single particle energy in the Lowest Landau Level 158
5.2 MF and LHY energy: Single vortex per unit cell 159

5.3 MF and LHY energy: Two vortices per unit cell 161

6 CONCLUSION 163

REFERENCES 165

CURRICULUM VITAE 175

LIST OF TABLES

TABLES

Table 1.1 Different order parameters of the spin-1 condensate. 52

Table 4.1 The rotating quantum droplet under confinement can be classified into four different regimes. We use the scales obtained by the energy ratios in (4.9) and (4.10) to quantify the regimes. 142

LIST OF FIGURES

FIGURES

Figure 1.1 The total energy of the condensate $E/N\hbar\omega$ in (1.67) vs. the variational cloud radius $\tilde{b} = b/a$, where a is the harmonic oscillator length scale. For any positive scattering length $a_s > 0$, the condensate can be stabilized by the harmonic potential, and the global minimum of the energy functional is always at a finite $\tilde{b}$ value. However, the attractive condensate $a_s < 0$ can only yield a local minimum for $\frac{Na_s}{a} > -0.67$, and the condensate is metastable. After this critical level, the local minimum disappears, and the density collapse is inevitable for the condensate in equilibrium. 12

Figure 1.2 Bogoliubov modes $\frac{E_{k,\pm}}{gn}$ vs. $\tilde{k} \equiv \sqrt{\frac{\hbar^2}{2mgn}}k$ for $\frac{g_{12}}{g} = -0.5$ (left panel) and $\frac{g_{12}}{g} = -1.2$ (right panel). As the ratio $\frac{g_{12}}{g}$ increases, two branches move away from each other. For $\frac{g_{12}}{g} = -1.2$, the low wavevectors, or greater wavelengths exhibit imaginary, therefore unstable, modes. 38

Figure 1.3 The MF phase diagram of the spin-1 condensate as a function of linear $p/|c_1|n$ and quadratic $q/|c_1|n$ Zeeman energies for (a) $c_1 > 0$, and (b) $c_1 < 0$. 52

Figure 1.4 The geometry of the unit cells for (a) Single vortex per unit cell, (b) Double vortex per unit cell. The black arrows show the basis vectors, whereas the red arrow is the relative position vector of the two vortices inside the same unit cell. 72

Figure 2.1 The kinetic, MF, LHY, and total energy densities of the Bose mixture for $\tilde{N} = 200$ (left panel) and $\tilde{N} = 20$ (right panel). The kinetic energy is negligible for the greater particle number, and the competing MF and LHY energies exhibit a global minimum. As $\tilde{N}$ decreases, the kinetic energy becomes comparable to the interaction energies. First, the energy's minimum shifts to a smaller radius length due to the decreasing $\tilde{N}$, then the local minimum disappears completely. Hence, there is a critical number of particles below which the droplet can not stabilize itself, and expands to infinity. 90

Figure 2.2 The numerical solutions to the extended GP equation (2.39) for different particle numbers. For sufficiently large $\tilde{N}$, the droplet profile approaches a flat-top shape, and its density converges to the equilibrium density of the infinite droplet. However, as the particle number decreases, the spatial gradient increases and the droplet expands to infinity below a critical number of particles. 91

Figure 3.1 A graphical representation of the phase diagram for a spin-1 Bose condensate is provided, with the quadratic Zeeman shift q and spin-spin interaction c_1 as variables, while the linear Zeeman energy p is set to zero. 99

Figure 3.2 The wavefunctions of the polar spin-1 condensate in the ground state for different combinations of particle number $\tilde{N}$ and Zeeman energy $t_1 = q/n_1|c_1|$. On the left side, the wavefunctions are shown for $q = 0$ (equivalently, $t_1 = 0$) with varying values of $\tilde{N}$. Below $\tilde{N} = 20$, the droplet can not stabilize itself. On the right side, the wavefunctions are depicted for a fixed $\tilde{N} = 500$ while varying t_1. This plot reveals a self-bound droplet until a critical value of the quadratic Zeeman energy $q_c \approx 1.5$ is reached. 102

Figure 3.3 The critical particle numbers $\tilde{N}_c$ for different values of $t_1 = q/n_1|c_1|$ using two methods: numerical solutions of the GP equation (shown in orange) and variational calculations employing the Gaussian ansatz (shown in blue). As observed in the graph, the density at the center of the droplet reduces as q increases. Eventually, the interplay between kinetic energy and LHY (Lee-Huang-Yang) pressure becomes dominant, overpowering the mean-field attraction, and causing the droplet to expand. This phenomenon is well-captured by the Gaussian variational calculation, which demonstrates good agreement with the GP solution. 105

Figure 3.4 The droplet wavefunctions in the ground state for $t_1 = -0.5, 0, 0.5$. The particle number for all the phases is the same, $\tilde{N} = 500$. 107

Figure 3.5 The phase diagram of a Rabi-coupled Bose mixture is represented as a function of two parameters: the Rabi frequency $\frac{2\hbar\omega_R}{\bar{g}n}$ and the detuning $\frac{\hbar\delta}{\bar{g}n}$, under the conditions $\frac{g_{12}}{g} < -1$ and $g > 0$. The color shading (indicated by the color bar) corresponds to the ratio $r = \sqrt{N_1/N_2}$ in the mean-field (MF) ground state, as given by the expression (3.18). The dashed red line marks the boundary above or below which the total MF two-particle interaction, with $g_{12}/g = -1.5$, becomes repulsive or attractive, respectively. On the other hand, the solid red line represents the boundary of the self-trapped droplet phase. In Region I of the diagram, the gas expands due to the repulsive MF interaction. In Region II, the MF energy is attractive, but the repulsive beyond-mean-field (BMF) energy is strong enough to cause expansion. In Region III, the MF attraction is stabilized by the repulsive BMF energy, resulting in the formation of a self-trapped droplet. 113

Figure 3.6 The integral I_+ in (3.28) as a function $\tilde{\omega}$ for varying r values. The scattering length ratio is fixed $g_{12}/g = -1.5$. 118

Figure 3.7 The ground state wavefunctions of the Rabi-coupled Bose mixture in the droplet phase are depicted for different combinations of $\tilde{\omega}_0^{(1)}$ and the ratio r. On the left side, the wavefunctions are shown for $\delta = 0$, corresponding to $r = 1$, and various values of $\tilde{\omega}_0^{(1)}$. Above a critical value $\tilde{\omega}_c$, the droplet can not sustain itself. On the right side, the wavefunctions are displayed for a fixed $\tilde{\omega}_0^{(1)} = 0.25$ while varying the ratio r. This plot reveals a self-bound droplet until a critical value of $r_c \approx 0.7$ is reached. The total particle number for both plots is $\tilde{N} = 500$. 119

Figure 3.8 The phase diagram of mechanical stability for the spin-1 droplet is presented concerning the quadratic Zeeman energy q/nc_1 and the linear Zeeman energy p/nc_1. The orange region in the diagram corresponds to the antiferromagnetic order. Outside the dashed blue lines, particularly when $|\tilde{p}| > 0.44$, the mean-field (MF) interaction is repulsive. Conversely, inside the dashed lines, where $|\tilde{p}| < 0.44$, the MF interaction becomes attractive. This occurs for a specific ratio of $c_1/c_0 = -5$, with c_0 being negative. The boundary of the droplet phase is represented by a solid purple line, indicating the region where the gas can be stabilized by beyond-mean-field (BMF) fluctuations. Three distinct regions are identifiable: In Region I, the repulsive MF interaction leads to gas expansion. In Region II, even though the MF energy is attractive, the BMF repulsion is relatively strong, causing expansion. In Region III, the MF attraction is stabilized by the repulsive BMF energy, resulting in a stable droplet phase.The total particle number in the system is $\tilde{N} = 500$. 124

Figure 3.9 The ground state wavefunctions of the spin-1 condensate in the antiferromagnetic (AF) phase are displayed for various combinations of the quadratic Zeeman energy $\tilde{q}_0^{(1)}$ and linear Zeeman energy $\tilde{p}$. The total particle number is fixed at $\tilde{N} = 500$, and the ratio c_1/c_0 is set to -5 with c_0 being negative. On the left plot, the wavefunctions are illustrated for a constant value of $\tilde{p} = 0.2$ while varying $\tilde{q}_0^{(1)}$. Above a critical value $\tilde{q}_c$, the formation of a self-bound droplet becomes unfeasible. On the right plot, the wavefunctions are shown for $|\tilde{q}_0^{(1)}| = 1$ with different values of $\tilde{p}$. Similarly, above a critical value $\tilde{p}_c$, the droplet is no longer self-trapped. Both plots clearly demonstrate how changes in the quadratic and linear Zeeman energies can significantly influence the formation and stability of the self-bound droplet in the spin-1 condensate within the antiferromagnetic phase. 125

Figure 4.1 (a) The local chemical potential $\mu_{loc}(\tilde{r}) = \tilde{\mu} - \frac{1}{2}\tilde{r}^2\left(1 - \tilde{\Omega}^2\right)$ in (4.11) vs. $|\tilde{\psi}|$ (Blue line). Since $\alpha_s > 1$ and β_{LHY} is positive, μ_{loc} shows a local negative minimum at $|\tilde{\psi}| = \sqrt{n_{min}}$, then monotonically increase with $|\tilde{\psi}|$. The solution to (4.11) for $\tilde{\mu} > \tilde{\mu}_{min}$ can be found by evaluating $\mu_{loc}(\tilde{r})$ for different $\tilde{r}$, along the curved arrow. The density jumps to 0 when the local chemical potential is equal to the minimum value μ_{min}. (b) The analytical solutions of the GP equation (4.11) of the rotating Bose mixture droplets in the strongly confined TF regime for various $\tilde{\Omega}$. The parameters are $\alpha_s = 1.05$, $\beta_{LHY} = 6 \times 10^{-3}$, $\gamma_{int} = 1$, $N = 10^5$. The convexity due to the strong confinement flattens and approaches the flat-top profile as $\tilde{\Omega} \to 1$. 143

Figure 4.2 The numerical solutions of the GP equation (4.2) of the rotating Bose mixture droplets for the parameters $\alpha_s = 1.05$, $\beta_{LHY} = 1 \times 10^{-3}$, $\gamma_{int} = 2$, $N = 10^5$, and (a) $\tilde{\Omega} = 0.80$,(b) $\tilde{\Omega} = 0.90$,(c) $\tilde{\Omega} = 0.97$. (upper panel) 2-D density profiles of the vortex lattices, (lower panel) the density profile of the vortex lattices along the x-axis (orange lines), and the rotating TF solution of the GP equation (4.11) (blue lines). . . . 144

Figure 4.3 The comparison of the radius of the condensates for the rotation frequency $\tilde{\Omega} \in [0, 1]$: Repulsive BEC in TF regime (dotted), Repulsive BEC in LLL regime (solid), and Droplet in the TF regime (dashed). The scattered data present the radius of the simulation results. The droplet radius converges to a finite value as $\tilde{\Omega} \to 1$, contrary to the diverging behavior of the repulsive BECs. 146

Figure 4.4 Density profile of the vortex lattice with $\tilde{\Omega} = 0.8$ in Fig.4.2(a). The insets show the 2D zooms of equal areas in the vortex lattice near the edge (Z1) and the center (Z2) of the droplet. The core size is larger, and the vortex unit cell area decreases near the edge. 148

Figure 4.5 (a) The vortex core area estimates by numerical solutions of 1-D (solid line) and 2-D (dashed line) healing length equation (4.14), analytical approximation (4.16) (dotted line) and the simulation data for (filled points) $\tilde{\Omega} = 0.8$. The density levels n_0 for the numerical and analytical solutions to (4.14) and (4.16) are taken from the strongly confined TF droplet equation (4.11). The difference in the core size along the TF droplet is more tractable than the repulsive BECs. (b) The vortex density of the rotating TF droplet calculated up to the first order in (4.17) for $\tilde{\Omega} = 0.80$ (gray), $\tilde{\Omega} = 0.90$ (black), $\tilde{\Omega} = 0.95$ (blue), and $\tilde{\Omega} = 0.97$ (red). The dotted lines represent the uniform vortex densities $n_{v0} = \tilde{\Omega}/\pi$. The scattered data shows the vortex density computed on the simulation data of Fig. 4.2, whereas the solid lines are the solutions to (4.17). The vortex density closely follows the uniform limit with an agreement on the corrections. 150

Figure 4.6 The vortex lattice of a rotating strongly confined droplet with a low filling factor. There are approximately 80 vortices for particle number $N = 500$, i.e. $\nu \approx 6.25$. The parameters are $\alpha_s = 1.25$, $\beta_{LHY} = 0.025$, $\gamma_{int} = 20$, and $\tilde{\Omega} = 0.99$. The color bar indicates the condensate density. 154

LIST OF ABBREVIATIONS

BEC	Bose-Einstein Condensate
MF	Mean-Field
LHY	Lee-Huang-Yang
BMF	Beyond Mean-Field
LLL	Lowest Landau-Level
TF	Thomas-Fermi
COM	Center-of-Mass
GP	Gross-Pitaevskii
LDA	Local Density Approximation

CHAPTER 1

WEAKLY INTERACTING BOSE CONDENSATES

The central interest of this thesis is the self-stabilized quantum droplet phases, in which the mean-field (MF) interactions in the Bose-Einstein condensate (BEC) favor the density collapse, whereas the beyond mean-field (BMF) interactions effectively act repulsive and stabilize the collapsing condensate [1]. This stabilization mechanism was theoretically studied by the microscopic Bogoliubov formulation of the weakly interacting condensates in the case of dipolar [2] and binary Bose mixtures[1]. Both types of droplets were recently realized in the ultracold gas experiments[3, 4], which are in good agreement with the estimations of the Bogoliubov theories. Here we raise two fundamental questions regarding the quantum droplets. First, we ask whether it is possible to obtain a droplet phase in spin-1 condensate. We also examine the properties of the spin-1 droplet and compare it to the Rabi-coupled Bose mixture droplets. Secondly, we investigate how the binary mixture droplets respond to the rotation. In particular, we address how the vortex lattices can form inside the quantum droplet. We define the properties of the vortex lattices and compare them to the counterparts in the repulsive BECs.

The leading theoretical approach to the weakly interacting Bose condensate is the Gross-Pitaevskii (GP) MF theory [5], in which the particles inside the condensate are assumed to occupy the same eigenstate. However, the MF theory is not sufficient to describe the droplet behavior, since the beyond MF fluctuations are the inevitable part of the stabilization mechanism. Therefore, the droplets are formulated by the microscopic Bogoliubov theories, which also take account of the Lee-Huang-Yang fluctuations[1].

We also study the vortex lattices inside the quantum droplets by two different ap-

proaches. First, we numerically solve the GP equation governing the rotating droplet and develop some analytical methods to define the properties of the vortex lattices. Secondly, we use the Jacobi-Theta formalism of the infinite perfect vortex lattices to calculate the MF and BMF energies of the quantum droplet. We generalize the single vortex per unit cell formulation of the Jacobi-Theta functions to the double vortex per unit cell cases.

This thesis is organized as follows. We write Ch.1 to provide a background on the weakly interacting Bose condensates and Jacobi-Theta formalism of the vortex lattices. In Ch.1.1 We summarize a general approach to the weakly interacting BEC, in which both the equations of the GP and Bogoliubov theories can be extracted. We discuss the mechanical stability of the repulsive and attractive single-component BEC using the GP approach. Then, we explain the microscopic Bogoliubov theory of the single component BEC. In Ch.1.2, we develop the same formalism for the binary Bose mixtures. In Ch.1.3 we derive the spin-1 Hamiltonian and summarize the MF and Bogoliubov theories of the spin-1 condensate. We discuss the MF phase diagram of the spin-1 condensate. Finally, in Ch.1.4 we review the Landau levels for rotating particles and summarize the Jacobi-Theta formalism for the infinite perfect vortex lattice. We discuss the theory of binary mixture quantum droplets in Ch.2.1. In Ch. 2.2, we list and explain the leading experimental works that realized the droplet phases in ultracold atomic gases. We discuss the theory of spin-1 droplets in Ch.3.1. We examine the Rabi-coupled binary mixture droplets, and polarized spin-1 droplets in Ch.3.2 and Ch.3.3, respectively. Ch.4 is devoted to the numerical results of the rotating quantum droplet, and the analytical formulas to explain its properties.

1.1 Ideal and Weakly Interacting Bose Condensates

The particles in the statistically classical limit rarely occupy the same single-particle eigenstates ν. Hence, the Boltzmann factor $\propto e^{-E_\nu/k_BT}$ successfully provides the occupancy of the different states ν. However, the quantum nature of the particles begins to manifest at sufficiently low temperatures. The Bosons tend to occupy the same eigenstate, whereas the Fermions can not. This difference significantly changes the distribution of the particles among the eigenstates.

For the system with chemical potential μ and temperature T, the probability of the eigenstate ν of energy ϵ_ν being occupied by n_ν particles is proportional to Gibbs factor $e^{-n_\nu(\epsilon_\nu-\mu)/k_BT}$, where k_B is the Boltzmann factor, $n_\nu = 0, 1, 2, ..$ for Bosons and $n_\nu = 0$ or 1 for Fermions. Hence, probability of the state ν being occupied by n_ν particles is given by [6]:

$$P(\nu, n_\nu) = \frac{e^{-n_\nu(\epsilon_\nu-\nu)/k_BT}}{Q}, \tag{1.1}$$

where $Q \equiv \sum_{\nu,n_\nu} e^{-n_\nu(\epsilon_\nu-\mu)/k_BT}$ is the grand canonical partition function. The summation is over all possible eigenstates ν and occupation numbers n_ν. Then, the expected occupancy of the state ν can be found by $\bar{n}_\nu = \sum_{n_\nu} n_\nu P(\nu, n_\nu)$:

$$\bar{n}_\nu = \sum_{n_\nu} \frac{n_\nu e^{-n_\nu(E_\nu-\mu)/k_BT}}{Q} = -\frac{1}{Q}\frac{\partial Q}{\partial \alpha}, \tag{1.2}$$

where $\alpha \equiv \frac{E_\nu-\mu}{k_BT}$, $\quad Q = \sum_{n_\nu=0}^{\infty} e^{-n_1\alpha} = \frac{1}{1-e^{-\alpha}}$. Hence Bose-Einstein distribution of the expected occupation number of particles in the state ν is:

$$\bar{n}_\nu = \frac{1}{e^{(\epsilon_\nu-\mu)/k_BT} - 1}. \tag{1.3}$$

This distribution function is interesting when compared to the classical $\bar{n}_v = e^{-\frac{(\epsilon_\nu-\mu)}{k_BT}}$ and Fermionic $\bar{n}_v = \frac{1}{e^{(\epsilon_\nu-\mu)/k_BT}+1}$ counterparts. Since Bosons can occupy the same eigenstate with an arbitrary number, the chemical potential μ cannot be greater than the ground state energy ϵ_0. This chemical potential $\mu = \epsilon_0$ is reached when the ground state $\nu = 0$ is substantially occupied with respect to the excited states $\nu \neq 0$. The macroscopic occupation of the eigenstate is the phenomenon called Bose-Einstein condensation. This behavior can be justified with the following argument.

Consider the occupation of the ground state N_0 and the rest of the states N_T for a finite temperature T, where $N = N_0 + N_T$ is the total number of particles that determines the chemical potential of the system:

$$N_0 = \frac{1}{e^{(\epsilon_0-\mu)/k_BT} - 1} \tag{1.4}$$

and

$$N_T = \sum_{\nu\neq 0} \frac{1}{e^{(\epsilon_\nu-\mu)/k_BT} - 1}. \tag{1.5}$$

As $\mu \to \epsilon_0$, N_0 diverges while $N_T = N_c = \sum_{\nu \neq 0} \frac{1}{e^{(\epsilon_\nu - \epsilon_0)/k_B T} - 1}$ is still finite. The particle number normalization $N = N_0 + N_T$ for $N > N_c$ ensures that the chemical potential μ is equal to the ground state energy ϵ_0. Then, the condensation occurs, i.e. the number of particles $N_0 = N - N_T$ occupy the ground state $\nu = 0$. Hence, the condition for the Bose condensation is [7]:

$$N \geq N_T(T, \mu = \epsilon_0) = \sum_{\nu \neq 0} \frac{1}{e^{(\epsilon_\nu - \epsilon_0)/k_B T} - 1}. \tag{1.6}$$

Ideally, non-interacting Bose-Einstein condensates (BEC) are hard to realize in the experiments due to the interactions among the particles that still manifest, even after a considerable dilution in the density [8]. Furthermore, the mechanical confinement of the condensates is achieved through the magnetic or optical traps, which are successfully modeled by the harmonic potentials [9]. Therefore, we now revisit the non-interacting BEC under a harmonic trap and discuss the depletion of the condensate due to thermal fluctuations.

1.1.1 Non-interacting BEC under the Harmonic Trap

Consider a Bose gas trapped by an isotropic harmonic potential [7]

$$V_{\text{ext}}(\vec{r}) = \frac{1}{2} m\omega^2 \left(x^2 + y^2 + z^2\right), \tag{1.7}$$

where ω is the oscillator frequency in all directions. The corresponding single-particle Hamiltonian is

$$\hat{H}_1 = -\frac{\hbar^2}{2m}\nabla^2 + V_{\text{ext}}(\vec{r}). \tag{1.8}$$

The eigenenergies are

$$\epsilon_{n_x, n_y, n_z} = \left(n_x + n_y + n_z + \frac{3}{2}\right)\hbar\omega, \tag{1.9}$$

where $n_{x,y,z} = 0, 1, 2, ...$ and $\epsilon_0 = \frac{3\hbar\omega}{2}$ is the zero-point energy of the 3-dimensional harmonic oscillator problem. The ground state wavefunction is:

$$\psi_0(\vec{r}) = \left(\frac{m\omega}{\hbar\pi}\right)^{3/4} \exp\left[-\frac{m\omega}{2\hbar} r^2\right], \tag{1.10}$$

where $r^2 = x^2 + y^2 + z^2$. The wavefunction of the condensate with N particles can be assumed to be

$$\Psi_0(\vec{r}) = \sqrt{N}\psi_0(\vec{r}), \tag{1.11}$$

where $n(\vec{r}) = |\Psi_0(r)|^2$ is the condensate density with normalization $\int d^3\vec{r} n(\vec{r}) = N$. The condensation condition can be calculated by the criteria $N \geqslant N_C = N_T(T, \mu = \epsilon_0)$, where $\epsilon_0 = \frac{3}{2}\hbar\omega$ and thermel depletion N_T [7]:

$$N_T = \sum_{n_x n_y, n_z} \frac{1}{\exp\left[\beta\left(n_x + n_y + n_z + \frac{3}{2} - \frac{3}{2}\right)\hbar\omega\right] - 1} \tag{1.12}$$

$$\simeq \int dn_x dn_y dn_z \frac{1}{\exp\left[\beta\left(n_x + n_y + n_z\right)\hbar\omega\right] - 1}, \tag{1.13}$$

where $\beta = 1/k_B T$. Define $\tilde{n}_i \equiv \beta\hbar\omega n_i, \quad d\tilde{n}_i = \beta\hbar\omega dn_i$. The integral becomes

$$N_T = \frac{1}{(\beta\hbar\omega)^3} \int_0^\infty d\tilde{n}_x d\tilde{n}_y d\tilde{n}_z \frac{1}{e^{\tilde{n}_x + \tilde{n}_y + \tilde{n}_z} - 1}. \tag{1.14}$$

Integrating over the region $n_x, n_y, n_z \geqslant 0$ with triangles $\tilde{n}_x + \tilde{n}_y + \tilde{n}_z = \tilde{x}$ of an area $\frac{\tilde{x}^2\sqrt{3}}{2}$ and distance to the origin $\frac{2\tilde{x}}{\sqrt{3}}$:

$$\begin{aligned} N_T &= \frac{1}{(\beta\hbar\omega)^3} \int_0^\infty d\tilde{x} \frac{2}{\sqrt{3}} \frac{\frac{\tilde{x}^2\sqrt{3}}{2}}{e^{\tilde{x}} - 1} \\ &= \frac{1}{(\beta\hbar\omega)^3} \int_0^\infty d\tilde{x} \frac{\tilde{x}^2}{e^{\tilde{x}} - 1} = \frac{\zeta(3)}{(\beta\hbar\omega)^3}. \end{aligned} \tag{1.15}$$

Then, critical temperature T_c for the condensation is [7]:

$$k_B T_c = \hbar\omega \left(\frac{N}{\zeta(3)}\right)^{1/3} = 0.94\hbar\omega N^{1/3}. \tag{1.16}$$

For the temperature $T \leqslant T_c$, $N_T = \frac{\zeta(3)\cdot(k_B T)^3}{(\hbar\omega)^3}$, since $\mu = \epsilon_0$ for this region. Then, the fraction of the condensed particles:

$$\begin{aligned} \frac{N_0}{N} &= \frac{N - N_T}{N} = 1 - \frac{\zeta(3)\left(k_B T\right)^3}{(\hbar\omega)^3} \frac{(\hbar\omega)^3}{\left(\hbar T_c\right)^3 \zeta(3)} \\ \frac{N_0}{N} &= 1 - \left(\frac{T}{T_c}\right)^3. \end{aligned} \tag{1.17}$$

For the non-interacting Bose gas, the depletion can occur only through the thermal fluctuations, since all the particles condense into the ground state as $T \to 0$. In the absence of thermal energy, the particles favor the ground state and no particle occupies the excited single-particle states. Taking thermal fluctuations into account is central to explaining various experiments and also manifests interesting phenomena [7, 8]. However, when the interactions among the particles are considered, the excitations to the excited states can also be triggered solely by quantum fluctuations. Even in the limit $T \to 0$, i.e. there is no excitation due to the thermal fluctuations, the quantum fluctuations can drastically change the properties and the dynamics of the BECs.

Since the examination of the interacting BECs at zero temperature is fundamental to understanding the arguments of this thesis, we first review the general approaches to the interacting systems.

1.1.2 Interacting BEC: General Approach

In this section, we closely follow the approach presented in [10]. The Hamiltonian of a Bose gas under a single-particle potential $V_{\text{ext}}(\vec{r})$ and two-body interactions $\mathcal{U}(\vec{r}_1 - \vec{r}_2)$ is written in terms of the field creation and annihilation operators $\hat{\psi}^\dagger(\vec{r}, t)$ and $\hat{\psi}(\vec{r}, t)$ as follows [11]:

$$\begin{aligned}\hat{H} = &\int d^3\vec{r}\hat{\psi}^\dagger(\vec{r}, t)\left[-\frac{\hbar^2}{2m}\hat{\nabla}^2 + V_{ext}(\vec{r})\right]\hat{\psi}(\vec{r}, t) \\ &+ \int d^3\vec{r}_1 \int d^3\vec{r}_2 \hat{\psi}^\dagger(\vec{r}_1, t)\,\hat{\psi}^\dagger(\vec{r}_2, t)\,\hat{\mathcal{U}}(\vec{r}_1 - \vec{r}_2)\,\hat{\psi}(\vec{r}_2, t)\,\hat{\psi}(\vec{r}_1, t)\,.\end{aligned} \tag{1.18}$$

Field operators obey the Bose commutation rules:

$$\begin{aligned}\left[\hat{\psi}(\vec{r}), \hat{\psi}(\vec{r}')\right] = 0, \quad \left[\hat{\psi}^\dagger(\vec{r}), \hat{\psi}^\dagger(\vec{r}')\right] = 0 \\ \left[\hat{\psi}(\vec{r}), \hat{\psi}^\dagger(\vec{r}')\right] = \delta(\vec{r} - \vec{r}').\end{aligned} \tag{1.19}$$

The interactions among the particles can be effectively modeled as the s-wave scattering process for the sufficiently dilute condensates in the cold temperature limit [9]. Hence, the two-body potential is regarded as contact interaction with a pseudo-potential:

$$\mathcal{U}(\vec{r}_1 - \vec{r}_2) = g\delta(\vec{r}_1 - \vec{r}_2)\,, \tag{1.20}$$

where $g = \frac{4\pi a_s \hbar^2}{m}$ is the interaction coupling constant, $\delta(\vec{r})$ is the Dirac delta function, and a_s is the s-wave scattering length. Then, the Hamiltonian becomes [10]:

$$\begin{aligned}\hat{H} = &\int d^3\vec{r}\hat{\psi}^\dagger(\vec{r}, t)\left[-\frac{\hbar^2}{2m}\hat{\nabla}^2 + V_{ext}(\vec{r})\right]\hat{\psi}(\vec{r}, t) \\ + &\frac{g}{2}\int d^3\vec{r}\hat{\psi}^\dagger(\vec{r}, t)\hat{\psi}^\dagger(\vec{r}, t)\hat{\psi}(\vec{r}, t)\hat{\psi}(\vec{r}, t).\end{aligned} \tag{1.21}$$

The exact Heisenberg equation of motion of the Bose field operator $\hat{\psi}(\vec{r})$:

$$-i\hbar\frac{\partial\hat{\psi}}{\partial t} = [\hat{H}, \hat{\psi}] = \hat{H}\hat{\psi} - \hat{\psi}\hat{H} \tag{1.22}$$

$$= \int d^3\vec{r}\left\{\hat{\psi}^\dagger\hat{\mathcal{T}}\hat{\psi}\hat{\psi} + \frac{g}{2}\hat{\psi}^\dagger\hat{\psi}^\dagger\hat{\psi}\hat{\psi}\hat{\psi} - \hat{\psi}\hat{\psi}^\dagger\hat{\mathcal{T}}\hat{\psi} - \frac{g}{2}\hat{\psi}\hat{\psi}^\dagger\hat{\psi}^\dagger\hat{\psi}\hat{\psi}\right\}, \tag{1.23}$$

where the single particle operator $\hat{\mathcal{T}} \equiv -\frac{\hbar^2}{2m}\hat{\nabla}^2 + V_{ext}(\vec{r})$. The commutation rules are used to simplify:

$$\begin{aligned} &\psi^\dagger\psi\psi^\dagger\psi\psi - \psi^\dagger\psi\psi - \psi\psi^\dagger\psi^\dagger\psi\psi \\ =&\underbrace{\left(\psi^\dagger\psi - \psi\psi^\dagger\right)}_{-1}\psi^\dagger\psi\psi - \psi^\dagger\psi\psi = -2\psi^\dagger\psi\psi. \end{aligned} \tag{1.24}$$

Similarly,

$$\hat{\psi}^\dagger\hat{\mathcal{T}}\hat{\psi}\hat{\psi} - \hat{\psi}\hat{\psi}^\dagger\hat{\mathcal{T}}\hat{\psi} = -\mathcal{T}\hat{\psi}. \tag{1.25}$$

Then, the exact equation of motion becomes for $\hat{K} = \hat{H} - \mu\hat{N}$ [10]:

$$\begin{aligned} i\hbar\frac{\partial\hat{\psi}}{\partial t} &= \left(-\frac{\hbar^2}{2m}\nabla^2 + V_{ext}(\vec{r}) - \mu\right)\hat{\psi}(\vec{r},t) \\ &+ g\hat{\psi}^\dagger(\vec{r},t)\hat{\psi}(\vec{r},t)\hat{\psi}(\vec{r},t), \end{aligned} \tag{1.26}$$

where μ is the Lagrange multiplier that ensures the fixed number of particles N. Now we search for the solutions with a static condensate $\Phi(\vec{r})$ and time-varying quantum fluctuations $\tilde{\psi}(\vec{r},t)$:

$$\hat{\psi}(\vec{r},t) = \Phi(\vec{r}) + \psi(\vec{r},t), \tag{1.27}$$

where $\Phi(\vec{r}) \equiv \langle\hat{\psi}(\vec{r},t)\rangle = \langle\hat{\psi}(\vec{r})\rangle$ is the condensate macroscopic Bose field and $\tilde{\psi}(\vec{r},t)$ represents the quantum fluctuations over the condensed Bose field with the time average $\langle\tilde{\psi}(\vec{r},t)\rangle = 0$. Using $\hat{\psi}\,(\vec{r})$, rewrite the interaction term:

$$\begin{aligned} \psi^\dagger\psi\psi &= (\Phi^* + \tilde{\psi}^\dagger)(\Phi + \tilde{\psi})(\Phi + \tilde{\psi}) \\ &= \left(|\Phi|^2 + \Phi^*\tilde{\psi} + \Phi\tilde{\psi}^\dagger + \tilde{\psi} + \tilde{\psi}\right)(\Phi + \tilde{\psi}) \\ &= |\Phi|^2\Phi + 2|\Phi|^2\tilde{\psi} + \Phi^*\tilde{\psi}\tilde{\psi} + \Phi^2\tilde{\psi}^\dagger + 2\Phi\tilde{\psi}^\dagger\tilde{\psi} + \tilde{\psi}^\dagger\tilde{\psi}\tilde{\psi}. \end{aligned} \tag{1.28}$$

The last term in the above expression $\tilde{\psi}^\dagger\tilde{\psi}\tilde{\psi}$ can be rewritten in the self-consistent MF approximation:

$$\tilde{\psi}^\dagger(\vec{r},t)\tilde{\psi}\,(\vec{r},t)\,\tilde{\psi}(\vec{r},t) \simeq 2\langle\tilde{\psi}^\dagger\tilde{\psi}\rangle\tilde{\psi}(\vec{r},t) + \langle\tilde{\psi}\tilde{\psi}\rangle\tilde{\psi}^\dagger(\vec{r},t). \tag{1.29}$$

Hence,

$$\hat{\psi}^\dagger\hat{\psi}\hat{\psi} = |\Phi|^2\Phi + 2\left[|\Phi|^2 + \langle\tilde{\psi}^\dagger\tilde{\psi}\rangle\right]\tilde{\psi} + \left[\Phi^2 + \langle\tilde{\psi}\tilde{\psi}\rangle\right]\tilde{\psi}^\dagger + 2\Phi\tilde{\psi}^\dagger\tilde{\psi} + \Phi^*\tilde{\psi}\tilde{\psi}. \tag{1.30}$$

To find the condensate wavefunction $\Phi(\vec{r})$, we take the time average of the equation of motion for $\hat{\psi}(\vec{r},t) = \Phi(\vec{r}) + \tilde{\psi}$:

$$\left[-\frac{\hbar^2}{2m}\nabla^2 + V_{ext}(\vec{r}) - \mu\right]\Phi(\vec{r}) + g\left\langle\psi^\dagger\psi\psi\right\rangle = 0, \tag{1.31}$$

where

$$\left\langle\psi^\dagger\psi\psi\right\rangle = |\Phi|^2\Phi + 2\Phi\langle\tilde{\psi}^\dagger\tilde{\psi}\rangle + \Phi^*\langle\tilde{\psi}\tilde{\psi}\rangle \tag{1.32}$$

since the time average of fluctuations $\langle\tilde{\psi}^\dagger\rangle = \langle\tilde{\psi}\rangle = 0$ vanish. Therefore, the equation for the condensate field $\Phi(\vec{r})$ becomes:

$$\left[-\frac{\hbar^2}{2m}\nabla^2 + V_{\text{ext}}(\vec{r}) - \mu\right]\Phi + g\left[|\Phi|^2 + 2\langle\tilde{\psi}^\dagger\tilde{\psi}\rangle\right]\Phi + g\langle\tilde{\psi}\tilde{\psi}\rangle\Phi^* = 0. \tag{1.33}$$

Define the condensate density $n_c(\vec{r}) \equiv |\Phi|^2$, normal average $\tilde{n}(\vec{r}) \equiv \langle\tilde{\psi}^\dagger\tilde{\psi}\rangle$, and anomalous average $\tilde{m}(\vec{r}) \equiv \langle\tilde{\psi}\tilde{\psi}\rangle$ [10]. Rewrite (1.33):

$$\left[-\frac{\hbar^2}{2m}\nabla^2 + V_{ext}(\vec{r}) - \mu\right]\Phi + g\left[n_c(\vec{r}) + 2\tilde{n}(\vec{r})\right]\Phi + g\tilde{m}(\vec{r})\Phi^* = 0. \tag{1.34}$$

Noticing that $\hat{\psi} = \Phi + \tilde{\psi}$ implies $\langle\hat{\psi}\rangle = \Phi$, the time evolution equation for the operator $\hat{\psi}$:

$$i\hbar\frac{\partial\hat{\psi}}{\partial t} = \left(\hat{\mathcal{T}} - \mu\right)\hat{\psi} + g\hat{\psi}^\dagger\hat{\psi}\hat{\psi} \tag{1.35}$$

can be reexpressed by taking the time average of both sides:

$$0 = (\hat{\mathcal{T}} - \mu)\Phi + g\langle\hat{\psi}^\dagger\hat{\psi}\hat{\psi}\rangle. \tag{1.36}$$

Subtracting the equations (1.35) and (1.36) gives:

$$i\hbar\frac{\partial\tilde{\psi}}{\partial t} = (\hat{\mathcal{T}} - \mu)\tilde{\psi} + g\left[\hat{\psi}^\dagger\hat{\psi}\hat{\psi} - \left\langle\hat{\psi}^\dagger\hat{\psi}\hat{\psi}\right\rangle\right]. \tag{1.37}$$

The last term can be written as:

$$\begin{aligned}\hat{\psi}^\dagger\hat{\psi}\hat{\psi} - \left\langle\hat{\psi}^\dagger\hat{\psi}\hat{\psi}\right\rangle \simeq\ & 2\left[|\Phi|^2 + \left\langle\tilde{\psi}^\dagger\tilde{\psi}\right\rangle\right]\tilde{\psi} \\ & + \left[\Phi^2 + \langle\tilde{\psi}\tilde{\psi}\rangle\right]\tilde{\psi}.\end{aligned} \tag{1.38}$$

This equation is obtained when the quadratic terms are treated with MF approximation:

$$\begin{aligned}\tilde{\psi}^\dagger\tilde{\psi} &\simeq \left\langle\tilde{\psi}^\dagger\tilde{\psi}\right\rangle, \\ \tilde{\psi}\tilde{\psi} &\simeq \langle\tilde{\psi}\tilde{\psi}\rangle.\end{aligned} \tag{1.39}$$

Hence, the equation of motion for the fluctuation operator $\tilde{\psi}$ becomes:

$$\begin{aligned} i\hbar\frac{\partial\tilde{\psi}}{\partial t} &= \left[-\frac{\hbar^2}{2m}\nabla^2 + V_{ext}(\vec{r})\mu\right]\tilde{\psi} + 2g\left[|\Phi|^2 + \tilde{n}(\vec{r})\right]\tilde{\psi} \\ &+ g\left[\Phi^2 + \tilde{m}(\vec{r})\right]\tilde{\psi}^\dagger. \end{aligned} \tag{1.40}$$

This results in coupled equations of motion for the condensate $\Phi(\vec{r})$ and fluctuation operator $\tilde{\psi}(\vec{r})$ [10]:

$$\begin{aligned} \left[-\frac{\hbar^2}{2m}\nabla^2 + V_{ext}(\vec{r}) - \mu\right]\Phi(\vec{r}) &+ g\left[|\Phi|^2 + 2\tilde{n}(\vec{r})\right]\Phi(\vec{r}) \\ &+ g\tilde{m}(\vec{r})\Phi^*(\vec{r}) = 0. \end{aligned} \tag{1.41}$$

These two equations must be solved self-consistently, i.e. the solution to Φ is dependent on fluctuations $\tilde{\psi}(\vec{r},t)$, whereas the $\tilde{\psi}(\vec{r},t)$ is also Φ dependent. Time-independent Gross-Pitaevskii equation is obtained when the normal $\tilde{n}(\vec{r})$ and anomalous fluctuations $\tilde{m}(\vec{r})$ are neglected in (1.41):

$$\left[-\frac{\hbar^2}{2m}\nabla^2 + V_{ext}(\vec{r})\right]\Phi(\vec{r}) + g|\Phi|^2\Phi(\vec{r}) = \mu\Phi(\vec{r}). \tag{1.42}$$

When any fluctuation is neglected on the condensate macroscopic field, the GP equation is mostly the appropriate method to study both the ground state and the dynamics of the problem [8]. It provides a closed and non-linear equation for the condensate wavefunction $\Phi(\vec{r})$. However, when the fluctuations over the condensate become non-negligible as with the thermal depletion or the quantum droplets, the effect of the non-condensate fraction on the condensate wavefunction $\Phi(\vec{r})$ should also be considered.

Bogoliubov's approach to finding the excitations over the GP MF solution still neglects the contributions of normal and anomalous fluctuations on the solution of the condensate wavefunction $\Phi(\vec{r})$ in (1.41) and beyond GP fluctuations $\tilde{\psi}(\vec{r},t)$ in (1.40) [10]. However, it calculates fluctuations over the MF using the condensate wavefunction $\Phi(\vec{r})$ [10]:

$$i\hbar\frac{\partial\tilde{\psi}}{\partial t} = \left[-\frac{\hbar^2}{2m}\nabla^2 + V_{ext}(\vec{r}) - \mu\right]\tilde{\psi}\left(\vec{r},t\right) + 2g|\Phi|^2\tilde{\psi} + g\Phi^2\tilde{\psi}^\dagger, \tag{1.43}$$

$$-i\hbar\frac{\partial\tilde{\psi}^\dagger}{\partial t} = \left[-\frac{\hbar^2}{2m}\nabla^2 + V_{\text{ext}}\left(\vec{r}\right) - \mu\right]\tilde{\psi}^\dagger\left(\vec{r},t\right) + 2g|\Phi|^2\tilde{\psi}^\dagger + g\Phi^{*^2}\tilde{\psi}. \tag{1.44}$$

Now search for solutions that are periodic in time, and satisfied for all times. Both positive and negative frequency components are necessary, since the equations for the $\tilde{\psi}$ and $\tilde{\psi}^*$ are coupled. Use the following ansatz [8]:

$$\begin{aligned}\tilde{\psi}(\vec{r},t) &= e^{-i\mu t/\hbar}\left[u(\vec{r})e^{-i\omega t} - v^*(\vec{r})e^{+i\omega t}\right],\\ \tilde{\psi}^\dagger(\vec{r},t) &= e^{+i\mu t/\hbar}\left[u^*(\vec{r})e^{+i\omega t} - v(\vec{r})e^{-i\omega t}\right],\end{aligned} \tag{1.45}$$

where the sign coefficients for the variables u and v are chosen to ensure both have the same sign.

Replace the operators in (1.45) into the coupled Bogoliubov equations (1.41) and (1.40), and obtain the coupled equations for the coefficients $u(\vec{r})$ and $v(\vec{r})$ [8]:

$$g|\Phi|^2 v = \left[\mathcal{T} + 2g|\Phi|^2 - \hbar\omega - \mu\right]u, \tag{1.46}$$

$$g|\Phi|^2 u = \left[\mathcal{T} + 2g|\Phi|^2 + \hbar\omega - \mu\right]v. \tag{1.47}$$

For the uniform gas, i.e. $V_{ext} = 0$, $u(\vec{r})$ and $v(\vec{r})$ can be chosen to ensure the excitations are in the form of plane waves [8]:

$$u(\vec{r}) = u_k\frac{e^{i\vec{k}\vec{r}}}{\sqrt{V}}, \quad v(\vec{r}) = v_k\frac{e^{i\vec{k}\vec{r}}}{\sqrt{v}}. \tag{1.48}$$

Then, the equations for $u(\vec{r})$ and $v(\vec{r})$ become:

$$gnv_k = \left(\tfrac{\hbar^2k^2}{2m} + gn - \hbar\omega\right)u_k, \tag{1.49}$$

$$gnu_k = \left(\tfrac{\hbar^2k^2}{2m} + gn + \hbar\omega\right)v_k, \tag{1.50}$$

where $\mu = gn$ is used for the uniform condensate. Solving $\hbar\omega$ by equalizing u_k/v_k, we obtain the Bogoilubov dispersion and transformation coefficients [8]:

$$E_k \equiv \hbar\omega = \sqrt{\epsilon_k\left(\epsilon_k + 2gn\right)}, \tag{1.51}$$

$$u_k^2 = \frac{1}{2}\left(1 + \frac{\epsilon_k + gn}{E_k}\right), \tag{1.52}$$

$$v_k^2 = \frac{1}{2}\left(-1 + \frac{\epsilon_k + gn}{E_k}\right). \tag{1.53}$$

Note that the coefficients v_k converge to zero as $1/k^2$ for large k in the positive energy solutions. This can be physically interpreted as an addition to the free particle with momentum $\hbar\vec{k}$, and a removal of a particle in the zero momentum state. Therefore, the Bogoliubov excitations are solely the excitations of a free particle out of a condensate.

Similarly, for smaller momenta, the excitations are the superpositions of the states in which $+\vec{k}$ atom is added and a condensate atom is removed, or a condensate atom is added and $-\vec{k}$ is removed. At longer wavelengths, the coefficients u_k and v_k are approximately equal to each other.

1.1.3 Interacting BEC: Mechanical Stability of BEC

Here we revisit the discussion on the mechanical stability of the weakly interacting condensate for both repulsive and attractive interactions in the GP regime [8]. Whether the condensates require external confinement to be mechanically stable is an important question to be addressed. Besides, how the interaction type, i.e. repulsive or attractive, affects the stability and time evolution of the condensate needs to be discussed.

Consider the energy functional of the condensate including the kinetic, trapping, and interaction energy in the GP regime. The GP approach assumes all the particles occupy the same state, which is not necessarily one of the eigenstates of the single particle Hamiltonian. Hence, assume $\psi(\vec{r}) = \sqrt{N}\phi(\vec{r})$ [8], where $\phi(\vec{r})$ is the state that all particles occupy. Use this GP wavefunction to calculate the total energy functional E when the Hamiltonian and the corresponding energy are [8]:

$$H = \sum_{i=1}^{N} \left[\frac{\mathbf{p}_i^2}{2m} + V_{ext}\left(\vec{r}_i\right) \right] + g \sum_{i<j} \delta\left(\vec{r}_i - \vec{r}_j\right), \tag{1.54}$$

$$E = \int d^3\vec{r} \left[\frac{\hbar^2}{2m} |\nabla\psi(\vec{r})|^2 + V_{\text{ext}}\left(\vec{r}\right)|\psi(\vec{r})|^2 + \frac{g}{2}|\psi(\vec{r})|^4 \right], \tag{1.55}$$

where g is the coupling constant of interaction and the V_{ext} is the external potential. Assume an external potential in the form of an isotropic harmonic trap

$$V_{\text{ext}}\left(\vec{r}\right) = \frac{1}{2} m\omega^2 r^2. \tag{1.56}$$

Minimize the energy functional with the constraint that the total number of particles is constant:

$$N = \int d^3\vec{r} |\psi(\vec{r})|^2, \tag{1.57}$$

$$\frac{\delta\left(E - \mu N\right)}{\delta\psi^*} = 0. \tag{1.58}$$

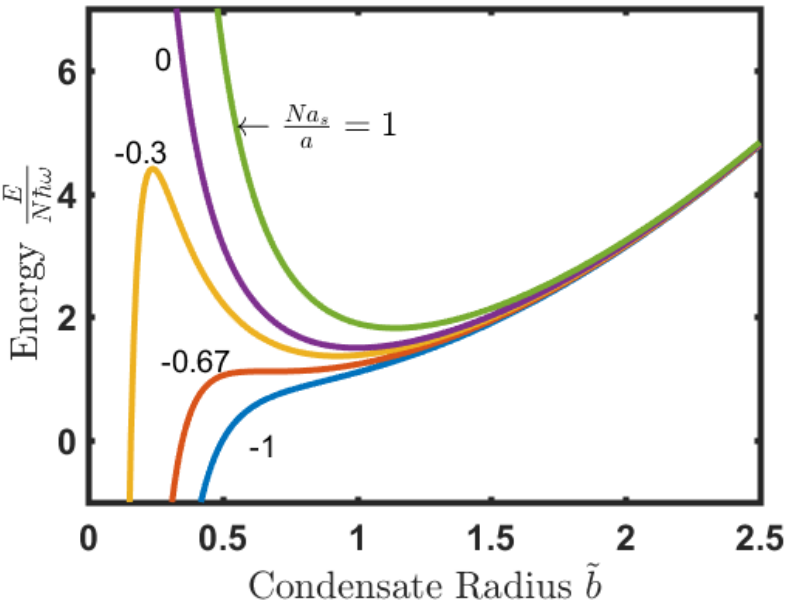

Figure 1.1: The total energy of the condensate $E/N\hbar\omega$ in (1.67) vs. the variational cloud radius $\tilde{b} = b/a$, where a is the harmonic oscillator length scale. For any positive scattering length $a_s > 0$, the condensate can be stabilized by the harmonic potential, and the global minimum of the energy functional is always at a finite $\tilde{b}$ value. However, the attractive condensate $a_s < 0$ can only yield a local minimum for $\frac{Na_s}{a} > -0.67$, and the condensate is metastable. After this critical level, the local minimum disappears, and the density collapse is inevitable for the condensate in equilibrium.

This variational analysis yields the same GP equation, as in (1.41):

$$-\frac{\hbar^2}{2m}\nabla^2\psi + V_{\text{ext}}(\vec{r})\psi + g|\psi|^2\psi = \mu\psi, \tag{1.59}$$

where g is positive for repulsive and negative for attractive interactions. To obtain this equation, the variation of the kinetic energy is computed with integration by parts, and $|\psi|^n = \psi^{n/2}(\psi^*)^{n/2}$, where n is an integer. The ground-state wavefunction in the absence of two-body interactions is the lowest energy eigenstate of the 3D harmonic oscillator problem is [8]:

$$\psi_0(\vec{r}) = \frac{\sqrt{N}}{\pi^{3/4}a^{3/2}}e^{-r^2/2a^2}, \tag{1.60}$$

where $a = \sqrt{\frac{\hbar}{m\omega}}$ is the oscillator length scale. In the existence of interactions, the condensate form may change depending on the strength and type of the interaction

but is expected to show a similar form. Therefore, assume a variational ansatz [8]:

$$\psi(\vec{r}) = \frac{\sqrt{N}}{\pi^{3/4}b^{3/2}}e^{-r^2/2b^2}, \tag{1.61}$$

where b is the condensate radius and the variational parameter. Let us now calculate the total energy of the condensate and minimize it with respect to the cloud size b.

$$\begin{aligned}
E_k &= \int d^3\vec{r}\frac{\hbar^2}{2m}|\nabla\psi|^2 = \int d^3\vec{r}\frac{\hbar^2}{2m}\left[\frac{\partial}{\partial r}\left(\frac{\sqrt{N}}{\pi^{3/4}b^{3/2}}e^{-r^2/2b^2}\right)\right]^2 \\
&= \frac{2\hbar^2 N}{m\pi^{1/2}b^7}\int_0^\infty drr^4e^{-r^2/b^2} \\
&= \frac{3\hbar^2 N}{4mb^2} = \frac{3\hbar\omega N}{4}\frac{1}{\tilde{b}^2}, \qquad (1.62) \\
E_{ext} &= \int d^3\vec{r}\frac{1}{2}m\omega^2r^2\left(\frac{\sqrt{N}}{\pi^{3/4}b^{3/2}}e^{-r^2/2b^2}\right)^2 \\
&= \frac{m\omega^2}{2}4\pi\frac{N}{\pi^{3/2}b^3}\int_0^\infty drr^4e^{-r^2/b^2} \\
&= \frac{3}{4}m\omega^2Nb^2 \\
&= \frac{3}{4}m\omega^2N\frac{b^2}{a^2}\frac{\hbar}{m\omega} = \frac{3\hbar\omega N}{4}\tilde{b}^2, \qquad (1.63) \\
E_{int} &= \frac{g}{2}\int d^3\vec{r}|\psi(\vec{r})|^4 = \frac{g}{2}4\pi\int_0^\infty drr^2\frac{N^2}{\pi^3b^6}e^{-2r^2/b^2} \\
&= \frac{2gN^2}{\pi^2b^6}\int_0^\infty drr^2e^{-2r^2/b^2} \\
&= \frac{1}{4\sqrt{2}\pi^{3/2}}\frac{gN^2}{b^3} = \frac{gN^2}{4\sqrt{2}\pi^{3/2}}\frac{1}{a^3}\frac{1}{\tilde{b}^3}, \qquad (1.64)
\end{aligned}$$

where $\tilde{b} \equiv b/a$. Then, the total energy of the condensate becomes:

$$\begin{aligned}
E &= \frac{3\hbar\omega N}{4}\left(\tilde{b}^2 + \frac{1}{\tilde{b}^2}\right) + \frac{gN^2}{4\sqrt{2}\pi^{3/2}}\frac{1}{a^3}\frac{1}{\tilde{b}^3} \qquad (1.65) \\
&= \frac{3\hbar\omega N}{4}\left[\tilde{b}^2 + \frac{1}{\tilde{b}^2} + \frac{1}{3\sqrt{2}\pi^{3/2}}\frac{gN}{a^3\hbar\omega}\frac{1}{\tilde{b}^3}\right]. \qquad (1.66)
\end{aligned}$$

Define $\tilde{g} \equiv \frac{g/a^3}{\hbar\omega} = \frac{4\pi a_s\hbar^2}{m}\frac{1}{a^3\hbar\omega} = \frac{a_s}{a}4\pi$ and rewrite the total energy:

$$\frac{E}{N\hbar\omega} = \frac{3}{4}\left[\tilde{b}^2 + \frac{1}{\tilde{b}^2} + \frac{4}{3\sqrt{2\pi}}\frac{Na_s}{a}\frac{1}{\tilde{b}^3}\right]. \tag{1.67}$$

For positive scattering length $a_s > 0$, the energy functional always yields a minimum for a finite radius $\tilde{b}$, as shown in Fig.1.1. However, for the attractive interaction $a_s < 0$, the interaction term globally favors a minimum at the limit $\tilde{b} \to 0$, i.e. the

condensate collapses. This collapse instability can be stabilized by a metastable minimum. This metastable minimum corresponds to $\frac{Na_s}{a} \approx -0.67$, below which there is no local minimum for a finite non-zero $\tilde{b}$. Hence, an upper limit exists for the number of particles to display at least a metastable minimum for the attractive interactions:

$$N < N_c = 0.67 \frac{a_{ho}}{a_s}. \tag{1.68}$$

1.1.4 Interacting BEC: Bogoliubov Microscopic Theory

We discussed different approaches to the problem of weakly interacting Bose condensate, including Gross-Pitaevskii and Bogoliubov theories. However, neither of the formalisms provides an explanation of the interacting condensate at the microscopic level. Here microscopic level means the distribution of the condensate atoms among the single particle eigenstates of a specified Hamiltonian. We now revisit the Bogoliubov theory at the microscopic level to understand the effect of the interactions on the distribution of the particles among the eigenstates. To simplify the discussion and obtain analytical formulas for the energy and condensate depletion, we consider a homogeneous Bose gas, $V_{ext}(\vec{r}) = 0$, in which non-interacting single-particle eigenstates are free particle eigenstates. We closely follow the approach provided by [8], and sometimes detail the reasoning and calculations.

Consider the Hamiltonian of the homogeneous weakly interacting Bose gas written in the second quantization formalism [8]:

$$\begin{aligned} \hat{H} &= \int d^3\vec{r}\hat{\psi}^\dagger(\vec{r}) \left(-\frac{\hbar^2}{2m}\nabla^2 \right) \hat{\psi}(\vec{r}) \\ &+ \frac{g}{2} \int d^3\vec{r}\hat{\psi}^\dagger(\vec{r})\hat{\psi}^\dagger(\vec{r})\hat{\psi}(\vec{r})\hat{\psi}(\vec{r}), \end{aligned} \tag{1.69}$$

where $g = \frac{4\pi a\hbar^2}{m}$ is the interaction coupling constant and $\hat{\psi}^\dagger$ and $\hat{\psi}$ are the field creation and annihilation operators, respectively. Note that the wavefunction in the momentum space is the Fourier transform of the wavefunction in the position space [7, 8]:

$$\phi(\vec{k}) = \int d^3\vec{r}\psi(\vec{r})e^{+i\vec{k}\vec{r}}, \tag{1.70}$$

$$\psi(\vec{r}) = \frac{\sqrt{V}}{(2\pi)^3} \int d^3\vec{k}\phi(\vec{k})e^{-i\vec{k}\vec{r}}. \tag{1.71}$$

Using the eigenstate transformations, rewrite the creation and annihilation operators in position space as a function of their duals in the momentum space:

$$\hat{\psi}(\vec{r}) = \frac{\sqrt{V}}{(2\pi)^3}\int d^3\vec{k}\hat{a}_{\vec{k}}e^{-i\vec{k}\vec{r}} = \frac{1}{\sqrt{V}}\sum_{\vec{k}}\hat{a}_{\vec{k}}e^{-i\vec{k}\vec{r}}, \tag{1.72}$$

$$\hat{\psi}^\dagger(\vec{r}) = \frac{\sqrt{V}}{(2\pi)^3}\int d^3\vec{k}\hat{a}^\dagger_{\vec{k}}e^{+i\vec{k}\vec{r}} = \frac{1}{\sqrt{V}}\sum_{\vec{k}}\hat{a}^\dagger_{\vec{k}}e^{+i\vec{k}\vec{r}}. \tag{1.73}$$

Replace the position operators with the momentum operators in the Hamiltonian (1.69):

$$\begin{aligned}
\hat{H} = \int d^3\vec{r} \quad & \left(\frac{1}{\sqrt{V}}\sum_{\vec{k}_1}\hat{a}^\dagger_{\vec{k}_1}e^{-i\vec{k}_1\vec{r}}\right)\left(\frac{-\hbar^2}{2m}\nabla^2\right)\left(\frac{1}{\sqrt{V}}\sum_{\vec{k}_2}\hat{a}^\dagger_{\vec{k}_2}e^{-i\vec{k}_2\vec{r}}\right) \\
+\frac{g}{2}\int d^3\vec{r} \quad & \left(\frac{1}{\sqrt{V}}\sum_{\vec{k}_1}\hat{a}^\dagger_{\vec{k}_1}e^{-i\vec{k}_1\vec{r}}\right)\left(\frac{1}{\sqrt{V}}\sum_{\vec{k}_2}\hat{a}^\dagger_{\vec{k}_2}e^{-i\vec{k}_2\vec{r}}\right) \\
& \left(\frac{1}{\sqrt{V}}\sum_{\vec{k}_3}\hat{a}_{\vec{k}_3}e^{-i\vec{k}_3\vec{r}}\right)\left(\frac{1}{\sqrt{V}}\sum_{\vec{k}_4}\hat{a}_{\vec{k}_4}e^{-i\vec{k}_4\vec{r}}\right) \\
= \frac{1}{V}\int d^3\vec{r} \quad & \sum_{\vec{k}_1,\vec{k}_2}\frac{\hbar^2k_2^2}{2m}e^{i(\vec{k}_1-\vec{k}_2)\vec{r}}\left(\hat{a}^\dagger_{\vec{k}_1}\hat{a}_{\vec{k}_2}\right) \\
+\frac{g}{2V^2}\int d^3\vec{r} \quad & \sum_{\vec{k}_1,\vec{k}_2,\vec{k}_3,\vec{k}_4}e^{i\left(\vec{k}_1+\vec{k}_2-\vec{k}_3-\vec{k}_4\right)\vec{r}}\left(\hat{a}^\dagger_{\vec{k}_1}\hat{a}^\dagger_{\vec{k}_2}\hat{a}_{\vec{k}_3}\hat{a}_{\vec{k}_4}\right),
\end{aligned} \tag{1.74}$$

where $\frac{1}{V}\int d^3\vec{r}e^{i\vec{k}\vec{r}} = \delta(\vec{r})$. Then, Hamiltonian becomes:

$$\hat{H} = \sum_{\vec{k}}\frac{\hbar^2k^2}{2m}\hat{a}^\dagger_{\vec{k}}\hat{a}_{\vec{k}} + \frac{g}{2V}\sum_{\vec{k}_1,\vec{k}_2,\vec{k}_3,\vec{k}_4}\delta\left(\vec{k}_1+\vec{k}_2-\vec{k}_3-\vec{k}_4\right)\hat{a}^\dagger_{\vec{k}_1}\hat{a}^\dagger_{\vec{k}_2}\hat{a}_{\vec{k}_3}\hat{a}_{\vec{k}_4}. \tag{1.75}$$

The Dirac delta term in interaction energy ensures the conservation of momentum for the two particles before and after a collision: $\vec{k}_1 + \vec{k}_2 = \vec{k}_3 + \vec{k}_4$. Hence, if the colliding particles of momentum $\vec{k}_3$ and $\vec{k}_4$ exchange momentum $\vec{q}$, the momentum of the particles after the collision are $\vec{k}_1 = \vec{k}_3 + \vec{q}$ and $\vec{k}_2 = \vec{k}_4 - \vec{q}$. Change the subindex $\vec{k}_3$ and $\vec{k}_4$ with $\vec{k}$ and $\vec{k'}$ [8]:

$$\hat{H} = \sum_{\vec{k}}\epsilon_k\hat{a}^\dagger_{\vec{k}}a_{\vec{k}} + \frac{g}{2V}\sum_{\vec{k},\vec{k'},\hat{q}}\hat{a}^\dagger_{\vec{k}+\vec{q}}\hat{a}^\dagger_{\vec{k'}-\hat{q}}\hat{a}_{\vec{k}}\hat{a}_{\vec{k'}}, \tag{1.76}$$

where $\epsilon_k \equiv \frac{\hbar^2k^2}{2m}$ is the free particle dispersion. Now consider the terms in the Hamiltonian. The first summation corresponds to the kinetic energy of the condensate, where $\hat{a}^\dagger_{\vec{k}}a_{\vec{k}}$ corresponds to the number of particles and ϵ_k is the energy of a single

particle in the $\vec{k}$-momentum state. The second summation is the interaction energy, which consists of the energies due to all possible s-wave collisions among the particles constraint to conserving the total momentum. The energy spectrum and the eigenstates of the total many-body system with the interaction in this general form are not analytically tractable. We need guidance in accordance with the physical properties of the system. This guidance for the weakly interacting Bose condensate comes from the intuition that a small fraction of the total particles leaves the ground state of the single-particle Hamiltonian. Hence, the macroscopic condensate field can be assumed to occupy the $\vec{k} = 0$ momentum state, whereas the quantum fluctuations above the condensate are any non-zero momentum state $\vec{k} \neq 0$. This approach constitutes the fundamental idea behind the Bogoliubov microscopic theory [12, 13]. Therefore, we approximate the interaction energy, which is quartic in terms of the operators $a_{\vec{k}}$, by at most quadratic in the non-zero momentum operators $a_{\vec{k}\neq 0}$, and ignore the higher order terms:

$$\sum_{\vec{k},\vec{k}',\vec{q}} \hat{a}^\dagger_{\vec{k}+\vec{q}} \hat{a}^\dagger_{\vec{k}-\vec{q}} \hat{a}_k \hat{a}_{k'} = a_0^\dagger \hat{a}_0^\dagger \hat{a}_0 \hat{a}_0 + \sum_{\substack{\vec{k} \\ \vec{q}=0 \\ \vec{k}'=0}}{}' \hat{a}^\dagger_k \hat{a}^\dagger_0 \hat{a}_k \hat{a}_0 + \sum_{\substack{\vec{k}' \\ \vec{q}=0 \\ \vec{k}=0}}{}' \hat{a}^\dagger_0 \hat{a}^\dagger_{\vec{k}'} \hat{a}_0 \hat{a}_{\vec{k}'} \tag{1.77}$$

$$+ \sum_{\substack{\vec{k}'=\vec{q} \\ \vec{k}=0}}{}' \hat{a}^\dagger_{\vec{q}} \hat{a}^\dagger_0 \hat{a}_0 \hat{a}_{\vec{q}} + \sum_{\substack{\vec{k}=-\vec{q} \\ \vec{k}'=0}}{}' \hat{a}^\dagger_0 \hat{a}^\dagger_{-\vec{q}} \hat{a}_{-\vec{q}} \hat{a}_0 + \sum_{\substack{\vec{q} \\ \vec{k}=0 \\ \vec{k}'=0}}{}' \hat{a}^\dagger_{\vec{q}} \hat{a}^\dagger_{-\vec{q}} \hat{a}_0 \hat{a}_0 + \sum_{\substack{\vec{k}=-\vec{q} \\ \vec{k}'=\vec{q}}}{}' \hat{a}^\dagger_0 \hat{a}^\dagger_0 \hat{a}_{\vec{q}} \hat{a}_{-\vec{q}}.$$

Assuming a scalar field for the macroscopic ground state $\hat{a}_0 \simeq \hat{a}_0^\dagger \simeq \sqrt{N_0}$.

$$\sum_{\vec{k},\vec{k}',\vec{q}} \hat{a}^\dagger_{\vec{k}+\vec{q}} \hat{a}^\dagger_{\vec{k}'-\vec{q}} \hat{a}_{\vec{k}} \hat{a}_{\vec{k}'} \simeq N_0^2 + N_0 \sum_{\vec{k}} \left(4\hat{a}^\dagger_{\vec{k}} \hat{a}_{\vec{k}} + a^\dagger_{\vec{k}} \hat{a}^\dagger_{-\vec{k}} + \hat{a}_{\vec{k}} \hat{a}_{-\vec{k}} \right) \tag{1.78}$$

where $N_0 = N - \sum_{\vec{k}\neq 0} \hat{a}^\dagger_{\vec{k}} a_{\vec{k}}$. We approximate $N_0^2 \simeq N^2 - 2N \sum_{\vec{k}} a^\dagger_{\vec{k}} a_{\vec{k}}$ since we ignore the term higher than the quadratic in the operators $\hat{a}_{\vec{k}}$. Then, the interaction Hamiltonian becomes:

$$\frac{g}{2V} \sum_{\vec{k},\vec{k}',\vec{q}} \hat{a}^\dagger_{k+q} \hat{a}^\dagger_{k'-q} \hat{a}_k \hat{a}_{k'} \simeq \frac{gN^2}{2V} + \frac{gN}{2V} \sum_{\vec{k}}{}' \left(2\hat{a}^\dagger_{\vec{k}} \hat{a}_{\vec{k}} + \hat{a}^\dagger_{\vec{k}} \hat{a}^\dagger_{\vec{k}} + \hat{a}_{\vec{k}} \hat{a}_{-\vec{k}} \right). \tag{1.79}$$

Hence, the total Hamiltonian becomes:

$$\begin{aligned} \hat{H} &= \frac{gN^2}{2V} + \sum_{\vec{k}}{}' \left(\epsilon_k + gn \right) a^\dagger_{\vec{k}} a_{\vec{k}} + \frac{gn}{2} \left(a^\dagger_{\vec{k}} a^\dagger_{\vec{k}} + a_{\vec{k}} a_{-\vec{k}} \right) \\ &= \frac{gN^2}{2V} + \sum_{\vec{k}}{}^{>} \left(\epsilon_k + gn \right) \left(a^\dagger_{\vec{k}} a_{\vec{k}} + a^\dagger_{-\vec{k}} a_{-\vec{k}} \right) + gn \left(a^\dagger_{\vec{k}} a^\dagger_{\vec{k}} + a_{\vec{k}} a_{-\vec{k}} \right), \end{aligned} \tag{1.80}$$

where superscript $'$ over the summation denotes the summation over $\vec{k} \neq 0$, and $^{>}$ denotes the summation over an half of the total $\vec{k}$-space. n is the density of the condensate. This Hamiltonian is quadratic and can be diagonalized by Bogoliubov transformation.

First, we revisit the Bogoliubov transformation for a single mode. From now on, we leave the vectorial notation of $\vec{k}$ and hat notation in the operators $\hat{a}$ for simplicity. Consider a toy Hamiltonian [8]:

$$\hat{H}_0 = \epsilon_1 \left(a_k^\dagger a_k + a_{-k}^\dagger a_{-k} \right) + \epsilon_2 \left(a_k^\dagger a_{-k}^\dagger + a_k a_{-k} \right) \tag{1.81}$$

$$= \begin{pmatrix} a_k & a_{-k}^\dagger \end{pmatrix} \begin{pmatrix} \epsilon_1 & \epsilon_2 \\ \epsilon_2 & \epsilon_1 \end{pmatrix} \begin{pmatrix} a_k^\dagger \\ a_{-k} \end{pmatrix} - \epsilon_1, \tag{1.82}$$

where $[a_k, a_k^\dagger] = 1$ is used to rewrite $a_k^\dagger a_k$ in the first part.

Now assume operator transformations in the form [8]:

$$\begin{aligned} b_k &= u a_k + v a_{-k}^\dagger \\ b_k^\dagger &= u a_k^\dagger + v a_{-k} \\ b_{-k} &= u a_{-k} + v a_k^\dagger \\ b_{-k}^\dagger &= u a_{-k}^\dagger + v a_k, \end{aligned} \tag{1.83}$$

where $u, v \in \mathcal{R}$. We expect the new quasiparticle creation and annihilation operators to obey the usual Bose commutation rules:

$$\begin{aligned} \left[b_k, b_k^\dagger \right] = 1 = b_k b_k^\dagger - b_k^\dagger b_k &= \left(u a_k + v a_{-k}^\dagger \right) \left(u a_k^\dagger + v a_{-k} \right) \\ &\quad - \left(u a_k^\dagger + v a_{-k} \right) \left(u a_k + v a_{-k}^\dagger \right) \\ &= u^2 a_k a_k^\dagger + uv \left(a_k a_{-k} + a_{-k}^\dagger a_k^\dagger \right) + v^2 a_{-k}^\dagger a_{-k} \\ &\quad - u^2 a_k^\dagger a_k - uv \left(a_{-k} a_k + a_k^\dagger a_{-k}^\dagger \right) - v^2 a_{-k} a_{-k}^\dagger \\ &= u^2 (\underbrace{a_k a_k^\dagger - a_k^\dagger a_k}_{=1}) + v^2 (\underbrace{a_{-k}^\dagger a_{-k} - a_{-k} a_{-k}^\dagger}_{=-1}) \\ &= u^2 - v^2 = 1. \end{aligned} \tag{1.84}$$

Using $u^2 - v^2 = 1$, one can rewrite a_k in terms of b_k :

$$\begin{aligned} a_k &= ub_k - vb^\dagger_{-k} \\ a_{-k} &= ub_{-k} - vb^\dagger_k \\ a^\dagger_k &= ub^\dagger_k - vb_{-k} \\ a^\dagger_{-k} &= ub^\dagger_{-k} - vb_k. \end{aligned} \tag{1.85}$$

In the matrix form:

$$\begin{pmatrix} a_k \\ a^\dagger_{-k} \end{pmatrix} = \begin{pmatrix} u & -v \\ -v & u \end{pmatrix} \begin{pmatrix} b_k \\ b^\dagger_{-k} \end{pmatrix} \tag{1.86}$$

and

$$\begin{pmatrix} a^\dagger_k & a_{-k} \end{pmatrix} = \begin{pmatrix} b^\dagger_k & b_{-k} \end{pmatrix} \begin{pmatrix} u & -v \\ -v & u \end{pmatrix}. \tag{1.87}$$

Then, $\hat{H}_0$ in the matrix form is:

$$\hat{H}_0 = \begin{pmatrix} b^\dagger_k & b_{-k} \end{pmatrix} \underbrace{\begin{pmatrix} u & -v \\ -v & u \end{pmatrix} \begin{pmatrix} \epsilon_1 & \epsilon_2 \\ \epsilon_2 & \epsilon_1 \end{pmatrix} \begin{pmatrix} u & -v \\ -v & u \end{pmatrix}}_{D=\begin{pmatrix} E_1 & 0 \\ 0 & E_1 \end{pmatrix}} \begin{pmatrix} b_k \\ b^\dagger_{-k} \end{pmatrix} - \epsilon_1. \tag{1.88}$$

Here D matrix should be diagonal for the transformations to diagonalize the Hamiltonian:

$$D = \begin{pmatrix} \left(u^2 + v^2\right)\epsilon_1 - 2uv\epsilon_2 & -2uv\epsilon_1 + \left(u^2 + v^2\right)\epsilon_2 \\ -2uv\epsilon_1 + \left(u^2 + v^2\right)\epsilon_2 & \left(u^2 + v^2\right)\epsilon_1 - 2uv\epsilon_2 \end{pmatrix}. \tag{1.89}$$

Choose u and v such that D is diagonal:

$$\left(u^2 + v^2\right)\epsilon_2 - 2uv\epsilon_1 = 0. \tag{1.90}$$

Remember that $u^2 - v^2 = 1$ is also required by the commutation rules. Appropriate parametrization for u and v can be found in the algebra of hyperbolic functions:

$$\begin{aligned} &\cosh^2\theta - \sinh^2\theta = 1 \\ &\cosh^2\theta + \sinh^2\theta = \cosh 2\theta \\ &2\sinh\theta\cosh\theta = \sinh 2\theta. \end{aligned} \tag{1.91}$$

Choosing $u = \cosh\theta$ and $v = \sinh\theta$ yields:

$$\begin{aligned} &\epsilon_2 \cosh 2\theta - \epsilon_1 \sinh 2\theta = 0 \\ &\tanh 2\theta = \frac{\epsilon_2}{\epsilon_1}, \quad \sinh 2\theta = \frac{\epsilon_2}{\sqrt{\epsilon_1^2 - \epsilon_2^2}}, \cosh 2\theta = \frac{\epsilon_1}{\sqrt{\epsilon_1^2 - \epsilon_2^2}}. \end{aligned} \tag{1.92}$$

The Bogoliubov spectrum E_k is found as:

$$\begin{aligned} E_k &= \epsilon_1 \cosh 2\theta - \epsilon_2 \sinh 2\theta \\ &= \frac{\epsilon_1^2 - \epsilon_2^2}{\sqrt{\epsilon_1^2 - \epsilon_2^2}} = \sqrt{\epsilon_1^2 - \epsilon_2^2} = \sqrt{(\epsilon_1 - \epsilon_2)(\epsilon_1 + \epsilon_2)}. \end{aligned} \tag{1.93}$$

The transformation coefficients u and v [8]:

$$\begin{aligned} u^2 = \cosh^2\theta &= \frac{1}{2}\left(1 + \frac{\epsilon_1}{\sqrt{\epsilon_1^2 - \epsilon_2^2}}\right) \\ v^2 = \sinh^2\theta &= \frac{1}{2}\left(-1 + \frac{\epsilon_1}{\sqrt{\epsilon_1^2 - \epsilon_2^2}}\right). \end{aligned} \tag{1.94}$$

The toy Hamiltonian H_0 is diagonalized as [8]:

$$H_0 = E_k - \epsilon + E_k\left(b_k^\dagger b_k + b_k^\dagger b_k\right). \tag{1.95}$$

The form of the transformations for the single mode Hamiltonian is sufficient to diagonalize the multimode Hamiltonian of the weakly interacting Bose gas (1.80). Replace $\epsilon_1 = \epsilon_k + gn$ and $\epsilon_2 = gn$, the Bogoliubov spectrum E_k, quasiparticle coefficients u_k and v_k become:

$$\begin{aligned} E_k &= \sqrt{\epsilon_k(\epsilon_k + 2gn)} \\ u_k^2 &= \frac{1}{2}\left(1 + \frac{\epsilon_k + gn}{E_k}\right) \\ v_k^2 &= \frac{1}{2}\left(-1 + \frac{\epsilon_k + gn}{E_k}\right). \end{aligned} \tag{1.96}$$

The Bogoliubov spectrum shows an interesting behavior for different $\mathrm{k} = |\vec{k}|$ limits. For sufficiently small k or long wavelengths, $\mathrm{k} \ll \frac{2\sqrt{mgn}}{\hbar}$, E_k is linear in k with $\frac{\hbar\sqrt{gn}}{m}$. This is similar to a phonon field with the sound velocity $s = \frac{\hbar\sqrt{gn}}{m}$. For high k or small wavelength, the interaction effect is negligible and the dispersion is the free particle dispersion. Now we express the total Hamiltonian in a diagonal form:

$$\hat{H} = \frac{gN^2}{2V} + \sum_{\vec{k}}{}^{>}(E_k - \epsilon_k - gn) + \sum_{\vec{k}}{}^{>} E_k\left(b_k^\dagger b_k + b_{-k}^\dagger b_{-k}\right), \tag{1.97}$$

where $b_k = u_k a_k + v_k a^\dagger_{-k}$ Here the total Hamiltonian is diagonalized in terms of the quasiparticle creation and annihilation operators. Hence, the interacting Bose gas can now be considered as the non-interacting Bose gas with zero point energy E_0:

$$E_0 = \frac{gN^2}{2V} + \frac{1}{2}{\sum_{\vec{k}}}' \left(E_k - \epsilon_k - gn\right), \tag{1.98}$$

where the half-space summation is only half of the summation over the whole $\vec{k}$-space since all of the arguments in the summation are symmetric under inversion. If this Hamiltonian is an ideal Bose condensate of the non-interacting quasiparticles, does it mean that there are no particles within the non-zero momentum state at zero temperature? No, because it does not have any excitation over the quasiparticle ground state, but it has excitations over the zero momentum single particle ground state. It means that the condensate has non-zero momentum atoms even at zero temperature. The interactions among the particles can excite the zero-momentum particles into the higher momentum state with the collision processes $\vec{0} + \vec{0} \rightarrow \vec{k} + -\vec{k}$.

Let us now revisit the calculation for the depletion of the condensate at zero temperature [8]. Depletion means the number of particles in the excited states of the single particle Hamiltonian. In this case, they are $\vec{k} \neq 0$ momentum states. The total number of particles in the $\vec{k} \neq 0$ states can be found by summing the expected value of the occupation operators overall $\vec{k} \neq 0$ states in the quasiparticle picture ground state $|GS\rangle$:

$$N_{ex} = \sum_{\vec{k}\neq 0} \left\langle GS \left| a^\dagger_k a_k \right| GS \right\rangle \quad \text{where} \quad b_k |GS\rangle = 0. \tag{1.99}$$

$$\begin{aligned} N_{ex} &= \sum_{\vec{k}\neq 0} \langle GS| \left(u_k b^\dagger_k - v_k b_{-k}\right) \left(u_k b_k - v_k b^\dagger_{-k}\right) |GS\rangle \\ &= {\sum_{\vec{k}}}' \left\langle GS \left| \left(u^2_k b^\dagger_k b_k - u_k v_k \left(b^\dagger_k b^\dagger_{-k} + b_k b_{-k}\right) + v^2_k b_- b^\dagger_{-k}\right) \right| GS \right\rangle \\ &= {\sum_{\vec{k}}}' \left\langle GS \left| v^2_k \right| GS \right\rangle = \sum_{\vec{k}} v^2_k \end{aligned} \tag{1.100}$$

since $\left\langle GS \left| b_k^\dagger b_{-k}^\dagger \right| GS \right\rangle = 0$ and $b_k b_k^\dagger = b_k^\dagger b_k + 1$.

$$\begin{aligned} N_{ex} &= \sum_{\vec{k}}{}' v_k^2 = \sum_{\vec{k}} \frac{1}{2}\left(-1 + \frac{\epsilon_k + gn}{E_k}\right) \\ &= \frac{V}{(2\pi)^3}\int d^3\vec{k}\frac{1}{2}\left(-1 + \frac{\epsilon_k + gn}{E_k}\right) \\ &= \frac{V}{(2\pi)^3}\frac{1}{2}4\pi\int dk k^2\left(-1 + \frac{\epsilon_k + gn}{\sqrt{\epsilon_k\left(\epsilon_k + 2gn\right)}}\right), \end{aligned} \tag{1.101}$$

where the summation is converted into the integral by the unit cell of volume $\left(\frac{2\pi}{L}\right)^3 = \frac{(2\pi)^3}{V}$ in the 3-dimensional $\vec{k}$-space. Make the substitution of the variable $\epsilon_k = gnx^2$:

$$N_{ex} = \frac{V}{(2\pi)^2}\left(\frac{2mgn}{\hbar^2}\right)^{3/2}\int_0^\infty dx x^2\left[-1 + \frac{x^2+1}{\sqrt{x^2\left(x^2+2\right)}}\right], \tag{1.102}$$

where the last integral is equal to $\sqrt{2}/3$. Rewrite $g = \frac{4\pi a\hbar^2}{m}$, and define excited particle density $n_{ex} = \frac{N_{ex}}{V}$ [8]:

$$\frac{n_{ex}}{n} = \frac{8}{3\sqrt{\pi}}\left(na^3\right)^{1/2}. \tag{1.103}$$

The depletion rate is proportional to $\sqrt{na^3}$. To have a consistent theory, the excited atom should be much less than the condensate atoms, i.e. $na^3 \ll 1$ inequality should be satisfied. It also means that the average interparticle spacing should be much smaller than the s-wave scattering length of the atoms. To satisfy this criterion is important to rely on the Bogoliubov approach.

Another interesting question is about the effect of the quantum fluctuations out of or into the macroscopic condensate on the ground state energy. If the single particle excited states are also occupied at the ground state of the interacting condensate even at the zero temperature, the difference in ground state energy of the many-body state with respect to the Hartree-Fock approximation draws attention. At zero temperature, there is no quasiparticle excitation, and the ground state energy is calculated by [8]:

$$\begin{aligned} E_0 &= \frac{gN^2}{2V} + \frac{1}{2}\sum_{\vec{k}}\left(E_k - \epsilon_k - gn\right) \\ &= \frac{gN^2}{2V} + \frac{1}{2}\sum_{\vec{k}}\left(\sqrt{\epsilon_k(\epsilon_k + 2gn)} - \epsilon_k - gn\right), \end{aligned} \tag{1.104}$$

where the first term is the mean-field energy and the second term is the Lee-Huang-Yang energy correction due to the quantum fluctuations out of and into the macro-

scopic part of the condensate. However, LHY energy summation linearly diverges for high momentum $\vec{k}$ [8]:

$$\begin{aligned}
&\lim_{k\to\infty}\left[\epsilon_k\sqrt{1+2\frac{gn}{\epsilon_k}}-\epsilon_k-gn\right]\\
&\simeq\lim_{k\to\infty}\left[\epsilon_k\left(1+\frac{gn}{\epsilon_k}-\frac{1}{8}\frac{(gn)^2}{(\epsilon_k)^2}\right)-\epsilon_k-gn\right]\\
&=\lim_{k\to\infty}-\frac{1}{8}\frac{(gn)^2}{\epsilon_k}
\end{aligned}\tag{1.105}$$

since $-\int\frac{d^3\vec{k}}{k^2}=-4\pi\int\frac{dkk^2}{k^2}\propto -k$. The reason behind this divergence is the incorrect treatment of the interacting atoms. The s-wave scattering theory models the collisions properly at sufficiently low $\vec{k}$. However, the second-order corrections to the scattering length should also be considered for high k (See [8]):

$$g\approx g_0+\frac{g_0^2}{V}\sum_{\vec{k}}\frac{1}{2\epsilon_k}.\tag{1.106}$$

Place the second-order correction for the coupling constant g in the MF energy term, the zero-point energy E_0 becomes:

$$\begin{aligned}
E_0&=\frac{N^2}{2V}\left(g+\frac{g^2}{V}\sum_{\vec{k}}\frac{1}{2\epsilon_k}\right)+\frac{1}{2}\sum_{\vec{k}}\left(E_k-\epsilon_k-gn\right)\\
&=\frac{gN^2}{2V}+\frac{1}{2}\sum_{\vec{k}}\left[E_k-\epsilon_k-gn+\frac{(gn)^2}{2\epsilon_k}\right].
\end{aligned}\tag{1.107}$$

Define the MF and LHY energy densities $\epsilon_{MF}\equiv\frac{E_{MF}}{V}$ and $\epsilon_{LHY}\equiv\frac{E_{LHY}}{V}$:

$$\epsilon_{MF}=\frac{gn^2}{2}\tag{1.108}$$

$$\epsilon_{LHY}=\frac{1}{2V}\sum_{\vec{k}}\left[E_k-\epsilon_k-gn+\frac{(gn)^2}{2\epsilon_k}\right],\tag{1.109}$$

$$\begin{aligned}
\epsilon_{LHY}&=\frac{1}{2V}\sum_{\vec{k}}\left[E_k-\epsilon_k-gn+\frac{(gn)^2}{2\epsilon_k}\right]\\
&\approx\frac{1}{2(2\pi)^3}\int d^3\vec{k}\left[E_k-\epsilon_k-gn+\frac{(gn)^2}{2\epsilon_k}\right]\\
&=\frac{4\pi}{2(2\pi)^3}\int dk\cdot k^2\left[\sqrt{\epsilon_k\left(\epsilon_k+2gn\right)}-\epsilon_k-gn+\frac{(gn)^2}{2\epsilon_k}\right].
\end{aligned}\tag{1.110}$$

Make the substitution $\epsilon_k=gnx^2$:

$$\epsilon_{LHY}=\frac{4\pi}{2(2\pi)^3}\left(\frac{2mgn}{\hbar^2}\right)^{3/2}gn\int_0^\infty dx\cdot x^2\left[\sqrt{x^2\left(x^2+2\right)}-x^2-1+\frac{1}{2x^2}\right].\tag{1.111}$$

To find the integral I in the last part, consider the limit:

$$\begin{aligned} I &= \lim_{l\to\infty} \int_0^l dx x^2 \left[x\sqrt{x^2+2} - x^2 - 1 + \frac{1}{2x^2} \right] \\ &= \lim_{l\to\infty} \int_0^l dx \left[x^3\sqrt{x^2+2} - x^4 - x^2 + \frac{1}{2} \right]. \end{aligned} \tag{1.112}$$

Make the substitution $u^2 = x^2 + 2$:

$$I = \lim_{l\to\infty} \left(l^3 + \frac{3l}{2} - l^3 - 2l + \frac{l}{2} + \frac{8\sqrt{2}}{15} \right) \tag{1.113}$$

$$= \frac{8\sqrt{2}}{15}. \tag{1.114}$$

Then, the LHY energy density becomes [8]:

$$\frac{E_{LHY}}{V} = \frac{8\sqrt{2}}{15} \frac{4\pi}{2(2\pi)^3} \left(\frac{2mgn}{\hbar^2} \right)^{3/2} gn \tag{1.115}$$

$$= \frac{gn^2}{2} \left[\frac{128}{15\sqrt{a}} \left(na^3 \right)^{1/2} \right]. \tag{1.116}$$

The total zero-point energy is:

$$\frac{E_0}{V} = \frac{gn^2}{2} \left[1 + \frac{128}{15\sqrt{\pi}} \left(na^3 \right)^{1/2} \right]. \tag{1.117}$$

Since $\sqrt{na_3} \ll 1$, the LHY correction is small in the weakly interacting regime $\sqrt{na^3}$, therefore mostly negligible. It does not cause any qualitatively important change in the condensate statics or dynamics, but only small quantitative corrections to the MF theory. However, this deviation is experimentally observed by exploiting the dependence of the pressure of the condensate on the chemical potential and the scattering length [14]. Consider the chemical potential $\mu = \partial E_0/\partial N$ with LHY correction:

$$\mu = gn \left[1 + \frac{32}{3\sqrt{\pi}} \left(na^3 \right)^{1/2} \right]. \tag{1.118}$$

The pressure of the condensate $P = \frac{\partial E_0}{\partial V}$ can be written as:

$$P(\mu, a) = \frac{\hbar^2}{ma^5} h(\nu), \tag{1.119}$$

where $\nu \equiv \mu a^3/g = \mu m a^2/\left(4\pi\hbar^2\right)$ and $h(\nu) = 2\pi\nu^2 \left(1 - \frac{128}{15\sqrt{\pi}}\sqrt{\nu} \right)$.

1.2 Two-Component Mixture Bose Condensates

1.2.1 Gross-Pitaevskii Mean-Field Theory of Bose Mixture

Consider a two-component Bose mixture, consisting of the atoms within the different hyperfine states of the same species of mass m. The condensate is assumed to be in the weakly interacting regime $na^3 \ll 1$ for any scattering length among the components. The interactions among the particles are modeled by the contact of the two hyperfine states. Hence, the coupling constants for the intracomponent interactions are g_{11} and g_{22}, and intercomponent interaction is g_{12}. The single particle Hamiltonian $\hat{H}_0$ consists of the kinetic and external potential energy of the mixture components [8]:

$$\hat{H}_0 = \sum_{i=1}^{2} \hat{h}_{0,i}, \tag{1.120}$$

where

$$\hat{h}_{0,i} = -\frac{\hbar^2}{2m}\hat{\nabla}_i^2 + \hat{V}_{\text{ext}}\left(\vec{r}_i\right). \tag{1.121}$$

The interaction part of the Hamiltonian consists of three fundamental contributions: intracomponent interactions for the hyperfine states 1 and 2, and the intercomponent interactions among the states. The total interaction Hamiltonian can be written in the second quantization formalism using the position field creation and annihilation operators [11]:

$$\begin{aligned}
\hat{H}_{\text{int}} &= \frac{g_{11}}{2}\int d^3\vec{r}_1 \hat{\psi}_1^\dagger\left(\vec{r}_1\right)\hat{\psi}_1^\dagger\left(\vec{r}_1\right)\hat{\psi}_1\left(\vec{r}_1\right)\hat{\psi}_1\left(\vec{r}_1\right) \\
&+ \frac{g_{22}}{2}\int d^3\vec{r}_2 \hat{\psi}_2^\dagger\left(\vec{r}_2\right)\hat{\psi}_2^\dagger\left(\vec{r}_2\right)\hat{\psi}_2\left(\vec{r}_2\right)\hat{\psi}_2\left(\vec{r}_2\right) \\
&+ g_{12}\int d^3\vec{r}\hat{\psi}_1^\dagger(\vec{r})\hat{\psi}_2^\dagger(\vec{r})\hat{\psi}_2(\vec{r})\hat{\psi}_1(\vec{r}) \\
&= \sum_{i,j=1}^{2}\frac{g_{ij}}{2}\int d^3\vec{r}\hat{\psi}_i^\dagger(\vec{r})\hat{\psi}_j^\dagger(\vec{r})\psi_j(\vec{r})\psi_i(\vec{r}),
\end{aligned} \tag{1.122}$$

where the coefficients of coupling constant for intracomponent is half of the intercomponent interactions because there is no overcounting among the different hyperfine states. The summation in the last line sums over 4 possible pairs $i, j = 1, 2$, with

$g_{21} = g_{12}$. The total Hamiltonian is:

$$\begin{aligned}\hat{H} = &\sum_{i=1,2} \int d^3\vec{r}\hat{\psi}_i^\dagger(\vec{r})\hat{h}_{0,i}\psi_i(\vec{r}) \\ &+ \sum_{i,j=1,2} \frac{g_{ij}}{2} \int d^3\vec{r}\hat{\psi}_i^\dagger(\vec{r})\hat{\psi}_j^\dagger(\vec{r})\hat{\psi}_j(\vec{r})\hat{\psi}_i(\vec{r}).\end{aligned} \tag{1.123}$$

The equations of motions can be calculated for both components $\hat{\psi}_i$ by Heisenberg equations of motion:

$$-i\hbar\frac{\partial\hat{\psi}_i}{\partial t} = \left[\hat{H}, \hat{\psi}_i\right], \tag{1.124}$$

where $\hat{\psi}_i$ and $\hat{\psi}_j$ obey the following commutation rules:

$$\begin{aligned}\left[\hat{\psi}_i\left(\vec{r}_1\right), \hat{\psi}_j\left(\vec{r}_2\right)\right] &= \left[\hat{\psi}_i^\dagger\left(\vec{r}_1\right), \hat{\psi}_j^\dagger\left(\vec{r}_2\right)\right] = 0, \\ \left[\hat{\psi}_i\left(\vec{r}_1\right), \hat{\psi}_j^\dagger\left(\vec{r}_2\right)\right] &= \delta_{ij}\delta\left(\vec{r}_1 - \vec{r}_2\right).\end{aligned} \tag{1.125}$$

Follow the similar steps as in the single component BEC and obtain the coupled equations of motion for the operators $\hat{\psi}_1$ and $\hat{\psi}_2$:

$$\begin{aligned}i\hbar\frac{\partial\hat{\psi}_1}{\partial t} &= -\frac{\hbar^2}{2m}\nabla^2\hat{\psi}_1 + V_{\text{ext}}\left(\vec{r}\right)\hat{\psi}_1 + g_{11}\hat{\psi}_1^\dagger\hat{\psi}_1\hat{\psi}_1 + g_{22}\hat{\psi}_2^\dagger\hat{\psi}_2\hat{\psi}_1, \\ i\hbar\frac{\partial\hat{\psi}_2}{\partial t} &= -\frac{\hbar^2}{2m}\nabla^2\hat{\psi}_2 + V_{\text{ext}}\left(\vec{r}\right)\hat{\psi}_2 + g_{22}\hat{\psi}_2^\dagger\hat{\psi}_2\hat{\psi}_2 + g_{12}\hat{\psi}_1^\dagger\hat{\psi}_1\hat{\psi}_2.\end{aligned} \tag{1.126}$$

The Gross-Pitaevskii equations for both components can be obtained by replacing the field operators with the classical fields $\hat{\psi}_i \simeq \Psi_i$ [7, 8]. The time-independent GP equations can be obtained by $\Psi_i(\vec{r}, t) = \psi_i(\vec{r})e^{-i\mu t/\hbar}$:

$$\begin{aligned}\mu_1\psi_1(\vec{r}) &= -\frac{\hbar^2}{2m}\nabla^2\psi_1(\vec{r}) + V_{\text{ext}}\left(\vec{r}\right)\psi_1(\vec{r}) + g_{11}\left|\psi_1\right|^2\psi_1 + g_{12}\left|\psi_2\right|^2\psi_1, \\ \mu_2\psi_2(\vec{r}) &= -\frac{\hbar^2}{2m}\nabla^2\psi_2(\vec{r}) + V_{\text{ext}}\left(\vec{r}\right)\psi_2(\vec{r}) + g_{22}\left|\psi_2\right|^2\psi_2 + g_{12}\left|\psi_1\right|^2\psi_2.\end{aligned} \tag{1.127}$$

These are coupled equations of motion in the sense that neither can be solved independently from the other due to the interactions among the different components. This GP approach to the Bose mixture problem can successfully predict and explain the interesting list of phenomena, including the miscibility and immiscibility of the components [7], vortices and vortex lattices for various ratios of $\frac{g_{12}}{\sqrt{g_{11}g_{22}}}$ [15, 16]. For instance, consider the homogenous miscible Bose mixture, consisting of $N = N_1 + N_2$ particles. Both components expand to the same volume V. The MF energy of this

miscible Bose mixture can be calculated by replacing the field operators by $\psi_i \approx \sqrt{N_i}$ and ignoring the kinetic and external potential energy [7]:

$$E_{MF,m} = \frac{1}{2} g_{11} \frac{N_1^2}{V} + \frac{1}{2} g_{22} \frac{N_2^2}{V} + g_{12} \frac{N_1 N_2}{V}. \tag{1.128}$$

We now consider the GP MF energy of the homogeneous immiscible Bose mixture. Assume the components are confined into the volumes V_1 and V_2, where $V_1 + V_2 = V$. Here the interaction energy only consists of intracomponent interactions, ignoring the domain wall between the components [7]:

$$E_{MF,i} = \frac{1}{2} g_{11} \frac{N_1^2}{V_1} + \frac{1}{2} g_{22} \frac{N_2^2}{V_2}. \tag{1.129}$$

Minimize the energy of the immiscible mixture to find the volume ratio of the components:

$$\begin{aligned} \frac{\partial E_{MF,i}}{\partial V_1} &= \frac{\partial}{\partial V_1} \left[\frac{1}{2} \left(g_{11} \frac{N_1^2}{V_1} + g_{22} \frac{N_2^2}{V - V_1} \right) \right] \\ &= \frac{1}{2} \left[-g_{11} \frac{N_1^2}{V_1^2} + g_{22} \frac{N_2^2}{(V - V_1)^2} \right] = 0. \end{aligned} \tag{1.130}$$

Then, $\frac{V_1^2}{V_2^2} = \frac{g_{11} N_1^2}{g_{22} N_2^2}$, and ratio becomes:

$$V_2 = V_1 \sqrt{\frac{g_{22}}{g_{11}}} \frac{N_2}{N_1}. \tag{1.131}$$

Since $V_1 + V_2 = V$, the volumes become:

$$V_1 = \frac{V}{1 + \sqrt{\frac{g_{22}}{g_{11}}} \frac{N_2}{N_1}}, V_2 = \frac{V}{1 + \sqrt{\frac{g_{11}}{g_{22}}} \frac{N_1}{N_2}}. \tag{1.132}$$

The total MF energy of the immiscible mixture becomes [7]:

$$E_{MF,i} = \frac{1}{2} g_{11} \frac{N_1^2}{V} + \frac{1}{2} g_{22} \frac{N_2^2}{V} + \sqrt{g_{11} g_{22}} N_1 N_2. \tag{1.133}$$

Compare the two MF energies (1.128) and (1.133) for uniform miscible and immiscible mixtures. The criteria for miscibility-immiscibility depends on the ratio $\frac{g_{12}}{\sqrt{g_{11} g_{22}}}$ [7]. If the intercomponent interaction is dominant, i.e. $g_{12} > \sqrt{g_{11} g_{22}}$, the energy of the miscible mixture is greater, hence, the ground state is the immiscible mixture of the components, i.e. the phases are separated. Certainly, this condition on the miscibility of the mixture requires a modification when external trapping is introduced. However, this straightforward analysis, relying on the MF approach, is still powerful enough to successfully estimate the experimental results.

Let us also briefly discuss the mechanical stability of the miscible Bose mixture on the MF level. If all of the interaction couplings are repulsive, the mixture condensate can be trapped by external confinement, similar to the discussion for the repulsive single component BEC. If all of the interactions are attractive, the mixture can only have a metastable local minimum in the existence of external trapping, similar to the analysis for the single component attractive condensate. If both of the intracomponent interactions are attractive and the intercomponent interaction is repulsive, the phases are separated and each component also displays density collapse [7]. A more interesting case appears when the intercomponent interactions are negative $g_{12} < 0$ and the intracomponent interactions $g_{ii} > 0$ are repulsive. In this case, the mixture becomes miscible due to the attraction between the two components. But both repulsive intracomponent interactions can dominate the stability behavior and may expand the mixture. To understand the different regimes of the stability, we first calculate the ratio of the component's particle numbers N_1/N_2 that minimizes the total MF energy with respect to N_1 and N_2:

$$\frac{\partial E_{MF}}{\partial N_1} = g_{11}\frac{N_1}{V} + g_{12}\frac{N_2}{V} = 0, \tag{1.134}$$

$$\frac{\partial E_{MF}}{V} = g_{12}\frac{N_2}{V} + g_{22}\frac{N_1}{V} = 0. \tag{1.135}$$

Then, $\frac{g_{11}}{-g_{12}} = \frac{N_2}{N_1} = \frac{-g_{12}}{g_{22}}$. Hence, the MF energy minimization locks the ratio:

$$\frac{N_1}{N_2} = \sqrt{\frac{g_{22}}{g_{11}}}. \tag{1.136}$$

Since $\sqrt{g_{11}}N_1 = \sqrt{g_{22}}N_2$, one can diagonalize the MF energy along this axis:

$$\begin{aligned} E_{MF} &= \frac{1}{2}\left(\sqrt{g_{11}}N_1 - \sqrt{g_{22}}N_2\right)^2 + \sqrt{g_{11}g_{22}}N_1N_2 + g_{12}N_1N_2 \\ &= \left(\sqrt{g_{11}g_{22}} + g_{12}\right)N_1N_2 \\ &= \delta g N_1 N_2, \end{aligned} \tag{1.137}$$

where $\delta g \equiv g_{12} + \sqrt{g_{11}g_{22}}$. If $\delta g = \sqrt{g_{11}g_{22}} - |g_{12}| < 0$, the mixture exhibits a density collapse. If it is positive, the mixture condensate tends to expand. However, there is an interesting regime here. The coefficient of the collapse at the MF level is δg, which is finely tunable by the available Feschbach resonances. Hence, one can engineer the level of attractive MF energy due to the three independent parameters: g_{11}, g_{22}, and g_{12}. Furthermore, thanks to the level of sophistication in the cold atom

experiments, the MF energy can be set to values close to zero in fractions [17, 18]. This facility will be vital for the experimental realization of the stabilization of the collapsing Bose mixture by the beyond Hartree-Fock fluctuations.

1.2.2 Bogoliubov Theory of Bose Mixture

We now consider the beyond GP MF energy for the Bose mixture condensate consisting of the same atomic species in two different hyperfine states of particle numbers N_1 and N_2, with $N = N_1 + N_2$. We again examine the homogeneous condensate. The Hamiltonian of the weakly interacting Bose mixture without external potential becomes:

$$\begin{aligned}\hat{H} = &\sum_{i=1,2} \int d^3\vec{r}\hat{\psi}_i^\dagger(\vec{r}) \left(-\frac{\hbar^2}{2m}\nabla_i^2\right) \hat{\psi}_i(\vec{r}) \\ &+ \sum_{i,j=1,2} \frac{g_{ij}}{2} \int d^3\vec{r}\hat{\psi}_i^\dagger(\vec{r})\hat{\psi}_j^\dagger(\vec{r})\hat{\psi}_j(\vec{r})\hat{\psi}_i(\vec{r}).\end{aligned} \tag{1.138}$$

Similar to the operator transformation in the single component theory (See. Ch.1.1), we rewrite the creation and annihilation operators in position space as the Fourier transforms of their duals in the momentum space. In this case, the transformations are written for both components, separately:

$$\begin{aligned}\hat{\psi}_1(\vec{r}) &= \frac{\sqrt{V}}{(2\pi)^3} \int d^3\vec{k}\hat{a}_{1,\vec{k}} e^{-i\vec{k}\vec{r}} = \frac{1}{\sqrt{V}} \sum_{\vec{k}} \hat{a}_{1,\vec{k}} e^{-i\vec{k}\vec{r}}, \\ \hat{\psi}_2(\vec{r}) &= \frac{\sqrt{V}}{(2\pi)^3} \int d^3\vec{k}\hat{a}_{2,\vec{k}} e^{-i\vec{k}\vec{r}} = \frac{1}{\sqrt{V}} \sum_{\vec{k}} \hat{a}_{2,\vec{k}} e^{-i\vec{k}\vec{r}}.\end{aligned} \tag{1.139}$$

Hence, the Hamiltonian becomes:

$$\begin{aligned}\hat{H} = &\sum_{\vec{k}} \left(\epsilon_{1,k} a_{1,k}^\dagger a_{1k} + \epsilon_{2,k} a_{2,k}^\dagger a_k\right) + \frac{g_{11}}{2V} \sum_{\vec{k},\vec{k'},\vec{q}} \left(a_{1,k+q}^\dagger a_{1,k'-q}^\dagger a_{1,k'} a_{1,k}\right) \\ &+ \frac{g_{22}}{2V} \sum_{\vec{k},\vec{k'},\vec{q}} \left(a_{2,k+q}^\dagger a_{2,k'-q}^\dagger a_{2,k'} a_{2,k}\right) + \frac{g_{12}}{V} \sum_{\vec{k},\vec{k'},\vec{q}} \left(a_{1,k'+q}^\dagger a_{2,k'-q}^\dagger a_{2,k'} a_{1,k}\right),\end{aligned} \tag{1.140}$$

where $\epsilon_{1,k} = \frac{\hbar^2 k^2}{2m_1}, \epsilon_{2,k} = \frac{\hbar^2 k^2}{2m_2}$. Since $m_1 = m_2 = m, \epsilon_k = \epsilon_{1,k} = \epsilon_{2,k}$. Now apply the Bogoliubov approximation and assume for both components: $\frac{N_1 - N_{10}}{N_1} \ll 1$ and $\frac{N_2 - N_{20}}{N_2} \ll 1$, where N_{i0} is the number of particles in $\vec{k} = 0$ momentum state

of the ith component. From now on, we leave the commas in the operator symbol $a_{i,k}$ between the component type and the momentum state, and instead use a_{ik} for simplicity. Approximate the quartic Hamiltonian terms up to the second order in the operators $\hat{a}_{1,0}$ and $\hat{a}_{2,0}$. Also, approximate up to the second order in the operators:

$$\begin{aligned} N_{i0}^2 &\simeq N_i^2 - 2N_i \sum_{\vec{k}}{}' a_{ik}^\dagger a_{ik}, \\ N_{10}N_{20} &\simeq N_1 N_2 - N_1 N_2 \sum_{\vec{k}}{}' \left(a_{1k}^\dagger a_{2k} + a_{2k}^\dagger a_{1k} \right). \end{aligned} \tag{1.141}$$

Then, we obtain [19]:

$$\begin{aligned} \hat{H} = &\sum_{\vec{k}} \epsilon_k \left(a_{1k}^\dagger a_{1k} + a_{2k}^\dagger a_{2k} \right) \\ &+ \frac{g_{11}N_1^2}{2V} + \frac{g_{11}N_1}{2V} \sum_{\vec{k}}{}' \left(2a_{1k}^\dagger a_{1k} + a_{1k}^\dagger a_{1-k}^\dagger + a_{1k}a_{1-k} \right) \\ &+ \frac{g_{22}N_2^2}{2V} + \frac{g_{22}N_2}{2V} \sum_{\vec{k}}{}' \left(2a_{2k}^\dagger a_{2k} + a_{2k}^\dagger a_{2-k}^\dagger + a_{2k}a_{2-k} \right) \\ &+ \frac{g_{12}N_1N_2}{V} + \frac{g_{12}\sqrt{N_1N_2}}{V} \sum_{\vec{k}}{}' \left(a_{1k}^\dagger a_{2k} + a_{2k}^\dagger a_{1k} + a_{1k}^\dagger a_{2-k}^\dagger + a_{1k}a_{2-k} \right). \end{aligned} \tag{1.142}$$

To diagonalize the Hamiltonian, express all the sums on the half of the total $\vec{k}$-space:

$$\begin{aligned} \hat{H} = &\frac{1}{2}g_{11}\frac{N_1^2}{V} + \frac{1}{2}g_{22}\frac{N_2^2}{V} + g_{12}\frac{N_1N_2}{V} \\ &+ \sum_{\vec{k}} \Big\{ \epsilon_k \left(a_{1k}^\dagger a_{1k} + a_{1-k}^\dagger a_{1-k} + a_{2k}^\dagger a_{2k} + a_{2-k}^\dagger a_{2-k} \right) \\ &\quad + g_{11}n_1 \left(a_{1k}^\dagger a_{1k} + a_{1-k}^\dagger a_{1-k} + a_{1k}^\dagger a_{1-k}^\dagger + a_{1k}a_{1-k} \right) \\ &\quad + g_{22}n_2 \left(a_{2k}^\dagger a_{2k} + a_{2-k}^\dagger a_{2-k} + a_{2k}^\dagger a_{2-k}^\dagger + a_{2k}a_{2-k} \right) \\ &\quad + g_{12}\sqrt{n_1n_2} \Big(a_{1k}^\dagger a_{2k} + a_{2k}^\dagger a_{1k} + a_{1k}^\dagger a_{2-k}^\dagger + a_{1k}a_{2-k} \\ &\quad + a_{1-k}^\dagger a_{2-k} + a_{2-k}^\dagger a_{1-k} + a_{1-k}^\dagger a_{2k}^\dagger + a_{1-k}a_{2k} \Big) \Big\}. \end{aligned} \tag{1.143}$$

Then, the total Hamiltonian can be written as the sum of MF energy and the quantum fluctuations:

$$\hat{H} = E_{0,MF} + \sum_{\vec{k}} \hat{H}_k, \tag{1.144}$$

where the ground state mean field energy $E_{0,MF}$ is:

$$E_{0,MF} = \frac{1}{2}g_{11}\frac{N_1^2}{V} + \frac{1}{2}g_{22}\frac{N_2^2}{V} + g_{12}\frac{N_1N_2}{V}, \tag{1.145}$$

and the energy of the Bogoliubov excitations $\sum \hat{H}_k$:

$$\begin{aligned}\hat{H}_k &= (\epsilon_k + g_{11}n_1)\left(a_{1k}^\dagger a_{1k} + a_{1-k}^\dagger a_{1-k}\right) + g_{11}n_1\left(a_{1k}^\dagger a_{1-k}^\dagger + a_{1k}a_{1-k}\right) \\ &+ (\epsilon_k + g_{22}n_2)\left(a_{2k}^\dagger a_{2k} + a_{2-k}^\dagger a_{2-k}\right) + g_{22}n_2\left(a_{2k}^\dagger a_{2-k}^\dagger + a_{2k}a_{2-k}\right) \\ &+ g_{12}\sqrt{n_1 n_2}\Big(a_{1k}^\dagger a_{2k} + a_{2k}^\dagger a_{1k} + a_{1k}^\dagger a_{2-k}^\dagger + a_{1k}a_{2-k} \\ &\qquad + a_{1-k}^\dagger a_{2-k} + a_{2-k}^\dagger a_{1-k} + a_{1-k}^\dagger a_{2k}^\dagger + a_{1-k}a_{2k}\Big).\end{aligned} \tag{1.146}$$

In this Hamiltonian, the time evolution of the operator a_{1k} is coupled not only with $a_{1-k}^\dagger$, but also with a_{2k} and $a_{2-k}^\dagger$. Hence the transformation should now combine $a_{1k}, a_{1-k}^\dagger, a_{2k}, a_{2-k}^\dagger$. Define a row vector of operations:

$$\vec{A}_k^\dagger = \begin{pmatrix} a_{1k}^\dagger & a_{1-k} & a_{2k}^\dagger & a_{2-k} \end{pmatrix}. \tag{1.147}$$

The corresponding column vector $\vec{A}_k$:

$$\vec{A}_k = \begin{pmatrix} a_{1k} \\ a_{1-k}^\dagger \\ a_{2k} \\ a_{2-k}^\dagger \end{pmatrix}, \tag{1.148}$$

where the $\dagger$ operator executes both the conjugate of the operators and the transpose of the vectors and matrices. The ^{T} operator takes only the transpose, without any conjugation on the number and operators.

$$\hat{H}_k \;=\; \vec{A}_k^\dagger \underline{\underline{H}} \vec{A}_k - (\epsilon_k + g_{11}n_1) - (\epsilon_k + g_{22}n_2), \tag{1.149}$$

where

$$\underline{\underline{H}} = \begin{pmatrix} \epsilon_k + g_{11}n_1 & g_{11}n_1 & g_{12}\sqrt{n_1 n_2} & g_{12}\sqrt{n_1 n_2} \\ g_{11}n_1 & \epsilon_k + g_{11}n_1 & g_{12}\sqrt{n_1 n_2} & g_{12}\sqrt{n_1 n_2} \\ g_{12}\sqrt{n_1 n_2} & g_{12}\sqrt{n_1 n_2} & \epsilon_k + g_{22}n_2 & g_{22}n_2 \\ g_{12}\sqrt{n_1 n_2} & g_{12}\sqrt{n_1 n_2} & g_{22}n_2 & \epsilon_k + g_{22}n_2 \end{pmatrix}. \tag{1.150}$$

Here $a_{ik}^\dagger a_{ik} = a_{ik}a_{ik}^\dagger - 1$ gives the constants at the last. The total Hamiltonian is:

$$\hat{H} = E_{0,MF} - \sum_{\vec{k}} \left[(\epsilon_k + g_{11}n_1) + (\epsilon_k + g_{22}n_2) + \vec{A}_k^\dagger \underline{\underline{H}} \vec{A}_k\right], \tag{1.151}$$

where $\underline{\underline{H}}$ is the 4-by-4 matrice in (1.150).

The Bose commutation rules for the operators a_{1k} and a_{2k} in the form of the vectors become:

$$\begin{aligned} &\vec{A}_k\vec{A}_k^{\dagger} - \left(\vec{A}_k^{\dagger}\right)^T\left(\vec{A}_k\right)^T = \underline{\underline{\eta}} \\ &\underline{\underline{\eta}} \equiv \begin{pmatrix} +1 & 0 & 0 & 0 \\ 0 & -1 & 0 & 0 \\ 0 & 0 & +1 & 0 \\ 0 & 0 & 0 & -1 \end{pmatrix}, \text{ and } \underline{\underline{\eta}}^2 = \underline{\underline{1}}. \end{aligned} \tag{1.152}$$

Now assume Bogoliubov transformation in the form [19]:

$$\vec{B}_k = \underline{\underline{T}}\vec{A}_k, \quad \vec{B}_k = \begin{pmatrix} b_{1k} \\ b_{1-k}^{\dagger} \\ b_{2k} \\ b_{2-k}^{\dagger} \end{pmatrix}, \tag{1.153}$$

where T is 4-by-4 matrix, and elements $T_{ij} \in \mathcal{R}$. We impose on the operators $b_{i,k}$ to obey the Bose commutation rules:

$$\vec{B}_k\vec{B}_k^{\dagger} - \left(\vec{B}_k^{\dagger}\right)^T\left(\vec{B}_k\right)^T = \eta \tag{1.154}$$

$$\underline{\underline{T}}\vec{A}_k\vec{A}_k^{\dagger}T^{\dagger} - \left(\underline{\underline{T}}^{\dagger}\right)^T\left(\vec{A}_k^{\dagger}\right)^T\left(\vec{A}_k\right)^T\underline{\underline{T}}^T = \eta \tag{1.155}$$

since $T_{ij} \in \mathbb{R}, \underline{\underline{T}}^{\dagger} = \underline{\underline{T}}^T$. Then, the transformation matrix satisfies:

$$T\left(\vec{A}_k\vec{A}_k^{\dagger} - \left(\vec{A}_k^{\dagger}\right)^T\left(\vec{A}_k\right)^T\right)T^T = \eta. \tag{1.156}$$

This implies:

$$T\eta T^T = \eta \tag{1.157}$$

$$T^{-1}\eta = \eta T^T \tag{1.158}$$

$$\left(T^{-1}\right)^T = \eta T \eta. \tag{1.159}$$

This set of equations for the transformation matrix reduces to the $u^2 - v^2 = 1$ for the single component Bose gas with $T = \begin{pmatrix} u & v \\ v & u \end{pmatrix}$.

If $\vec{B}_k = T\vec{A}_k$, then

$$\begin{aligned} \vec{A}_k &= T^{-1}\vec{B}_k \\ \vec{A}_k^{\dagger} &= \vec{B}_k^{\dagger}\left(T^{-1}\right)^T. \end{aligned} \tag{1.160}$$

Hence, the summation in the Hamiltonian can be written as:

$$\begin{aligned}\vec{A}_k^\dagger H_0 \vec{A}_l &= \vec{B}_k^\dagger \left(T^{-1}\right)^T H_0 T^{-1} \vec{B}_k \\ &= \vec{B}_k^\dagger D \vec{B}_k,\end{aligned} \tag{1.161}$$

where $D = \left(T^{-1}\right)^T H_0 T^{-1}$ is expected to be a diagonal matrix in the form:

$$D \equiv \begin{pmatrix} E_1 & 0 & 0 & 0 \\ 0 & E_1 & 0 & 0 \\ 0 & 0 & E_2 & 0 \\ 0 & 0 & 0 & E_2 \end{pmatrix}. \tag{1.162}$$

The diagonal elements are degenerate because the dispersion of the corresponding Bogoliubov mode is only the symmetric one with respect to the origin of the $\vec{k}-$space. To find the eigenvalue equation whose eigenvectors are the vectors of the transformation matrix, and whose eigenvalues are the dispersion of the Bogoliubov modes, use the properties of the transformation matrix [19]:

$$DT = \left(T^{-1}\right)^T H_0 \tag{1.163}$$

$$= \eta T \eta H_0, \tag{1.164}$$

where $(T^{-1})^T = \eta T \eta$ is used. Then, the eigenvalue equation becomes:

$$H_0 \eta T^T = \eta T^T D, \tag{1.165}$$

where

$$D\eta = \begin{pmatrix} E_1 & 0 & 0 & 0 \\ 0 & -E_1 & 0 & 0 \\ 0 & 0 & E_2 & 0 \\ 0 & 0 & 0 & -E_2 \end{pmatrix}, \tag{1.166}$$

and

$$\eta H_0 = \begin{pmatrix} \epsilon_k + g_{11}n_1 & -g_{11}n_1 & g_{12}\sqrt{n_1 n_2} & -g_{12}\sqrt{n_1 n_2} \\ g_{11}n_1 & -\epsilon_k - g_{11}n_1 & g_{12}\sqrt{n_1 n_2} & -g_{12}\sqrt{n_1 n_2} \\ g_{12}\sqrt{n_1 n_2} & -g_{12}\sqrt{n_1 n_2} & \epsilon_k + g_{22}n_2 & -g_{22}n_2 \\ g_{12}\sqrt{n_1 n_2} & -g_{12}\sqrt{n_1 n_2} & g_{22}n_2 & -\epsilon_k - g_{22}n_2 \end{pmatrix} \tag{1.167}$$

$$= \begin{pmatrix} C_1 & -2B_1 & d & -d \\ 2B_1 & -C_1 & d & -d \\ d & -d & C_2 & -2B_2 \\ d & -d & 2B_2 & -C_2 \end{pmatrix}, \tag{1.168}$$

where $C_i = \epsilon_k + g_{ii} n_i$ $B_i = g_{ii}/2$, and $d = g_{12}\sqrt{n_1 n_2}$. The transformation matrix T is:

$$T = \begin{pmatrix} u_1 & v_1 & \mu_1 & \nu_1 \\ v_1 & u_1 & \nu_1 & \mu_1 \\ u_2 & v_2 & \mu_2 & \nu_2 \\ v_2 & u_2 & \nu_2 & \mu_2 \end{pmatrix}. \tag{1.169}$$

The eigenvalue equation is:

$$\begin{pmatrix} C_1 & -2B_1 & d & -d \\ 2B_1 & -C_1 & d & -d \\ d & -d & C_2 & -2B_2 \\ d & -d & 2B_2 & -C_2 \end{pmatrix} \begin{pmatrix} u_1 \\ v_1 \\ \mu_1 \\ \nu_1 \end{pmatrix} = E_1 \begin{pmatrix} u_1 \\ v_1 \\ \mu_1 \\ \nu_1 \end{pmatrix}. \tag{1.170}$$

The first two rows of operations yield:

$$\begin{aligned} C_1 u_1 - 2B_1 v_1 + d\,(\mu_1 - \nu_1) &= E u_1, \\ 2B_1 u_1 - C_1 v_1 + d\,(\mu_1 - \nu_1) &= E v_1. \end{aligned} \tag{1.171}$$

These equations can be rearranged as:

$$\begin{aligned} (C_1 + 2B_1)\,(u_1 - v_1) + 2d\,(p_1 - v_1) &= E\,(u_1 + v_1)\,, \\ (C_1 - 2B_1)\,(u_1 + v_1) &= E\,(u_1 - v_1)\,. \end{aligned} \tag{1.172}$$

Remember that $\epsilon_1 = \sqrt{\epsilon_k\,(\epsilon_k + 2g_{11}n_1)} = \sqrt{(C_1 - 2B_1)\,(C_1 + 2B_1)}$. Then, $C_1 + 2B_1 = \frac{\epsilon_1^2}{\epsilon_k}$, $C_1 - 2B_1 = \epsilon_k$. Hence, one can rewrite the above set of equations in terms of the dispersions:

$$\begin{aligned} \frac{\epsilon_1^2}{\epsilon_k}\,(u_1 - v_1) + 2d\,(\mu_1 - \nu_1) &= E\,(u_1 + v_1)\,, \\ \epsilon_k\,(u_1 + v_1) &= E\,(u_1 - v_1)\,. \end{aligned} \tag{1.173}$$

Similarly, for the last two row operations:

$$\begin{aligned} \frac{\epsilon_2^2}{\epsilon_k}\,(\mu_1 - \nu_1) + 2d\,(u_1 - v_1) &= E\,(\mu_1 + \nu_1)\,, \\ \epsilon_k\,(\mu_1 + \nu_1) &= E\,(\mu_1 - \nu_1)\,. \end{aligned} \tag{1.174}$$

Hence, the ratio of the quasiparticle coefficients is:

$$\frac{u_1}{v_1} = \frac{E + \epsilon_k}{E - \epsilon_k} = \frac{\mu_1}{\nu_1}. \tag{1.175}$$

Replacing u_1 in terms of v_1, and μ_1 in terms of ν_1 gives:

$$v_1 \frac{2\epsilon_k \left(\epsilon_1^2 - E^2\right)}{E - \epsilon_k} + \frac{4d\epsilon_k^2}{E - \epsilon_k} \nu_1 = 0 \tag{1.176}$$

and

$$\nu_1 \frac{2\epsilon_k \left(\epsilon_2^2 - E^2\right)}{E - \epsilon_k} + \frac{4d\epsilon_k^2}{E - \epsilon_k} v_1 = 0. \tag{1.177}$$

Equating the ratios $\frac{v_1}{\nu_1}$:

$$E^4 - \left(\epsilon_1^2 + \epsilon_2^2\right) E^2 + \epsilon_1^2 \epsilon_2^2 - 4d^2 \epsilon_k^2 = 0. \tag{1.178}$$

The solution to the above equation gives the energy dispersion of two Bogoliubov modes $E_\pm$ [19]:

$$E_\pm^2 = \frac{1}{2} \left\{ \epsilon_1^2 + \epsilon_2^2 \pm \sqrt{\left(\epsilon_1^2 - \epsilon_2^2\right)^2 + 16\epsilon_k^2 g_{12}^2 n_1 n_2} \right\}, \tag{1.179}$$

where $\epsilon_i = \sqrt{\epsilon_k(\epsilon_k + 2g_{ii}n_i)}$. To find the transformation coefficients, using $T^{-1} = \eta T^T \eta$ and $TT^{-1} = 1$ gives:

$$\left(u_1^2 - v_1^2\right) + \left(\mu_1^2 - \nu_1^2\right) = 1. \tag{1.180}$$

Use this equation and the ratio expressions for $\frac{u_1}{v_1}$, $\frac{\nu_1}{v_1}$, and $\frac{\nu_1}{\mu_1}$ found above and obtain:

$$v_1^2 = \frac{\epsilon_k d^2 \left(E - \epsilon_k\right)^2}{E \left[4\epsilon_k^2 d^2 + \left(E^2 - \epsilon_1^2\right)^2\right]}. \tag{1.181}$$

Note that $4\epsilon_k^2 d^2$ can be rewritten as $\left(E^2 - \epsilon_1^2\right)\left(E^2 - \epsilon_2^2\right)$. Hence, the coefficients become [19]:

$$v_1^2 = \frac{\epsilon_k \left(E - \epsilon_k\right)^2 \left(E^2 - \epsilon_2^2\right)}{4\epsilon_k^2 E \left(2E^2 - \epsilon_1^2 - \epsilon_2^2\right)}, \tag{1.182}$$

$$u_1^2 = \frac{\epsilon_k \left(E + \epsilon_k\right)^2 \left(E^2 - \epsilon_2^2\right)}{4\epsilon_k^2 E \left(2E^2 - \epsilon_1^2 - \epsilon_2^2\right)}, \tag{1.183}$$

$$\nu_1^2 = \frac{\epsilon_k \left(E - \epsilon_k\right)^2 \left(E^2 - \epsilon_1^2\right)}{4\epsilon_k^2 E \left(2E^2 - \epsilon_1^2 - \epsilon_2^2\right)}, \tag{1.184}$$

$$\mu_1^2 = \frac{\epsilon_k \left(E + \epsilon_k\right)^2 \left(E^2 - \epsilon_1^2\right)}{4\epsilon_k^2 E \left(2E^2 - \epsilon_1^2 - \epsilon_2^2\right)}. \tag{1.185}$$

In this approach, the Bogoliubov modes are obtained by solving the eigenvalues of the 4-by-4 matrix. However, there is an obvious inversion symmetry in the eigenvalues

due to the formalism of the problem. We can take advantage of this symmetry to reduce the 4-by-4 matrix to a 2-by-2 matrix. For more general case of, say, spin-f Hamiltonian, the square matrices of size $2(2f+1) \times 2(2f+1)$ can be reduced to $(2f+1) \times (2f+1)$ by using the same method [20]. Consider the transformation [20]

$$\vec{B}_k = \underline{\underline{U}}_k \vec{A}_k + \underline{\underline{V}}_k \vec{A}_{-k}, \tag{1.186}$$

where $\vec{B}_k = \begin{pmatrix} b_{1k} \\ b_{2k} \end{pmatrix}$, $\vec{A}_k = \begin{pmatrix} a_{1k} \\ a_{2k} \end{pmatrix}$, $\vec{A}^*_{-k} = \begin{pmatrix} a^\dagger_{1-k} \\ a^\dagger_{2-k} \end{pmatrix}$. Note that the * operator does not make any transpose operation, but only takes the conjugate of the Hermitian operators. ^{T} operation will only take the transpose of the vector or matrix, whereas † operator executes both the conjugation and transposition. The operators b_{1k} and b_{2k} should obey Bose commutation rules:

$$[b_{ik}, b^\dagger_{jk'}] = \delta_{ij}\delta_{k,k'}, \tag{1.187}$$

$$\vec{B}_k \vec{B}^\dagger_k - \vec{B}^*_k \vec{B}^T_k = I. \tag{1.188}$$

$$\begin{pmatrix} b_{1k} \\ b_{2k} \end{pmatrix} \begin{pmatrix} b^\dagger_{1k} & b^\dagger_{2k} \end{pmatrix} - \begin{pmatrix} b^\dagger_{1k} \\ b^\dagger_{2k} \end{pmatrix} \begin{pmatrix} b_{1k} & b_{2k} \end{pmatrix} = I. \tag{1.189}$$

$$\begin{aligned} &\left(U_k \vec{A}_k + V_k \vec{A}^*_{-k}\right)\left(\vec{A}^\dagger_k U^T_k + \vec{A}^\dagger_{-k} V^T_k\right) \\ &- \left(U_k \vec{A}^*_k i + V_k \vec{A}_{-k}\right)\left(\bar{A}^T_k U^T_k + \vec{A}^T_{-k} V^T_k\right) \\ &= U_k \left(\vec{A}_k \vec{A}^\dagger_k - \vec{A}^*_k \vec{A}^T_k\right) U^T_k + V_k \left(\vec{A}^*_{-k} \vec{A}^\dagger_{-k} - \vec{A}_{-k} \vec{A}^T_{-k}\right) V^T_k \\ &= U_k U^\dagger_k - V_k V^T_k = I = (U_k + V_k)^T (U_k - V_k) \end{aligned} \tag{1.190}$$

since $U^T_k V_k = V^T_k U_k$. Then, the following equations are satisfied for the addition and subtraction of U_k and V_k:

$$\begin{aligned} (U_k - V_k)^{-1} &= (U_k + V_k)^\dagger, \\ U_k - V_k &= \left((U_k + V_k)^T\right)^{-1}. \end{aligned} \tag{1.191}$$

Now consider the time evolution of the operators:

$$\begin{aligned} \partial_t \vec{A}_k &= M_k \vec{A}_k + N_k \vec{A}^*_{-k} \\ \partial_t \vec{A}^*_{-k} &= M_k \vec{A}^*_{-k} + N_k \vec{A}_k, \end{aligned} \tag{1.192}$$

where $\partial_t \equiv i\hbar\frac{\partial}{\partial t}$, and M_k, N_k are 2-by-2 matrices determined from the Hamiltonian of the problem. if $M_k, N_k \in \mathbb{R}$ and symmetric:

$$\begin{aligned}\partial_t\left(\vec{A}_k + \vec{A}^*_{-k}\right) &= (M_k + N_k)\left(\vec{A}_k + \vec{A}^*_{-k}\right),\\ \partial_t\left(\vec{A}_k - \vec{A}^*_{-k}\right) &= (M_k - N_k)\left(\vec{A}_k - \vec{A}^*_{-k}\right).\end{aligned} \tag{1.193}$$

In this form, the summed and subtracted operators become diagonal. Express B_k in term of $\left(\vec{A}_k + \vec{A}^*_{-k}\right)$ and $\left(\vec{A}_k - \vec{A}^*_{-k}\right)$:

$$\vec{B}_k = \frac{1}{2}\left[(U_k + V_k)\left(\vec{A}_k + \vec{A}^*_{-k}\right) + (U_k - V_k)\left(\vec{A}_k - \vec{A}^*_{-k}\right)\right]. \tag{1.194}$$

We expect B_k yield a non-interacting quasiparticle picture with eigenenergies E_k:

$$\partial_t\vec{B}_k = E_k\vec{B}_k = E_k\left(U_k\vec{A}_k + V_k\vec{A}^*_{-k}\right). \tag{1.195}$$

Then, the time evolution of B_k becomes [20]:

$$\partial_t\vec{B}_k = \frac{1}{2}\big[\,(U_k + V_k)\underbrace{\partial_t\left(\vec{A}_k + \vec{A}^*_{-k}\right)}_{(M_k+N_k)\left(\vec{A}_k+\vec{A}^*_{-k}\right)} + (U_k - V_k)\underbrace{\partial_t\left(\vec{A}_k - \vec{A}^*_{-k}\right)}_{(M_k-N_k)\left(\vec{A}_k-\vec{A}^*_{-k}\right)}\,\big]. \tag{1.196}$$

Then,

$$\begin{aligned}\partial_t\vec{B}_k = \frac{1}{2}\Big[&(U_k + V_k)(M_k + N_k)\left(\vec{A}_k + \vec{A}^*_{-k}\right)\\ &+ (U_k - V_k)(M_k - N_k)\left(\vec{A}_k - \vec{A}^*_{-k}\right)\Big].\end{aligned} \tag{1.197}$$

Compare this time evolution equation with (1.195). The following coupled equations are obtained:

$$\begin{aligned}(U_k + V_k)(M_k + N_k) + (U_k - V_k)(M_k - N_k) &= 2E_kU_k,\\ (U_k + V_k)(M_k + N_k) - (U_k - U_k)(M_k - N_k) &= 2E_kV_k.\end{aligned} \tag{1.198}$$

By summing and subtracting two equations, we obtain:

$$\begin{aligned}(U_k + V_k)(M_k + N_k) &= E_k(U_k + V_k),\\ (U_k - V_k)(M_k - N_k) &= E_k(U_k - V_k).\end{aligned} \tag{1.199}$$

Use the inversion and transposition properties of the sum and subtract of U_k and V_k and obtain:

$$(M_k + N_k)(M_k - N_k)(U_k + V_k)^\dagger = (U_k + V_k)^\dagger E_b^2. \tag{1.200}$$

Therefore, $\underline{\underline{G}} = (\underline{\underline{M}} + \underline{\underline{N}})(\underline{\underline{M}} - \underline{\underline{N}})$ gives the eigenvalues E_k^2 [20]. M_k and N_k should be determined from the Hamiltonian [20]:

$$\begin{aligned} H =& \frac{1}{2} g_{11} \frac{N_1^2}{V} + \frac{1}{2} g_{22} \frac{N_2^2}{V} + g_{12} \frac{N_1 N_2}{V} \\ &+ \sum_{\vec{k}}^{>} \Big\{ \epsilon_k \left(a_{1k}^\dagger a_{1k} + a_{1-k}^\dagger a_{1-k} + a_{2k}^\dagger a_{2k} + a_{2-k}^\dagger a_{2-k} \right) \\ &\quad + g_{11} n_1 \left(a_{1k}^\dagger a_{1k} + a_{1-k}^\dagger a_{1-k} + a_{1k}^\dagger a_{1-k}^\dagger + a_{1k} a_{1-k} \right) \\ &\quad + g_{22} a_2 \left(a_{2k}^\dagger a_{2k} + a_{2-k}^\dagger a_{2k} + a_{2k}^\dagger a_{2-k}^\dagger + a_{2k} a_{2-k} \right) \\ &\quad + g_{12} \sqrt{n_1 n_2} \Big(a_{1k}^\dagger a_{2k} + a_{2k}^\dagger a_{1k} + a_{1k}^\dagger a_{2-k}^\dagger + a_{1k} a_{2-k} \\ &\quad + a_{1-k}^\dagger a_{2-k} + a_{2-k}^\dagger a_{1-k} + a_{1-k}^\dagger a_{2k}^\dagger + a_{1-k} a_{2k} \Big) \end{aligned} \tag{1.201}$$

$$\begin{aligned} \partial_t \vec{A}_k = M_k \vec{A}_k + N_k \vec{A}_{-k}^* &= M_k \begin{pmatrix} a_{1k} \\ a_{2k} \end{pmatrix} + N_k \begin{pmatrix} a_{1-k}^\dagger \\ a_{2-k}^\dagger \end{pmatrix} \\ &= i\hbar \frac{\partial}{\partial t} \begin{pmatrix} a_{1k} \\ a_{2k} \end{pmatrix} = \left[\vec{A}_k, \hat{H} \right]. \end{aligned} \tag{1.202}$$

The commutations are calculated as:

$$\begin{aligned} \left[a_{1k}, \hat{H} \right] &= (\epsilon_k + g_{11} n_1)\, a_{1k} + g_{11} n_1 a_{1-k}^\dagger + g_{12} \sqrt{n_1 n_2} \left(a_{2k} + a_{2-k}^\dagger \right) \\ \left[a_{2k}, \hat{H} \right] &= (\epsilon_k + g_{22} n_2)\, a_{2n} + g_{22} n_2 a_{2-k}^\dagger + g_{12} \sqrt{n_1 n_2} \left(a_{1k} + a_{1-k}^\dagger \right). \end{aligned} \tag{1.203}$$

Hence, the time evolutions in the vectorial form can be written as:

$$i\hbar \frac{\partial}{\partial t} \vec{A}_k = \underbrace{\begin{pmatrix} \epsilon_k + g_{11} n_1 & g_{12} \sqrt{n_1 n_2} \\ g_{22} \sqrt{n_1 n_2} & \epsilon_k + g_{22} n_2 \end{pmatrix}}_{M_k} \vec{A}_k + \underbrace{\begin{pmatrix} g_{11} n_1 & g_{12} \sqrt{n_1 n_2} \\ g_{12} \sqrt{n_1 n_2} & g_{22} n_2 \end{pmatrix}}_{N_k} \vec{A}_{-k}^*. \tag{1.204}$$

The matrix $\underline{\underline{G}} = (\underline{\underline{M}} + \underline{\underline{N}})(\underline{\underline{M}} - \underline{\underline{N}})$ is:

$$\begin{aligned} &= \begin{pmatrix} \epsilon_k + 2 g_{11} n_1 & 2 g_{12} \sqrt{n_1 n_2} \\ 2 g_{12} \sqrt{n_1 n_2} & \epsilon_k + 2 g_{22} n_2 \end{pmatrix} \begin{pmatrix} \epsilon_k & 0 \\ 0 & \epsilon_k \end{pmatrix} \\ &= \begin{pmatrix} \epsilon_1^2 & 2 g_{12} \epsilon_k \sqrt{n_1 n_2} \\ 2 g_{12} \epsilon_k \sqrt{n_1 n_2} & \epsilon_2^2 \end{pmatrix}, \end{aligned} \tag{1.205}$$

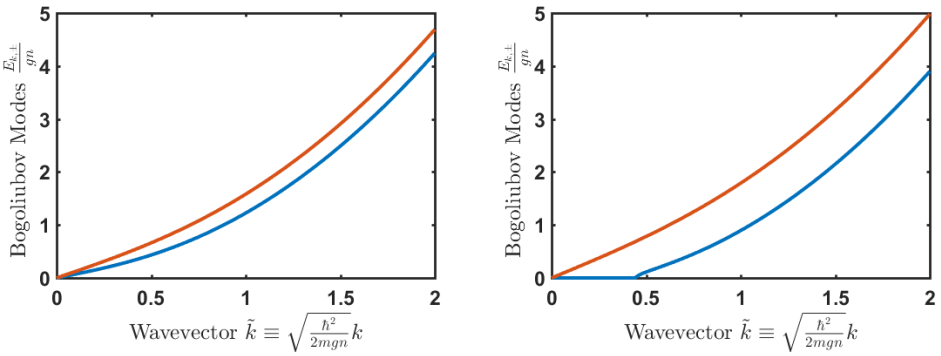

Figure 1.2: Bogoliubov modes $\frac{E_{k,\pm}}{gn}$ vs. $\tilde{k} \equiv \sqrt{\frac{\hbar^2}{2mgn}}k$ for $\frac{g_{12}}{g} = -0.5$ (left panel) and $\frac{g_{12}}{g} = -1.2$ (right panel). As the ratio $\frac{g_{12}}{g}$ increases, two branches move away from each other. For $\frac{g_{12}}{g} = -1.2$, the low wavevectors, or greater wavelengths exhibit imaginary, therefore unstable, modes.

where $\epsilon_i = \sqrt{\epsilon_k(\epsilon_k + 2g_{ii}n_i)}$, $i = 1, 2$ are the dispersion relations of the single component weakly interacting Bose gas. The eigenvalues of $\underline{\underline{G}}$ are E_k^2:

$$\begin{aligned} \left(\epsilon_1^2 - E_k^2\right)\left(\epsilon_2^2 - E_k^2\right) &= 4\epsilon_k^2 g_{12}^2 n_1 n_2, \\ E_k^4 - \left(\epsilon_1^2 + \epsilon_2^2\right)E_k^2 + \epsilon_1^2\epsilon_2^2 - 4\epsilon_k^2 g_{12}^2 n_1 n_2 &= 0. \end{aligned} \tag{1.206}$$

The energy of the Bogoliubov modes for the Bose mixture is:

$$E_{k,\pm}^2 = \frac{1}{2}\left\{\epsilon_1^2 + \epsilon_2^2 \pm \sqrt{\left(\epsilon_1^2 - \epsilon_2^2\right)^2 + 16\epsilon_k^2 g_{12}^2 n_1 n_2}\right\}, \tag{1.207}$$

which is exactly the same result obtained through the calculations on the 4-by-4 matrix. Let us now briefly discuss how these two modes behave for various values of the ratio $\frac{g_{12}}{g}$, where $g_{11} = g_{22} = g$ is chosen for simplicity. $n_1/n_2 = 1$ and $\epsilon_1 = \epsilon_2 = \sqrt{\epsilon_k(\epsilon_k + gn)}$. Then, two Bogoliubov branches become:

$$E_{k,\pm} = \sqrt{\epsilon_k(\epsilon_k + (g \pm g_{12})n}. \tag{1.208}$$

Assume $g > 0$. For $|g_{12}| \leq 1$, all of the modes have real energy, whereas some modes become imaginary, hence unstable when $|g_{12}| > 1$. Furthermore, as g_{12} deviates from 0, the two modes drift apart. For $g_{12} = 0$, both modes are totally coincide. Both of these behaviors are illustrated in Fig. (1.2) for $\frac{g_{12}}{g} = -0.5$ and $\frac{g_{12}}{g} = -1.2$. The

diagonalized Hamiltonian can be written as:

$$\begin{aligned}\hat{H} = \quad & E_{0,MF} - \sum_{\vec{k}}{}^{>} (\epsilon_k + g_{11}n_1) + (\epsilon_k + g_{22}n_2) \\ & + \sum_{\vec{k}}{}^{>} \left[E_+(b_{1k}b_{1k}^\dagger + b_{1-k}^\dagger b_{1-k}) + E_-(b_{2k}b_{2k}^\dagger + b_{2-k}^\dagger b_{2-k}) \right]. \quad (1.209)\end{aligned}$$

Use the commutation relations for the operators b_{ik} to convert the half-space summations to the whole space. Then, the Hamiltonian expression can be written as:

$$\begin{aligned}\hat{H} = E_{0,MF} + \frac{1}{2}\sum_{\vec{k}} & \left[E_+ + E_- - (\epsilon_k + g_{11}n_1) - (\epsilon_k + g_{22}n_2) \right] \\ & + \sum_{\vec{k}} E_+ b_{1k}^\dagger b_{1k} + E_- b_{2k}^\dagger b_{2k}.\end{aligned} \quad (1.210)$$

For the ground state energy of the Bose mixture, there is no quasiparticle excitation: no energy contribution from Bogoliubov modes. Hence the zero point energy with the quantum fluctuations becomes [19]:

$$\begin{aligned}E_0 = & \frac{1}{2}g_{11}\frac{N_1^2}{V} + \frac{1}{2}g_{22}\frac{N_2^2}{V} + g_{12}\frac{N_1 N_2}{V} \\ & + \frac{1}{2}\sum_{\vec{k}} \left[E_+ + E_- - (\epsilon_k + g_{11}n_1) - (\epsilon_k + g_{22}n_2) \right].\end{aligned} \quad (1.211)$$

Similar to the linear divergence in the single component condensate, the second order contribution to the scattering length is required to renormalize the ground state energy. The renormalized coupling coefficients are:

$$g_{ij} \approx g_{ij} + \frac{g_{ij}^2}{V}\sum_{\vec{k}} \frac{1}{2\epsilon_k}. \quad (1.212)$$

The zero-point energy with the renormalization becomes:

$$\begin{aligned}E_0 = E_{0,MF} + \frac{1}{2}\sum_{\vec{k}} & \left[E_+ + E_- - (\epsilon_k + g_{11}n_1) - (\epsilon_k + g_{22}n_2) \right. \quad (1.213) \\ & \left. + \frac{(g_{11}n_1)^2 + (g_{22}n_2)^2 + 2\left(g_{12}\sqrt{n_1 n_2}\right)^2}{2\epsilon_k} \right], \quad (1.214)\end{aligned}$$

where

$$E_\pm = \sqrt{\frac{1}{2}\left(\epsilon_1^2 + \epsilon_2^2 \pm \sqrt{(\epsilon_1^2 - \epsilon_2^2)^2 + 16\epsilon_k^2 g_{12}^2 n_1 n_2} \right)}. \quad (1.215)$$

Remember that MF energy minimization locks the ratio: $\frac{n_1}{n_2} = \sqrt{\frac{g_{22}}{g_{11}}}$. Apply the change of variables $\epsilon_k = \frac{\hbar^2 k^2}{2m} \equiv g_{11} n_1 x^2$. Then, the LHY energy of the Bose mixture becomes:

$$E_{LHY} = \frac{1}{2(2\pi)^3} 4\pi \int_0^\infty dk\, k^2 \Bigg[E_+ + E_- - (\epsilon_k + g_{11} n_1) - (\epsilon_k + g_{22} n_2) + \frac{(g_{11} n_1)^2 + (g_{22} n_2)^2 + 2\left(g_{12}\sqrt{n_1 n_2}\right)^2}{2\epsilon_k} \Bigg]. \tag{1.216}$$

$$E_{LHY} = \frac{1}{(2\pi)^2} \left(\frac{2m g_{11} n_1}{\hbar^2}\right)^{3/2} g_{11} n_1 \int_0^\infty dx x^2 \times \tag{1.217}$$
$$\left[\frac{E_+}{g_{11} n_1} + \frac{E_-}{g_{11} n_1} - \left(x^2 + 1\right) - \left(x^2 + \sqrt{\frac{g_{22}}{g_{11}}}\right) + \frac{1 + \frac{g_{22}}{g_{11}} + 2\frac{g_{12}^2}{g_{11}^2}\sqrt{\frac{g_{11}}{g_{22}}}}{2x^2} \right].$$

One can find the dimensionless ratio $\frac{E_\pm}{g_{11} n_1}$ as follows:

$$\begin{aligned} \frac{E_\pm}{g_{11} n_1} &= \frac{1}{g_{11} n_1 \sqrt{2}} \sqrt{\epsilon_1^2 + \epsilon_2^2 \pm \sqrt{\left(\epsilon_1^2 - \epsilon_2^2\right)^2 + 16 \epsilon_k^2 g_{12}^2 n_1 n_2}} \\ &= x\sqrt{x^2 + 1 + \alpha \pm \sqrt{(1 - 1\alpha)^2 + 4\beta}}, \end{aligned} \tag{1.218}$$

where $\alpha = \sqrt{\frac{g_{22}}{g_{11}}}$, and $\beta = \frac{g_{12}^2 \sqrt{g_{11}}}{g_{11}^2 \sqrt{g_{22}}}$. Hence, the integral expression I in the LHY energy becomes:

$$I = \int dx x^2 \Bigg[x\sqrt{x^2 + 1 + \alpha + \sqrt{(1-\alpha)^2 + 4\beta}} + x\sqrt{x^2 + 1 + \alpha - \sqrt{(1-\alpha)^2 + 4\beta}} - \left(x^2 + 1\right) - \left(x^2 + \alpha\right) + \frac{1 + \alpha^2 + 2\beta}{2x^2} \Bigg]. \tag{1.219}$$

Analyze the limit $x \to \infty$ to divide the total LHY energy into the contributions of the two Bogoliubov branches. Note that

$$x\sqrt{x^2 + a \pm b} \simeq x^2 \sqrt{1 + \frac{a \pm b}{x^2}} \simeq x^2 \left(1 + \frac{a \pm b}{2x^2} - \frac{(a \pm b)^2}{8x^4}\right). \tag{1.220}$$

Hence, divide the integral into two parts $E_{LHY} = E_{LHY,+} + E_{LHY,-}$:

$$E_{LHY,\pm} = \frac{1}{(2\pi)^2} \left(\frac{2m g_{11} n_1}{\hbar^2}\right)^{3/2} g_{11} n_1 I_\pm, \tag{1.221}$$

where

$$I_{\pm} = \int dx x^2 \quad \left[x\sqrt{x^2+1+\alpha \pm \sqrt{(1-\alpha)^2+4\beta}} - \left(x^2 + \frac{1+\alpha\pm\sqrt{(1-\alpha)^2+4\beta}}{2} \right) + \frac{\left(1+\alpha\pm\sqrt{(1-\alpha)^2+4\beta}\right)^2}{8x^2} \right]. \tag{1.222}$$

Define a constant $f_{\pm} \equiv f_{\pm}(\alpha,\beta) = 1+\alpha \pm \sqrt{(1-\alpha)^2+4\beta}$. Then, $I_{\pm}$ becomes:

$$I_{\pm} = \int_0^{\infty} dx x^2 \left[x\sqrt{x^2+f_{\pm}} - \left(x^2 + \frac{f_{\pm}}{2} \right) + \frac{f_{\pm}^2}{8x^2} \right]. \tag{1.223}$$

Apply the change of variables $u^2 = x^2 + f_{\pm}$. The integrals become:

$$I_{\pm} = \lim_{l\to\infty} \int_0^l dx x^3 \sqrt{x^2+f_{\pm}} - \frac{l^5}{5} - \frac{f_{\pm}}{2}\frac{l^3}{3} + \frac{f_{\pm}^2}{8} l. \tag{1.224}$$

The first integral on the right-hand side is:

$$\begin{aligned} \lim_{l\to\infty} \int_0^l dx x^3 \sqrt{x^2+f_{\pm}} &= \lim_{l\to\infty} \int_{\sqrt{f_{\pm}}}^{\sqrt{l^2+f_{\pm}}} du u^2 \left(u^2 - f_{\pm}\right) \\ &= \lim_{l=\infty} \left(\frac{u^5}{5} - f_{\pm}\frac{u^3}{3} \right)_{\sqrt{f_{\pm}}}^{\sqrt{l^2+f_{\pm}}}. \end{aligned} \tag{1.225}$$

Expand (1.225) in Taylor series around $f_{\pm}/l$ and put into (1.224):

$$I_{\pm} = \frac{2f_{\pm}^{5/2}}{15}. \tag{1.226}$$

Then, the two branches of the LHY energy become [1]:

$$E_{LHY,\pm} = \frac{\sqrt{2}}{15\pi^2}\frac{m^{3/2}}{\hbar^3}\left(g_{11}n_1\right)^{5/2}\left[1+\alpha\pm\sqrt{(1-\alpha)^2+4\beta}\right]^{5/2}, \tag{1.227}$$

where $\alpha = \sqrt{\frac{g_{22}}{g_{11}}}$, and $\beta = \frac{g_{12}^2\sqrt{g_{11}}}{g_{11}^2\sqrt{g_{22}}}$.

1.3 Spin-1 Bose Condensates

The spin-1 condensate consists of atoms in the hyperfine manifold $|1,-1\rangle$, $|1,0\rangle$, and $|1,1\rangle$, in which the spin exchange processes, such as $|1\rangle + |-1\rangle \rightarrow |0\rangle + |0\rangle$, are allowed. Furthermore, the dipolar moment is assumed to be sufficiently weak such

that the long-range interactions among the particles are negligible, and the time scale of dipolar relaxation into the lowest Zeeman level is much larger than the time scale of the spin collisions. Therefore, the total longitudinal magnetization is conserved, and applying an external magnetic field does not change the condensate overall magnetization [21, 22]. The interactions among the atoms are assumed to be s-wave scattering collisions. Due to the symmetry properties of the two-body wavefunction of the indistinguishable particles, the collision channels only with the even total spins F are allowed ([22]).

The spin-exchange collisions are feasible under an external magnetic field only if the hyperfine splitting remains within the linear region. This constraint ensures that the total energy of the colliding particles is conserved. Therefore, there is an upper threshold for the magnetic field to preserve the spinor nature of the condensate[22], and the magnetic Feshbach resonances can not be used to tune the spinor scattering lengths.

The spin-1 condensate exhibits spin-dependent interaction energy which leads to various magnetic order parameters in the ground state. These ground states can be reached by the spin-exchange collisions. Furthermore, the magnetic properties can also be tuned by the linear p and quadratic Zeemen q energies. Depending on the sign and the magnitude of the parameters p, q, and the spin coupling constant c_1, a rich phase diagram emerges, including the phases such as ferromagnetic, polar, antiferromagnetic, and broken-axis symmetric [21].

To understand the ground state properties and the MF and LHY energies of each magnetic order, we first revisit the derivation of the Hamiltonian for spin-1 condensate and find the MF energy. Then, we apply the Bogoliubov theory to calculate the LHY energies for each order parameter. In this section, we frequently refer to the calculations shown in [21, 23].

1.3.1 Spin-1 Bose Gas Hamiltonian

The many-body wavefunction of two indistinguishable particles of spin-f shifts a phase factor of $(-1)^{2f}$ under an exchange. The same exchange operations cause a

change of $(-1)^{F+2f}$ and $(-1)^{L}$ for the spin and orbital parts of the wavefunction, respectively, where F is the total spin and L is the relative orbital angular momentum. To be consistent, the change in the phase factors should not cause any different physical behavior, i.e. $(-1)^{2f} = (-1)^{F+2f+L}$ which indicates that $\mathrm{F}+\mathrm{L}$ is even [22]. This condition must be satisfied regardless of the statistical nature of the particles.

Since we model the two body interactions in the s-wave scattering regime, the relative orbital angular momentum can be assumed to be zero $\mathrm{L} = 0$. Therefore, the collision channels only with the even total spin of the two particles are allowed, i.e. $F = 0, 2, 4, \ldots$, 2f. This property of the spinor condensates suggests to express the interaction Hamiltonian using the projection operators on the even total spin [22]:

$$\hat{V}_{\text{int}} = \sum_{F=0,2\ldots,2f} \hat{V}^{(F)}, \tag{1.228}$$

where

$$\hat{V}^{(F)} = \frac{g_F}{2} \int d^3\vec{r} \sum_{\substack{m_1,m_2,\\ m_1'm_2'=-f}}^{+f} \Big[\psi^\dagger_{m_1'}(\vec{r})\psi^\dagger_{m_2'}(\vec{r}) \quad \langle f, m_1'; f, m_2'|\, f, m_1; f, m_2\rangle \psi_{m_1}(\vec{r})\psi_{m_2}(\vec{r}) \Big]$$

$$= \frac{g_F}{2} \int d^3\vec{r} \sum_{M=-F}^{+F} \sum_{\substack{m_1,m_2,\\ m_1'm_2'=-f}}^{+f} \psi^\dagger_{m_1'}\psi^\dagger_{m_2'} \langle f, m_1'; f, m_2'|F, M\rangle \underbrace{\langle F, M|f, m_1; f, m_2\rangle}_{\text{Clebsch-Gordon Coefficients}} \psi_{m_1}\psi_{m_2}$$

$$= \frac{g_F}{2} \int d^3\vec{r} \sum_{M=-F}^{+F} \hat{A}^\dagger_{FM}\hat{A}_{FM}, \tag{1.229}$$

where the operator $\hat{A}_{FM}$ annihilates the pair of particles with spin $|m_1\rangle$ and $|m_2\rangle$ and project onto the total spin channel $|F, M\rangle$:

$$\hat{A}_{FM} = \sum_{\substack{m_1,m_2,\\ m_1'm_2'=-f}}^{+f} \langle F, M|f, m_1; f, m_2\rangle \psi_{m_1}\psi_{m_2}. \tag{1.230}$$

Here $\psi_m(\vec{r})$ and $\psi^\dagger_m(\vec{r})$ represent the field annihilation and creation operators with spin state $|f, m\rangle$, respectively, and g_F is the interaction coupling constant along the

total spin channel F. The particles with spin $|f, m_1\rangle$ and $|f, m_2\rangle$ collide, and the particles with $|f, m_1'\rangle$ and $|f, m_2'\rangle$ are created after the collision. The total interaction Hamiltonian is [21]:

$$\hat{V} = \frac{1}{2}\int d^3\vec{r} \sum_{\substack{m_1,m_2,\\ m_1',m_2'}} C_{m_1,m_2}^{m_1',m_2'} \psi_{m_1'}^\dagger \psi_{m_2'}^\dagger \psi_{m_1}\psi_{m_2}, \tag{1.231}$$

where the Clecsch-Gordon coefficients are:

$$C_{m_1,m_2}^{m_1',m_2'} = \sum_{F=0,2,..,2f} g_F \left\langle f, m_1'; f, m_2' \middle| \hat{P}_F \middle| f, m_1; f, m_2 \right\rangle, \tag{1.232}$$

where $\hat{P}_F \equiv \sum_{M=-F}^{+F} |F, M\rangle\langle F, M|$ is the projection operator onto the total spin channel F.

To understand the significance of the allowance only of even total spin channels, let us first revise the Clebsh-Gordon coefficients for the total angular momentum of two spin-1 particles and discuss the possible collision scenarios. In the following, we use the notation $|F, M\rangle$ for the total spin $\vec{F} = \vec{F}_1 + \vec{F}_2$, whereas $|m_1\rangle |m_2\rangle \equiv |f = 1, m_1; f = 1, m_2\rangle$ represent the spinor part of the two-body wavefunction. Note the ladder operators for the total spin:

$$L_\pm|\ell, m\rangle = \hbar\sqrt{\ell(\ell+1) - m(m\pm 1)}|\ell, m\pm 1\rangle, \tag{1.233}$$

while $\vec{F}_\pm = \vec{F}_{1,\pm} + \vec{F}_{2,\pm}$, where $\vec{F}_{i,\pm}$ represents the ladder operator for the particle i. Start from the identity $|2, 2\rangle = |1\rangle |1\rangle$ and apply the ladder operators to find [24]:

$$\begin{aligned}
|2,2\rangle &= |1\rangle|1\rangle, \\
|2,1\rangle &= \frac{1}{\sqrt{2}}(|1\rangle|0\rangle + |0\rangle|1\rangle), \\
|2,0\rangle &= \frac{1}{\sqrt{6}}(|-1\rangle|1\rangle + 2|0\rangle|0\rangle + |1\rangle|-1\rangle), \\
|2,-1\rangle &= \frac{1}{\sqrt{2}}(|-1\rangle|0\rangle + |0\rangle|-1\rangle), \\
|2,-2\rangle &= |-1\rangle|-1\rangle.
\end{aligned} \tag{1.234}$$

Similarly, two-body spinors $|m_1\rangle |m_2\rangle$ can be written in terms of the total spin basis

$|F, M\rangle$ [24]:

$$\begin{aligned}
|1\rangle|1\rangle &= |2,2\rangle, \\
|1\rangle|0\rangle &= \frac{1}{\sqrt{2}}(|2,1\rangle + |1,1\rangle), \\
|0\rangle|1\rangle &= \frac{1}{\sqrt{2}}(|2,1\rangle - |1,1\rangle), \\
|1\rangle\,|-1\rangle &= \frac{1}{\sqrt{6}}|2,0\rangle + \frac{1}{\sqrt{2}}|1,0\rangle + \frac{1}{\sqrt{3}}|0,0\rangle, \\
|-1\rangle\,|1\rangle &= \frac{1}{\sqrt{6}}|2,0\rangle - \frac{1}{\sqrt{2}}|1,0\rangle + \frac{1}{\sqrt{3}}|0,0\rangle, \\
|0\rangle|0\rangle &= \sqrt{\frac{2}{3}}|2,0\rangle - \frac{1}{\sqrt{3}}|0,0\rangle.
\end{aligned} \tag{1.235}$$

Using the above equations, one can also express $|1,1\rangle$,$|1,0\rangle$ and $|0,0\rangle$ in terms of $|m_1\rangle\,|m_2\rangle$ [24]:

$$\begin{aligned}
|0,0\rangle &= \frac{1}{\sqrt{3}}(|1\rangle\,|-1\rangle - |0\rangle\,|0\rangle + |-1\rangle\,|1\rangle), \\
|1,1\rangle &= \frac{1}{\sqrt{2}}(|1\rangle\,|0\rangle - |0\rangle\,|1\rangle), \\
|1,0\rangle &= \frac{1}{\sqrt{3}}(|1\rangle\,|-1\rangle - |-1\rangle\,|1\rangle).
\end{aligned} \tag{1.236}$$

Let us now discuss some collision scenarios. First, consider the collision of two particles with spin state $|1\rangle$. In this case, the collision can only occur through the total spin-2 channel with the state $|2,2\rangle = |1\rangle\,|1\rangle$. Then the created particles after the collision can only be two $|1\rangle$ particles. If the colliding particles have spin parts of $|1\rangle$ and $|0\rangle$ with the quantum state $1/\sqrt{2}(|0\rangle\,|1\rangle + |1\rangle\,|0\rangle)$, we obtain only the even total spin channel $|2,1\rangle$. The odd total spin channel of $|1,1\rangle$ being forbidden is also demonstrated here by the Clebsch-Gordon coefficients. However the state $|2,1\rangle$ can only yield again two particles with $|0\rangle$ and $|1\rangle$. Therefore, this collision channel does not cause any spin exchange process.

Now consider the collision with spin $|1\rangle$ and $|-1\rangle$. This collision with the quantum state $1/\sqrt{(}2)(|1\rangle\,|-1\rangle + |-1\rangle\,|1\rangle)$ can occur through either total spin-0 channel of state $|0,0\rangle$ with the probability $2/3$ or a total spin-2 channel of state $|2,0\rangle$ with probability $1/3$. Furthermore, both of the states $|2,0\rangle$ and $|0,0\rangle$ can create pair of particles with spins either $|0\rangle\,|0\rangle$ or $|1\rangle\,|-1\rangle$. Note that there is a possibility of a spin exchange process in which the entangled state $1/\sqrt{2}(|1\rangle\,|-1\rangle + |-1\rangle\,|1\rangle)$ is converted into the

state $|0\rangle\,|0\rangle$. Similarly, when two particles of state $|0\rangle$ collide, the spin exchange process can occur in the reverse direction $|0\rangle + |0\rangle \rightarrow |1\rangle + |-1\rangle$. These processes are physically realizable as long as the perturbation of the single particle eigenenergy manifold by the external fields is linear, which ensures the conservation of energy during the exchange processes. Furthermore, whether a spin exchange occurs or not during the collision, the longitudinal magnetization is conserved during a considerable time scale even under an external magnetic field for the spin-1 condensates with a low dipolar relaxation rate. In these condensates, the time scale to condense into the lowest Zeeman energy is assumed to be sufficiently larger than the collision time scale [21, 22].

The spin-exchange processes are the fundamental physical mechanisms for the rich magnetic orders encountered in the spinor condensates. Depending on the strength of the scattering lengths along the total spin channels, different magnetic order parameters may emerge such as ferromagnetic, polar, etc [21, 22].

Now let us define some operators to express the spin-1 Hamiltonian in a physically intuitive way. The total density operator $n(\vec{r})$:

$$n(\vec{r}) \equiv \sum_{m=-f}^{+f} \psi_m^\dagger(\hat{r})\psi_m(\hat{r}). \tag{1.237}$$

Spin-density operator:

$$\hat{F}_\nu(\vec{r}) \equiv \sum_{m,m'=-f}^{+f} (f_\nu)_{mm'}\, \psi_m^\dagger(\vec{r})\psi_{m'}(\vec{r}), \tag{1.238}$$

where $\nu = x, y, z$ are the spatial directions and the elements of the spin component matrices are [24]:

$$(f_x)_{mm'} = \frac{1}{2} \quad \Big[\sqrt{(f-m+1)(f+m)}\delta_{m-1,m'} + \sqrt{(f+m+1)(f-m)}\delta_{m+1,m'}\Big], \tag{1.239}$$

$$(f_y)_{mm'} = \frac{1}{2i} \quad \Big[\sqrt{(f-m+1)(f+m)}\delta_{m-1,m'} - \sqrt{(f+m+1)(f-m)}\delta_{m+1,m'}\Big], \tag{1.240}$$

$$(f_z)_{mm'} = m\delta_{mm'}. \tag{1.241}$$

Consider the spin-f Hamiltonian in (1.228) and (1.229), which are in terms of $\hat{A}_{FM}$ operators. To rewrite it in terms of the density $\hat{n}^2(\vec{r})$ and spin coupling operators $\sum_\nu (\hat{F}_\nu)_{m_1 m_1'} (\hat{F}_\nu)_{m_2 m_2'}$, consider the following relations:

$$\mathcal{N}\left(n^2(\vec{r})\right) = \sum_{m_1,m_2=-f}^{+f} \psi^\dagger_{m_1}\psi^\dagger_{m_2}\psi_{m_2}\psi_{m_1} \tag{1.242}$$

$$= \sum_{F=0,2,..,2F} \sum_{M=-F}^{+F} \hat{A}^\dagger_{FM}(\vec{r})\hat{A}_{FM}(\vec{r}), \tag{1.243}$$

where $\mathcal{N}$ is the normal ordering operator which places the creation operators to the latest in operator orders. The spin coupling between the pair can be written in terms of the total and single spin operators as:

$$\vec{f}_1 \cdot \vec{f}_2 = \frac{1}{2}\left[\left(\vec{f}_1 + \vec{f}_2\right)^2 - \vec{f}_1^2 - \vec{f}_2^2\right] = \frac{1}{2}\vec{F}^2_{tot} - f(f+1). \tag{1.244}$$

Therefore, the spin coupling operator becomes:

$$\mathcal{N}\left[\vec{F}_1(\vec{r}) \cdot \vec{F}_2(\vec{r})\right] = \sum_{F=0,2...,2f} \left[\frac{1}{2}F(F-1) - f(f+1)\right] \sum_{M=-F}^{F} A^\dagger_{FM}(\vec{r})A_{FM}(\vec{r}). \tag{1.245}$$

For spin-$f = 1$, the relations become:

$$\hat{n}^2(\vec{r}) = \sum_M A^\dagger_{2M}A_{2M} + A^\dagger_{00}A_{00} \tag{1.246}$$

$$\hat{\vec{F}}_1 \cdot \hat{\vec{F}}_2 = -2A^\dagger_{00}A_{00} + \sum_m A^\dagger_{2M}A_{2M}. \tag{1.247}$$

Therefore, the operators $\hat{n}^2$, $\hat{\vec{F}}_1 \cdot \hat{\vec{F}}_2$, and the singlet pair operator A_{00} are not independent [21]. Consider the interaction energy for the spin-1 condensate [21]:

$$\begin{aligned}
\hat{V}_{\text{int}} &= V^{(0)} + V^{(2)} \\
&= \int d^3\vec{r}\left\{\frac{1}{2}g_0 A^\dagger_{00}A_{00} + \frac{1}{2}g_2 \sum_{M=-F}^{+F} A^\dagger_{2M}A_{2M}\right\} \\
&= \frac{1}{2}\int d^3\vec{r}\left\{g_0\frac{\hat{n}^2 - \vec{F}_1\cdot\vec{F}_2}{3} + g_2\frac{2\hat{n}^2 + \vec{F}_1\cdot\overrightarrow{F_2}}{3}\right\} \\
&= \frac{1}{2}\int d^3\vec{r}\left\{\frac{g_0+2g_2}{3}\hat{n}^2 + \frac{g_2-g_0}{3}\bar{F}_1\cdot\vec{F}_2\right\} \\
&= \frac{1}{2}\int d^3\vec{r}\left\{c_0\hat{n}^2 + c_1\vec{F}_1\cdot\vec{F}_2\right\},
\end{aligned} \tag{1.248}$$

where the density coupling constant is $c_0 = \frac{g_0+2g_2}{3}$ and spin coupling constant is $c_1 = \frac{g_2-g_0}{3}$.

Similar reasoning applies to find the Hamiltonian for the higher spins [21]. For $f = 2$:

$$\hat{n}^2(\tilde{r}) = \sum_M A^\dagger_{4M} A_{4M} + \sum_M A^\dagger_{2M} A_{2M} + A^\dagger_{00} A_{00} \tag{1.249}$$

$$\hat{\vec{F}}_1 \cdot \hat{\vec{F}}_2 = -6A^\dagger_{00}A_{00} - 3\sum_m A^\dagger_{2M}A_{2M} + 4\sum_m A^\dagger_{4M}A_{4M} \tag{1.250}$$

and

$$\begin{aligned}
\hat{V}_{\text{int}} &= V^{(0)} + V^{(2)} + V^{(4)} \\
&= \int d^3\vec{r} \left\{ \frac{1}{2} g_0 A^\dagger_{00} A_{00} + \frac{1}{2} g_2 \sum_{M=-2}^{+2} A^\dagger_{2M} A_{2M} + \frac{1}{2} g_4 \sum_{M=-4}^{+4} A^\dagger_{4M} A_{4M} \right\} \\
&= \frac{1}{2} \int d^3\vec{r} \Big\{ g_0 \hat{A}^\dagger_{00}\hat{A}_{00} + \frac{g_2}{7}(4\hat{n}^2 - \vec{F}_1 \cdot \vec{F}_2 - 10\hat{A}^\dagger_{00}\hat{A}_{00}) \\
&\qquad + \frac{g_4}{7}(3\hat{n}^2 + \vec{F}_1 \cdot \vec{F}_2 + 3\hat{A}^\dagger_{00}\hat{A}_{00}) \Big\} \\
&= \frac{1}{2} \int d^3\vec{r} \left\{ \frac{4g_2+3g_4}{7}\hat{n}^2 + \frac{g_4-g_2}{7}\vec{F}_1 \cdot \vec{F}_2 + \frac{3g_4-10g_2+7g_0}{7}\hat{A}^\dagger_{00}\hat{A}_{00} \right\} \\
&= \frac{1}{2} \int d^3\vec{r} \Big\{ c_0\hat{n}^2 + c_1 \vec{F}_1 \cdot \vec{F}_2 + c_2 \hat{A}^\dagger_{00}\hat{A}_{00} \Big\},
\end{aligned} \tag{1.251}$$

where $c_0 = \frac{4g_2+3g_4}{7}$, $c_1 = \frac{g_4-g_2}{7}$, and $c_2 = \frac{3g_4-10g_2+7g_0}{7}$.

When the spin-1 condensate is placed under a magnetic field applied along the $z-$axis, the single particle part H_0 of the total Hamiltonian needs also to cooperate with the linear and quadratic Zeeman energies [21]:

$$\begin{aligned}
\hat{H}_0 &= \int d^3\vec{r} \sum_{m,m'=f}^{+f} \psi^\dagger_m \left[-\frac{\hbar^2\nabla^2}{2m} - p\left(f_z\right)_{mm'} + q\left(f_z^2\right)_{mm'} \right] \psi_{m'} \\
&= \int d^3\vec{r} \sum_{m=-f}^{+f} \psi^\dagger_m \left[-\frac{\hbar^2\nabla^2}{2m} - pm + qm^2 \right] \psi_m,
\end{aligned} \tag{1.252}$$

where linear Zeeman energy $p = g_L\mu_B B$, in which g_L is the Landé $g-$factor, μ_B is the Bohr magneton, and B is the magnitude of the applied static magnetic field. The quadratic Zeeman energy $q = q_B + q_{MW}$, where q_B denotes the Zeeman shift due to the static magnetic field, which can be calculated from the second-order perturbation theory as $q_B \equiv \frac{(g_L\mu_B B)^2}{\Delta E_{hf}}$, where ΔE_{hf} denotes the energy spacing between the hyperfine states. One can also independently tune the quadratic Zeeman energy

q_{MW} by applying a microwave field [22]. Therefore, the total spin-1 gas Hamiltonian $\hat{H} = \hat{H}_0 + \hat{V}_{int}$ becomes [23]:

$$\begin{aligned}\hat{H} &= \int d^3\vec{r} \sum_{m=-1}^{+1} \psi_m^\dagger \left[-\frac{\hbar^2\nabla^2}{2M} - pm + qm^2 \right] \psi_m \\ &+ \frac{1}{2}\int d^3\vec{r} \sum_{m,m'=-1}^{+1} c_0 \psi_m^\dagger \psi_{m'}^\dagger \psi_{m'} \psi_m \\ &+ \frac{1}{2}\int d^3\vec{r} \sum_{\nu=x,y,z} \sum_{\substack{m_1,m_2,\\ m_1',m_2'=-1}}^{+1} c_1 \psi_{m_2'}^\dagger \psi_{m_1'}^\dagger (\hat{F}_\nu)_{m_1,m_1'} (\hat{F}_\nu)_{m_2,m_2'} \psi_{m_1} \psi_{m_2}.\end{aligned} \tag{1.253}$$

1.3.2 MF Theory of Spin-1 Condensate

The corresponding MF energy can be calculated by replacing the field operators with the classical fields, i.e. $\hat{\psi}(\vec{r}) = \Psi(\vec{r})$ [21]:

$$E_{MF} = -p\,\langle F_z\rangle + q\langle F_z^2\rangle + \frac{c_0 n}{2} + \frac{c_1 n}{2}\langle\vec{F}\rangle^2, \tag{1.254}$$

where the operator $\langle\hat{\mathcal{O}}\rangle = \langle\Psi|\hat{\mathcal{O}}|\Psi\rangle$ denotes the expectation value of the operator $\hat{\mathcal{O}}$ in the state Ψ. The most interesting part of the MF energy function is its dependence on the magnetic properties of the condensate such as $\langle\vec{F}\rangle^2$, $\langle F_z^2\rangle$, and $\langle F_z\rangle$. The comparative strength of the coefficients p, q, and c_1 can result in various magnetic orders, whereas the coefficient c_0 has no effect on the magnetic order parameter [21], but plays a significant role in the mechanical stability of the condensate. The ground state order parameters for $c_1 < 0$, $c_1 = 0$, and $c_1 > 0$ are provided for the various levels of linear $p/c_1 n$ and quadratic $q/c_1 n$ Zeeman energies in Fig.(1.3).

First consider the case in which there is no magnetic field applied on the condensate, i.e. $p = 0$, $q = 0$. The only spin-relevant part of the MF energy functional is $E_{MF,spin} = \frac{c_1 n}{2}\langle\vec{F}\rangle^2$. The minimization of $E_{MF,spin}$ is straightforward, and the ground state magnetic order $\tau = (\tau_1\ \tau_0\ \tau_{-1})$ can be directly determined by the sign of the spin coupling constant $c_1 = \frac{g_2 - g_0}{3}$. When c_1 is negative, the particles condensed into a fully magnetized state, i.e. $\langle\vec{F}\rangle = 1$. Here the direction of magnetization can be arbitrary since the rotational symmetry is not broken when $p = 0$ and $q = 0$. This is the ferromagnetic phase, hence, the spin coupling constant $c_1 < 0$ is named a ferromagnetic interaction. If c_1 is positive, the magnetic order is set to minimize

the magnitude of the total magnetization $\langle \vec{F} \rangle = 0$. This region will be named the anti-ferromagnetic (AF) interaction even though there is no Neel order in the spatial configuration of the atoms.

Secondly, consider the case of zero linear Zeeman energy $p = 0$, but finite quadratic Zeeman energy $q \neq 0$. For the ferromagnetic interaction $c_1 < 0$, if $q < 0$, the magnetic order is required to maximize both $\langle \vec{F} \rangle$ and $\langle F_z^2 \rangle$. This can be achieved by the full magnetization along either $+z$ and $-z$ axis: $\tau_F = (1\ 0\ 0)$ or $(0\ 0\ 1)$ (See the regions I and II in Fig. 1.3). However, if $q > 0$, the ground state magnetic order requires more careful treatment since one needs to achieve the minimization of $\langle F_z^2 \rangle$ and maximization of $\langle \vec{F} \rangle$ with the same order parameter. It is obvious that, for a sufficiently large $q > 2|c_1|n$, the ground state order parameter is $\tau_P = (0\ 1\ 0)$, which yields $\langle F_z^2 \rangle = 0$, $\langle \vec{F} \rangle = 0$ (See region IV in Fig. 1.3). In this limit, the magnetization is zero, but its effect on the energy is negligible compared to the coefficient q. For finite values of q comparable to the interaction energy $c_1 n$, the competition between the maximization of total magnetization and minimization of $\langle F_z^2 \rangle$ can exhibit more interesting order parameters with partial magnetization, whose determination requires a more quantitative approach as shown below.

Consider the general form of the order parameter for the spin-1 state:

$$|\tau\rangle = \begin{pmatrix} \tau_1 \\ \tau_0 \\ \tau_{-1} \end{pmatrix} = \begin{pmatrix} |\tau_1| e^{i\phi_1} \\ |\tau_0| e^{i\phi_0} \\ |\tau_{-1}| e^{i\phi_{-1}} \end{pmatrix}, \tag{1.255}$$

where $\tau_i \in \mathcal{C}$, and $|\tau_1|^2 + |\tau_1|^2 + |\tau_{-1}|^2 = 1$. The expected values are written as

$$\langle \hat{F}_z \rangle = |\tau_1|^2 - |\tau_{-1}|^2, \tag{1.256}$$

$$\langle \hat{F}_z^2 \rangle = |\tau_1|^2 + |\tau_{-1}|^2. \tag{1.257}$$

The vectorial spin operator is $\hat{\vec{F}} = \hat{e}_x F_x + \hat{e}_y F_y + \hat{e}_z F_z$, where the matrix representa-

tions of each spin component are [24]:

$$\hat{F}_x = \frac{1}{\sqrt{2}} \begin{pmatrix} 0 & 1 & 0 \\ 1 & 0 & 1 \\ 0 & 1 & 0 \end{pmatrix}, \hat{F}_y = \frac{i}{\sqrt{2}} \begin{pmatrix} 0 & -1 & 0 \\ 1 & 0 & -1 \\ 0 & 1 & 0 \end{pmatrix}, \\ \hat{F}_z = \begin{pmatrix} 1 & 0 & 0 \\ 0 & 0 & 0 \\ 0 & 0 & -1 \end{pmatrix}. \tag{1.258}$$

The expected values of the magnetization along the different axes:

$$\langle \hat{F}_x \rangle = \frac{1}{\sqrt{2}} \left[\tau_0^* \tau_1 + \left(\tau_1^* + \tau_1^* \right) \tau_0 + \tau_0^* \tau_1 \right], \tag{1.259}$$

$$\langle \hat{F}_y \rangle = \frac{i}{\sqrt{2}} \left[\tau_0^* \tau_1 - \tau_1^* \tau_0 + \tau_{-1}^* \tau_0 - \tau_0^* \tau_{-1} \right], \tag{1.260}$$

$$\langle \hat{F}_z \rangle = |\tau_1^2| - |\tau_{-1}^2|. \tag{1.261}$$

Then, calculate:

$$\langle \vec{F} \rangle^2 = \left[|\tau_1|^2 - |\tau_{-1}|^2 \right]^2 + 2 \left| \tau_1^* \tau_0 + \tau_{-1} \tau_0^* \right|^2. \tag{1.262}$$

The latest term in the summation can also be expressed in terms of the magnitude of the order parameter and a single phase variable $\theta \equiv \phi_1 + \phi_{-1} - \phi_0$ as follows [21]:

$$\begin{aligned} &\left| |\tau_1||\tau_0| e^{i(\phi_0 - \phi_1)} + |\tau_{-1}||\tau_0| e^{i(\phi_{-1} - \phi_0)} \right|^2 \\ &= |\tau_0|^2 \left\{ |\tau_1|^2 + |\tau_{-1}|^2 + |\tau_1||\tau_{-1}| e^{i(2\phi_0 - \phi_1 - \phi_{-1})} + |\tau_{-1}||\tau_1| e^{-i(2\phi_0 - \phi_1 - \phi_{-1})} \right\}, \end{aligned} \tag{1.263}$$

and

$$\langle \vec{F} \rangle^2 = \left(|\tau_1|^2 - |\tau_{-1}|^2 \right)^2 + 2 |\tau_0|^2 \left[|\tau_1|^2 + |\tau_1|^2 + 2|\tau_1||\tau_{-1}| \cos\theta \right]. \tag{1.264}$$

The total spin relevant MF energy functional becomes [21]:

$$\begin{aligned} E_{MF,spin} &= -p \left(|\tau_1|^2 - |\tau_{-1}|^2 \right) + q \left(|\tau_1|^2 + |\tau_{-1}|^2 \right) \\ &+ \frac{c_1 n}{2} \left\{ \left(|\tau_1|^2 - |\tau_{-1}|^2 \right)^2 + 2 |\tau_0|^2 \left[|\tau_1|^2 + |\tau_{-1}|^2 + 2|\tau_1||\tau_{-1}| \cos\theta \right] \right\}. \end{aligned} \tag{1.265}$$

If $c_1 > 0$ ($c_1 < 0$), $cos(\theta) = -1$ ($cos(\theta) = +1$) should be chosen to minimize the MF energy. In either case, the argument inside the square bracket takes a quadratic form $(|\tau_1| \pm |\tau_{-1}|)^2$. Furthermore, by using the normalization of the spinor vector, one can

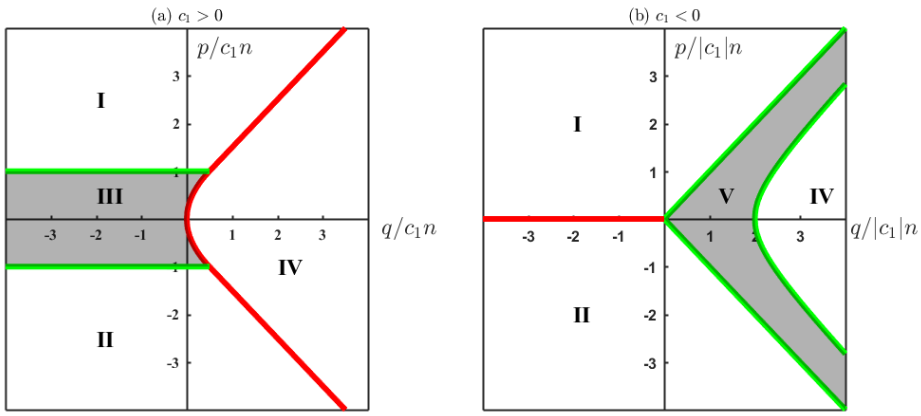

Figure 1.3: The MF phase diagram of the spin-1 condensate as a function of linear $p/|c_1|n$ and quadratic $q/|c_1|n$ Zeeman energies for (a) $c_1 > 0$, and (b) $c_1 < 0$.

express $|\tau_0|$ in terms of $|\tau_1|$ and $|\tau_{-1}|$. Therefore, the total MF energy functional can be written solely in terms of $|\tau_1|$ and $|\tau_{-1}|$:

$$\begin{aligned} E_{MF,spin} &= -p\left(|\tau_1|^2 - |\tau_{-1}|^2\right) + q\left(|\tau_1|^2 + |\tau_{-1}|^2\right) \\ &+ \frac{c_1 n}{2}\left\{\left(|\tau_1|^2 - |\tau_{-1}|^2\right)^2 + 2(1 - |\tau_1|^2 - |\tau_{-1}|^2)\left[|\tau_1| \pm |\tau_{-1}|\right]^2\right\}. \end{aligned} \tag{1.266}$$

Consider the previously discussed order parameters and their MF ground state ener-

Table 1.1: Different order parameters of the spin-1 condensate.

	Phase	Order parameter τ^{T}
(I)	F	$\left(e^{i\phi_1}, 0, 0\right)$
(II)	F	$\left(0, 0, e^{i\phi_{-1}}\right)$
(III)	AF	$\left(e^{i\phi_1}\sqrt{\frac{1+p/(c_1 n)}{2}}, 0, e^{i\phi_{-1}}\sqrt{\frac{1-p/(c_1 n)}{2}}\right)$
(IV)	P	$\left(0, e^{i\phi_0}, 0\right)$
(V)	BA	Eqs. (1.278)

gies:

$$\tau_F = \begin{pmatrix} 1 \\ 0 \\ 0 \end{pmatrix} \Rightarrow \quad E_F = E_I = -p + q + \tfrac{c_1 n}{2},$$
$$\tau_F = \begin{pmatrix} 0 \\ 0 \\ 1 \end{pmatrix} \Rightarrow \quad E_F = E_{II} = +p + q + \tfrac{c_1 n}{2}, \tag{1.267}$$
$$\tau_p = \begin{pmatrix} 0 \\ 1 \\ 0 \end{pmatrix} \Rightarrow \quad E_P = E_{IV} = 0.$$

Now consider the parameter regime $c_0 > 0$ and $q < 0$. Here $cos(\theta) = -1$ and $|\tau_0| = 0$ are required to minimize the MF energy. Therefore the ground state order parameter τ_{AF} can be parametrized as:

$$\tau_{AF} = \begin{pmatrix} \cos\alpha \\ 0 \\ \sin\alpha \end{pmatrix}, \tag{1.268}$$

and the corresponding MF energy is:

$$E_{MF,spin} = -p\cos 2\alpha + q + \frac{c_1 n}{2}(\cos 2\alpha)^2. \tag{1.269}$$

Minimizing this energy concerning the parameter α yields the order parameter [21]:

$$\tau_{AF} = \frac{1}{2}\begin{pmatrix} \sqrt{1 + \frac{p}{c_1 n}} \\ 0 \\ \sqrt{1 - \frac{p}{c_1 n}} \end{pmatrix}, \tag{1.270}$$

with the energy:

$$E_{AF} = E_{\text{III}} = q - \frac{p^2}{2c_1 n}. \tag{1.271}$$

Now also consider the parameter regime $c_1 < 0$ ($cos\theta = +1$) and $q > 0$. Consider the general form of the order parameter [21]:

$$\tau_{BA} = \begin{pmatrix} \tau_1 \\ \sqrt{1 - \tau_1^2 - \tau_{-1}^2} \\ \tau_{-1} \end{pmatrix}, \tag{1.272}$$

where BA stands for the broken axis phase since the magnetization along a direction other than the longitudinal axis is favored. Minimize the energy functional (1.267) with respect to $|\tau_1|$ and $|\tau_{-1}|$ by:

$$\frac{\partial E_{MF}}{\partial|\tau_1|} = 0, \tag{1.273}$$

$$\frac{\partial E_{MF}}{\partial|\tau_{-1}|} = 0. \tag{1.274}$$

Evaluation of the differentials gives the following relations:

$$\frac{q}{c_1 n} = (|\tau_1| + |\tau_{-1}|)^2 \frac{(|\tau_1| + |\tau_{-1}|)^2 - 1}{2|\tau_1||\tau_{-1}|}, \tag{1.275}$$

$$\frac{p}{c_1 n} = \left(|\tau_1|^2 - |\tau_{-1}|^2\right) \frac{(|\tau_1| + |\tau_{-1}|)^2 - 1}{2|\tau_1||\tau_{-1}|}. \tag{1.276}$$

Therefore,

$$\tau_{\pm 1} = \frac{q \pm p}{2q} \sqrt{\frac{q^2 - p^2}{2q^n c_1} + 1}, \tag{1.277}$$

$$\tau_0 = \sqrt{\frac{(q^2 - p^2)\left(-p^2 - q^2 + 2c_1 nq\right)}{4c_1 nq^3}}, \tag{1.278}$$

with the magnetization along $\langle F_z \rangle$ and perpendicular $\langle F_+ \rangle$ to the external magnetic fields are:

$$\langle F_z \rangle = \frac{p\left(-p^2 + q^2 + 2qc_1 n\right)}{2c_1 nq^2}, \tag{1.279}$$

$$\langle F_+ \rangle = \frac{\sqrt{(q^2 - p^2)\left\{(p^2 - 2c_1 nq)^2 - q^4\right\}}}{2\left|c_1\right| nq^2}, \tag{1.280}$$

which signals a tilt against the direction of the external magnetic field whose angle can be determined by using the above components [21].

The BA phase has the MF spin-dependent interaction energy [21]:

$$E_{BA} = E_V = \frac{(q^2 - p^2 + 2c_1 nq)^2}{8c_1 nq^2}. \tag{1.281}$$

Since all the order parameters and corresponding MF energies are calculated, the phase boundaries in the phase diagram of the spin-1 condensate under a magnetic field can now be derived more quantitatively. As shown in Fig. 1.3(a), the analytical equality that defines the phase boundary between phases III and IV can be found by:

$$\begin{aligned} E_{III} &= E_{IV}, \\ q - \frac{p^2}{2c_1 n} &= 0. \end{aligned} \tag{1.282}$$

Then, $p^2 = 2c_1nq$ successfully separates the polar and AF phases. Similarly, the ferromagnetic (I) and polar phase (IV) are separated by the equation $p = q + \frac{c_1 n}{2}$.

For the ferromagnetic interactions $c_1 < 0$, the broken-axis phase (V) is separated from the polar phase (IV) by:

$$\begin{aligned} E_V &= E_{IV}, \\ \frac{\left(-p^2 + q^2 + 2qc_1 n\right)^2}{8c_1 n q^2} &= 0, \end{aligned} \tag{1.283}$$

which gives the equation of the phase boundary as $p^2 = q^2 - 2\left|c_1\right| nq$. Note that the yellow and red phase boundaries indicate the second- and first-order phase transitions [21], in which the MF energy changes concerning p and q, continuously and discontinuously, respectively.

1.3.3 Bogoliubov Theory of Spin-1 Condensate

We now revisit the Bogoliubov theory of spin-1 condensate by following the calculations in [23]. Even though the fundamental assumptions are the same, the calculational differences emerge due to the multi-component and spin-dependent structure of the spin-1 condensate. Consider the spin-1 Hamiltonian in (1.254). Change the basis of the creation and annihilation operators from the position to the momentum space, the same process as in Sections 1.1 and 1.2.

$$\begin{aligned} \hat{H} &= \sum_{\vec{k}} \sum_{m} \left(\varepsilon_k + qm^2\right) a^\dagger_{k,m} a_{k,m} \\ &+ \frac{c_0}{2V} \sum_{\vec{k},\vec{k}',\vec{q}} \sum_{m,m'} a^\dagger_{\vec{k}+\vec{q},m} a^\dagger_{\vec{k}'-\vec{q},m'} a_{\vec{k}',m'} a_{\vec{k}',m} \\ &+ \frac{c_1}{2V} \sum_{\vec{k},\vec{k}',\vec{q}} \sum_{\substack{m_1,m_2,\\ m_1',m_2'}} \sum_{\nu=x,y,z} a^\dagger_{\vec{k}+\vec{q},m_2'} a^\dagger_{\vec{k}'-\vec{q},m_1'} \left(F_\nu\right)_{m_1,m_1'} \left(F_\nu\right)_{m_2,m_2'} a_{\vec{k}',m_2} a_{\vec{k}',m_1}. \end{aligned} \tag{1.284}$$

The relation between the number of particles in the $\vec{k} = 0$ state N_0 and the total number of particles N is:

$$N_0 + {\sum_{\vec{k}}}' \sum_{m} a^\dagger_{k,m} a_{k,m} = N. \tag{1.285}$$

Bogoliubov approximation assumes:

$$\begin{aligned}
&\hat{a}_{0,m} \simeq \sqrt{N_0}\tau_m, \\
&\hat{a}^{\dagger}_{0,m} \simeq \sqrt{N_0}\tau^*_m, \\
&N_0^2 \simeq N^2 - 2N \sum_{\vec{k}}{}' \sum_m a^{\dagger}_{k,m} a_{k,m},
\end{aligned} \tag{1.286}$$

where $\tau = (\tau_1 \ \tau_0 \ \tau_{-1})^T$ is the spinor vector. Using the Bogoliubov approximations, rewrite the Hamiltonian up to the quadratic order in $a_{k,m}$. The first line of the Hamiltonian (1.285):

$$\begin{aligned}
&\sum_k \sum_m \left(\varepsilon_k + qm^2\right) a^{\dagger}_{k,m} a_{k,m} \\
&= \sum_m qm^2 \tau^*_m \tau_m N_0 + \sum_k{}' \sum_m \left(\varepsilon_k + qm^2\right) a^{\dagger}_{k,m} a_{k,m} \\
&= q\left\langle F_z^2 \right\rangle N + \sum_k{}' \sum_m \left[\varepsilon_k + qm^2 - q\left\langle F_z^2 \right\rangle\right] a^{\dagger}_{km} a_{km}.
\end{aligned} \tag{1.287}$$

The density coupling interaction energy is:

$$\begin{aligned}
&\frac{c_0}{2V} \sum_{\vec{k},\vec{k}',\vec{q}} \sum_{m,m'} a^{\dagger}_{\vec{k}+\vec{q},m} a^{\dagger}_{\vec{k}'-\vec{q},m'} a_{\vec{k}',m'} a_{\vec{k}',m} = \frac{c_0}{2V} \sum_{m,m'} \{N_0^2 \left|\tau_m\right|^2 \left|\tau_{m'}\right|^2 \\
&+ \sum_{\vec{k}}{}' a^{\dagger}_{k,m} \sqrt{N_0}\tau^*_{m'} \sqrt{N_0}\tau_{m'} a_{k,m} + \sum_{\vec{k}'}{}' \sqrt{N_0}\tau^*_m a^{\dagger}_{k',m'} a_{k',m'} \sqrt{N_0}\tau_m \\
&+ \sum_{\vec{k}'}{}' a^{\dagger}_{k',m} \sqrt{N_0}\tau^*_{m'} \sqrt{N_0}\tau_m a_{k',m'} + \sum_{\vec{k}}{}' a^{\dagger}_{k,m'} \sqrt{N_0}\tau^*_m \sqrt{N_0}\tau_{m'} a_{k,m} \\
&+ \sum_{\vec{q}}{}' a^{\dagger}_{q,m} a^{\dagger}_{-q,m'} \sqrt{N_0}\tau_{m'} \sqrt{N_0}\tau_m + \sum_{\vec{q}}{}' \sqrt{N_0}\tau^*_m \sqrt{N_0}\tau^*_{m'} a_{q,m'} a_{q,m}\} \\
&= \frac{c_0 N^2}{2V} + \frac{c_0 N}{2V} \sum_{\vec{k}}{}' \left[2\hat{D}^{\dagger}_k \hat{D}_k + \hat{D}^{\dagger}_k \hat{D}^{\dagger}_{-k} + \hat{D}_k \hat{D}_{-k}\right],
\end{aligned} \tag{1.288}$$

where $\hat{D}_k \equiv \sum_m \tau^*_m \hat{a}_{k,m}$ and $\hat{D}^{\dagger}_k \equiv \sum_m \tau_m \hat{a}^{\dagger}_{k,m}$ are the density fluctuation operators.

The spin coupling interaction energy is:

$$
\begin{aligned}
&\frac{c_1}{2V}\sum_{\vec{k},\vec{k}',\vec{q}}\sum_{\substack{m_1,m_2,\\ m_1',m_2'}}\sum_{\nu=x,y,z} a^{\dagger}_{\vec{k}+\vec{q},m_2'}a^{\dagger}_{\vec{k}'-\vec{q},m_1'}\left(F_\nu\right)_{m_1,m_1'}\left(F_\nu\right)_{m_2,m_2'}a_{\vec{k}',m_2}a_{\vec{k}',m_1}\\
&=\frac{c_1}{2V}\sum_{\substack{m_1,m_1',\\ m_2,m_2'}}\sum_{\nu}\Bigg\{N_0^2\left(F_\nu\right)_{m_1,m_1'}\left(F_\nu\right)_{m_2,m_2'}\tau^*_{m_2'}\tau^*_{m_1'}\tau_{m_1}\tau_{m_2}\\
&+N_0\sum_{k}{}'a^{\dagger}_{k,m_2'}\tau^*_{m_1'}\left(F_\nu\right)_{m_1,m_1'}\left(F_\nu\right)_{m_2,m_2'}\tau_{m_1}a_{k,m_2}\\
&+N_0\sum_{k'}{}'a^{\dagger}_{k',m_1'}\tau^*_{m_2'}\left(F_\nu\right)_{m_1,m_1'}\left(F_\nu\right)_{m_2,m_2'}\tau_{m_2}a_{k',m_1}\\
&+N_0\sum_{k'}{}'a^{\dagger}_{k',m_2'}\tau^*_{m_1'}\left(F_\nu\right)_{m_1,m_1'}\left(F_\nu\right)_{m_2,m_2'}\tau_{m_2}a_{k',m_1}\\
&+N_0\sum_{k}{}'a^{\dagger}_{k,m_1'}\tau^*_{m_2'}\left(F_\nu\right)_{m_1,m_1'}\left(F_\nu\right)_{m_2,m_2'}\tau_{m_1}a_{k,m_2}\\
&+N_0\sum_{k}{}'a^{\dagger}_{k,m_1'}a^{\dagger}_{-k,m_2'}\left(F_\nu\right)_{m_1,m_1'}\left(F_\nu\right)_{m_2,m_2'}\tau_{m_1}\tau_{m_2}\\
&+N_0\sum_{k}{}'\tau^*_{m_1'}\tau^*_{m_2'}\left(F_\nu\right)_{m_1,m_1'}\left(F_\nu\right)_{m_2,m_2'}a_{k,m_1}a_{-k,m_2}\Bigg\}\\
&=\frac{c_1N^2\langle\vec{F}\rangle^2}{2V}-\sum_{\vec{k}}{}'\sum_{m}\langle\vec{F}\rangle^2c_1na^{\dagger}_{k,m}a_{k,m}\\
&+\sum_{\vec{k}}{}'\sum_{m,m'}c_1n\langle\vec{F}\rangle\cdot\left(\vec{F}\right)_{mm'}a^{\dagger}_{k,m'}a_{k,m}\\
&+\frac{c_1n}{2}\sum_{\vec{k}}{}'\left(2\vec{F}^{\dagger}_k\cdot\vec{F}_k+\vec{F}^{\dagger}_k\cdot\vec{F}^{\dagger}_{-k}+\vec{F}_k\cdot\vec{F}_{-k}\right),
\end{aligned}
\tag{1.289}
$$

where

$$
\begin{aligned}
\hat{\vec{F}}_k&\equiv\sum_{m,m'}(\hat{F})_{mn'}\tau^*_m\hat{a}_{k,m'}\\
\hat{\vec{F}}^{\dagger}_k&=\sum_{m',m}(\hat{F})_{mm'}\tau_m\hat{a}^{\dagger}_{k,m'}
\end{aligned}
\tag{1.290}
$$

are the spin fluctuation operators. Then, the effective Hamiltonian of the quadratic form in terms of the creation and annihilation operators of the momentum states is

[23]:

$$\begin{aligned}\hat{H}_{eff} &= \frac{Vn^2}{2}\left[c_0 + c_1\langle\vec{F}\rangle^2\right] + qN\langle F_z^2\rangle \\ &+ \sum_{\vec{k}}{}' \sum_{m} \left[\varepsilon_k + qm^2 - q\left\langle F_z^2\right\rangle - nc_1\langle\vec{F}\rangle^2\right] a_{k,m}^{\dagger} a_{k,m} \\ &+ \sum_{\vec{k}}{}' \sum_{m,m'} c_1 n\langle\vec{F}\rangle\cdot(\vec{F})_{mm'} a_{k,m'}^{\dagger} a_{k,m} \\ &+ \frac{c_0 n}{2V}\sum_{\vec{k}}{}' \left(2\hat{D}_k^{\dagger}\hat{D}_k + \hat{D}_k^{\dagger}\hat{D}_{-k}^{\dagger} + \hat{D}_k\hat{D}_{-k}\right) \\ &+ \frac{c_1 n}{2}\sum_{\vec{k}}{}' \left(2\vec{F}_k^{\dagger}\cdot\vec{F}_k + \vec{F}_k^{\dagger}\cdot\vec{F}_{-k}^{\dagger} + \vec{F}_k\cdot\vec{F}_{-k}\right).\end{aligned} \tag{1.291}$$

Here the first line of (1.292) is the MF energy, and the rest of the terms contribute to the energy of the quantum fluctuations. The knowledge of the spinor order parameter is necessary to proceed with the calculations of the dispersion relations and the corresponding LHY energy. Even if the total energy including the LHY correction can slightly shift the MF phase boundaries and the ground state order parameters, we will stick with the MF ground state order parameters since the corrections are sufficiently small for a dilute condensate. Note that our end purpose with the LHY corrections is the feasibility of the droplet phase, which emerges with the collapse of the condensate. The collapsing condensate at its initial stage can be successfully modeled by the MF picture. Then, as the density grows, the LHY correction becomes significant in means of mechanical stability, rather than the magnetic order. Therefore, the use of the MF order parameters to calculate the LHY energy is a reasonable approach.

In the following, we follow the calculations of the Bogoliubov dispersions and the LHY energies for the ferromagnetic, polar, and antiferromagnetic order parameters in [23].

1.3.3.1 Ferromagnetic Order

In the ferromagnetic phase, the order parameter is $\tau_F = (1\ 0\ 0)^T$. This order parameter yields the following magnetic properties:

$$\langle\vec{F}\rangle = \hat{e}_z, \langle F_z\rangle = 1, \left\langle F_z^2\right\rangle = 1. \tag{1.292}$$

The density and spin fluctuation operators become:

$$\hat{D}_k = \hat{a}_{k,1}\hat{\vec{F}}_k = \hat{e}_z a_{k,1} - \hat{e}_y \frac{i}{\sqrt{2}} a_{k,0} + \hat{e}_x \frac{1}{\sqrt{2}} a_{k,0}. \tag{1.293}$$

The effective Hamiltonian becomes:

$$\begin{aligned}
\hat{H}_{eff} \quad &= \frac{Vn^2}{2}\left(c_0 + c_1\right) + qN \\
&+ {\sum_{\vec{k}}}' \Big\{ \left(\varepsilon_k + \left(c_1 + c_0\right) n\right) a^\dagger_{k,1} a_{k,1} + \frac{\left(c_1 + c_0\right) n}{2} \left[a^\dagger_{k,1} a^\dagger_{-k,1} + a_{k,1} a_{-k,1} \right] \\
&+ \left(\varepsilon_k - q\right) a^\dagger_{k,0} a_{k,0} + \left(\varepsilon_k - 2nc_1\right) a^\dagger_{k,-1} a_{k,-1} \Big\}.
\end{aligned} \tag{1.294}$$

Rewrite the summations in the Hamiltonian over half of the total $\vec{k}$ space:

$$\begin{aligned}
\hat{H}_{eff} \quad &= E_{MF,F} + {\sum_{\vec{k}}}' \Big\{ \left[\varepsilon_k + \left(c_1 + c_0\right) n\right] \left(a^\dagger_{k,1} a_{k,1} + a^\dagger_{-k,1} a_{-k,1} \right) \\
&+ \left(c_1 + c_0\right) n \left(a^\dagger_{k,1} a^\dagger_{-k,1} + a_{k,1} a_{-k,1} \right) \\
&+ \left(\varepsilon_k - q\right) \quad \left(a^\dagger_{k,0} a_{k,0} + a^\dagger_{k,0} a_{-k,0} \right) \\
&+ \left(\varepsilon_k - 2nc_1\right) \left(a^\dagger_{k,-1} a_{k,-1} + a^\dagger_{-k,-1} a_{-k,-1} \right) \Big\}.
\end{aligned} \tag{1.295}$$

It is clear from the form of the coefficients of the quadratic operators that the modes $a_{k,0}$ and $a_{k,-1}$ are not coupled to any other mode. These modes do not make any contribution to the ground state energy. However, the fluctuations among the atoms with state $|1\rangle$ require a diagonalization, and the quadratic form is the same as the previous Bogoliubov calculations. To clarify these points, we express the ferromagnetic Hamiltonian $H_{eff,F}$ in the matrix form:

$$H_{eff,F} = E_{MF} + {\sum_{\vec{k}}}' \left[\vec{a}^\dagger_k \underline{H}_0 \vec{a}_k - \left(\varepsilon_k + g_2 n\right) - \left(\varepsilon_k - q\right) - \left(\varepsilon_k - 2nc_1\right) \right], \tag{1.296}$$

where

$$\vec{a}_k = \begin{pmatrix} a_{k,1} & a_{k,1}^\dagger & a_{k,0} & a_{k,0}^\dagger & a_{k,-1} & a_{k,-1}^\dagger \end{pmatrix}, \tag{1.297}$$

$$\vec{a}_k^\dagger = \begin{pmatrix} a_{k,1}^\dagger \\ a_{k,1} \\ a_{k,-1}^\dagger \\ a_{k,0} \\ a_{k,-1}^\dagger \\ a_{k,-1} \end{pmatrix}, \tag{1.298}$$

$$\underline{H}_0 = \left(\begin{array}{cc|cc|cc} \varepsilon_k + g_2 n & g_2 n & 0 & 0 & 0 & 0 \\ g_2 n & \varepsilon_k + g_2 n & 0 & 0 & 0 & 0 \\ \hline 0 & 0 & \varepsilon_k - q & 0 & 0 & 0 \\ 0 & 0 & 0 & \varepsilon_k - q & 0 & 0 \\ \hline 0 & 0 & 0 & 0 & \varepsilon_k - 2nc_1 & 0 \\ 0 & 0 & 0 & 0 & 0 & \varepsilon_k - 2nc_1 \end{array}\right). \tag{1.299}$$

The matrix $\underline{H}_0$ is block diagonal, and only the first block diagonal is sufficient to calculate the Bogoliubov dispersion:

$$E_k = \sqrt{\varepsilon_k \left(\varepsilon_k + 2g_2 n\right)}, \tag{1.300}$$

and the LHY energy:

$$E_{LHY} = \frac{1}{2} \sum_{\vec{k}} \left(E_k - \varepsilon_k - g_2 n + \text{ renormalization term }\right), \tag{1.301}$$

where the renormalization energy is obtained by the same approach in single-component BEC [23], which yields the following interaction energy density:

$$\frac{E_0^F}{V} = qn + \frac{2\pi\hbar^2 n^2}{M} a_2 \left(1 + \frac{128}{15\sqrt{\pi}} \sqrt{n a_2^3}\right). \tag{1.302}$$

Note that the total ground state energy differs from the single component BEC energy only by the term of qn, which is a second-order energy shift due to the applied magnetic field. This result is expected since the ferromagnetic order favors all the atoms inside the condensate to occupy the same spin state $|1\rangle$ or $|-1\rangle$. In this distribution, the only available collision channels are $|2,2\rangle$ or $|2,-2\rangle$, and the atoms collide and

are created back as the atoms with the same spins. Therefore, the spin-1 condensate in the ferromagnetic order behaves as a single-component BEC, and the resulting LHY energy has the same form as the single-component BEC.

1.3.3.2 Polar Order

The order parameter in the polar phase is $\tau_P = (0\ 1\ 0)^T$. The magnetic properties of the polar phase are:

$$\langle F_z \rangle = 0, \langle F_z^2 \rangle = 0, \langle \vec{F} \rangle = 0. \tag{1.303}$$

The density and spin fluctuation operators are:

$$\hat{D}_k = \hat{a}_{k,0}, \tag{1.304}$$

$$\hat{\vec{F}}_k = \hat{e}_x \frac{1}{\sqrt{2}} \left(a_{k,1} + a_{k-1}\right) + \hat{e}_y \frac{i}{\sqrt{2}} \left(a_{k,1} - a_{k,-1}\right). \tag{1.305}$$

Replacing the expected values and the operator expressions into the effective spin-1 Hamiltonian (1.292), and summing the momentum states over the half plane gives:

$$\begin{aligned}
\hat{H}_{eff,P} &= \frac{Vn^2c_0}{2} \\
&+ \sum_{\vec{k}}{}^{>} \Big\{ (\varepsilon_k + nc_0) \left(a_{k,0}^\dagger a_{k,0} + a_{-k,0}^\dagger a_{-k,0} \right) + nc_0 \left(a_{k,0}^\dagger a_{-k,0}^\dagger + a_{k,0} a_{-k,0} \right) \\
&+ (\varepsilon_k + q + nc_1) \left(a_{k,1}^\dagger a_{k,1} + a_{-k,1}^\dagger a_{-k,1} + a_{k,-1}^\dagger a_{k,-1} + a_{-k,-1}^\dagger a_{-k,-1} \right) \\
&+ nc_1 \left(a_{k,1}^\dagger a_{k,-1}^\dagger + a_{-k,1}^\dagger a_{k,-1}^\dagger + a_{k,1} a_{k,-1} + a_{-k,1} a_{-k,-1} \right) \Big\}.
\end{aligned} \tag{1.306}$$

In the polar phase, there exist fluctuations between the different momentum states of the two atoms in spin $|0\rangle$ and atoms of the spin $|1\rangle$ and $|-1\rangle$. We use the reduction of the Hamiltonian matrix [20] (See Section. 1.3) to obtain a 3-by-3 matrix to be diagonalized:

$$i\hbar \frac{d\vec{A}_k}{dt} = \underline{M}_k \vec{A}_k + \underline{N}_k \vec{A}_{-k}^* = \begin{pmatrix} [H, a_{k,1}] \\ [H, a_{k,0}] \\ [H, a_{k,-1}] \end{pmatrix}, \tag{1.307}$$

where

$$\vec{A}_k = \begin{pmatrix} a_{k,1} \\ a_{k,0} \\ a_{k,-1} \end{pmatrix}, \quad \vec{A}_{-k}^* \equiv \begin{pmatrix} a_{-k,1}^\dagger \\ a_{-k,0}^\dagger \\ a_{-k,-1}^\dagger \end{pmatrix}. \tag{1.308}$$

We calculate the commutations:

$$\begin{aligned}\left[\hat{H}, a_{k,0}\right] &= (\varepsilon_k + nc_0)\, a_{k,0} + nc_0 a^{\dagger}_{-k,0},\\ \left[\hat{H}, a_{k,1}\right] &= (\varepsilon_k + q + nc_1)\, a_{k,1} + nc_1 a^{\dagger}_{k,-1},\\ \left[\hat{H}, a_{k,-1}\right] &= (\varepsilon_k + q + nc_1)\, a_{k,-1} + nc_1 a^{\dagger}_{k,1}.\end{aligned} \tag{1.309}$$

Therefore, $\underline{M}_k$ and $\underline{N}_k$ matrices are:

$$\underline{M_k} = \begin{pmatrix} \varepsilon_k + q + nc_1 & 0 & 0 \\ 0 & \varepsilon_k + nc_0 & 0 \\ 0 & 0 & \varepsilon_k + q + nc_1 \end{pmatrix}, \tag{1.310}$$

$$\underline{N}_k = \begin{pmatrix} 0 & 0 & nc_1 \\ 0 & nc_0 & 0 \\ nc_1 & 0 & 0 \end{pmatrix}. \tag{1.311}$$

Then, $\underline{G}_k = (\underline{M}_k + \underline{N}_k)(\underline{M}_k - \underline{N}_k)$ becomes:

$$\underline{G}_k = \begin{pmatrix} (\varepsilon_k + q)\,(\varepsilon_k + q + 2nc_1) & 0 & 0 \\ 0 & \varepsilon_k\,(\varepsilon_k + 2nc_0) & 0 \\ 0 & 0 & (\varepsilon_k + q)\,(\varepsilon_k + q + 2nc_1) \end{pmatrix}. \tag{1.312}$$

The eigenvalues of the matrix $\underline{G}_k$ provide the Bogoliubov dispersions E_k^2 of each mode:

$$\begin{aligned}E_0 &= \sqrt{\varepsilon_k\,(\varepsilon_n + 2nc_0)},\\ E_{\pm 1} &= \sqrt{(\varepsilon_k + q)\,(\varepsilon_k + q + 2nc_1)}.\end{aligned} \tag{1.313}$$

Note that the two Bogoliubov modes that combine the excitations in spin $|1\rangle$ and $|-1\rangle$ yield the same dispersive behavior. The Bogoliubov mode that emerges through the momentum fluctuations among the same spin $|0\rangle$ particles yields another branch differing in both dispersion and LHY energy. The total LHY energy is:

$$E_{LHY} = E_{LHY,0} + E_{LHY,1} + E_{LHY,-1}, \tag{1.314}$$

where

$$E_{LHY,0} = \frac{1}{2}\sum_{\vec{k}} \left[\sqrt{\varepsilon_k\,(\varepsilon_k + 2nc_0)} - (\varepsilon_k + nc_0)\right], \tag{1.315}$$

$$E_{LHY,\pm 1} = \frac{1}{2}\sum_{k} \left[\sqrt{(\varepsilon_k + q)\,(\varepsilon_k + q + 2nc_1)} - (\varepsilon_k + q + nc_1)\right]. \tag{1.316}$$

However, both of these summations linearly diverge in k. A similar renormalization correction should be applied before the calculation of the LHY energy integral. Since the renormalization correction is due to the MF energy term $Vn^2c_0/2$, we need to find the second-order correction in the T-matrix treatment of the scattering process to the coupling constant c_0 [23]:

$$\begin{aligned} c_0 = \frac{g_0 + 2g_2}{3} &\approx \frac{g_0 + 2g_2}{3} + \frac{g_0^2 + 2g_2^2}{3V} \sum_{\vec{k}}{}' \frac{1}{2\varepsilon_k} \\ &\approx c_0 + \left(c_0^2 + 2c_1^2\right) \frac{1}{V} \sum_{\hat{k}}{}' \frac{1}{2\varepsilon_k}. \end{aligned} \tag{1.317}$$

Therefore, the MF energy is corrected as:

$$\frac{Vn^2c_0}{2} \approx \frac{Vn^2c_0}{2} + \frac{n^2c_0^2}{2} \sum_{\vec{k}}{}' \frac{1}{2\varepsilon_k} + \frac{2n^2c_1^2}{2} \sum_{\vec{k}}{}' \frac{1}{2\varepsilon_k} \tag{1.318}$$

We now distribute the last two sums in the renormalization energy into each Bogoliubov branch so that none diverges:

$$\begin{aligned} E_{LHY,0} &= \frac{1}{2} \sum_{\vec{k}} \left[\sqrt{\varepsilon_k \left(\varepsilon_k + 2nc_0\right)} - \left(\varepsilon_k + nc_0\right) + \frac{n^2c_0^2}{2\varepsilon_k} \right] \\ E_{LHY,\pm1} &= \frac{1}{2} \sum_{\vec{k}} \left[\sqrt{\left(\varepsilon_k + q\right)\left(\varepsilon_k + q + 2nc_1\right)} - \left(\varepsilon_k + q + nc_1\right) + \frac{n^2c_1^2}{2\varepsilon_k} \right] \end{aligned} \tag{1.319}$$

The energy integral becomes:

$$\begin{aligned} \varepsilon_{LHY,0} &= \frac{1}{(2\pi)^2} \int dk k^2 \left[\sqrt{\varepsilon_k \left(\varepsilon_k + 2nc_0\right)} - \varepsilon_k - nc_0 + \frac{\left(nc_0\right)^2}{2\varepsilon_k} \right] \\ &= \frac{1}{(2\pi)^2} \left(\frac{2Mc_0n}{\hbar^2} \right)^{3/2} c_0 n \underbrace{\int_0^\infty dx x^2 \left[\sqrt{x^2\left(x^2+2\right)} - x^2 - 1 + \frac{1}{2x^2} \right]}_{\frac{8\sqrt{2}}{15}} \\ &= \frac{n^2c_0}{2} \left[\frac{16}{15\pi^2} \frac{M^{3/2}}{\hbar^3} \sqrt{nc_0^3} \right] \end{aligned} \tag{1.320}$$

where the substitution of variables is executed by $\varepsilon_k \equiv c_0 n x^2 = \frac{\hbar^2 k^2}{2M}$. The form of the LHY energy for the spin $|0\rangle$ is the same as the single-component BECs. This is due to the fact that spin $|0\rangle$ atoms constitute their own Bogoliubov quasiparticles without any coupling with the other spin manifold. The LHY energies due to the other two

branches are identical:

$$\begin{aligned}
\varepsilon_{LHY,\pm 1} &\approx \frac{1}{(2\pi)^2}\int dk k^2 \\
&\times \left[\sqrt{(\varepsilon_k+q)\left(\varepsilon_k+q+2nc_1\right)}-\left(\varepsilon_k+q+nc_1\right)+\frac{\left(nc_1\right)^2}{2\varepsilon_k}\right] \\
&= \frac{1}{(2\pi)^2}\left(\frac{2Mc_1n}{\hbar^2}\right)^{3/2} c_1 n\int_0^\infty dx x^2 \\
&\times \left[\sqrt{(x^2+t)\left(x^2+t+2\right)}-\left(x^2+t+1\right)+\frac{1}{2x^2}\right] \\
&= \frac{c_1n^2}{2}\left(\frac{16}{15\pi^2}\frac{M^{3/2}}{\hbar^2}\sqrt{nc_1^3}\right) I(t)
\end{aligned} \tag{1.321}$$

where $\varepsilon_k = \frac{\hbar^2k^2}{2m} \equiv c_1 n x^2$ and $t \equiv \frac{q}{nc_1}$. The integral $I(t)$ is

$$I(t) \equiv \frac{15}{8\sqrt{2}}\int^\infty dx x^2\left[\sqrt{(x^2+t)\left(x^2+t+2\right)}-\left(x^2+t+1\right)+\frac{1}{2x}\right] \tag{1.322}$$

where $I(0) = 1$. $I(t)$ is a monotonically increasing function of t, which is proportional to the quadratic Zeeman energy. It means that the LHY energy for the polar phase is dependent on, and can be tuned by the parameter q. Note that this is not the case for the ferromagnetic order parameter.

The total interaction energy for the polar phase becomes [23]:

$$E_{0,p} = \frac{n^2c_0}{2}\left[1+\frac{16M^{3/2}}{15\pi^2\hbar^3}\sqrt{nc_0^3}\right]+\frac{16M^{3/2}}{15\pi^2\hbar^3}n^2c_1\sqrt{nc_1^3}I(t). \tag{1.323}$$

1.3.3.3 Anti-ferromagnetic Order

The order parameter in this regime is $\tau_{AF} = 1/\sqrt{2}(1\ 0\ 1)$. The magnetic properties of the condensate are:

$$\langle\vec{F}\rangle = 0, \langle F_z\rangle = 0, \left\langle F_z^2\right\rangle = 1. \tag{1.324}$$

The density and spin fluctuations become:

$$\hat{D}_k = \frac{1}{\sqrt{2}}\left(a_{k,1}+a_{k,-1}\right), \tag{1.325}$$

$$\hat{\vec{F}}_k = \hat{e}_z\frac{1}{\sqrt{2}}\left(a_{k,1}-a_{k,-1}\right)+\hat{e}_x a_{k,0}. \tag{1.326}$$

Then, the effective Hamiltonian becomes [23]:

$$\begin{aligned}
&\hat{H}_{eff,AF} = \frac{Vn^2c_0}{2} + qN \\
+ &\sum_{\vec{k}}{}^{>} \Big\{ (\varepsilon_k - q + nc_1) \left(a^\dagger_{k,0}a_{k,0} + a^\dagger_{-k,0}a_{-k,0} \right) + nc_1 \left(a^\dagger_{k,0}a^\dagger_{-k,0} + a_{k,0}a_{-k,0} \right) \\
+ &\left(\varepsilon_k + \frac{n\left(c_0+a_1\right)}{2} \right) \left(a^\dagger_{k,1}a_{k,1} + a^\dagger_{-k,1}a_{-k,1} + a^\dagger_{k,-1}a_{k,-1} + a^\dagger_{-k,-1}a_{-k,-1} \right) \\
+ &\frac{n\left(c_0+c_1\right)}{2} \left(a^\dagger_{k,1}a^\dagger_{-k,1} + a^\dagger_{k,-1}a^{-1}_{-k,-1} + a_{k,1}a_{-k,1} + a_{k,-1}a_{-k,-1} \right) \\
+ &\frac{n\left(c_0-c_1\right)}{2} \Big(a^\dagger_{k,1}a^\dagger_{k,-1} + a^\dagger_{k,-1}a^{-1}_{k,1} + a^\dagger_{-k,1}a_{-k,-1} + a^\dagger_{-k,-1}a_{-k,1} \\
&\qquad + a_{k,1}a_{-k,-1} + a^\dagger_{k,1}a^\dagger_{-k,-1} + a_{k,-1}a_{-k,1} + a^\dagger_{k,-1}a^\dagger_{-k,1} \Big) \Big\}. \qquad (1.327)
\end{aligned}$$

The corresponding commutation relations to find $\underline{M}_k$ and $\underline{N}_k$ matrices are:

$$\begin{aligned}
\left[\hat{a}_{k,1}, \hat{H} \right] &= \left(\varepsilon_k + \frac{n\left(c_0+c_1\right)}{2} \right) a_{k,1}, \\
&\quad + \frac{n\left(c_0+c_1\right)}{2} a^\dagger_{-k,1} + \frac{n\left(c_0-c_1\right)}{2} \left(a_{k,-1} + a^\dagger_{-k,-1} \right), \\
\left[\hat{a}_{k,-1}, \hat{H} \right] &= \left(\varepsilon_k + \frac{n\left(c_0+c_1\right)}{2} \right) a_{k,-1}, \\
&\quad + \frac{n\left(c_0+c_1\right)}{2} a^\dagger_{-k,-1} + \frac{n\left(c_0-c_1\right)}{2} \left(a_{k,1} + a^\dagger_{-k,1} \right), \\
\left[a_{k,0}, \hat{H} \right] &= \left(\varepsilon_k - q + nc_1 \right) a_{k,0} + nc_1 a^\dagger_{-k,0}. \qquad (1.328)
\end{aligned}$$

Then, the matrices $\underline{M}_k$ and $\underline{N}_k$ are found to be:

$$\underline{M}_k = \begin{pmatrix} \varepsilon_k + \frac{n(c_c+c_1)}{2} & \frac{n(c_0-c_1)}{2} & 0 \\ \frac{n(c_0-c_1)}{2} & \varepsilon_k + \frac{n(c_0+c_1)}{2} & 0 \\ 0 & 0 & \varepsilon_k - q + nc_1 \end{pmatrix}, \qquad (1.329)$$

$$\underline{N}_k = \begin{pmatrix} \frac{n(c_0+c_h)}{2} & \frac{n(c_0-c_1)}{2} & 0 \\ \frac{n(c_0-c_1)}{2} & \frac{n(c_0+c_1)}{2} & 0 \\ 0 & 0 & nc_1 \end{pmatrix}. \qquad (1.330)$$

The matrix $\underline{G}_k = (\underline{M}_k + \underline{N}_k)(\underline{M}_k - \underline{N}_k)$ becomes:

$$\underline{G}_k = \begin{pmatrix} \varepsilon_k \left(\varepsilon_k + n\left(c_0+c_1\right) \right) & \varepsilon_k n\left(c_0-c_1\right) & 0 \\ \varepsilon_k n\left(c_0-c_1\right) & \varepsilon_k \left(\varepsilon_k + n\left(c_0+c_1\right) \right) & 0 \\ 0 & 0 & \left(\varepsilon_k - q\right)\left(\varepsilon_k - q + 2nc_1\right) \end{pmatrix}.$$

The energy of the Bogoliubov modes can be found by finding the eigenvalues of the matrix $\underline{G}_k$ [20]:

$$E_{k,0} = \sqrt{(\varepsilon_k - q)\,(\varepsilon_k - q + 2nc_1)}, \tag{1.331}$$

$$E_{k,+1} = \sqrt{\varepsilon_k\,(\varepsilon_k + 2nc_0)}, \tag{1.332}$$

$$E_{k,-1} = \sqrt{\varepsilon_k\,(\varepsilon_k + 2nc_1)}, \tag{1.333}$$

where $q < 0$. The LHY energies can be calculated by the similar procedure shown in the previous subsection. The resulting total interaction energy is [23]:

$$\begin{aligned} E_0^{AF} = qn + \frac{n^2 c_0}{2}\left[1 + \frac{16M^{3/2}}{15\pi^2\hbar^3}\sqrt{nc_0^3}\right] \\ + \frac{8M^{3/2}n^2c_1}{15\pi^2\hbar^3}\sqrt{nc_1^3}\,(1 + I(t))\,, \end{aligned} \tag{1.334}$$

where $t = \frac{|q|}{nc_1}$.

1.4 Vortex Lattices in the Interacting Bose Condensates

The rotation of the superfluids shows peculiar phenomena compared to the classical fluids [7, 8]. The interesting phenomena emerge due to the coherent wavefunction of the Bose condensates [8]:

$$\Psi(\vec{r}) = |\Psi(\vec{r})|e^{i\phi(\vec{r})}, \tag{1.335}$$

where $\phi(\vec{r})$ is the phase of the condensate wavefunction. The momentum density of a quantum state with the wavefunction $\Psi(\vec{r})$ can be calculated by [8]:

$$\vec{j} = \frac{\hbar}{2i}\left(\Psi^*\boldsymbol{\nabla}\Psi - \Psi\boldsymbol{\nabla}\Psi^*\right). \tag{1.336}$$

The relation between the momentum density and superfluid velocity flow is [8]:

$$\vec{j} = mn\vec{v}. \tag{1.337}$$

The velocity field for the coherent condensate wavefunction is calculated as

$$\vec{v} = \frac{\hbar}{m}\nabla\phi(\vec{r}). \tag{1.338}$$

This formula implies that the condensate flow is irrotational $\nabla \times \phi = 0$ unless there exists a singularity in the phasor of the wavefunction, which can be attributed to a

zero density. In the existence of the phase singularities, the angular momentum can be carried through the vortex.

At the rapid rotation, the triangular vortex lattices are observed with more than 80 vortices [25]. The average vortex density can be approximately calculated for the rapidly rotating condensate. Consider the Hamiltonian of a condensate with N particles rotating with the angular frequency Ω in the rotating frame [8]:

$$\begin{aligned} H' =& H - \vec{\Omega} \cdot \vec{L} \\ =& \sum_{i=1}^{N} \left(\frac{\vec{p}_i^2}{2M} + V_{ext}\left(\vec{r}_i\right) - \vec{\Omega} \cdot \left(\vec{r}_i \times \vec{p}_i\right) \right) + U_0 \sum_{i<j} \delta\left(\vec{r}_i - \vec{r}_j\right) \\ =& \sum_{i=1}^{N} \left(\frac{\left(\vec{p}_i - M\Omega \times \vec{r}_i\right)^2}{2m} + V\left(\vec{r}_i\right) - \frac{M}{2}\left(\Omega \times \vec{r}_i\right)^2 \right) \\ & + U_0 \sum_{i<j} \delta\left(\vec{r}_i - \vec{r}_j\right). \end{aligned} \tag{1.339}$$

The first term is the kinetic energy of the rotating condensate in the rotating frame. This term should vanish for a classical fluid since the velocity field mimics a rotating rigid body with each particle having $\vec{v}_i = \vec{p}_i/M = \vec{\Omega} \times \mathbf{r}_i$. This field ensures $\vec{\nabla} \times \vec{v} = 2\Omega$ for any point in the fluid. However, the condensate velocity field cannot be in this form, because there needs to have singularities in the density profile. Therefore, a velocity field that approximates rigid-body rotation can be created by forming vortex lattices. If the number n_{v} of vortices per unit area in the plane perpendicular to Ω is uniform and equal to

$$n_{\mathrm{v}} = \frac{2m\Omega}{h} = \frac{1}{\pi a_\Omega^2}, \tag{1.340}$$

where $a_\Omega = \sqrt{\hbar/m\Omega}$ is the scale for the average intervortex distance.

The deviations from the classical fluid velocity profile are negligible for the condensates with many vortices [7, 8]. This can be understood by the following reasoning. Consider the rotational kinetic energy of the condensate as a whole: $M\Omega^2 R^2$, where R is the condensate radial size. The kinetic energy per particle due to the swirling motion around a vortex is around $\hbar^2/ma_\Omega^2 = \hbar\Omega = m\Omega^2 a_\Omega^2$. The ratio of the two energy scales yields $a_\Omega^2/R^2 \approx 1/N_v$, where N_v is the number of vortices. Therefore, as N_v increases, the swirling kinetic energy becomes relatively small with respect to

the rotation kinetic energy as a whole. This point will also be used to derive the GP equation for the coarse-grained density profile of the vortex lattices.

Now we first revisit the single particle Hamiltonian of a rotating neutral particle and the corresponding Landau levels. Then, the Jacobi-Theta formalism for the vortex lattices in the lowest Landau level regime is revisited [15, 16]. Finally, we present our results on the generalization of the Jacobi-Theta formalism to the vortex lattices with two vortices per unit cell.

1.4.1 Single Particle Hamiltonian under Rotation and Landau Levels

Consider a particle of mass M confined by the radial plane with the trapping frequency $w_\perp$. Assume the particle is rotated around the rotation axis $\hat{e_z}$. The Hamiltonian of the rotating particle in the rotating frame is given by [15]:

$$\hat{H} = \left(\frac{p_x^2}{2M} + \frac{1}{2} M \omega_\perp^2 x^2 + \frac{p_y^2}{2M} + \frac{1}{2} M \omega_\perp^2 y^2 \right) - \vec{\Omega} \cdot \hat{\vec{L}}, \tag{1.341}$$

where $\vec{L} = \hat{e}_z L_z = \hat{e}_z (x p_y - y p_x)$ is the angular momentum, and the $\vec{\Omega} = \hat{e}_z \Omega$ is the rotation frequency. Therefore, one can rewrite the Hamiltonian in terms of the position and momentum operators in 2D:

$$\hat{H} = \left(\frac{p_x^2}{2M} + \frac{1}{2} M \omega_\perp^2 x^2 + \frac{p_y^2}{2M} + \frac{1}{2} M \omega_\perp^2 y^2 \right) - \Omega (x p_y - y p_x). \tag{1.342}$$

The ladder operators for the 2D harmonic oscillator problem are [24]:

$$\begin{aligned}
a_x^\dagger &= \frac{1}{\sqrt{2\hbar M \omega_\perp}} \left(M \omega_\perp \hat{x} - i \hat{p}_x \right), \\
a_x &= \frac{1}{\sqrt{2\hbar M \omega_\perp}} \left(M \omega_\perp \hat{x} + i \hat{p}_x \right), \\
a_y^\dagger &= \frac{1}{\sqrt{2\hbar M \omega_\perp}} \left(M \omega_\perp \hat{y} - i \hat{p}_y \right), \\
a_y &= \frac{1}{\sqrt{2\hbar M \omega_\perp}} \left(M \omega_\perp \hat{y} + i \hat{p}_y \right).
\end{aligned} \tag{1.343}$$

The position and momentum operators in terms of the ladder operators are:

$$\hat{x} = \sqrt{\frac{\hbar}{2M\omega_\perp}}\left(a_x^\dagger + a_x\right), \tag{1.344}$$

$$\hat{p}_x = i\sqrt{\frac{\hbar M\omega_\perp}{2}}\left(a_x^\dagger - a_x\right), \tag{1.345}$$

$$\hat{y} = \sqrt{\frac{\hbar}{2M\omega_\perp}}\left(a_y^\dagger + a_y\right), \tag{1.346}$$

$$\hat{p}_y = i\sqrt{\frac{\hbar M\omega_\perp}{2}}\left(a_y^\dagger - a_y\right). \tag{1.347}$$

Writing the rotating single particle Hamiltonian (1.342) in terms of the ladder operators gives:

$$\begin{aligned}\hat{H} &= h\omega_\perp\left(a_x^\dagger a_x + \frac{1}{2} + a_y^\dagger a_y + \frac{1}{2}\right) - \Omega\left(xp_y - yp_x\right)\\ &= \hbar\omega_\perp\left(a_x^\dagger a_x + a_y^\dagger a_y + 1\right) + i\hbar\Omega\left(a_x^\dagger a_y - a_x a_y^\dagger\right).\end{aligned} \tag{1.348}$$

The modes a_x and a_y are coupled, i.e. $[\hat{H}, \hat{a}_x] \propto a_x, a_y$. Apply the following set of transformations:

$$\begin{aligned} b_x &= \tfrac{1}{\sqrt{2}}\left(a_x + ia_y\right) \quad b_y = \tfrac{1}{\sqrt{2}}\left(a_x - ia_y\right)\\ b_x^\dagger &= \tfrac{1}{\sqrt{2}}\left(a_x^\dagger - ia_y^\dagger\right) \quad b_y^\dagger = \tfrac{1}{\sqrt{2}}\left(a_x^\dagger + ia_y^\dagger\right).\end{aligned} \tag{1.349}$$

Here the operators b_i, where $i = x, y$ still obey the Bose commutation rules:

$$\left[b_i, b_j^\dagger\right] = \delta_{ij} \quad \text{and} \quad [b_i, b_j] = \left[b_i^\dagger, b_j^\dagger\right] = 0. \tag{1.350}$$

The ladder operators a_j in terms of b_j are written as:

$$a_x = \frac{1}{\sqrt{2}}\left(b_x + b_y\right) \quad a_y = \frac{i}{\sqrt{2}}\left(b_y - b_x\right) \tag{1.351}$$

$$a_x^\dagger = \frac{1}{\sqrt{2}}\left(b_x^\dagger + b_y^\dagger\right) \quad a_y^\dagger = -\frac{i}{\sqrt{2}}\left(b_y^\dagger - b_x^\dagger\right). \tag{1.352}$$

Replace the a_j operators in the Hamiltonian (1.348) by b_j operators:

$$\hat{H} = \hbar\omega_\perp + \hbar\left(\omega_\perp + \Omega\right)b_x^\dagger b_x + \hbar\left(\omega_\perp - \Omega\right)b_y^\dagger b_y. \tag{1.353}$$

The Hamiltonian in this form is diagonalized, and the two modes are controlled by the corresponding ladder operators b_x and b_y. The energy steps introduced by each mode are $\hbar\left(\omega_\perp + \Omega\right)$ and $\hbar\left(\omega_\perp - \Omega\right)$, respectively. The eigenenergies can be denoted by two quantum numbers n, and m with the eigenenergies $E_{n,m}$ are given by:

$$E_{n,m} = \hbar\omega_\perp + \hbar\left(\omega_\perp + \Omega\right)n + \hbar\left(\omega_\perp - \Omega\right)m, \tag{1.354}$$

where $n, m = 0, 1, ..$ Note that in the limit rotation frequency Ω approaches trapping frequency $\omega_\perp$, the states with the quantum number m become degenerate while the states n are separated by an energy difference $\sim 2\hbar\omega_\perp$ [15]. The eigen levels with different n are called Landau levels, and the level $n = 0$ is called the lowest Landau level (LLL). In the LLL state, there are still plenty of available quantum states, whose energy levels are slightly separated at the rapid rotation limit. This is an interesting point in the means that both Fermionic and Bosonic many-body systems can exhibit similar physical behavior regardless of the statistical nature of the particles. We denote the state in the nth Landau level, and mth orbital by $|n, m\rangle$. The lowest Landau levels are $|0, m\rangle$, where $m = 0, 1, 2, ...$ Note that the LLL states satisfy the following equation [15]:

$$b_x |0, m\rangle = 0, \tag{1.355}$$

whereas $|0, 0\rangle$ needs also to satisfy:

$$b_y |0, 0\rangle = 0. \tag{1.356}$$

Using these equations, one can derive the wavefunctions for the LLL states as follows:

$$\begin{aligned}
&(a_x + ia_y) |0, 0\rangle = 0 \\
&\left[m\omega_\perp x + ip_x + i\left(m\omega_\perp y + ip_y\right)\right] X(x)Y(y) = 0 \\
&\underbrace{\left(m\omega_\perp x + \frac{\hbar}{x}\frac{\partial X}{\partial x}\right)}_{-k} + i\underbrace{\left(m\omega_\perp y + \frac{\hbar}{Y}\frac{\partial Y}{\partial y}\right)}_{-ik} = 0 \\
&X(x) = e^{-\frac{m\omega_\perp x^2}{2\hbar}\frac{kx}{\hbar}}, Y(y) = e^{-\frac{m\omega_\perp y^2}{2\hbar}\frac{iky}{\hbar}} \\
&|0, 0\rangle \propto e^{-\frac{m\omega_\perp}{2\hbar}\left(x^2+y^2\right)} e^{-\frac{k}{\hbar}(x+iy)}
\end{aligned} \tag{1.357}$$

Applying also the condition $b_y |0, 0\rangle = 0$ yields:

$$|0, 0\rangle = \frac{1}{a_\perp\sqrt{2\pi}} e^{\frac{x^2+y^2}{2a_\perp^2}}, \tag{1.358}$$

where $a_\perp = \sqrt{\frac{\hbar}{M\omega_\perp}}$ is the harmonic oscillator length scale. We now apply the ladder operator $b_y^\dagger$ to calculate the other states in the LLL:

$$|0, m\rangle = (b_y^\dagger)^m |0, 0\rangle . \tag{1.359}$$

Noticing the ladder operation $b_y^\dagger |0,m\rangle = \sqrt{m+1}\,|0,m+1\rangle$ and $b_y^\dagger = \frac{1}{\sqrt{2}}\left(a_x^\dagger + i a_y^\dagger\right)$ yield the expression [15]:

$$|0,m\rangle = \frac{1}{a_\perp \sqrt{2\pi m!}} \left(\frac{x+iy}{a_\perp}\right)^m e^{-r^2/2a_\perp^2}, \tag{1.360}$$

where $r^2 = x^2 + y^2$ is the radial distance.

1.4.2 Infinite Perfect Lattices in the Lowest Landau Level: Single Vortex per Unit Cell

If the condensate is in the limit of rapid rotation $\tilde{\Omega} = \Omega/\omega_\perp \to 1$, and the interaction among the particles is sufficiently weak $gn_0 \ll 2\hbar\omega_\perp$, one can assume the rotating particles occupy either of the LLL states [26]:

$$u_{0,m} = |0,m\rangle \propto \left(\frac{x+iy}{a_\perp}\right)^m e^{-r^2/2a_\perp^2}. \tag{1.361}$$

Therefore, the condensate wavefunction $\Psi(\vec{r},z)$ can be expressed in terms of the superposition of the LLL eigenstates $u_{0,m}(\vec{r})$, and a density profile along $z-$axis [26]:

$$\Psi(\vec{r},z) = \sqrt{n_z(z)}\phi(\vec{r}), \tag{1.362}$$

where

$$\phi(\vec{r}) = \sum_m c_m u_{0,m}(\vec{r}) \propto \left(\sum_m c_m w^m\right) e^{-r^2/2a_\perp^2}. \tag{1.363}$$

Here $w \equiv \frac{x+iy}{a_\perp}$ is complex-valued space variable. This form of expression for the LLL state wavefunction is valuable to realize that the wavefunction is a polynomial function of a complex variable w of an order ν, where ν is the number of vortices in the condensate if all the vortices are single poled. Otherwise, the order of the polynomial is the number of the poles in total.

Note that the vortex positions are the points in space where the condensate density vanishes and the phase winds by an integer multiple of 2π. Therefore, one expects to find the zeros of the wavefunction, that defines the vortex lattice, at the locations of the vortices. The fundamental theory of algebra proves that any polynomial of order ν with complex number coefficients has a ν number of roots [16]. In our case, it physically means that the roots of the polynomial $\sum_m c_m w^m$ correspond to the location of

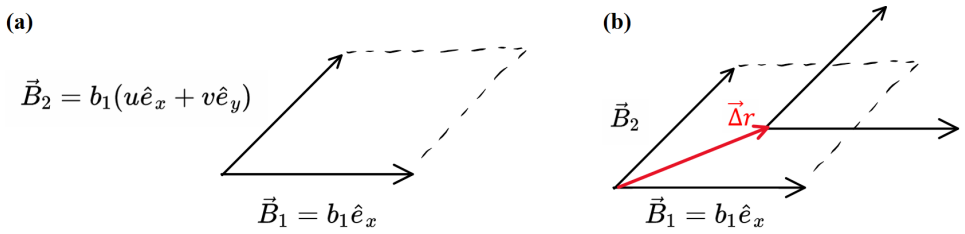

Figure 1.4: The geometry of the unit cells for (a) Single vortex per unit cell, (b) Double vortex per unit cell. The black arrows show the basis vectors, whereas the red arrow is the relative position vector of the two vortices inside the same unit cell.

the vortex center in the vortex lattice. Therefore, the vortex lattice wavefunction $\phi(\vec{r})$ can be written as [16]:

$$\phi(\vec{r}) \propto \prod_{\alpha=1}^{\nu}(w - w_\alpha) = \lambda\left[\prod_{\alpha}(w - w_\alpha)\right] e^{-r^2/2a_\perp^2}, \tag{1.364}$$

where w_α denotes the location of vortex with number α. If this is a representation of a perfect vortex lattice with the same unit cell throughout the whole condensate, the density profile of the lattice should satisfy a form [16]:

$$|\phi(\vec{r})|^2 \propto g(\vec{r}) = g(\vec{r} + \vec{R}) = \sum_{veck} g_{\vec{k}} e^{i\vec{K}\vec{r}}, \tag{1.365}$$

where $\vec{R} = n_1\vec{B}_1 + n_2\vec{B}_2$, and $\vec{B}_1$ and $\vec{B}_2$ are the basis vectors of the lattice. (See Fig. 1.4(a).) $\vec{K}$ is the reciprocal lattice vector. Without loss of generality, assume a unit cell in the form:

$$\begin{aligned} \vec{B}_1 &= b_1\hat{e}_x, \\ \vec{B}_2 &= b_1\left(u\hat{e}_x + v\hat{e}_y\right), \end{aligned} \tag{1.366}$$

and $v_c = b_1^2 v$ is the area of the unit cell. For instance, the parameters $u = 0$, and $v = 1$ create a perfect square lattice. $u = 1/2$ and $v = \sqrt{3}/2$ gives the triangular vortex lattice configuration. The corresponding reciprocal lattice vectors are:

$$\begin{aligned} &\vec{K}_1 = \frac{2\pi}{v_c}\vec{B}_2 \times \hat{e}_z, \vec{K}_2 = \frac{2\pi}{v_c}\hat{e}_z \times \vec{B}_1, \\ &\vec{K}_1 = \frac{2\pi b_1}{v_c}\left(-u\hat{e}_y + v\hat{e}_x\right), \vec{K}_2 = \frac{2\pi b_1}{v_c}\hat{e}_y, \\ &\vec{K} = m_1\vec{K}_1 + m_2\vec{K}_2 = \frac{2\pi b_1}{v_c}\left[m_1 v\hat{e}_x + (m_2 - m_1 u)\,\hat{e}_y\right], \\ &v_c|\vec{K}|^2 = \frac{(2\pi)^2}{v}\left[(m_1 v)^2 + (m_2 - m_1 u)^2\right]. \end{aligned} \tag{1.367}$$

To determine the Fourier coefficients $g_{\vec{K}}$ of the spatially periodic function $g(\vec{r})$, we consider the Jacobi-Theta function $\theta(\zeta,\tau)$ [15, 16]:

$$\theta(\zeta,\tau)=(-i)\sum_{n=-\infty}^{\infty}(-1)^n e^{i\pi\tau\left(n+\frac{1}{2}\right)^2}e^{i2\pi\zeta\left(n+\frac{1}{2}\right)}, \tag{1.368}$$

with quasiperiodic properties:

$$\begin{aligned}\theta(\zeta+1,\tau)&=\theta(\zeta,\tau),\\ \theta(\zeta+\tau,\tau)&=-e^{-i\pi(\tau+2\zeta)}\theta(\zeta,\tau).\end{aligned} \tag{1.369}$$

Choose $\zeta=\frac{x+iy}{b_1}$, $\tau=u+iv$ so that the periodicity of the vortex lattice is satisfied for the proposed unit cell. The θ function is quasiperiodic in the sense that the amplitude along the y-axis diverges due to the $-e^{-i\pi(\tau+2(x+iy))}$ term in the second property.

To obtain g_K, calculate $|\theta|^2$:

$$\begin{aligned}|\theta|^2=\theta\cdot\theta^*&=\left[\sum_{m=-\infty}^{\infty}(-1)^m\cdot e^{i\pi(u+iv)\left(m+\frac{1}{2}\right)^2}e^{i2\pi(\bar{x}+i\bar{y})\left(m+\frac{1}{2}\right)}\right]\\ &\times\left[\sum_{m'=-\infty}^{\infty}(-1)^{m'}e^{-i\pi(u-iv)\left(m'+\frac{1}{2}\right)^2}e^{-i2\pi(x-i\bar{y})\left(m'+\frac{1}{2}\right)}\right]\\ &=\sum_{m,m'}(-1)^{m+m'}e^{i\pi u(m-m')(m+m'+1)}e^{-\pi v\left[\left(m+\frac{1}{2}\right)^2+\left(m'+\frac{1}{2}\right)^2\right]}\\ &\quad\times e^{i2\pi\bar{x}(m-m')}e^{-2\pi y(m+m'+1)}.\end{aligned} \tag{1.370}$$

The double summation can be written as:

$$\begin{aligned}\sum_{m=-\infty}^{\infty}\sum_{m'=-\infty}^{\infty}&=\sum_{\substack{n=m-m'\\ \text{odd}}}\sum_{\substack{n'=m+m'+1\\ \text{even}}}+\sum_{\substack{n=m-m'\\ \text{even}}}\sum_{\substack{n'=m+m'+1\\ \text{odd}}}\\ &=\sum_{n=-\infty}^{\infty}\sum_{n'=-\infty}^{\infty}\left[1-(-1)^{n+n'}\right]\frac{1}{2}.\end{aligned} \tag{1.371}$$

Then, rewrite $|\theta|^2$ by summing over $n=m-m'$ and $n'=m+m'+1$:

$$\begin{aligned}|\theta|^2&=\sum_{n,n'}\frac{1}{2}\left[1-(-1)^{n+n'}\right](-1)^{n'-1}e^{i\pi unn'}e^{-\pi v\frac{n^2+n'^2}{2}}e^{i2\pi\bar{x}n}e^{-2\pi\bar{y}n'}\\ &=\sum_{n=-\infty}^{\infty}e^{i2\pi\bar{x}n}e^{-\pi v\frac{n^2}{2}}\sum_{n'=-\infty}^{\infty}\frac{(-1)^{n'-1}}{2}\left[1-(-1)^{n+n'}\right]e^{i\pi unn'}e^{-2\pi\bar{y}n'}e^{-\pi v\frac{n'^2}{2}}.\end{aligned} \tag{1.372}$$

Here $\frac{(-1)^{n'-1}}{2}\left[1-(-1)^{n+n'}\right] = \frac{(-1)^{n}}{2}\left[1-(-1)^{n^1+n}\right]$, therefore, $|\theta|^2$ becomes [15, 16]:

$$\begin{aligned}|\theta|^2 &= \sum_{n=-\infty}^{\infty}(-1)^n e^{i2\pi\bar{x}n}e^{-\pi v\frac{n^2}{2}}\sum_{n'=-\infty}^{\infty}\frac{1}{2}\left[1-(-1)^{n'+n}\right]e^{i\pi unn'}e^{-2\pi\bar{y}n'}e^{-\pi vn'^2/2}\\ &= \sum_{n=-\infty}^{\infty}(-1)^n e^{i2\pi\bar{x}n}e^{-\pi v\frac{n^2}{2}}L_n, \end{aligned} \tag{1.373}$$

where

$$L_n = \sum_{n'=-\infty}^{\infty}\frac{1}{2}\left[1-(-1)^{n'+n}\right]e^{i\pi unn'}e^{-2\pi\bar{y}n'}e^{-\pi vn'^2/2}. \tag{1.374}$$

To obtain a form of $|\theta|^2$ with an ingredient $e^{i\vec{K}\vec{r}}$, where $\vec{K}$ is the reciprocal vector in (1.367), apply the Poisson summation formula and rewrite L_n [15, 16]. Remember that a periodic function $f(x) = f(x+T_0)$ can be written as a Fourier sum:

$$f(x) = \sum_{n=-\infty}^{\infty}a_n e^{i2\pi f_0 nx}, \tag{1.375}$$

$$a_n = \frac{1}{T_0}\int_0^{T_0} f(x)e^{-i2\pi f_0 nx}dx, \tag{1.376}$$

where $T_0 = \frac{1}{f_0}$ is the period of the function. For a periodic train of impulses, the Fourier sum becomes:

$$\begin{aligned} f(x) &= \sum_{n=-\infty}^{\infty}\delta(x-nT),\\ a_n &= \frac{1}{T}\int_0^{T}\sum_{n=-\infty}^{\infty}\delta(x-nT)e^{-i\frac{2\pi}{T}nx}dx. \end{aligned} \tag{1.377}$$

Then, $a_n = 1/T$. Multiply both sides of the equation by a function $g(x)$ and integrate over the variable x:

$$\sum_{n=-\infty}^{\infty}g(nT) = \frac{1}{T}\sum_{k=-\infty}^{\infty}\int_{-\infty}^{\infty}g(x)e^{i\frac{2\pi}{T}kx}dx, \tag{1.378}$$

which is the Poisson summation formula [15].

Let's first evaluate summation L_n for different even-odd configurations of n and n'. If n is odd, only the even n' terms are non-zero. Similarly, if n is even, only the odd n' terms are non-zero. Consider both summation channels, and the function $g(x)$ with the periodicity $T = 2$ due to the even-odd parity of the summations:

$$g(x) = e^{i\pi unx}e^{-2\pi\bar{y}x}e^{-\pi v\frac{x^2}{2}}. \tag{1.379}$$

Use the integral formula:

$$\int_{-\infty}^{\infty} e^{-a^2x/2} e^{iJx} dx = \sqrt{\frac{2\pi}{a}} e^{-J^2/2a}, \tag{1.380}$$

with $a \equiv \pi v$ and $J \equiv \pi \left(um^2 + k + i2\bar{y} \right)$. We obtain for L_n [15, 16]:

$$L_n = \frac{1}{2} \sum_{k=-\infty}^{\infty} \sqrt{\frac{2}{v}} e^{i\pi k(n+1)} e^{-\frac{\pi}{2v}(un+k+i2\bar{y})}. \tag{1.381}$$

Therefore, $|\theta|^2$ becomes [15, 16]:

$$\begin{aligned} |\theta|^2 = \sum_{m_1,m_2} \quad & \frac{1}{2}\sqrt{\frac{2}{v}} (-1)^{m_1+m_2+m_1m_2} e^{i2\pi\bar{x}m_1} \\ & \times e^{-\pi v \frac{m_1^2}{2}} e^{-\frac{\pi}{2v}(m_1u+m_2)^2} e^{\frac{\pi}{2v}4\bar{y}^2} e^{-\frac{\pi}{v}2\bar{y}(m_1u+m_2)}. \end{aligned} \tag{1.382}$$

Remember the form of the reciprocal lattice vector $\vec{K}$ and $v_c|\vec{K}|^2$, one can rewrite the square of the Jacobi-Theta function as [15, 16]:

$$|\theta(\zeta,\tau)|^2 = \frac{1}{2} \left(\sum_{m_1,m_2} g_{\vec{K}} e^{i\vec{K}\vec{r}} \right) e^{2\pi\bar{y}/v}, \tag{1.383}$$

where

$$g_{\vec{k}} = \sqrt{\frac{2}{v}} (-1)^{m_1+m_2+m_1m_2} e^{-v_c|\vec{K}|^2/8\pi}. \tag{1.384}$$

Note that $|\theta|^2$ function includes a multiplication $e^{2\pi\bar{y}/v}$, which breaks the cylindrical symmetry. In this form, it does not exhibit a perfect spatial periodicity but only carries the positions of the vortices in a correct array. We need a further modification on the $|\phi(\vec{r})|^2$ function without losing the vortex lattice geometry provided by the $|\theta|^2$ function. This modification can be introduced by the following multiplication [15, 16]:

$$|\phi(\vec{r})|^2 = |\theta(\zeta,\tau)|^2 |h(\zeta)|^2 e^{-r^2/a_\perp^2}, \tag{1.385}$$

where $h(\zeta)$ is an entire function without any zeros. It should be entire to ensure that it is still a multiplicative term in the $\sum_m c_m w^m$ polynomial. It should be without zeros to ensure that the perfect lattice geometry provided by the Jacobi-Theta function is not distorted. The exponential function of ζ matches the above requirements:

$$h(\zeta) = e^{c_1\zeta + c_2\zeta^2}. \tag{1.386}$$

The density profile $|\phi(\vec{r})|^2$ becomes:

$$\begin{aligned} |\phi(\vec{r})|^2 &= \left(\sum_{\vec{K}} g_{\vec{K}} e^{i\vec{K}\vec{r}} e^{2\pi\bar{y}^{-2}/v^2}\right) \left| e^{c_1\bar{x}} e^{ic_1\bar{y}}\, e^{c_2\left(\bar{x}^2-\bar{y}^2\right)} e^{ic_2 2\bar{x}\bar{y}} \right| e^{-r^2/a_\perp^2} \\ &= e^{2\pi\bar{y}^2/v} e^{c_1\bar{x}} e^{c_2\bar{x}^2} e^{-c_2\bar{y}^2} e^{-r^2/a_\perp^2} \sum_{\vec{K}} g_{\vec{K}} e^{i\vec{K}\vec{r}}. \end{aligned} \tag{1.387}$$

To conserve the cylindrical symmetry around the origin:

$$c_1 = 0, \tag{1.388}$$

$$\frac{2\pi}{v_c} - c_2 = c_2. \tag{1.389}$$

Then, $c_2 = \pi/v_c$. Therefore, the density profile takes the form [15, 16]:

$$|\phi(\vec{r})|^2 = A \sum_{\hat{K}} g_{\vec{K}} e^{i\vec{K}\vec{r}} e^{-r^2/\sigma^2}, \tag{1.390}$$

where the condensate radius, harmonic oscillator length, and the unit cell area are related by:

$$\frac{1}{\pi\sigma^2} = \frac{1}{\pi a_\perp^2} - \frac{1}{v_c}. \tag{1.391}$$

Note that as the condensate radius approaches infinity, the length scale of the trapping harmonic oscillator and the intervortex spacing become on the same order of magnitude.

The normalization of the wavefunction $\int d^2\vec{r}|\phi(\vec{r})|^2 = 1$ gives the constant A:

$$A = \frac{1}{\pi\sigma^2} \frac{1}{\sum_{\vec{K}} g_{\vec{K}} e^{-|\vec{K}|^2\sigma^2/4}} \approx \frac{1}{\pi\sigma^2 g_{\vec{0}}}, \tag{1.392}$$

where the last approximation follows from the multiplication of $e^{-v_c\left|\vec{K}\right|^2/8\pi}$ in $g_{\vec{K}}$ and $e^{-|\vec{K}|^2\sigma^2/4}$ in the sum, in which only $|\vec{K}| = 0$ term can significantly contribute to the total summation, since $\pi\sigma^2 \gg v_c$ in the rapidly rotating limit. Therefore, the normalized condensate density profile is [15, 16]:

$$|\phi(\vec{r})|^2 = \frac{1}{\pi\sigma^2} \sum_{\vec{K}} \tilde{g}_{\vec{K}} e^{i\vec{K}\vec{r}} e^{-r^2/\sigma^2}, \tag{1.393}$$

where

$$\tilde{g}_{\vec{K}} = \frac{g_{\vec{K}}}{\sum_{\vec{K}} g_{\vec{K}} e^{-\frac{|\vec{K}|^2\sigma^2}{4}}} \simeq \frac{g_{\vec{K}}}{g_0}. \tag{1.394}$$

The form of the density function $|\phi(\vec{r})|^2$ is quite suitable to calculate the MF energy, which scales as $\propto |\phi(\vec{r})|^4$. However, the LHY energy requires an odd power $\propto |\phi(\vec{r})|^5 = |\phi(\vec{r})|^4|\phi(\vec{r})|$, which means that we need a formula also for $|\phi(\vec{r})|$.

Note that the periodic properties of the function $|\phi(\vec{r})|^2$ are also valid for the odd power $|\phi(\vec{r})|$, since the unit cell geometry and corresponding reciprocal lattices are exactly the same. Therefore, we can naively expect a form:

$$|\phi(\vec{r})| = \frac{1}{\sqrt{\pi\sigma^2}} e^{-r^2/2\sigma^2} \sum_{\vec{K}} \tilde{h}_{\vec{K}} e^{i\vec{K}\vec{r}}, \tag{1.395}$$

where $\tilde{h}_{\vec{K}}$ is the Fourier coefficients of the periodic and real function $|\phi(\vec{r})|$ such that $|\phi(\vec{r})|^2 = |\phi(\vec{r})||\phi(\vec{r})|$. This holds true if:

$$\sum_{\vec{K}} \tilde{g}_{\vec{K}} e^{i\vec{K}\vec{r}} = \sum_{\vec{K}',\vec{K}''} \tilde{h}_{\vec{K}'} \tilde{h}_{\vec{K}''} e^{i\left(\vec{K}'+\vec{K}''\right)\vec{r}}, \tag{1.396}$$

since for any $\vec{r}$, the equation $\vec{K} = \vec{K}' + \vec{K}''$ must be satisfied. Furthermore, this summation is a convolution of a 2-dimensional discrete function $\tilde{h}_{\vec{K}}$ by itself. In the form of indices m_1, m_2 that spans the reciprocal lattice vector $\vec{K} = m_1\vec{K}_1 + m_2\vec{K}_2$, the convolution sum can be written as:

$$\tilde{g}\left[m_1, m_2\right] = \sum_{m_3,m_4} \tilde{h}\left[m_3, m_4\right] \tilde{h}\left[m_1 - m_3, m_2 - m_4\right], \tag{1.397}$$

where $\tilde{g}\left[m_1, m_2\right] = (-1)^{m_1+m_2+m_1m_2} e^{-v_c|\vec{K}|^2/8\pi}$.

Remember the definition of discrete Fourier transform $X(w)$ of a 1-dimensional discrete function $x[n]$ and its properties [27]:

$$\begin{aligned} X(\omega) &= \sum_{n=-\infty}^{\infty} x[n] e^{j\omega n}, \\ x[n] &= \frac{1}{2\pi} \int_{-\pi}^{-\pi} X(\omega) e^{-j\omega n} d\omega. \end{aligned} \tag{1.398}$$

The self-convolution $y[n] = \sum_{n'} x\left[n'\right] x\left[n - n'\right]$ becomes a multiplication $Y(\omega) = X(\omega)X(\omega) = X^2(\omega)$ in the frequency domain. In our case, the formalism needs to be extended to 2-dimensions:

$$G\left(x, y\right) = \sum_{m_1,m_2} \tilde{g}\left[m_1, m_2\right] e^{ixm_1} e^{iym_2}. \tag{1.399}$$

Here $G(x,y) = H(x,y)^2$ where $H(x,y)$ is the discrete Fourier transform of $\tilde{h}[m_1, m_2]$:

$$\begin{aligned}\tilde{h}[m_1,m_2] &= \frac{1}{(2\pi)^2}\int_{-\pi}^{\pi}\int_{-\pi}^{\pi} dxdy H(x,y)e^{-ixm_1}e^{-iym_2} \\ &= \frac{1}{(2\pi)^2}\int_{-\pi}^{\pi}\int_{-\pi}^{\pi} dxdy \sqrt{G(x,y)}e^{-ixm_1}e^{-iym_2}, \end{aligned} \tag{1.400}$$

where

$$G(x,y) = \sum_{m_1,m_2} \tilde{g}[m_1,m_2]e^{ixm_1}e^{iym_2}. \tag{1.401}$$

Using equations (1.400) and (1.401), we can numerically find the $\tilde{h}_{\vec{K}}$ coefficients, and we reconstruct the function $|\phi(\vec{r})|$:

$$|\phi(\vec{r})| = \frac{1}{\sqrt{\pi\sigma^2}} e^{-r^2/2\sigma^2} \sum_{\vec{K}} \tilde{h}_{\vec{K}} e^{i\vec{K}\vec{r}}. \tag{1.402}$$

1.4.3 Infinite Perfect Lattices in the Lowest Landau Level: Two Vortices per Unit Cell

The Jacobi-Theta function formalism presented in the previous section implicitly assumes that there exists a single vortex per unit cell. This assumption is embedded in the form of the Jacobi-Theta function and its pole locations in the variable $\zeta = \bar{x} + i\bar{y}$. We generalize this formulation to the vortex lattices with two vortices per unit cell. Both vortices inside the unit cell have the same basis vectors defined as in the previous section:

$$\begin{aligned}\vec{B}_1 &= b_1\hat{e}_x, \\ \vec{B}_2 &= b_1\left(u\hat{e}_x + v\hat{e}_y\right),\end{aligned} \tag{1.403}$$

whereas the relative position vector between the vortices inside the same cell is (See Fig. 1.4(b).):

$$\Delta\vec{r} = \Delta x\hat{e}_x + \Delta y\hat{e}_y. \tag{1.404}$$

The new form of the wavefunction $\phi_2(\vec{r})$:

$$\begin{aligned}\phi_2(\vec{r}) &= \theta_1(\zeta,\tau)\theta_2(\zeta,\tau)h(\zeta)e^{-r^2/2a_\perp^2} \\ &= \underbrace{\theta(\zeta,\tau)}_{\text{Zeros on } \vec{R}_i}\underbrace{\theta\left(\zeta-\Delta x-i\Delta y,\tau\right)}_{\text{Zeros on } \vec{R}_i+\Delta\vec{r}} h(\zeta)e^{-r^2/2a_\perp^2},\end{aligned} \tag{1.405}$$

where $\zeta = \bar{x} + i\bar{y}$ and $\tau = u + iv$. Here $h(\zeta)$ is again an entire function without zeros, helping to normalize the diverging part of the Jacobi-Theta function. The density profile $|\phi_2(\vec{r})|^2$ gives:

$$|\phi_2(\vec{r})|^2 = |\theta(\zeta,\tau)|^2 \left|\theta\left(\zeta - \Delta x - i\Delta y, \tau\right)\right|^2 |h(\zeta)|^2 e^{-r^2/2a_\perp^2}, \tag{1.406}$$

where

$$|\theta(\zeta,\tau)|^2 = \frac{1}{v_c}\sum_{\vec{K}} g_{\vec{K}} e^{i\vec{K}\vec{r}} e^{\frac{2\pi y^2}{v_c}}, \tag{1.407}$$

$$|\theta(\zeta - \Delta x - i\Delta y, \tau)|^2 = \frac{1}{v_c}\sum_{\vec{K}} g_{\vec{K}} e^{i\vec{K}\vec{r}} e^{-i\vec{K}\Delta\vec{r}} e^{\frac{2\pi(y-\Delta y)^2}{v_c}}. \tag{1.408}$$

Assume an entire function $h(\zeta) = e^{c_1\zeta} e^{c_2\zeta^2}$, where $c_1 = c_{1,r} + ic_{1,i}$ is a complex variable and $c_2 \in \mathcal{R}$.

$$|h(\zeta)|^2 = e^{2c_{1,r}\bar{x} - 2c_{1,i}\bar{y}} e^{2c_2\left(\bar{x}^2 - \bar{y}^2\right)}. \tag{1.409}$$

In order for the density profile to have a cylindrical symmetry, the constraints on the coefficients are:

$$c_{1,r} = 0, \tag{1.410}$$

$$c_{1,i} = -\frac{2\pi\Delta y}{v_c}, \tag{1.411}$$

$$c_2 = \frac{\pi}{v}. \tag{1.412}$$

Then, the density function becomes:

$$|\phi_2(\vec{r})|^2 = Ae^{-r^2/\sigma^2} \sum_{\vec{K},\vec{K}'} g_K g_{K'} e^{i\vec{K}\vec{r}} e^{i\vec{K}'(\vec{r}-\Delta\vec{r})}, \tag{1.413}$$

where

$$\frac{1}{\sigma^2} = \frac{1}{a_\perp^2} - \frac{2\pi}{v_c}. \tag{1.414}$$

The condensate size σ expression differs from the case of the single vortex per unit cell by only a factor of 2 in the unit cell, which is expected since the recent formulation includes two vortices per unit cell.

Normalize $\phi_2(\vec{r})$ by the integration:

$$\begin{aligned}\int d^2\vec{r}|\phi_2(\vec{r})|^2 &= A\sum_{\vec{K},\vec{K}'} g_K g_{K'} e^{-i\vec{K}'\Delta\vec{r}} \underbrace{\int d^2\vec{r} e^{i(\vec{K}+\vec{K}')r} e^{-r^2/\sigma^2}}_{\pi\sigma^2 e^{-|\vec{K}+\vec{K}'|^2\sigma^2/4}} \\ &= A\pi\sigma^2 \sum_{\vec{K},\vec{K}'} g_K g_{K'} e^{-i\vec{K}'\Delta\vec{r}} e^{-|\vec{K}+\vec{K}'|^2\sigma^2/4}.\end{aligned} \tag{1.415}$$

Here only the terms with $|\vec{K}+\vec{K}'| = 0$ contribute to the summation. Since $g_{\vec{K}} = g_{-\vec{K}}$, the summation can be approximated as:

$$1 \approx A\pi\sigma^2 \sum_{\vec{K}} g_K^2 e^{-i\vec{K}'\Delta\vec{r}}. \tag{1.416}$$

Therefore, the density function becomes:

$$|\phi_2(\vec{r})|^2 = \frac{e^{-r^2/\sigma^2}}{\pi\sigma^2} \sum_{\vec{K},\vec{K}'} \hat{g}_K \hat{g}_{K'} e^{i\vec{K}\vec{r}} e^{-i\vec{K}'(\vec{r}-\Delta\vec{r})}, \tag{1.417}$$

where

$$\hat{g}_{\vec{K}} = \frac{g_{\vec{K}}}{\left(\sum_{\vec{K}''} g_{\vec{K}''}^2 e^{-i\vec{K}''\cdot\Delta\vec{r}}\right)^{1/2}}. \tag{1.418}$$

By applying a reasoning similar to the one vortex per unit cell formalism, we find the expression of $|\phi_2(\vec{r})|$:

$$|\phi_2(\vec{r})| = \frac{e^{-r^2/2\sigma^2}}{\sqrt{\pi\sigma^2}} \sum_{\vec{K},\vec{K}'} \hat{h}_{\vec{K}} \hat{h}_{\hat{K}'} e^{i\vec{K}\vec{r}} e^{i\vec{K}'(\vec{r}-\Delta\vec{r})}, \tag{1.419}$$

where

$$\hat{h}_k = \tilde{h}_k \frac{1}{\left(\sum_{\vec{K}} \left(\frac{g_k}{g_0}\right)^2 e^{-i\vec{K}\vec{r}}\right)^{1/4}}. \tag{1.420}$$

Now we are ready to calculate the kinetic and interact energy including both MF and LHY energies for both single and two vortex per unit cells (See Ch.5).

CHAPTER 2

BOSE MIXTURE DROPLETS

2.1 Theory of Bose Mixture Droplet

We discussed the mechanical stabilization of the attractive and repulsive single and two-component Bose condensates in Chapter 1.1. We concluded that the external traps can stabilize the repulsive and attractive BEC. In the latter case, the equilibrium is only metastable and there is an upper bound for the number of particles to exhibit this local minimum in the energy dependence on the cloud size. During the whole discussion, the system interaction is modeled by the MF picture, and the LHY corrections are neglected. Even though the LHY energy is experimentally demonstrated [14], it is only considered as negligible corrections to the physical observables, such as the pressure of the condensate.

We also concluded that the effective MF interaction energy is highly tunable for the Bose mixture such that the overall MF energy can be chosen to be slightly attractive. In this case, an obvious choice for stabilization might again be external confinement. However, it is also possible that sufficiently weak MF energy can be stabilized by the quantum fluctuations, i.e. repulsive LHY energy [1]. In this case, the stabilization can be realized without any external trap. This approach is interesting from two points of view. Firstly, mechanical stabilization without any external potential is never achieved in equilibrium conditions. Secondly, the LHY energy manifests itself as the key mechanism to the stabilization. Before it was only considered as neglected corrections.

From now on, this section summarizes the reasoning and formulation of the paper [1].

Let us discuss this argument more quantitatively. Consider the total interaction energy E_0 of the homogeneous Bose mixture, including both MF and LHY energies (See Chapter 1.2):

$$\begin{aligned} E_0 &= E_{MF} + E_{LHY,+} + E_{LHY,-}, \\ E_{MF} &= \frac{1}{2} g_{11} \frac{N_1^2}{V} + \frac{1}{2} g_{22} \frac{N_2^2}{V} + g_{12} \frac{N_1 N_2}{V} \qquad (2.1) \\ E_{LHY,\pm} &= \frac{\sqrt{2}V}{15\pi^2} \frac{m^{3/2}}{\hbar^3} (g_{11} n_1)^{5/2} \left[1 + \alpha \pm \sqrt{(1-\alpha)^2 + 4\beta} \right]^{5/2}, \qquad (2.2) \end{aligned}$$

where $\alpha = \sqrt{\frac{g_{22}}{g_{11}}}$, and $\beta = \frac{g_{12}^2 \sqrt{g_{11}}}{g_{11}^2 \sqrt{g_{22}}}$. If any mechanical stabilization is realized without an external trap, this will be firstly triggered by the collapse tendency of the MF energy. At the beginning of the collapsing behavior, the density is lower than the expected equilibrium density of the droplet. Hence, the ratio of the particles N_1/N_2 is approximately determined by the minimization of the MF energy. This analysis is already done in the Ch.1.2. We find that the MF interaction energy tends to lock the ratio :

$$\frac{N_1}{N_2} = \sqrt{\frac{g_{22}}{g_{11}}}. \qquad (2.3)$$

Rewrite $E_{0,MF}$ to emphasize the locked ratio, i.e. diagonalize the MF energy along this density scale:

$$\begin{aligned} E_{MF} &= \frac{1}{2V} \left(\sqrt{g_{11}} N_1 - \sqrt{g_{22}} N_2 \right)^2 + \sqrt{g_{11} g_{22}} \frac{N_1 N_2}{V} + g_{12} \frac{N_1 N_2}{V} \\ &= \left(\sqrt{g_{11} g_{22}} + g_{12} \right) \frac{N_1 N_2}{V} \qquad (2.4) \\ &= \delta g \frac{N_1 N_2}{V}, \end{aligned}$$

where $\delta g = \sqrt{g_{11} g_{22}} + g_{12}$. Note that we have the freedom to choose the MF energy $\propto \delta g$ to be negative while the LHY energy is repulsive. Assume $g_{11} > 0$ and $g_{22} > 0$, but $g_{12} < 0$, such that $\delta g \lesssim 0$. For this choice of parameters, the LHY energy contribution is always positive, i.e. repulsive. Hence, the MF energy $\propto n^2$ can trigger the collapse, but the LHY energy $\propto n^{5/2}$ can stop the collapsing density since it scales with a higher exponent on the condensate density n. Note that this analysis ignores the effect of kinetic energy, hence the spatial gradient of the density profile. A more careful treatment seems necessary to understand the stability mechanism for the finite droplets. However, this equilibrium mechanism seems obvious for the homogeneous infinite droplet since the approach only considers the MF and LHY interaction energies.

Before the quantitative analysis of the infinite droplet in equilibrium, we like to emphasize another theoretically interesting point. As shown in the lower panel of Fig. 1.2, when $|g_{12}| > \sqrt{g_{11}g_{22}}$, the long wavelength modes in one of the branches of the Bogoliubov modes, namely the soft mode due to a smoother profile, yields imaginary values [1]. This implies that these modes are unstable at least from the perspective of the Bogoliubov theory. Whether this instability is in the nature of the droplets so that it cannot be eliminated by any other contribution from higher-order terms or it is an artifact of treating the problem with the Bogoliubov theory so that other interacting many-body methods can resolve this instability is an interesting problem. In this line of research, there are various proposals to resolve the issue, including Bosonic pairing [28], Balieav damping [29]. In any case, the fundamental idea behind droplet stabilization is successfully captured by the Bogoliubov theory. From now on, we ignore the Bogoliubov mode with imaginary modes, assuming that this does not change the qualitative analysis, but only lacks small quantitative differences.

2.1.1 Infinite Bose Mixture Droplet

Let us now consider the equilibrium of the attractive MF and repulsive LHY energy for the homogeneous infinite Bose mixture condensate. Ignoring the LHY energy contribution from the Bogoliubov branch including the unstable modes, the total energy of the condensate becomes:

$$E_0 = E_{MF} + E_{LHY,+}, \tag{2.5}$$

where the MF and LHY energies are:

$$E_{MF} = \delta g \frac{N_1 N_2}{V}, \tag{2.6}$$

$$E_{LHY,+} = \frac{\sqrt{2}V}{15\pi^2}\frac{m^{3/2}}{\hbar^3}\left(g_{11}n_1\right)^{5/2}\left[1+\alpha+\sqrt{(1-\alpha)^2+4\beta}\right]^{5/2} \tag{2.7}$$

$$= \frac{\sqrt{2}V}{15\pi^2}\frac{m^{3/2}}{\hbar^3}\left(g_{11}n_1\right)^{5/2} h^{5/2}(\alpha,\beta), \tag{2.8}$$

where $h(\alpha,\beta) \equiv \left[1+\alpha+\sqrt{(1-\alpha)^2+4\beta}\right]$. The condition on the equilibrium is the absence of pressure for the infinite homogeneous system:

$$P = -\frac{\partial E_0}{\partial V} = -\frac{\partial\left(E_{MF}+E_{LHY}\right)}{\partial V} = 0, \tag{2.9}$$

where

$$
\begin{aligned}
-\frac{\partial E_{MF}}{\partial V} &= \delta g n_1 n_2 \\
-\frac{\partial E_{LHY}}{\partial V} &= \frac{\sqrt{2}}{10\pi^2}\frac{m^{3/2}}{\hbar^3}\left(g_{11}n_1\right)^{5/2} h^{5/2}(\alpha,\beta) \\
P = 0 &= n_1 n_2\left[\delta g + \frac{\sqrt{2}}{10\pi^2}\frac{m^{3/2}}{\hbar^3} g_{11}^{5/2} h^{5/2}(\alpha,\beta)\frac{n_1}{n_2}\sqrt{n_1}\right].
\end{aligned}
\tag{2.10}
$$

Note that the pressure contribution of the MF energy is compressive since $\delta g < 0$, whereas the LHY applies an effectively repulsive force. This creates the mechanism to equilibrate the collapsing condensate. This mechanism is only possible since the MF and LHY energy scales with the condensate density with a different power. Then the equilibrium density for the first component $n_{1,eq}$ becomes [1]:

$$
\sqrt{n_{1,eq}} = \frac{5\sqrt{2}\pi^2\hbar^3}{m^{3/2}}\frac{|\delta g|}{g_{11}^{5/2}h^{5/2}}\sqrt{\frac{g_{11}}{g_{22}}},
\tag{2.11}
$$

where $n_1/n_2 = g_{22}/g_{11}$ is used. Now use $g = \frac{4\pi a\hbar^2}{m}$ to rewrite the equilibrium density in terms of the scattering lengths:

$$
n_{1,eq} = \frac{25\pi}{32}\frac{a_{11}}{a_{22}}\frac{|\delta a|^2}{a_{11}^5 h^5(\alpha,\beta)}.
\tag{2.12}
$$

Note that $n_{1,eq} = \frac{n_{eq}\sqrt{a_{22}}}{\sqrt{a_{22}}+\sqrt{a_{11}}}$, where the total density of the droplet is $n_{eq} = n_{1,eq} + n_{2,eq}$. Then, n_{eq} becomes:

$$
n_{eq} = \frac{25\pi}{32}\frac{a_{11}}{a_{n2}}\frac{|\delta a|^2}{a_{11}^5 h^5}\frac{\sqrt{a_{11}}+\sqrt{a_{22}}}{\sqrt{a_{22}}},
\tag{2.13}
$$

where

$$
h \equiv 1 + \sqrt{\frac{a_{22}}{a_{11}}} + \sqrt{\left(1-\sqrt{\frac{a_{22}}{a_{11}}}\right)^2 + 4\frac{a_{12}^2}{a_{11}^2}\sqrt{\frac{a_{11}}{a_{22}}}}.
\tag{2.14}
$$

$\delta g \propto \delta a \lesssim 0$ implies $a_{12}^2 \sim a_{11}a_{22}$. Hence, the function h can be approximated as:

$$
h \simeq 2 + 2\sqrt{\frac{a_{22}}{a_{11}}} = 2\left(\frac{\sqrt{a_{11}}+\sqrt{a_{22}}}{\sqrt{a_{11}}}\right).
\tag{2.15}
$$

Then equilibrium density becomes:

$$
n_{eq} = \frac{25\pi}{1024}\frac{a_{11}}{a_{22}}\frac{|\delta a|^2}{a_{11}^{5/2}\sqrt{a_{22}}}\frac{1}{\left(\sqrt{a_{11}}+\sqrt{a_{22}}\right)^4},
\tag{2.16}
$$

where $n_{1,\text{eq}} = \frac{n_{eq}\sqrt{a_{22}}}{\sqrt{a_{22}}+\sqrt{a_{11}}}$ and $\frac{n_{2,\text{eq}}}{n_{1,\text{eq}}} = \sqrt{\frac{a_{11}}{a_{22}}}$. n_{eq} are functions of all three scattering lengths, allowing one to tune the equilibrium density at a fine scale.

This section discussed whether the competing interactions on the MF and LHY levels could result in a self-stable droplet phase for the infinite homogeneous binary Bose mixture. We conclude that the Bose mixture condensate can stabilize itself against the MF density collapse for the right choice of parameters. The parameters need to ensure the criteria that the MF energy coefficient $\propto \delta g$ is sufficiently small such that the equilibrium density is still in the weakly interacting regime of the condensate. Otherwise, the Bogoliubov analysis becomes insufficient to model the stabilizing behavior due to the violation of the assumption that the atoms mostly occupy the ground state of the single particle Hamiltonian.

The number of particles and the cloud size are limited for real experiments. Hence, the droplet theory also needs to account for the inhomogeneous, finite droplets with a surface. The following section discusses the theory of finite droplets by following [1].

2.1.2 Finite Bose Mixture Droplet

It requires a careful examination to pass from the analysis of infinite, homogeneous to finite-size, inhomogeneous droplets. Firstly, the MF and LHY interaction energies were calculated for the homogeneous gas, i.e. there is no spatial gradient in the density. So one needs to either motivate another approach to calculate the inhomogeneous condensate energy, which is analytically intractable in general, or find a regime in which the homogeneous energy expressions are approximately acceptable. Secondly, the equilibrium condition for the mixture droplets was derived in the absence of the kinetic energy. However, density gradient introduces kinetic energy. Therefore, one needs to extend the theoretical analysis to also account for the kinetic energy. In fact, as we will prove in this section, the effectively repulsive kinetic energy will play a significant role in the minimum number of particles required to obtain a droplet phase. Finally, the Bose mixture condensate consists of two components, which require two scalar fields for the component wavefunctions. This point also needs to be addressed by the finite droplet theory.

To resolve the issue of MF and LHY interaction energies of the inhomogeneous droplet, we apply the local density approximation (LDA) in which the droplet locally

exhibits a similar behavior to a homogeneous gas. Hence, the component densities n_1 and n_2 in the energy expression can be replaced by the local density operators $n_1(\vec{r}) = |\psi_1(\vec{r})|^2$ and $n_2(\vec{r}) = |\psi_2(\vec{r})|^2$, where $\psi_1(\vec{r})$ and $\psi_2(\vec{r})$ are the wavefunctions of the components. The MF and LHY energy density expressions become:

$$\varepsilon_{MF}(\vec{r}) \approx \frac{E_{MF}}{V} = \delta g n_1(\vec{r}) n_2(\vec{r}), \tag{2.17}$$

$$\varepsilon_{LHY}(\vec{r}) \approx \frac{E_{LHY,+}}{V} = \frac{\sqrt{2}}{15\pi^2}\frac{m^{3/2}}{\hbar^3}\left(g_{11} n_1(\vec{r})\right)^{5/2} h^{5/2}(\alpha,\beta), \tag{2.18}$$

where the interaction energies are now calculated by the following integrals:

$$E_{MF} = \int d^3\vec{r}\,\varepsilon_{MF}(\vec{r}), \tag{2.19}$$

$$E_{LHY} = \int d^3\vec{r}\,\varepsilon_{LHY}(\vec{r}). \tag{2.20}$$

To address the problem of the kinetic energy of the finite droplet due to the spatial gradient, we define the kinetic energy density functional consisting of both components:

$$\varepsilon_k(\vec{r}) = \frac{\hbar^2}{2m}\left[|\nabla\psi_1|^2 + |\nabla\psi_2|^2\right]. \tag{2.21}$$

Then, the total energy density functional and the total energy become:

$$\varepsilon(\vec{r}) = \varepsilon_k(\vec{r}) + \varepsilon_{MF}(\vec{r}) + \varepsilon_{LHY}(\vec{r}), \tag{2.22}$$

$$E = \int d^3\vec{r}\,\varepsilon(\vec{r}). \tag{2.23}$$

Lastly, we assume that the different components are totally in phase. Hence, the ratio between the densities of components is constant throughout the droplet. We call this assumption a 'locked-in' approximation since it implies that both components lock onto each other and write:

$$\frac{|\psi_1(\vec{r})|^2}{|\psi_2(\vec{r})|^2} = \frac{n_1}{n_2} = \sqrt{\frac{a_{22}}{a_{11}}}. \tag{2.24}$$

Now we are ready to express the total energy integral. We assume that intra-component scattering lengths are equal to each other, i.e. $a_{11} = a_{22} = a$. Then, $n_1/n_2 = 1$. This simplifies the problem algebraically, without losing the fundamental points of quantum droplet physics. In fact, the more general case $a_{11}/a_{22} \neq 1$ is also analytically tractable, but not more instructive than this approach. We non-dimensionalize the

problem with respect to the density scale of the infinite droplet in equilibrium, n_{eq}:

$$n_1(\vec{r}) = n_{eq}|\phi_1(\vec{r})|^2, \tag{2.25}$$

$$n_2(\vec{r}) = n_{eq}|\phi_2(\vec{r})|^2, \tag{2.26}$$

where $|\phi_1|^2 + |\phi_2|^2 = |\phi|^2$ and the total number of particles $\tilde{N} = \int d^3\vec{r}|\phi|^2$. For $a_{11} = a_{22}$, $h(\alpha, \beta) = 4$ and $n_1 = n_2 = n/2$. The equilibrium density becomes $n_{eq} = \frac{15\pi}{1024}\frac{|\delta a|^2}{16a^5}$. The interaction and kinetic energies are:

$$\varepsilon_{MF} = \frac{\delta g}{4} n_{eq}^2 |\phi|^4, \tag{2.27}$$

$$\varepsilon_{LHY} = \frac{8}{15\pi^2}\frac{m^{3/2}}{\hbar^3} g^{5/2} n_{eq}^{5/2} |\phi|^5, \tag{2.28}$$

$$\varepsilon_K = \frac{\hbar^2 n_{eq}}{2m}|\nabla\phi|^2. \tag{2.29}$$

Choose the energy scale of $\frac{1}{6}n_{eq}^2|\delta g|$ to simplify the expression in the governing equations, the total energy density becomes [1]:

$$\varepsilon = \frac{1}{6}n_{eq}^2|\delta g|\left[\frac{1}{2}|\tilde{\nabla}\phi|^2 - \frac{3}{2}|\phi|^4 + |\phi|^5\right], \tag{2.30}$$

where $\tilde{\nabla} = \frac{\partial}{\partial\tilde{r}}$ denotes the dimensionless space derivation, i.e. $\frac{\partial}{\partial r} = \frac{\partial}{\xi\partial\tilde{r}}$ and $\xi = \frac{4\sqrt{6}}{10\pi}\sqrt{\frac{a^5}{|\delta a|^3}}$ is the coherence length of the droplet. We replaced the expression for n_{eq} in the coefficient of the LHY energy to reduce it to 1. Remember that the normalization condition $\tilde{N} = \int d^3\tilde{r}|\phi|^2$ must be obeyed by the dimensionless wavefunction ϕ.

Let us now discuss the different regimes of the problem. We first note that the MF and LHY interaction energies scale with density as n^2 and $n^{5/2}$, respectively, whereas the kinetic energy $\propto n$ is a single particle operator. This dimensional analysis directly implies that the kinetic energy is negligible for sufficiently large particle numbers. This is the Thomas-Fermi (TF) regime. Indeed, in the thermodynamic limit $\tilde{N} \to \infty$, the droplet becomes homogeneous and reaches the equilibrium density of the infinite homogeneous droplet n_{eq}. For the finite particle numbers in the TF regime, the wavefunction of the droplet is expected to show a flat-top profile near the center and a rapid fall at the surface. However, the kinetic energy becomes relevant as $\tilde{N}$ decreases. For small $\tilde{N}$, effectively repulsive kinetic energy introduces a density gradient and the stabilization mechanism due to the different powers of the MF and

LHY energies is significantly affected. The condensate profile is expected to show a convex curvature even at the center. The droplet is still self-stabilized, but its density does not reach the TF equilibrium. In this weak droplet regime, the Gaussian ansatz can be useful to scale the energies and quantify the different regimes.

Assume the wavefunction of the isotropic droplet with radius $\tilde{R}$ to have a Gaussian form:

$$\phi(\tilde{r}) = Ae^{-\tilde{r}^2/2\tilde{R}^2}, \tag{2.31}$$

where A is the normalization constant found by the condition:

$$\iiint |\phi|^2 \tilde{r}^2 d\tilde{r} \sin\theta d\theta d\phi = \tilde{N}. \tag{2.32}$$

Use the integrals:

$$\begin{aligned} \int_0^\infty e^{-\frac{a}{2}x^2} x^2 dx &= \sqrt{\frac{\pi}{2}} \frac{1}{a^{3/2}}, \\ \int_0^\infty e^{-\frac{a}{2}x^2} x^4 dx &= \sqrt{\frac{\pi}{2}} \frac{3}{a^{5/2}}, \end{aligned} \tag{2.33}$$

to calculate the normalization constant A. The normalized wavefunction is:

$$\phi(\tilde{r}) = \frac{\sqrt{\tilde{N}}}{\left(\pi\tilde{R}^2\right)^{3/4}} e^{-\tilde{r}^2/2\tilde{R}^2}. \tag{2.34}$$

Use the normalized wavefunction to calculate the kinetic, MF, and LHY energies:

$$\begin{aligned} E_K &= \int d^3\tilde{r} \frac{1}{2} |\tilde{\nabla}\phi(\tilde{r})|^2 \\ &= \frac{1}{2} 4\pi \int d\tilde{r}\tilde{r}^2 \frac{\tilde{N}}{\left(\pi\tilde{R}^2\right)^{3/2}} \left[\frac{\partial}{\partial\tilde{r}} \left(e^{-\tilde{r}^2/2\tilde{R}^2}\right)\right]^2 \\ &= \frac{2\tilde{N}}{\sqrt{\pi}\tilde{R}^7} \int_0^\infty d\tilde{r}\tilde{r}^4 e^{-\tilde{r}^2/\tilde{R}^2} \\ &= \frac{3}{4} \frac{\tilde{N}}{\tilde{R}^2}. \end{aligned} \tag{2.35}$$

$$\begin{aligned} E_{MF} &= -\frac{3}{2} \int d^3\tilde{r} |\phi|^4 \\ &= -\frac{3}{2} 4\pi \int_0^\infty d\tilde{r}\tilde{r}^2 \frac{\tilde{N}^2}{\left(\pi\tilde{R}^2\right)^3} e^{-2\tilde{r}^2/\tilde{R}^2} \\ &= -\frac{3\sqrt{2}}{8\pi^{3/2}} \frac{\tilde{N}^2}{R^3}. \end{aligned} \tag{2.36}$$

$$
\begin{aligned}
E_{LHY} &= \int d^3\tilde{r}|\phi|^5 \\
&= \frac{4\tilde{N}^{5/2}}{\pi^{11/4}\tilde{R}^{15/2}} \int_0^\infty e^{-5\tilde{r}^2/2\tilde{R}^2}\tilde{r}^2 d\tilde{r} \\
&= \frac{2\sqrt{2}}{\pi^{9/4}5^{3/2}} \frac{\tilde{N}^{5/2}}{\tilde{R}^{9/2}}.
\end{aligned} \tag{2.37}
$$

We first note that the kinetic and LHY energies are effectively repulsive, whereas the MF energy is attractive. Furthermore, kinetic energy scales with $\propto \tilde{N}/\tilde{R}^2$, where as MF and LHY energies scale with $\propto -\tilde{N}^2/\tilde{R}^3$ and $\propto \tilde{N}^{5/2}/\tilde{R}^{9/2}$, respectively. This dimensional analysis supports the argument for the TF regime. As $\tilde{N}$ goes to infinity, the kinetic energy can be neglected, and a novel density scale emerges for the equilibrium density.

The total energy $E = E_K + E_{MF} + E_{LHY}$ as a function of the radius $\tilde{R}$ is shown for the number of particles $\tilde{N} = 200$ and $\tilde{N} = 20$. Expectedly, the greater number of particles implies that the kinetic energy is negligible, and the attractive MF energy is stabilized by the repulsive LHY energy. This creates a minimum in the energy vs. radius graph, as shown in Fig. 2.1. However, as $\tilde{N}$ decreases, the kinetic energy becomes relevant, and it effectively repulses the condensate. This firstly shifts the minimum of the energy to the lower cloud sizes. Then, the minimum of the energy functional disappears. This corresponds to the fact that there is a minimum number of particles below which the condensate can not self-stabilize, but rather expand to infinity. More quantitative approaches are possible to determine the critical particle number. The equation $\frac{\partial E}{\partial R} = 0$ can not give a real and finite root for the sufficiently low number of particles.

The Gaussian ansatz is useful for this problem in the weak droplet regime. For more general cases, we can obtain the extended GP equation for the droplet and numerically solve it to find the groundstate wavefunctions for different numbers of particles. The variational analysis yields the time-independent GP equation:

$$
\frac{\delta E - \mu\tilde{N}}{\delta\phi*} = 0, \tag{2.38}
$$

where $E = \int d^3\tilde{r}\varepsilon(\tilde{r})$ is the total energy, μ is the chemical potential of the droplet. This results in the extended GP equation:

$$
\mu\phi = -\frac{1}{2}\tilde{\nabla}^2\phi - 3|\phi|^2\phi + \frac{5}{2}|\phi|^3\phi. \tag{2.39}
$$

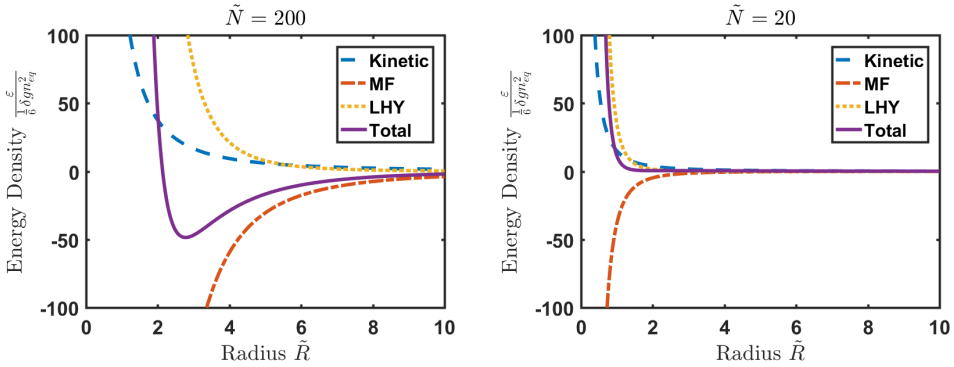

Figure 2.1: The kinetic, MF, LHY, and total energy densities of the Bose mixture for $\tilde{N} = 200$ (left panel) and $\tilde{N} = 20$ (right panel). The kinetic energy is negligible for the greater particle number, and the competing MF and LHY energies exhibit a global minimum. As $\tilde{N}$ decreases, the kinetic energy becomes comparable to the interaction energies. First, the energy's minimum shifts to a smaller radius length due to the decreasing $\tilde{N}$, then the local minimum disappears completely. Hence, there is a critical number of particles below which the droplet can not stabilize itself, and expands to infinity.

The numerical solutions of the extended GP equation are demonstrated in Fig (2.2) for different $\tilde{N}$ values. A Gaussian profile replaces the flat-top profile as the particle number decreases from 3000 to 20. The self-stabilization is evident for high $\tilde{N}$ values, where the limiting density of the condensate is slightly larger than n_{eq}, the equilibrium density of the infinite homogeneous droplet. The critical particle number of the system is around $\tilde{N} \sim 19$, below which there is no droplet phase as the ground state.

2.2 Bose Mixture Droplet Experiments

The Bose mixture droplets were experimentally realized by several groups after D. Petrov offered the theory in 2015 [1]. The droplets are realized for both homo- and heteronuclear binary mixtures. Here we discuss the experimental signatures of the droplets for the successful experiments in chronological order. Note that we only focus on the proof-of-the-concept experiments. Otherwise, the droplet experiments are also successfully completed for other theoretical and experimental purposes such

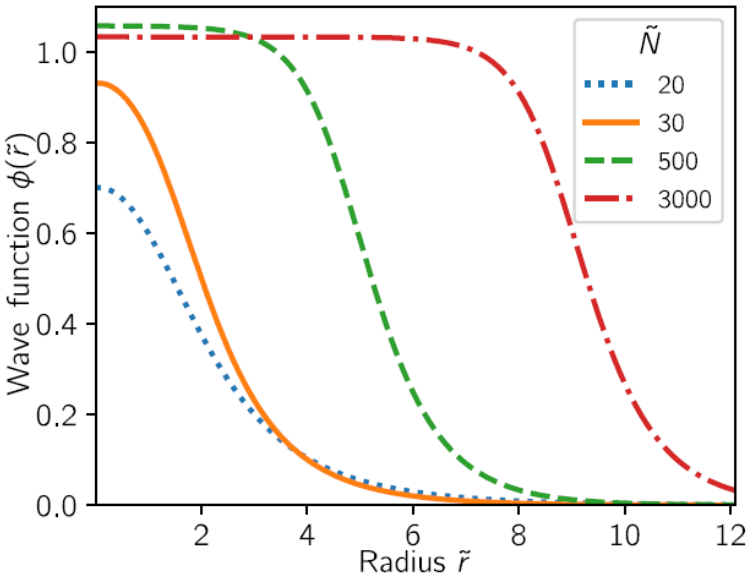

Figure 2.2: The numerical solutions to the extended GP equation (2.39) for different particle numbers. For sufficiently large $\tilde{N}$, the droplet profile approaches a flat-top shape, and its density converges to the equilibrium density of the infinite droplet. However, as the particle number decreases, the spatial gradient increases and the droplet expands to infinity below a critical number of particles.

as the collision of the self-bound droplets [30], bright soliton-to-droplet crossover [31], and near-cancellation of the MF energy [32].

2.2.1 ICFO Group

[3] conducted experiment on the mixture of the two hyperfine states $|1,-1\rangle$ and $||1,0\rangle$ of ^{49}K atoms with an initial number of atom around 25×10^3. A sufficiently weak trapping frequency along the direction of gravity $\omega_z/2\pi = 635Hz$ is chosen to compensate for the gravity, but the condensate is still in 3D. The mixture is first prepared within the miscible regime with $\delta a \sim 7a_0$. The balanced mixture is obtained and verified by the measurement of the spin compositions via Stern-Gerlach separation during the time-of-flight expansion. The repulsive δa is adiabatically turned into the attractive regime $\delta a < 0$. Then, the optical dipole trap which ensures the horizontal stability is switched off, and the time-of-flight (TOF) images are taken for different regimes: $\delta a > 0$, $\delta a < 0$, $a < 0$.

It is evident that if the intra-component interactions are attractive, the condensate exhibits a collapse instability in a relatively short time scale. Similarly, when $\delta a > 0$, the MF energy is dominated by the repulsive interactions, then the condensate expands when released. However, in the droplet phase $\delta a < 0$, the self-stable phase that sustains its profile for a considerable amount of time after the switch-off is evident, as shown in the middle row. In this case, the peak density of $n_0 \approx 2^1 4 atoms/cm^3$ is obtained, which is orders of magnitudes dilute than the classical liquids.

This experiment also studied the dependence of the critical number of particles N_c on the scattering length δa. It is shown [3] how the N_c changes with respect to δa. As evident from the results, the experimental results on the critical number of particles clearly deviate from the theoretical estimates. In fact, the droplets seem more sustainable than what Bogoliubov theory estimates, since N_c is lower than the predictions.

2.2.2 LENS Group

[33] also used the hyperfine states of ^{39}K atoms to obtain a homonuclear droplet. They first prepare the atoms in $|1, -1\rangle$ state with the initial number of particles around 4×10^5. The trapping frequencies are $\omega_x = 2\pi \times 195 Hz$, $\omega_y = 2\pi \times 180 Hz$, and $\omega_x = 2\pi \times 220 Hz$. Then, they apply an RF pulse for 10 microseconds to transfer half of the atoms to the state $|1, 0\rangle$. The laser beam along the $z-$axis is modulated with 4 kHz to achieve compensation towards the gravitational force. The mean-field parameter δa is tuned negative, then the condensate is released. A similar self-stabilizing behavior is also observed in this experiment.

2.2.3 Beijing Group

[34] realized the quantum droplets for a heteronuclear mixture of ^{23}Na and ^{87}Rb atoms, which are prepared in their lowest energy hyperfine states $|1, 1\rangle$. Both components have around 10^4 particles. They define dimensionless parameter $\tilde{\delta g} \equiv \frac{\delta g}{\bar{g}}$, where $\bar{g} = (g_{11} + g_{22})/2$. The theory predicts the observation of the droplet phase for $\tilde{\delta g} \in [-0.247, -0.110]$. They discuss the significance of adiabatic switching off of the trap potentials and claim that the droplet phase parameter regime for $\tilde{\delta g}$ is

narrower due to the perturbation introduced by the non-adiabatic switch off. They show in the TOF images that the condensate stays nearly the same for $\tilde{\delta g} \approx -0.173$. For $\tilde{\delta g} \approx +0.322$, the gas becomes repulsive in the MF regime, and the cloud size increases constantly.

CHAPTER 3

SPIN-1 AND RABI-COUPLED DROPLETS

3.1 Spin-1 Droplets

The droplets with self-stabilization due to the quantum fluctuations have been realized in the binary Bose mixture and dipolar condensates experiments. Here we consider spin-1 Bose condensates as another potential candidate for a droplet phase. We find that the actual spin fluctuations yield self-trapped states for two different magnetic orders, in which the mean-field picture predicts collapse. Polar ground states can be stabilized for the full regime of te spin-dependent coupling, whereas the antiferromagnetic ground state requires a negative quadratic Zeeman energy for the stabilization. Interestingly, The LHY energy of the spin-1 gas can be varied by the external free parameter of quadratic Zeeman coupling. It can provide a novel mechanism to independently set the comparative strength of LHY energy. We also explore the required parameters for experimentally achieving spin-1 droplets.

Bose-Einstein condensates (BECs) have commonly been described using the Gross-Pitaevskii mean-field (MF) approach to explain various experimental findings. The MF theories of interacting BECs offer a reasonable quantitative agreement and a qualitative understanding of complex phenomena, including the dynamics of condensate collapse or expansion, collective modes, bright and dark solitons, and the shift of critical temperature due to interactions [5, 7, 8, 35–38]. The Bogoliubov theory, which calculates the quantum fluctuations beyond the Gross-Pitaevskii mean-field, introduces additional processes, such as the scattering of two atoms in the condensate to states with momenta $\mathbf{p}$ and $-\mathbf{p}$. Experimental verification of these quantum fluctuations is achieved by measuring condensate excitations[14, 39], revealing deviations

from the MF predictions in terms of energy dispersion and non-condensate depletion. However, a more remarkable demonstration of quantum fluctuations is recently observed in self-bound Bose droplets[1, 3, 4].

The conventional repulsively interacting Bose-Einstein condensates (BECs) are stabilized and prevented from expanding through confinement using magnetic or optical traps [7], as discussed in Ch.1.1. In the case of attractive interactions, higher densities become energetically favorable. I causes the collapse of the gas into a high-density non-trapped phase, unless a metastable state like a bright soliton exists [40]. The key innovation in the self-bound droplets lies in utilizing quantum fluctuations to establish mechanically stable BECs in a regime where mean-field theories predict collapse. This stability can be achieved without violating the diluteness assumption for the gas, as long as distinct physical parameters govern the mean-field interaction energy and the quantum fluctuation contribution [1].

Recent experiments have successfully created two types of ultracold droplets: binary mixture droplets [3, 33, 41] and dipolar droplets [4, 42]. These droplets demonstrate adjustable competitions among different interactions and relatively weak Lee-Huang-Yang (LHY) corrections, which can stabilize the residual mean-field (MF) energy. In the case of dipolar droplets, long-range and short-range interactions compete at the MF level, and the LHY correction is a function of the short-range interaction. In the binary mixture droplets, the interspecies and intraspecies short-range interactions determine both MF and LHY energies. Interestingly, the set of free parameters is sufficient to tune the MF and LHY energies independently. In binary mixture droplets, the MF interaction energy is determined by parameters related to s-wave scattering lengths, where $a_{11} > 0$ and $a_{22} > 0$ represent intraspecies interactions and $a_{12} < 0$ represents interspecies interactions. The residual MF interaction is proportional to $n^2\delta a$, with $\delta a = -|a_{12}| + \sqrt{a_{11}a_{22}}$. When δa is negative, the MF energy favors higher densities, leading to potential collapse. However, the presence of the LHY interaction energy, expressed as $(a_+ n)^{5/2}$, where $a_+ > 0$ is the effective scattering length for quantum fluctuations [1], increases rapidly with density and effectively prevents collapse. As long as the equilibrium density obeys the diluteness assumption of the Bogoliubov theory, an ultra-dilute, yet liquid-like self-bound droplet can form.

The experimental findings concerning binary mixture droplets in both homonuclear [3, 33] and heteronuclear [41] systems are reasonably consistent with theories based on the Gross-Pitaevskii approximation with local Lee-Huang-Yang (LHY) corrections. However, there is a need for a deeper understanding of the droplet states for two primary reasons. Firstly, achieving better quantitative agreement with experimental data is necessary [3, 28]. Secondly, these systems present an opportunity to test the validity of various theoretical proposals in the field of quantum many-body physics. For instance, the stability of soft Bogoliubov modes in the theory of binary mixture droplets has been a subject of interest [28, 43]. Some recent studies suggest that these modes can be stabilized due to exotic many-body effects like bosonic pairing [28] or beyond LHY contributions [29, 44]. However, other theories ignore these effects, claiming that any instability would occur at such a slow rate that it might not be observed in experiments. By expanding the range of droplets [45–49] and introducing new stabilization mechanisms, novel phenomena may emerge, and improve our understanding of droplet theories even further.

In this part of the thesis, we explore the spin-1 Bose-Einstein condensate (BEC) gas as a potential candidate for creating self-bound droplets. We demonstrate that spin fluctuations can stabilize both the polar and antiferromagnetic phases of the spin-1 gas in a parameter range where the mean-field (MF) theory predicts collapse. It's worth noting that altering the s-wave scattering lengths of spinor gases using standard Feshbach resonances is not possible [50–52]. However, there are promising proposals, such as optical Feshbach resonances [53, 54], which might provide new avenues for tuning the gas into the droplet regime in future experiments. As more atom species are cooled to ultracold temperatures, it becomes crucial to investigate hyperfine manifolds with unstable mean-field ground states and explore the possibility of stable self-bound droplets. Whether achieved by controlling the scattering lengths or through naturally occurring scattering lengths in certain hyperfine manifolds, a droplet stabilized with spin fluctuations can offer additional means to study the nature of beyond-mean-field equilibrium. The LHY energy can be independently tuned by the external free parameter, namely the quadratic Zeeman energy. This is interesting because the effect of LHY energy on the stable phases can be examined more in detail.

We investigate a Bose-Einstein condensate (BEC) composed of spin-1 atoms, where s-wave interactions are present, and the system is subjected to a uniform and static magnetic field aligned with the z-axis. We assume a low dipolar relaxation rate, preserving the total magnetization along the z-axis. By setting this conserved magnetization to zero and excluding the linear Zeeman terms from the Hamiltonian, we focus on considering the effects of the quadratic Zeeman energy q in the system. in [22, 23]. The Hamiltonian is given by

$$\begin{aligned}\hat{H} \quad &= \int d\mathbf{x}\ \hat{\Psi}_m^\dagger(\mathbf{x}) \left(-\frac{\hbar^2\nabla^2}{2M} + qm^2\right) \hat{\Psi}_m(\mathbf{x}) \\ &+\frac{c_0}{2}\int d\mathbf{x}\ \hat{\Psi}_m^\dagger(\mathbf{x})\hat{\Psi}_{m'}^\dagger(\mathbf{x})\hat{\Psi}_{m'}(\mathbf{x})\hat{\Psi}_m(\mathbf{x}) \\ &+\frac{c_1}{2}\int d\mathbf{x}\ \hat{\Psi}_m^\dagger(\mathbf{x})\hat{\Psi}_{m'}^\dagger(\mathbf{x})\ \mathbf{F}_{mn}\cdot\ \mathbf{F}_{m'n'}\hat{\Psi}_{n'}(\mathbf{x})\hat{\Psi}_n(\mathbf{x}),\end{aligned} \tag{3.1}$$

where $\hat{\Psi}_m^\dagger(\mathbf{x})$ and $\hat{\Psi}_m(\mathbf{x})$ are creation and annihilation operators of spin-1 atoms with the magnetic quantum number m, $\mathbf{F}_{mm'} = (F^x_{mm'}, F^y_{mm'}, F^z_{mm'})$ are the set of spin-1 matrices, represented in the basis of z-axis eigenstates, and the repeated indices imply the summation over -1, 0 and 1. Density and spin coupling constants, c_0 and c_1, are written as $c_0 = (g_0 + 2g_2)/3$ and $c_1 = (g_2 - g_0)/3$. Here, g_0 and g_2 are the bare coupling constants of the s-wave collisions of two spin-1 bosons with total spin-0 and 2, which are given in terms of the corresponding scattering lengths $a_{0,2}$ as $g_{0,2} = 4\pi a_{0,2}\hbar^2/M$. To eliminate the ultraviolet divergence in the beyond-mean-field energy, we apply standard T-matrix perturbation up to the second order to renormalize the bare coupling constants $g_{0,2}$. It is important to mention that the strength of the quadratic Zeeman energy q can be modified using either static magnetic fields or RF (radio frequency) pulses [55, 56].

Using Bogoliubov theory, we replace the operators $\hat{a}_{\mathbf{0},m}$ with the c-numbers $\sqrt{N_0}\tau_m$ and keep the terms with $\hat{a}_{\mathbf{k}\neq\mathbf{0},m}$ and $\hat{a}^\dagger_{\mathbf{k}\neq\mathbf{0},m}$ up to the second order, where N_0 is the number of particles in the $\mathbf{k} = 0$ state, τ is the ground state order parameter in the spin-1 manifold and $\hat{a}_{\mathbf{k},m}$ are the Fourier components $\hat{\Psi}_m(\mathbf{x}) = V^{-1/2}\sum_{\mathbf{k}}\hat{a}_{\mathbf{k},m}e^{i\mathbf{kx}}$.

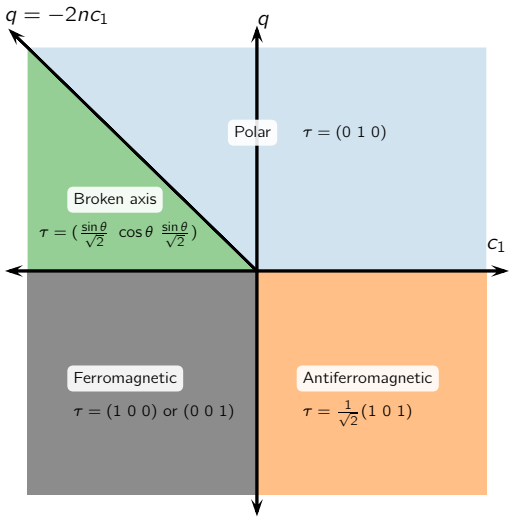

Figure 3.1: A graphical representation of the phase diagram for a spin-1 Bose condensate is provided, with the quadratic Zeeman shift q and spin-spin interaction c_1 as variables, while the linear Zeeman energy p is set to zero.

Then, the effective Bogoliubov Hamiltonian for spin-1 Bose gas becomes [23]:

$$\begin{aligned}\hat{H}_{eff} = \quad & \frac{Vn^2}{2}(c_0 + c_1\langle\mathbf{F}\rangle^2) + qN\langle F_z^2\rangle \\ & + \sum_{\mathbf{k}\neq\mathbf{0}} \Big\{ \left[\epsilon_{\mathbf{k}} - nc_1\langle\mathbf{F}\rangle^2 + qm^2 - q\langle F_z^2\rangle\right] \hat{a}^\dagger_{\mathbf{k},m}\hat{a}_{\mathbf{k},m} \\ & + nc_1\langle\mathbf{F}\rangle\cdot\mathbf{F}_{mm'}\hat{a}^\dagger_{\mathbf{k},m}\hat{a}_{\mathbf{k},m'} \\ & + \frac{nc_0}{2}(2\hat{D}^\dagger_{\mathbf{k}}\hat{D}_{\mathbf{k}} + \hat{D}_{\mathbf{k}}\hat{D}_{-\mathbf{k}} + \hat{D}^\dagger_{\mathbf{k}}\hat{D}^\dagger_{-\mathbf{k}}) \\ & + \frac{nc_1}{2}(2\hat{\mathbf{F}}^\dagger_{\mathbf{k}}\hat{\mathbf{F}}_{\mathbf{k}} + \hat{\mathbf{F}}_{\mathbf{k}}\hat{\mathbf{F}}_{-\mathbf{k}} + \hat{\mathbf{F}}^\dagger_{\mathbf{k}}\hat{\mathbf{F}}^\dagger_{-\mathbf{k}})\Big\}, \end{aligned} \tag{3.2}$$

where $\epsilon_{\mathbf{k}} = \hbar^2\mathbf{k}^2/2M$ is the free particle dispersion, $\langle\mathbf{F}\rangle \equiv \sum_{m,m'}\mathbf{F}_{mm'}\tau^*_m\tau_{m'}$ is the expectation value of the spin-1 order parameter, $\hat{D}_{\mathbf{k}} \equiv \sum_m \tau^*_m\hat{a}_{\mathbf{k},m}$ and $\hat{\mathbf{F}}_{\mathbf{k}} \equiv \sum_{m,m'}\mathbf{F}_{mm'}\tau^*_m\hat{a}_{\mathbf{k},m'}$ are the density and spin fluctuation operators, respectively. The first line in (3.2) represents the MF energy functional of the spin-1 BEC

$$\frac{E_{\rm MF}}{V} = \quad \frac{n^2}{2}(c_0 + c_1\langle\mathbf{F}\rangle^2) + qn\langle F_z^2\rangle, \tag{3.3}$$

where the remaining terms in the summation account for quantum fluctuations. Unlike Bose-Bose mixtures, the quantum fluctuations in spinor gases involve not only pseudo-spin labeling of different components but actual spin fluctuations. The minimization of the spinor MF functional (3.3) reveals a wide range of magnetic orders

and quantum phase transitions in spin-1 systems [22], which are briefly summarized below for completeness. A schematic phase diagram is presented in Fig. 3.1. For $c_1 < 0$ and $q < 0$, the MF ground state exhibits ferromagnetism with two possible order parameters: $\tau^{\mathrm{F}} = (1\ 0\ 0)$ or $(0\ 0\ 1)$. This results in $\langle \mathbf{F} \rangle^2 = 1$ and $\langle F_z^2 \rangle = 1$. For $c_1 < 0$ and $q > 0$, the ground state depends on the magnitude of q: If $q > 2|c_1|n$, the order parameter becomes $\tau^{\mathrm{P}} = (0\ 1\ 0)$ known as the polar phase, and if $0 < q < 2|c_1|n$ the order parameter becomes $\tau^{\mathrm{BA}} = (\sin\theta/\sqrt{2}\ \cos\theta\ \sin\theta/\sqrt{2})$ where $\sin\theta = \sqrt{1/2 - q/(4|c_1|n)}$. This is referred as the broken-axisymmetric phase. When $c_1 > 0$ and $q > 0$, MF energy is minimized with the polar order parameter τ^{P} again. Finally, for $c_1 > 0$ and $q < 0$, the antiferromagnetic phase is obtained with order parameter $\tau^{\mathrm{AF}} = (1\ 0\ 1)/\sqrt{2}$.

Let us now examine the mechanical instabilities for all the mean-field phases. In the ferromagnetic phase, where $\langle \mathbf{F} \rangle^2 = 1$ and $\langle F_z^2 \rangle = 1$, the MF energy density can be expressed as $n^2(c_0 + c_1)/2 + qn$. This indicates a potential density collapse if $c_0 + c_1 \equiv g_2 < 0$. Conversely, for $g_2 > 0$, the perpetual expansion would occur, requiring the presence of a confining potential [23].

In the ferromagnetic phase, a uniform condensate can host either $m = 1$ or $m = -1$ spin states, with the constraint of the conservation of total magnetization along the z-axis. Consequently, two spin-1 bosons, each having $m = 1$ (or $m = -1$), can only scatter in a single collision channel with a total spin of 2. As a result, the ferromagnetic spin-1 gas behaves like a single-component BEC, and the well-known Lee-Huang-Yang (LHY) energy contributes to the total beyond-mean-field energy

$$\frac{E_0^F}{V} = qn + \frac{2\pi\hbar^2 n^2}{M} a_2 \left(1 + \frac{128}{15\sqrt{\pi}} \sqrt{n a_2^3}\right), \tag{3.4}$$

which is expressed in terms of scattering length a_2 for convenience. Note that the mean-field (MF) collapse with $g_2 \propto a_2 < 0$ cannot be prevented by the Lee-Huang-Yang (LHY) term, which also involves the same overall factor a_2. As a result, the LHY energy cannot serve as a stability mechanism for the spinor gas in the ferromagnetic phase [23].

Additionally, it is worth noting that the LHY correction for the ferromagnetic order remains unaffected by the quadratic Zeeman energy. A similar analysis conducted for the broken-axisymmetric phase reveals that droplet formation is not feasible since

both the mean-field and LHY terms are governed by the same parameter.

Consider the polar phase with $c_1 > 0$ and $q > 0$ (first quadrant in Fig. 3.1), which has the order parameter $\tau^P = (0\ 1\ 0)$ and the MF ground state energy $E^P_{MF} = Vn^2c_0/2$ resulting in a density collapse for $c_0 < 0$. Including the LHY corrections, the total ground state energy becomes for $c_1 > 0$ and $q > 0$ [23]:

$$\frac{E_0^P}{V} = \frac{n^2 c_0}{2}\left[1 + \alpha\sqrt{nc_0^3}\right] + \alpha n^2|c_1|\sqrt{n|c_1|^3}I(t), \tag{3.5}$$

where $\alpha = 16\sqrt{M^3}/15\pi^2\hbar^3$, $t \equiv q/n|c_1| = |q|/n|c_1|$ since $q > 0$, and

$$\begin{aligned} I(t) &\equiv -\frac{15}{8\sqrt{2}}\int_0^\infty dx\, x^2 \\ &\times\left(x^2 + t + 1 - \sqrt{(x^2+t)(x^2+t+2)} - \frac{1}{2x^2}\right). \end{aligned} \tag{3.6}$$

We provide an approximate analytical expression for $I(t)$ in 3.56:

$$I(t) \approx \frac{15\pi}{32\sqrt{2}}\left[\sqrt{t+1} - \frac{1}{32}\frac{1}{(t+1)^{3/2}}\right]. \tag{3.7}$$

to a sufficiently large accuracy.

Importantly, in the polar phase, the beyond mean-field (MF) correction includes contributions from both density and spin fluctuations. These contributions involve terms proportional to c_0 and c_1 in (3.5) and are also influenced by the quadratic Zeeman coupling q, which is in stark contrast to the ferromagnetic phase discussed earlier. When $q = 0$, the parameters t and I approach 0 and 1, respectively, with I monotonically increasing with q. Consequently, spin fluctuations increase with the quadratic Zeeman energy q, leading to a rise in the total ground state energy. In the ultra-low density limit, the MF energy and density fluctuations scale with n^2 and $n^{5/2}$, respectively, while spin fluctuations scale with n^2 due to the $\sqrt{t+1}$ term in (3.7). The crucial observation here is that collapse instability emerges in the density channel when the interactions are attractive ($c_0 < 0$) at the MF level. This attraction can be counterbalanced by quantum fluctuations in the spin channel (c_1), which can be controlled using the Zeeman field q. On the other hand, fluctuations in the density channel play a less significant role. This point shows parallels with quantum mechanical stabilization of Bose-Bose mixtures in Ref. [1]. There, the weak attractive interaction between the two components induces also an MF-level instability, which is balanced by one of

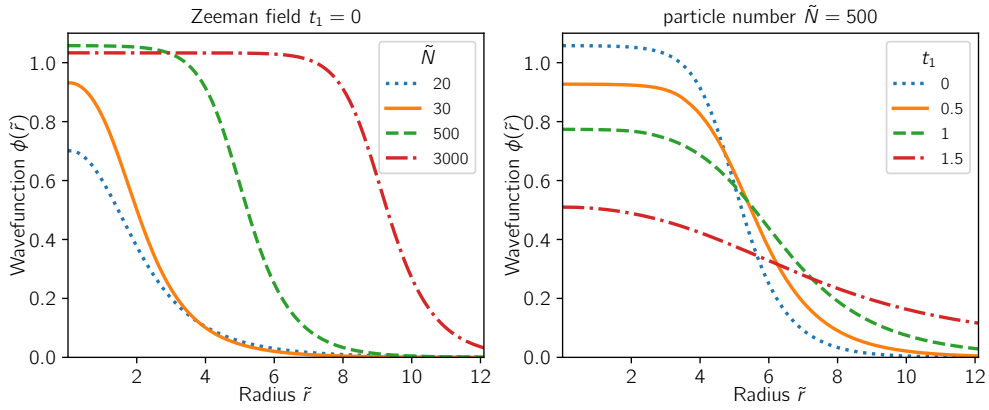

Figure 3.2: The wavefunctions of the polar spin-1 condensate in the ground state for different combinations of particle number $\tilde{N}$ and Zeeman energy $t_1 = q/n_1|c_1|$. On the left side, the wavefunctions are shown for $q = 0$ (equivalently, $t_1 = 0$) with varying values of $\tilde{N}$. Below $\tilde{N} = 20$, the droplet can not stabilize itself. On the right side, the wavefunctions are depicted for a fixed $\tilde{N} = 500$ while varying t_1. This plot reveals a self-bound droplet until a critical value of the quadratic Zeeman energy $q_c \approx 1.5$ is reached.

the two terms in the total LHY fluctuation. The other LHY term gives a negligible "soft-mode" contributions that are routinely neglected in the literature of quantum droplets [1, 33, 43, 57–59]. In the subsequent analysis, we will also ignore these fluctuations and focus on investigating the stability condition between the MF energy in the density channel and the LHY correction in the spin channel.

3.1.1 Polar Spin-1 Droplets

In the polar phase of an infinite homogeneous spin-1 gas, the equilibrium between the MF and the LHY energies can be calculated by the vanishing pressure condition. We obtain by solving the thermodynamic identity for pressure $P = -(\partial E/\partial V)_N$:

$$P = \frac{n^2 c_0}{2} + \frac{\alpha n^2 |c_1|}{2}\sqrt{n|c_1|^3} f(t), \tag{3.8}$$

where $f(t) \equiv 3I(t) - 2tI'(t)$ with $f(0) = 3$. $P = 0$ condition yields the equilibrium density n_0 as

$$n_0 = \frac{|c_0|^2}{\alpha^2 |c_1|^5 f^2(t_0)}, \tag{3.9}$$

which is an implicit equation with $t_0 = q/n_0|c_1|$. Here, n_0 provides an intuition on the density scales of the problem: It approximates the value of the limiting density in finite droplets where the kinetic energy is negligible. We deduce that the equilibrium density monotonically decreases as quadratic Zeeman energy q increases. This is due to the fact that the function $f(t)$ is a monotonically increasing function of t. Greater q means a stronger fluctuation energy in the polar phase. Hence, equilibrium density becomes lower when the MF energy is negative.

Now we quantitatively discuss the feasibility of a finite spin-1 condensate in the polar phase. The polar MF ground state wavefunction is $\Psi(\mathbf{r}) = \psi(\mathbf{r})\tau^P$. The total energy density functional is

$$\begin{aligned} \mathcal{E}[\psi^*, \psi] &= \frac{\hbar^2}{2M}|\nabla\psi|^2 \\ &+ \frac{c_0}{2}|\psi|^4 + \alpha|c_1|^{5/2}|\psi|^5 I\left[\frac{q}{|c_1||\psi|^2}\right], \end{aligned} \tag{3.10}$$

and non-dimensionalize the wavefunction $\psi(\mathbf{r}) = \sqrt{n_1}\phi(\mathbf{r})$ with $n_1 = |c_0|^2/9\alpha^2|c_1|^5$, which is the equilibrium density of the infinite droplet obtained from (3.9) for $q = 0$. The minimization of the total energy constraint to the fixed total number of particles $N = \int d^3\mathbf{r}|\psi|^2$ results in the modified GP equation. Hence the canonical ensemble energy is $E = \int d^3\mathbf{r}\mathcal{E}[\psi^*, \psi] - \mu N$ where μ is the chemical potential, and the variational analysis over the wavefunction $\phi*$, i.e. $\frac{\partial E}{\partial \phi*} = 0$, yields:

$$\begin{aligned} \tilde{\mu}\phi \quad &= -\frac{1}{2}\tilde{\nabla}^2\phi - 3|\phi|^2\phi \\ &+ \left[\frac{5}{2}I\left(\frac{t_1}{|\phi|^2}\right)|\phi|^3 - I'\left(\frac{t_1}{|\phi|^2}\right)t_1\,|\phi|\right]\phi, \end{aligned} \tag{3.11}$$

which is written in dimensionless form $\tilde{\mathbf{r}} = \mathbf{r}/\xi$, where $\xi = \sqrt{3\hbar^2/M|c_0|n_1}$ is the coherence length and $t_1 = q/n_1|c_1|$. Dimensionless chemical potential $\tilde{\mu}$ is determined by solving $\tilde{N} = \int d^3\tilde{r}|\phi(\tilde{\mathbf{r}})|$. The relation between the actual N and scaled total number $\tilde{N}$ in the droplet is $\tilde{N} = N/n_1\xi^3$.

In the absence of quadratic Zeeman energy $q = 0$, the modified GP equation of Ref. [1] is obtained.

Here it is beneficial to closely examine the relationship between the polar spinor and binary mixture droplets. The MF instability condition $c_0 < 0$ in the polar spinor corresponds to $\delta g < 0$ in the binary mixture, where $\delta g = g_{12} + \sqrt{g_{11}g_{22}}$ is expressed

in terms of the inter- and intra-component coupling constants g_{12} and g_{11}-g_{22}, respectively. The quantum fluctuations that stabilize this instability in the polar phase, denoted as $n^{5/2}|c_1|^{5/2}$, correspond to the out-of-phase term $n^{5/2}a_+^{5/2}$ in binary mixtures. Conversely, the "soft modes" that are neglected, represented as $n^{5/2}|c_0|^{5/2}$ in the polar phase, corresponding to the in-phase term $n^{5/2}a_-^{5/2}$ in binary mixtures.

We solve the modified Gross-Pitaevskii (GP) equation (3.11) numerically using imaginary time propagation to determine the ground state wavefunctions for various values of the quadratic Zeeman coupling q and the total number of particles $\tilde{N}$ [60]. The results are presented in Fig.(3.2).In the left panel of Fig.(3.2), we display the wavefunctions for different $\tilde{N}$ values, while q is fixed at $q = 0$. The polar spinor gas forms a self-bound quantum droplet for particle numbers above a critical value near $\tilde{N}_c \approx 19$, similar to the behavior observed in Bose-Bose mixtures [1]. Below this critical level $\tilde{N}_c$, the repulsive pressure due to the kinetic energy dominates over the MF attraction, leading to the expansion of the droplet to infinity.

In the right panel of Fig.(3.2), we present the ground state wavefunctions for various q (or t) values while keeping $\tilde{N} = 500$ fixed. As q increases, the LHY energy from spin fluctuations becomes stronger, resulting in a decrease in the maximum density of the droplet. Beyond a critical value of the Zeeman energy, $q_c \approx 1.5$, the combined repulsion from the LHY energy and the quantum pressure arising from the kinetic energy overpowers the MF attraction, leading to the expansion of the droplet to infinity. Consequently, the quadratic Zeeman coupling offers a means to control the particle density at the center of the droplet.

Note also that greater Zeeman energy also increases the critical value of N_c. To study this relationship, we utilize a Gaussian ansatz, since the droplet wavefunction is approximately Gaussian near the critical region. We examine q_c vs. N_c by comparing the Gaussian ansatz with the numerical solution for different values of $t_1 = q/n_1|c_1|$. As depicted in Fig.(3.3), N_c monotonically increases with t_1.

The discussion of polar droplets has focused on the parameter region where $c_1 > 0$ and $q > 0$ until now. However, it is important to note that the ground state can also exhibit polar order with ferromagnetic coupling $c_1 < 0$ and a strong Zeeman shift $q > -2nc_1$ (depicted as the blue region in the second quadrant of Fig. 3.1). In this

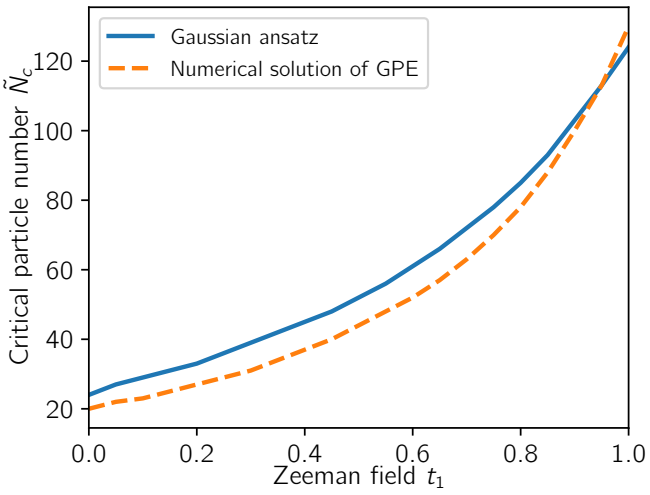

Figure 3.3: The critical particle numbers $\tilde{N}_c$ for different values of $t_1 = q/n_1|c_1|$ using two methods: numerical solutions of the GP equation (shown in orange) and variational calculations employing the Gaussian ansatz (shown in blue). As observed in the graph, the density at the center of the droplet reduces as q increases. Eventually, the interplay between kinetic energy and LHY (Lee-Huang-Yang) pressure becomes dominant, overpowering the mean-field attraction, and causing the droplet to expand. This phenomenon is well-captured by the Gaussian variational calculation, which demonstrates good agreement with the GP solution.

particular regime, the LHY energy is obtained by replacing $I(t)$ with $I(t-2)$ in all the previous calculations. Interestingly, we find that droplet formation is feasible for all parameter regimes with a polar ground state.

3.1.2 AF Spin-1 Droplets

The total GS energy of the antiferromagnetic phase, which is realized when $c_1 > 0$ and $q < 0$ with an order parameter $\tau^{AF} = (1\ 0\ 1)/\sqrt{2}$:

$$\begin{aligned}\frac{E_0^{AF}}{V} &= qn + \frac{n^2 c_0}{2}\left[1 + \alpha\sqrt{nc_0^3}\right] \\ &\quad + \frac{\alpha n^2|c_1|}{2}\sqrt{n|c_1|^3}\left[1 + I(t)\right], \end{aligned} \tag{3.12}$$

where $t = |q|/nc_1 \equiv |q|/n|c_1|$ since $c_1 > 0$ here. We follow the similar reasoning given in Sec. 3.1.1. we first consider the attraction induced in the MF level with

$c_0 < 0$. This attraction can drive the density collapse and the stabilization with the fluctuations in the spin channel is possible. We again ignore the soft mode in the density channel.

We calculate the pressure with the same approach:

$$P \quad = \frac{n^2 c_0}{2} + \frac{\alpha n^2 |c_1|}{4} \sqrt{n|c_1|^3}\, g(t), \tag{3.13}$$

where $g(t) \equiv 3 + 3I(t) - 2tI'(t)$. The equilibrium density for the antiferromagnetic droplet is again calculated by the vanishing pressure condition as:

$$n_0 \quad = \frac{4|c_0|^2}{\alpha^2 c_1^5\, g^2(t_0)}, \tag{3.14}$$

where $t_0 = |q|/n_0 c_1$. Note that the equilibrium density is finite and positive. Besides, $g(t)$ increases monotonically as t increases, when $t \geq 0$.

Now consider the wavefunction $\Psi(\mathbf{r}) = \psi(\mathbf{r})\tau^{AF}$ of the antiferromagnetic phase. We can write the corresponding energy density functional:

$$\begin{aligned} \mathcal{E}[\psi^*, \psi] &= \frac{\hbar^2}{2M}|\nabla\psi|^2 + q|\psi|^2 + \frac{c_0}{2}|\psi|^4 \\ &+ \frac{\alpha}{2}|c_1|^{5/2}|\psi|^5 \left(1 + I\left[\frac{q}{|c_1||\psi|^2}\right]\right). \end{aligned} \tag{3.15}$$

We again use the locked-in approximation to express the droplet wavefunction as $\psi(\mathbf{r}) = \sqrt{n_1}\phi(\mathbf{r})$ where $n_1 = |c_0|^2/9\alpha^2|c_1|^5$ where n_1 is obtained from n_0 calculated at the limit $q \to 0$. Define $t_1 \equiv |q|/n_1 c_1$, the modified GP equation is obtained by the variational analysis of energy in the grand canonical ensemble:

$$\begin{aligned} \tilde{\mu}\phi \quad &= -\frac{1}{2}\tilde{\nabla}^2\phi + 3t_1\frac{|c_1|}{|c_0|}\phi - 3|\phi|^2\phi \\ &+ \left\{\frac{5}{4}\left[1 + I\left(\frac{t_1}{|\phi|^2}\right)\right]|\phi|^3 - \frac{1}{2}I'\left(\frac{t_1}{|\phi|^2}\right)t_1|\phi|\right\}\phi. \end{aligned} \tag{3.16}$$

The same form of Eq. (3.11) is obtained when $q \to 0$, i.e. $t_1 \to 0$. Although the antiferromagnetic (AF) phase yields the same ground-state wavefunctions as the polar case when $q = 0$, the effect of non-zero $|q|$ values differs between the AF and polar cases. In the AF phase, the droplet is stabilized through contributions from both density and spin fluctuations, whereas in the polar case, spin fluctuations serve as the only stabilizing mechanism.

To explore the stability of a finite-sized AF spinor droplet, we numerically solve the modified GP equation and calculate the ground state wavefunctions, as shown in

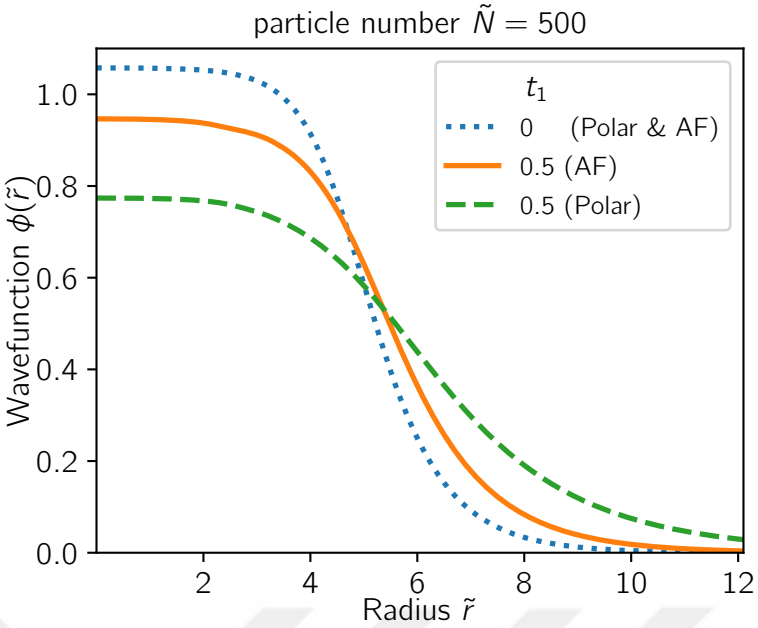

Figure 3.4: The droplet wavefunctions in the ground state for $t_1 = -0.5, 0, 0.5$. The particle number for all the phases is the same, $\tilde{N} = 500$.

Fig.(3.4). As with the polar phase, a stronger quadratic Zeeman shift leads to lower density within the central region of the droplet. An additional increase in $|q|$ results in the expansion of the droplet, similar to the behavior observed in the polar phase. Consequently, the quadratic Zeeman effect can be utilized to control the density of the droplet in both the AF and polar phases.

3.1.3 Discussion of experimental realization and Conclusion

The phase diagram and stability of spin-1 Bose-Einstein condensates (BECs) are governed by three parameters: density-density interaction c_0, spin-spin interaction c_1, and the quadratic Zeeman energy q. A self-trapped droplet arises when the mean-field (MF) instability towards mechanical collapse, induced by $c_0 < 0$, is balanced by the Lee-Huang-Yang (LHY) quantum fluctuations. The LHY energy is derived using a perturbative expansion within the Bogoliubov theory and requires diluteness, which is satisfied when $|c_0|/|c_1|$ is sufficiently small. In the case of finite droplets, additional quantum pressure from kinetic energy, the total particle number constraint, and the quadratic Zeeman shift contribute to a complex interplay that determines full stability.

Presently, the experimentally available spinor BECs are not suitable for droplet formation as they are all mechanically stable with $c_0 > 0$ [22, 50, 51, 55, 61, 62]. c_0 is an order of magnitude larger than $|c_1|$ [22] for the most commonly used alkali atoms Na and Rb. For Lithium, $|c_0|/|c_1| \sim 0.46$ [63]. However, favorable parameters for droplet formation could potentially emerge in novel hyperfine manifolds as more atomic gases are trapped and cooled with new species and mixtures. While the spin-1 condensates lack the standard magnetic Feshbach resonance for tuning the interaction strength, there are theoretical proposals for using optical Feshbach resonances [53, 54], which might soon be realized experimentally. Notably, the required changes in the condensate properties to enter the self-trapped droplet regime are not exceptionally large. Hypothetically, a droplet with favorable parameters could be self-trapped when certain atom-atom scattering lengths are considered. Furthermore, the quadratic Zeeman shifts allow for control over the droplet's stability and density. For instance, consider an atom with 0-channel and 2-channel scattering lengths $a_0 = -100a_B$ and $a_2 = +45a_B$, which yields $c_0 = \frac{4\pi\hbar^2}{M}(-\frac{10}{3}a_B) < 0$ and $c_1 = \frac{4\pi\hbar^2}{M}(\frac{145}{3}a_B) > 0$ with the ratio $\frac{c_0}{c_1} \simeq -0.07$. For an atom with the mass of 23 amu, the expected density near the center of a Thomas-Fermi droplet is $n_1 \approx 13 \times 10^{14} cm^{-3}$ when $q = 0$ and a droplet with $N = 25,000$ particles could be self-stabilized. The correlation length becomes $\xi \simeq 1\mu m$. For total number of particles $130,000$ ($\tilde{N} = 100$), the droplet will be stable up to $t_1 \simeq 1$, thus the quadratic Zeeman shift can be varied between 0 to 20 kHz. The droplet size is in the $3 - 6\mu m$ interval for $N \approx 25,000 - 150,000$ particles.

In summary, similar to droplet formations in dipolar and binary mixture gases, we predict the existence of self-trapped droplets in the spin-1 gas in both polar and antiferromagnetic phases. This stability arises from the competition between MF attraction and LHY repulsion induced by spin fluctuations. The quadratic Zeeman effect can be used to control the droplet's stability and density. We anticipate that experimentally favorable parameters for droplet formation could be achieved in new cold atom species or by adjusting scattering lengths. Our findings can be extended to non-zero magnetization, spin-2 gases, and spinor mixtures. Additionally, exploring other manifestations of beyond MF interactions within spinor BECs offers an exciting avenue for future research.

3.2 Rabi-coupled Bose Mixture Droplets

Self-trapped quantum droplets arise when the natural tendency of the gas to collapse at the mean-field level is counteracted by effectively repulsive beyond mean-field fluctuations. These beyond mean-field effects are influenced by the Rabi-frequency ω_R in Rabi-coupled Bose mixtures and the quadratic Zeeman effect q in spinor gases. Previous investigations of quantum droplets have primarily focused on unpolarized Rabi-coupled Bose mixtures and unpolarized spinor gases, analyzing the effects of varying ω_R and q.In this part of the thesis, we extend the exploration to investigate the stability of the droplet phase in polarized Rabi-coupled Bose mixtures and polarized spinor gases. We calculate the beyond mean-field corrections for both systems, considering the polarized order parameters. The resulting phase diagram for the droplets is constructed in the parameter space of the Rabi-frequency ω_R and detuning δ for Rabi-coupled mixtures and the quadratic Zeeman energy q and linear Zeeman energy p for spinor gases. We draw comparisons between the two systems, highlighting their similarities and differences, and discuss the potential for experimental realization.

3.2.1 Introduction

Theoretical predictions and experimental observations of bosonic droplets have emphasized the significant role of beyond mean-field (BMF) effects, which typically provide minor corrections. Self-trapping of a collapsing Bose-Einstein condensate (BEC) becomes possible only when considering BMF fluctuations [1, 2]. In a trapped single-component BEC with attractive interactions, the mean-field (MF) interaction energy scales as $-N^2|a|/R^3$, where N is the number of particles, R is the condensate's radius, and a is the s-wave scattering length ($a < 0$) [8]. The trapping potential $\propto NR^2$ and kinetic energy $\propto N/R^2$ can balance this attractive MF interaction, resulting in a metastable BEC only if the particle number stays below a certain maximum value [8]. However, the situation is profoundly different for self-bound droplets. In this case, the MF collapse is stabilized solely by the BMF quantum fluctuations, even without a confining potential [1–4, 33, 41, 42, 46, 47, 49, 57, 64–67], and these droplets exhibit a minimum particle number below which the gas is no longer stable [1]. As the particle number N decreases, the kinetic energy eventually becomes

dominant, causing the gas to expand.

The stability of droplets is not only determined by the particle number constraints but also relies on the interaction parameters. Different classes of Bose droplets, including dipolar [2], binary mixture [1], and spinor [64] droplets, have distinct sets of fundamental interaction parameters. For dipolar droplets, the dipole interaction strength ϵ_{dd} and contact interactions a_s are crucial. For binary mixtures, the intraspecies contact interactions a_{11} and a_{22}, along with the interspecies interaction a_{12}, play a key role. In the case of spin-1 gases, the total spin-0 channel interaction a_0 and the total spin-2 channel interaction a_2 are the relevant parameters to be considered. These interaction parameters need to be carefully adjusted to drive the mean-field energy of the system towards collapse and simultaneously balance it with the beyond mean-field (BMF) energy for the mechanical stabilization.

The main theoretical approach used to study quantum droplets is the Bogoliubov theory [1, 2, 64], which effectively captures the underlying physics of the droplet phase. However, there is a notable quantitative discrepancy between the theoretical predictions and experimental observations regarding the critical number of particles [3, 4, 68]. Various proposals have been put forward to address this disagreement, including higher-order contributions [29, 44], bosonic pairing [28], beyond Born-approximation [69], or general Gaussian-state ansatzes [70]. In this thesis, we rely on the Bogoliubov theory, which offers a satisfactory qualitative understanding of the droplet phenomena. However, to rely on the results of the Bogoliubov theory, it is important to ensure that the gas needs to remain in the dilute regime $\sqrt{na^3} \ll 1$, where n is the density of the condensate and a is the scattering length. This stringent fine-tuning requirement motivates us to explore additional methods to control droplet properties in ultracold atom experiments.

Lately, there has been growing interest in Bose mixtures featuring Rabi-coupling between the hyperfine states of particles, primarily due to their intriguing many-body effects, such as effective tunable three-body interactions [67, 71–73]. The coupling between the two levels of the system causes the BMF energy to depend on the Rabi frequency ω_R [72], offering an additional method to control the droplet density. Similar to a critical particle number, there exists a critical Rabi frequency ω_c, beyond which

the droplet is no longer self-trapped [67]. In the case of spinor droplets, the BMF correction of the spinor gas, which depends on the quadratic Zeeman energy, plays a similar role, with a maximum value q_c above which the droplet expands [64]. Furthermore, introducing a non-zero quadratic Zeeman energy or Rabi frequency causes one of the gapless Bogoliubov modes to become gapped in both spinor and Rabi-coupled mixtures. The mean-field energies can be controlled by adjusting the detuning δ for Rabi-coupled gases and the linear Zeeman energy p for spinor gases. These similarities lead us to conduct a comparative investigation of their droplet states.

Until now, both the Rabi-coupled binary mixture droplets [67] and the spinor gas droplets [64] have been examined under the condition of zero net polarization. In the case of Rabi-coupled droplets, the detuning δ is assumed to be zero, resulting in an unpolarized ground state order parameter within the mean-field (MF) analysis. Similarly, in the study of spinor droplets [64], the mean-field ground states are studied with zero magnetization $\langle \mathbf{F} \rangle$. In this study, we conduct a theoretical investigation into the formation of droplets in the polarized Rabi-coupled binary mixture and the spin-1 gas. We explore how the presence of non-zero polarization impacts the MF and BMF energies, and we discuss the possibility of droplet phases under finite polarization. For the Rabi-coupled binary mixtures, introducing a non-zero detuning δ causes an asymmetry in the particle number between the two levels within the MF ground state. The finite polarization also leads to changes in both the MF and BMF interaction energies. For a given Rabi-frequency ω_R, there exists a critical value of the detuning δ_c beyond which the droplet is no longer self-trapping. Similarly, in the case of the spin-1 droplet, the presence of finite magnetization alters the MF and BMF interactions. Here, a critical magnetization $\tilde{p}_c$ exists for a given quadratic Zeeman energy q, above which the droplet expands. By utilizing these critical values, we determine the droplet phase boundary of the Rabi-coupled mixture in the ω_R-δ plane and the spinor gas in the q-p plane, respectively.

In Section 3.2.2, we provide an overview of the Bogoliubov Theory applied to Rabi-coupled binary mixtures. We discuss the MF ground states and examine the mechanical stability of the mixture. In Section 3.2.4, we present the formulation of the polarized Rabi-coupled droplet and show our numerical findings regarding the droplet phase boundary in the ω_R-δ plane. Moving on to Section 3.3.1, we summarize the

Bogoliubov Theory applied to polarized spin-1 gas and investigate the mean-field order parameters in the case of anti-ferromagnetic interactions with $c_1 > 0$. In Section 3.3.4, we develop the formulation of the polarized spinor droplet and present the droplet phase boundary in the $p - q$ plane. Finally, in Section 4.7, we discuss the feasibility of observing the proposed phenomena in experiments and highlight the similarities and differences between the polarized Rabi-coupled and spinor droplets.

3.2.2 Rabi-Coupled Bose Mixtures: Bogoliubov Theory

We examine a Bose-Einstein condensate (BEC) containing N atoms with two internal states labeled as $m = 1, 2$. The BEC exhibits s-wave scattering lengths denoted by a_{11}, a_{22}, and a_{12} for the corresponding interactions. These internal states are interconnected through a Rabi frequency ω_R and a detuning parameter δ. By applying the rotating wave approximation to remove the explicit time dependence, the Hamiltonian describing this system of a Rabi-coupled binary mixture can be expressed as [72]:

$$\begin{aligned}\hat{H} \quad &= \int d\mathbf{x} \left\{ \sum_{m=1,2} \hat{\Psi}_m^\dagger(\mathbf{x}) \left(-\frac{\hbar^2 \nabla^2}{2M} \right) \hat{\Psi}_m(\mathbf{x}) \right. \\ &+ \sum_{m,m'} \left(\frac{g_{mm'}}{2} \, \hat{\Psi}_m^\dagger(\mathbf{x}) \hat{\Psi}_{m'}^\dagger(\mathbf{x}) \hat{\Psi}_{m'}(\mathbf{x}) \hat{\Psi}_m(\mathbf{x}) \right) \\ &- \hbar\omega_R \left(\hat{\Psi}_1^\dagger(\mathbf{x}) \hat{\Psi}_2(\mathbf{x}) + \hat{\Psi}_2^\dagger(\mathbf{x}) \hat{\Psi}_1(\mathbf{x}) \right) \\ &\left. - \hbar\frac{\delta}{2} \left(\hat{\Psi}_2^\dagger(\mathbf{x}) \hat{\Psi}_2(\mathbf{x}) - \hat{\Psi}_1^\dagger(\mathbf{x}) \hat{\Psi}_1(\mathbf{x}) \right) \right\}, \end{aligned} \tag{3.17}$$

where $g_{mm'} = 4\pi a_{mm'} \hbar^2 / M$ represents the coupling constant of the s-wave interaction among the atoms of mass M within the internal states m and m'. $\hat{\Psi}_m^\dagger(\mathbf{x})$ and $\hat{\Psi}_m(\mathbf{x})$ are the field operators that create and annihilate the particle with internal state m at position $\mathbf{x}$, respectively.

In order to comprehend the ground state order parameter at the MF level and its distinctions from the binary mixture without Rabi-coupling, we focus on the MF energy of the gas with equal intra-species scattering lengths, where $g_{11} = g_{22} = g$, for simplicity. The MF energy is given by [73, 74] (See Appendix 3.2.3 for details):

$$\frac{E_{MF}}{N} = -\hbar\omega_R \sin\theta - \frac{\hbar\delta}{2} \cos\theta + \frac{gN}{2V} - \frac{\bar{g}N}{2V} \sin^2\theta, \tag{3.18}$$

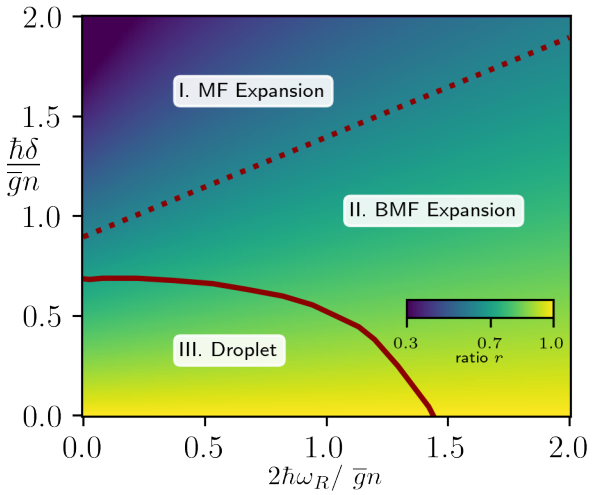

Figure 3.5: The phase diagram of a Rabi-coupled Bose mixture is represented as a function of two parameters: the Rabi frequency $\frac{2\hbar\omega_R}{\bar{g}n}$ and the detuning $\frac{\hbar\delta}{\bar{g}n}$, under the conditions $\frac{g_{12}}{g} < -1$ and $g > 0$. The color shading (indicated by the color bar) corresponds to the ratio $r = \sqrt{N_1/N_2}$ in the mean-field (MF) ground state, as given by the expression (3.18). The dashed red line marks the boundary above or below which the total MF two-particle interaction, with $g_{12}/g = -1.5$, becomes repulsive or attractive, respectively. On the other hand, the solid red line represents the boundary of the self-trapped droplet phase. In Region I of the diagram, the gas expands due to the repulsive MF interaction. In Region II, the MF energy is attractive, but the repulsive beyond-mean-field (BMF) energy is strong enough to cause expansion. In Region III, the MF attraction is stabilized by the repulsive BMF energy, resulting in the formation of a self-trapped droplet.

where $\bar{g} = \frac{g-g_{12}}{2}$. The wavefunctions of the condensate components $(\psi_1\ \psi_2) = \sqrt{n}(\sin\theta/2\ \cos\theta/2)$ where $\theta \in [0, \pi]$ is the polar angle on the Bloch sphere. Given a fixed total number of particles N, the task of determining the mean-field (MF) ground state involves finding the value of θ that minimizes the energy expressed in Equation (3.18). [67] computed the ground state MF order parameter $r \equiv \sqrt{N_1/N_2} = \tan(\theta/2)$ for any g_{12}/g with $\delta = 0$.

In this analysis, we focus on the parameter space where δ is not equal to zero. Our objective is to investigate the order parameters that lead to system collapse within the MF framework. For this purpose, we assume $g_{12}/g < -1$ and $g > 0$, which results

in collapse without phase separation, and within this range, $\overline{g} > 0$. In Figure 3.5, we depict the ratio r between particle numbers in the MF ground state for different values of ω_R and δ. When there is no detuning ($\delta = 0$), the MF energy is minimized with $\theta = \pi/2$ or $r = 1$ for any ω_R. This corresponds precisely to the order parameter used by [67] in their droplet analysis. However, when detuning δ becomes non-zero, the MF ground state becomes polarized, and $r \neq 1$. The polarization becomes more pronounced as either $\omega_R \to 0$ or $\delta \to \infty$, leading to $r \to 0$ or $\theta \to 0$. The order parameter $r = \tan(\theta/2)$, where $\theta \in [0, \pi/2]$, undergoes a smooth change across the parameter space. (Refer to Figure 3.5).

Now let us discuss how the two-body interaction part ($\frac{gN^2}{2V} - \frac{\bar{g}N^2}{2V}\sin^2\theta$) of the MF energy (3.18) changes with the detuning δ.long the ω_R-axis, the MF ground state yields $r = 1$ or $\theta = \pi/2$, leading to a two-body interaction proportional to $(g - \bar{g})n^2 = (g + g_{12})n^2/2$, where $n = N/V$ represents the density of the gas. Since $g_{12}/g < -1$, the MF picture indicates a density collapse. However, along the δ-axis, the MF ground state yields $r = 0$ or $\theta = 0$ for $\hbar\delta/\bar{g}n > 2$. Consequently, the MF two-body interaction is proportional to gn^2, implying that the gas is expected to expand within the MF framework since $g > 0$. It is worth noting that as the detuning δ increases from zero to infinity, the gas becomes more polarized. As the polarization of the gas increases (i.e., $r \to 0$), the effective MF interaction first becomes less attractive and then becomes repulsive. Consequently, there exists a critical value of $\theta = \sin^{-1}\sqrt{g/\bar{g}}$, below which the MF interaction becomes repulsive. For the case when $g_{12}/g = -1.5$, the boundary separating this attractive and repulsive MF interaction is illustrated with the dashed red line in Figure 3.5. In region I of Figure 3.5, the MF energy is repulsive, favoring gas expansion. On the other hand, in regions II and III of Figure 3.5, the MF energy is attractive.

From now on, ω_R, r, g_{12}, g, and N are considered as the free parameters of the Rabi-coupled mixture problem. In addition, we utilize dimensionless parameters $\tilde{\omega} = \frac{\hbar\omega_R}{gn}$ and $\gamma = g_{12}/g$ as needed. The outcomes are depicted as functions of the parameter set ($\tilde{\omega}$, r), which can then be translated to the parameter plane (ω_R, δ) when required.

The BMF energy of each corresponding Bogoliubov mode are separately calculated. For the seperation of the modes, we use $E^{\pm}_{BMF} = \frac{1}{2}\sum_{\mathbf{k}}\left(E^{\pm}_{\mathbf{k}} - \lim_{\mathbf{k}\to\infty} E^{\pm}_{\mathbf{k}}\right)$, where

$E^{\pm}_{\mathbf{k}}$ are the Bogoliubov dispersions. Then we obtain (See Appendix 3.2.3 for details):

$$\frac{E^{\pm}_{BMF}}{V} = \alpha(gn)^{5/2} I_{\pm}(\tilde{\omega}, \gamma, r), \tag{3.19}$$

where $\alpha = \frac{M^{3/2}}{\sqrt{2}\pi^2\hbar^3}$. See Ch. 3.2.3 for $I_{\pm}(\tilde{\omega}, \gamma, r)$. In the limit $\tilde{\omega} \to 0$ and $r = 1$, (3.19) recovers the BMF energy of the Bose mixture without Rabi-coupling. In the limit $r \to 1$ for any $\tilde{\omega}$, the $E^{\pm}_{BMF}$ expressions of [67] are recovered for both modes. For more general cases where $r \neq 1$, we numerically calculate I_+ for various r values. In the interval $r \in [0.6, 1]$ where the MF energy is attractive and $\gamma = -1.5$, the BMF energy (3.19) increases with the increase of either $\tilde{\omega}$ or the ratio r. This behavior is due to the fact that I_+ is a monotonically increasing function of both variables.

3.2.3 The Bogoliubov Theory of Rabi-coupled Mixture

We obtain the MF energy and BMF fluctuations using the Bogoliubov theory in the Hamiltonian (3.17). We express the field operators in terms of Fourier modes $\hat{\Psi}_m(\mathbf{x}) = V^{-1/2} \sum_{\mathbf{k}} \hat{a}_{\mathbf{k},m} e^{i\mathbf{kx}}$ by assuming a homogeneous condensate, and rewrite the operators $\hat{a}_{\mathbf{k},m} = \hat{a}_{\mathbf{0},m} + \sum_{\mathbf{k}\neq 0} \hat{a}_{\mathbf{k},m}$ retaining the terms only up to the quadratic order in $\hat{a}_{\mathbf{k}\neq\mathbf{0},m}$. We replace the operators with the classical number $\hat{a}_{\mathbf{0},m} \approx \sqrt{N_{0,m}}$, where $N_{0,m}$ is the number of particles with internal state m in the $\mathbf{k} = 0$ state. The Hamiltonian (3.17) becomes:

$$\begin{aligned}
\hat{H} \quad &= -2\hbar\omega_R\sqrt{N_1 N_2} - \frac{\hbar\delta}{2}(N_2 - N_1) + \sum_{m,m'} \frac{g_{mm'} N_m N_{m'}}{2V} \\
&+ \sum_{\mathbf{k}\neq 0} \Bigg\{ \left(\epsilon_{\mathbf{k}} + g_{11} n_1 + \hbar\omega_R \sqrt{\frac{N_2}{N_1}} \right) \hat{a}^{\dagger}_{\mathbf{k},1} \hat{a}_{\mathbf{k},1} \\
&+ \left(\epsilon_{\mathbf{k}} + g_{22} n_2 + \hbar\omega_R \sqrt{\frac{N_1}{N_2}} \right) \hat{a}^{\dagger}_{\mathbf{k},2} \hat{a}_{\mathbf{k},2} \\
&+ \frac{g_{11} n_1}{2} \left(\hat{a}^{\dagger}_{\mathbf{k},1} \hat{a}^{\dagger}_{-\mathbf{k},1} + \hat{a}_{\mathbf{k},1} \hat{a}_{-\mathbf{k},1} \right) \\
&+ \frac{g_{22} n_2}{2} \left(\hat{a}^{\dagger}_{\mathbf{k},2} \hat{a}^{\dagger}_{-\mathbf{k},2} + \hat{a}_{\mathbf{k},2} \hat{a}_{-\mathbf{k},2} \right) \\
&+ g_{12}\sqrt{n_1 n_2} \left(\hat{a}^{\dagger}_{\mathbf{k},1} \hat{a}^{\dagger}_{-\mathbf{k},2} + \hat{a}_{\mathbf{k},1} \hat{a}_{-\mathbf{k},2} \right) \\
&+ \left(g_{12}\sqrt{n_1 n_2} - \hbar\omega_R \right) \left(\hat{a}^{\dagger}_{\mathbf{k},1} \hat{a}_{\mathbf{k},2} + \hat{a}^{\dagger}_{\mathbf{k},2} \hat{a}_{\mathbf{k},1} \right) \Bigg\},
\end{aligned} \tag{3.20}$$

where $\epsilon_{\mathbf{k}} = \frac{\hbar^2 k^2}{2M}$ is the free particle dispersion. The first line of (3.20) is the MF energy of the Rabi-coupled binary mixture gas. The subsequent terms correspond to the quantum fluctuations that constitute the BMF energy.

The MF energy of Rabi-coupled gas reads:

$$E_{MF} \quad = -2\hbar\omega_R\sqrt{N_1 N_2} - \frac{\hbar\delta}{2}(N_2 - N_1) + \sum_{m,m'} \frac{g_{mm'} N_m N_{m'}}{2V}. \tag{3.21}$$

In the case of equal intraspecies coupling, $g_{11} = g_{22} = g$, and using the parameterization of the particle number ratio for the components, $\tan(\theta/2) = N_1/N_2$, with $N_1 + N_2 = N$, MF energy in Equation (3.21) can be expressed as follows:

$$\frac{E_{MF}}{N} = -\hbar\omega_R \sin\theta - \frac{\hbar\delta}{2}\cos\theta + \frac{gN}{2V} - \frac{\bar{g}N}{2V}\sin^2\theta. \tag{3.22}$$

We find the corresponding Bogoliubov modes for polarized Rabi-coupled mixture by applying the Bogoliubov transformation [72] on the quadratic Hamiltonian (3.20):

$$E_{\pm,\mathbf{k}} = \sqrt{D_{\mathbf{k}} \pm \sqrt{D_{\mathbf{k}}^2 - T_{\mathbf{k}}^2}} \tag{3.23}$$

$$D_{\mathbf{k}} = \frac{1}{2}\sum_{m=1,2}\left[\left(\epsilon_{\mathbf{k}} + \hbar\omega_R\sqrt{\frac{n_{\bar{m}}}{n_m}}\right)\left(\epsilon_{\mathbf{k}} + 2gn_m + \hbar\omega_R\sqrt{\frac{n_{\bar{m}}}{n_m}}\right) - \hbar\omega_R(2g_{12}\sqrt{n_1 n_2} - \hbar\omega_R)\right] \tag{3.24}$$

$$T_{\mathbf{k}}^2 = \epsilon_{\mathbf{k}}\left(\epsilon_{\mathbf{k}} + \hbar\omega_R\left(r + \frac{1}{r}\right)\right) \times \left[\left(\epsilon_{\mathbf{k}} + 2gn_1 + \hbar\omega_R\frac{1}{r}\right)(\epsilon_{\mathbf{k}} + 2gn_2 + \hbar\omega_R r) - (2g_{12}\sqrt{n_1 n_2} - \hbar\omega_R)^2\right], \tag{3.25}$$

where $\bar{m} = 3 - m$, $n_1 = \frac{r^2}{r^2+1}n$ and $n_2 = \frac{1}{r^2+1}n$. These Bogoliubov modes reduce to the results of [67] for $r = 1$ and non-zero ω_R, and they recover the usual Bose mixture results without Rabi coupling for $\omega_R = 0$ and $r = 1$.

The total BMF energy is the zero-point energy of the Bogoliubov excitations:

$$E_{BMF} = \frac{1}{2}\sum_{\mathbf{k}}\left\{E_{+,\mathbf{k}} + E_{-,\mathbf{k}} - 2\epsilon_{\mathbf{k}} - \left(r + \frac{1}{r}\right)\hbar\omega_R - gn_1 - gn_2 + \frac{g^2 n_1^2 + g^2 n_2^2 + 2g_{12}^2 n_1 n_2}{2\epsilon_{\mathbf{k}}}\right\}, \tag{3.26}$$

where the last term within the summation is the T-matrix renormalization energy for the Bose mixture [1].

To compute the BMF energy for each mode individually, we distribute the renormalization energy among the two modes in a way that ensures neither mode results in a divergence. We calculate each respective Bogoliubov mode separately using the formula $E^{\pm}_{BMF} = \frac{1}{2}\sum_{\mathbf{k}} \left(E^{\pm}_{\mathbf{k}} - \lim_{\mathbf{k}\to\infty} E^{\pm}_{\mathbf{k}}\right)$, leading to the following expression:

$$\frac{E^{\pm}_{BMF}}{V} = \alpha(gn)^{5/2} I_{\pm}(\tilde{\omega}, \gamma, r), \tag{3.27}$$

where $\alpha = \frac{M^{3/2}}{\sqrt{2}\pi^2\hbar^3}$, $\tilde{\omega} = \frac{\hbar\omega_R}{gn}$, the particle number ratio $r = \sqrt{\frac{N_1}{N_2}}$, and coupling constant ratio $\gamma = \frac{g_{12}}{g}$.

The integral expression for the function $I_{\pm}(\tilde{\omega}, r, \gamma)$ within the BMF energy (3.27) is given by:

$$\begin{aligned} I_{\pm}(\tilde{\omega}, \gamma, r) \equiv & \left(\frac{r^2}{r^2+1}\right)^{5/2} \int_0^{\infty} dy y^2 \\ & \times \left\{ \sqrt{(y^4 + \beta_2 y^2 + \beta_0) \pm \sqrt{(\beta_2^2 + 2\beta_0 - z_4)y^4 + (2\beta_0\beta_2 - z_6)y^2 + \beta_0^2}} \right. \\ & \left. -y^2 \left[1 + \frac{\beta_2 \pm \sqrt{\beta_2^2 + 2\beta_0 - z_4}}{2y^2} + \frac{\beta_0 \pm \frac{\beta_0\beta_2 - z_6/2}{\sqrt{\beta_2^2+2\beta_0-z_4}} - \frac{(\beta_2 \pm \sqrt{\beta_2^2+2\beta_0-z_4})^2}{4}}{2y^4} \right] \right\}, \end{aligned} \tag{3.28}$$

where

$$\beta_0 \equiv \frac{(r^2+1)^2}{r^4}\left[\frac{2r\tilde{\omega}}{r^2+1}(1-\gamma) + \tilde{\omega}^2 + \frac{\tilde{\omega}^2}{2r^2} + \frac{\tilde{\omega}^2 r^2}{2}\right] \tag{3.29}$$

$$\beta_2 \equiv \left(1 + \frac{1}{r^2}\right)\left(1 + \frac{\tilde{\omega}}{r} + \tilde{\omega}r\right) \tag{3.30}$$

$$\begin{aligned} z_4 \equiv & \left(2 + \frac{\tilde{\omega}(r^2+1)}{r^3}\right)\left(\frac{2}{r^2} + \frac{\tilde{\omega}(r^2+1)}{r}\right) \\ & + \tilde{\omega}\frac{(r^2+1)^3}{r^5}\left(2 + \frac{\tilde{\omega}(r^2+1)}{r}\right) - \left(\frac{2\gamma}{r} - \frac{\tilde{\omega}(r^2+1)}{r^2}\right)^2 \end{aligned} \tag{3.31}$$

$$\begin{aligned} z_6 \equiv & \tilde{\omega}\frac{(r^2+1)^2}{r^3}\left[\left(2 + \frac{\tilde{\omega}(r^2+1)}{r^3}\right)\left(\frac{2}{r^2} + \frac{\tilde{\omega}(r^2+1)}{r}\right)\right. \\ & \left. \left(\frac{2\gamma}{r} - \frac{\tilde{\omega}(r^2+1)}{r^2}\right)^2\right], \end{aligned} \tag{3.32}$$

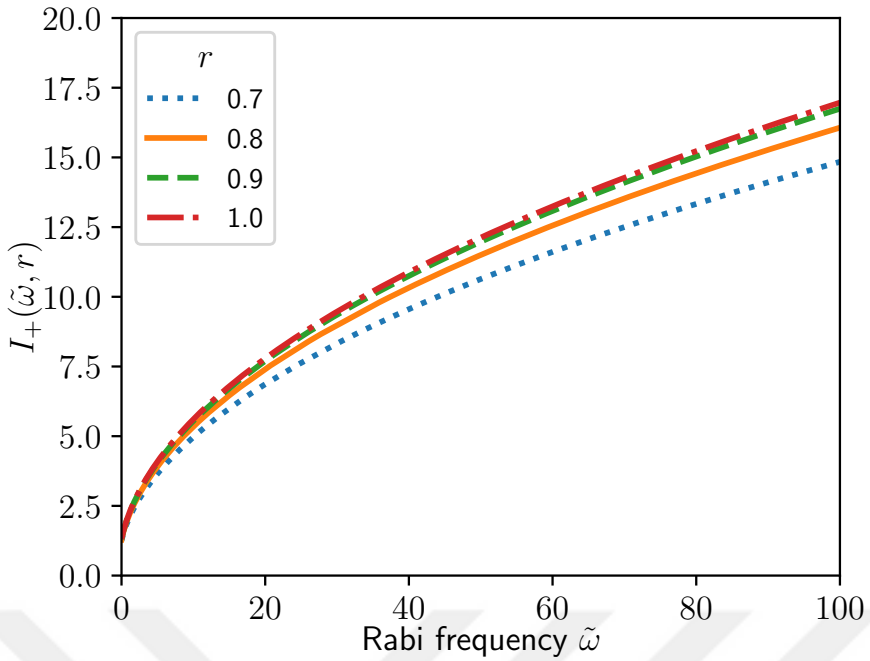

Figure 3.6: The integral I_+ in (3.28) as a function $\tilde{\omega}$ for varying r values. The scattering length ratio is fixed $g_{12}/g = -1.5$.

where $gn_1y^2 \equiv \epsilon_{\mathbf{k}}$. Check Fig. 3.6 to see how $I_+(\tilde{\omega}, \gamma, r)$ behaves for various r values as $\tilde{\omega}$ changes.

3.2.4 Rabi-Coupled Bose Mixture Droplet

We will now explore the potential for self-trapping. We follow previous works such as Refs. [1, 57, 64], and we will disregard the contribution from the 'soft' Bogoliubov mode $E^-_{\mathbf{k}}$. First, let's consider the case of an infinite and homogeneous Rabi-coupled Bose mixture. The gas pressure can be calculated using the formula $P = -\partial \left(E_{MF} + E^+_{BMF}\right)/\partial V$, which yields:

$$P = \frac{g(1+r^4) + 2g_{12}r^2}{2(r^2+1)^2} n^2 + \alpha (gn)^{5/2} f(\tilde{\omega}), \tag{3.33}$$

where $f(\tilde{\omega}) = \frac{3}{2} I_+(\tilde{\omega}) - \tilde{\omega} I'_+(\tilde{\omega})$. For any value of g_{12}/g, there exists a certain value of r within the range of $r \in [0, 1]$ above which the pressure due to the MF energy becomes negative. However, this negative pressure can be balanced and stabilized by a positive contribution from the BMF energy, given that $g > 0$ and $f(\tilde{\omega})$ is positive for any $\tilde{\omega}$. In such cases, the condition of vanishing pressure $P = 0$ can be achieved.

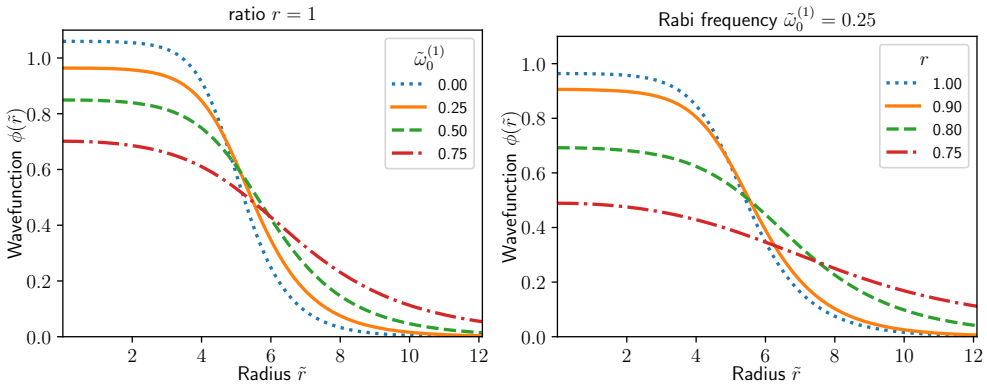

Figure 3.7: The ground state wavefunctions of the Rabi-coupled Bose mixture in the droplet phase are depicted for different combinations of $\tilde{\omega}_0^{(1)}$ and the ratio r. On the left side, the wavefunctions are shown for $\delta = 0$, corresponding to $r = 1$, and various values of $\tilde{\omega}_0^{(1)}$. Above a critical value $\tilde{\omega}_c$, the droplet can not sustain itself. On the right side, the wavefunctions are displayed for a fixed $\tilde{\omega}_0^{(1)} = 0.25$ while varying the ratio r. This plot reveals a self-bound droplet until a critical value of $r_c \approx 0.7$ is reached. The total particle number for both plots is $\tilde{N} = 500$.

As a result, we obtain an implicit equation for the equilibrium density:

$$n_0 = \frac{\left[g(1+r^4) + 2g_{12}r^2\right]^2}{4(r^2+1)^4\alpha^2 g^5 f^2(\tilde{\omega}_0)}, \tag{3.34}$$

where $\tilde{\omega}_0 = \frac{\hbar\omega_R}{gn_0}$. When $\omega_R = 0$ and $r = 1$, the equilibrium density is given by $n_0^{(1)} = \frac{25|\delta g|^2}{16\alpha^2 g^5(1+|\gamma|)^5}$, where $\delta g \equiv g_{12} + g$. Here, $n_0^{(1)}$ also serves as an approximation for the density of finite droplets where the kinetic energy is negligible. As the Rabi frequency $\tilde{\omega}$ increases while keeping the ratio r fixed, both the function $f(\tilde{\omega})$ and the BMF energy become larger, resulting in a decrease in the equilibrium density of the droplet.

We examine the feasibility of the finite droplet in a more quantitative manner by deriving the governing Gross-Pitaevskii Equation (GPE). To facilitate this analysis, we utilize the locked-in approximation, where different components of the droplet are in phase within any given region, and the density ratio of the components remains fixed throughout the condensate. Consequently, a single scalar wavefunction suffices to represent both components. We assume a droplet wavefunction $\Psi(\mathbf{r}) = \psi(\mathbf{r})(\tau_1\ \tau_2)^T$, where $\tau_1/\tau_2 = r$, and $|\tau_1|^2 + |\tau_2|^2 = 1$. By employing $n(\mathbf{r}) = |\Psi(\mathbf{r})|^2$, we express

the energy functional of the droplet as follows:

$$\begin{aligned}\mathcal{E}[\psi^*,\psi] &= \frac{\hbar^2}{2M}|\nabla\psi|^2 + \left(-\frac{2\hbar\omega_R r}{r^2+1} - \frac{\hbar\delta(1-r^2)}{2(1+r^2)}\right)|\psi|^2 \\ &+ \left(\frac{g}{2} - \frac{2\bar{g}r^2}{(1+r^2)^2}\right)|\psi|^4 \\ &+ \alpha g^{5/2} I_+\left(\frac{\hbar\omega_R}{g|\psi|^2}, \gamma, r\right)|\psi|^5, \end{aligned} \tag{3.35}$$

and write the wavefunction in dimensionless form $\psi(\mathbf{r}) = \sqrt{n_0^{(1)}}\phi(\mathbf{r})$. We proceed by minimizing the total energy in the grand canonical ensemble, given by $E = \int d^3\mathbf{r}\mathcal{E}[\psi^*,\psi] - \mu N$, where the chemical potential is constrained by the total number of particles $N = \int d^3\mathbf{r}|\psi|^2$. This minimization leads to the resulting modified Gross-Pitaevskii equation :

$$\begin{aligned}\tilde{\mu}\phi &= -\frac{1}{8}\left(r+\frac{1}{r}\right)^2\tilde{\nabla}^2\phi \\ &+ \left[2\alpha_4|\phi|^2 + \frac{5\alpha_5}{2}I_+\left(\frac{\tilde{\omega}_0^{(1)}}{|\phi|^2}, r, \gamma\right)|\phi|^3\right. \\ &- \left.\alpha_5\tilde{\omega}_0^{(1)} I_+'\left(\frac{\tilde{\omega}_0^{(1)}}{|\phi|^2}, r, \gamma\right)|\phi|\right]\phi, \end{aligned} \tag{3.36}$$

where $\tilde{\omega}_0^{(1)} = \frac{\hbar\omega_R}{g n_0^{(1)}}$, $\alpha_4 = \frac{3}{2|\delta g|}\left(\frac{(r^2+1)^2 g}{2r^2} - 2\bar{g}\right)$, and $\alpha_5 = \frac{15}{8(1+|\gamma|)^{5/2}}\left(r+\frac{1}{r}\right)^2$. The equation (3.36) is written in the dimensionless form $\tilde{\mathbf{r}} = \mathbf{r}/\xi$, with $\xi = \sqrt{\frac{6\hbar^2}{M|\delta g|n_0^{(1)}}}$ is the coherence length of the droplet and the total particle number is scaled by $\tilde{N} = N/n_0^{(1)}\xi^3$. This modified GPE reduces to the form obtained by Petrov [1] when $\omega_R = 0$ and $r = 1$, since $\alpha_4 = -3/2$ and $\alpha_5 I_+(0,1,\gamma) = 1$ in this limit. From now on, the scattering length ratio is fixed $\gamma = -1.5$, as in [67].

We use imaginary time evolution to numerically solve the modified Gross-Pitaevskii Equation (3.36) and obtain the ground state wavefunction for a fixed total particle number $\tilde{N} = 500$. We then identify the critical value of $\tilde{\omega}0^{(1)}$ above which the droplet expands to infinity. Interestingly, driving the gas to region II in Fig. 3.5, where the mean-field (MF) energy is attractive, would normally result in gas collapse. However, the repulsion due to the BMF energy is strong enough to lead to an expansion instead. To intuitively understand this, let's consider a condensate with particle number $\tilde{N}$ and radius $\tilde{R}$. The total energy $\tilde{E}$ comprises an attractive MF energy $\propto -\tilde{N}^2/\tilde{R}^3$, a repulsive BMF energy $\propto I + \tilde{N}^{5/2}/\tilde{R}^{9/2}$, and the kinetic energy $\propto \tilde{N}/\tilde{R}^2$. As the

BMF energy increases with larger I_+, the equilibrium radius $\tilde{R}$ of the droplet grows. Consequently, the kinetic energy ($\propto \tilde{R}^{-2}$) becomes significant relative to both MF ($\propto \tilde{R}^{-3}$) and BMF ($\propto \tilde{R}^{-9/2}$) energies. As a result, the minimum of $\tilde{E}(\tilde{R})$ shifts to larger $\tilde{R}$ and eventually disappears. For the case of $\tilde{N} = 500$ and $\delta = 0$, or $r = 1$, the critical frequency is $\tilde{\omega}_c = 0.9$, above which the gas expands. Fig. 3.7 illustrates the increase in the droplet radius with increasing $\tilde{\omega}_0^{(1)}$ up to the critical $\tilde{\omega}_c$ in the left panel.

As r decreases, the MF interaction energy (α_4 term in (3.18)) initially decreases and then becomes repulsive for $r < 0.62$. The BMF energy (3.19) also decreases with r. However, since the MF energy shrinks at a higher rate, we expect $\tilde{\omega}_c$ to decrease as r decreases. As r changes from 1 to 0.7, $\tilde{\omega}_c$ changes from 0.9 to 0, and we do not observe a droplet phase below $r = 0.7$. For $0.62 < r < 0.70$, the MF interaction of the gas is attractive. However, the MF energy is relatively weak, so any BMF repulsion results in an expansion. The right panel of Fig. 3.7 shows the droplet wavefunction for various ratios r with fixed $\tilde{N} = 500$ and $\tilde{\omega}_0^{(1)} = 0.25$.

To determine the droplet phase boundary, we numerically obtain the critical $\tilde{\omega}_c$ values for different r while keeping $\tilde{N} = 500$ and $|\gamma| = 1.5$, as shown in Fig. 3.5.

The parameters discussed in the phase diagrams above are achievable within the current experimental capabilities for Rabi-coupled gases. For example, a mixture of ^{39}K atoms in hyperfine states $|F = 1, m_F = 0\rangle$ and $|F = 1, m_F = -1\rangle$ can be utilized. By tuning the intracomponent scattering lengths to $a_{11} = a_{22} = 40a_B$ and the intercomponent scattering length to $a_{12} = -60a_B$ using Feshbach resonance around $B \approx 54.5\ G$, we can obtain a ratio of interactions $\gamma = \frac{g}{g_{12}} = -1.5$. In the absence of detuning and Rabi coupling, a droplet with a radius of $0.4\ \mu m$ and a peak density of $n_0 = 4.12 \times 10^{16} cm^{-3}$ can be formed with approximately $N \approx 23,000$ particles. Introducing a Rabi-coupling $\omega_R = 2\pi f_R$ up to $f_R \approx 51\ kHz$ causes the droplet to expand to a radius of $r \approx 0.65\ \mu m$ and the central density to decrease to $n_0 \approx 0.8 \times 10^{16} cm^{-3}$. Above $51\ kHz$, the droplet will not be self-bound. By setting the Rabi-frequency to $f_R = 10.2\ kHz$ for the same number of particles, the role of non-zero detuning can be tested. The critical detuning level for these parameters is $\delta_c = 41\ kHz$, which results in a density of $n_0 = 3.75 \times 10^{16} cm^{-3}$ and a radius of

$7.4\ \mu m$ beyond which it is no longer self-bound.

3.3 Polarized Spin-1 Droplet

In the previous chapter 3.3.4, we investigated the behavior of a spin-1 gas with zero magnetization ($\langle \mathbf{F} \rangle = 0$). Our findings showed that a spinor droplet can exist in both the polar and antiferromagnetic phases under specific conditions: negative density interaction ($c_0 < 0$) and positive spin interaction ($c_1 > 0$). In the spin-1 condensate, the quadratic Zeeman energy q plays a role similar to the Rabi-frequency ω_R in Bose mixtures, as both parameters are capable of controlling the droplet's density. When the value of q increases, the droplet expands due to the influence of the greater BMF energy. However, beyond a critical threshold of q, the gas loses its self-binding ability. Additionally, we draw parallels between the detuning parameter δ in the Rabi-coupled mixture and the linear Zeeman shift p in the spinor gas. Both of these parameters have analogous effects in their respective systems.

3.3.1 Polarized Spin-1 Gases: Bogoliubov Theory

We broaden our thesis of spinor droplets to account for the impact of non-zero magnetization ($p \neq 0$). The ground state order parameter experiences modifications solely within the antiferromagnetic phase (refer to Fig. 3.8), while it induces a constant shift in the mean-field energy for the polar phase [21, 22, 62].

The following Hamiltonian describes the spin-1 condensate with s-wave interactions and a uniform magnetic field along the z-axis:

$$\begin{aligned} \hat{H} \quad &= \int d\mathbf{x} \left\{ \hat{\Psi}^\dagger_m(\mathbf{x}) \left(-\frac{\hbar^2 \nabla^2}{2M} + qm^2 - pm \right) \hat{\Psi}_m(\mathbf{x}) \right. \\ &+ \frac{c_0}{2}\ \hat{\Psi}^\dagger_m(\mathbf{x}) \hat{\Psi}^\dagger_{m'}(\mathbf{x}) \hat{\Psi}_{m'}(\mathbf{x}) \hat{\Psi}_m(\mathbf{x}) \\ &+ \left. \frac{c_1}{2}\ \hat{\Psi}^\dagger_m(\mathbf{x}) \hat{\Psi}^\dagger_{m'}(\mathbf{x})\ \mathbf{F}_{mn} \cdot\ \mathbf{F}_{m'n'} \hat{\Psi}_{n'}(\mathbf{x}) \hat{\Psi}_n(\mathbf{x}) \right\}, \end{aligned} \tag{3.37}$$

where $\hat{\Psi}^\dagger_m(\mathbf{x})$ and $\hat{\Psi}_m(\mathbf{x})$ create and annihilate spin-1 atom in the magnetic quantum state $m = -1, 0, 1$, $\mathbf{F}_{mm'} = (F^x_{mm'}, F^y_{mm'}, F^z_{mm'})$ are the spin-1 matrices in z-axis

basis, and summation convention is used for m indices. The linear Zeeman energy, denoted by p, arises from the product of the Land'e g_L-factor, the Bohr magneton μ_B, and the applied magnetic field B, expressed as $p = -g_L\mu_B B$. On the other hand, the quadratic Zeeman energy, represented as $q = q_B + q_{MW}$, can be adjusted using both an external static field $q_B = \frac{(g\mu_B B)^2}{\Delta E_{hf}}$ and a microwave field q_{MW}. Consequently, while the linear Zeeman energy p is set using the static magnetic field B, the quadratic Zeeman energy q can be independently controlled by the microwave fields [22].

The density and spin interactions are parameterized by the coupling constants $c_0 = \frac{g_0+2g_2}{3}$ and $c_1 = \frac{g_2-g_0}{3}$, respectively. Here, g_0 and g_2 represent the total coupling constants for the spin-0 and spin-2 channels, respectively.

The MF ground state order parameter τ is determined by minimizing the MF energy [22] (See section 3.3.2 for derivation):

$$\frac{E_{\rm MF}}{V} = \frac{n^2}{2}(c_0 + c_1\langle\mathbf{F}\rangle^2) + qn\langle F_z^2\rangle - pn\langle F_z\rangle. \tag{3.38}$$

We study the magnetic orders in the presence of positive spin coupling constants ($c_1 > 0$) as depicted in Fig. 3.8. When $p = 0$, the order parameter takes the form of $\tau_P = (0\ 1\ 0)$ for $q > 0$, or $\tau_{AF} = \frac{1}{\sqrt{2}}(1\ 0\ 1)$ for $q < 0$. When $q > 0$, the introduction of a non-zero p does not lead to any changes in τ_P along the q-axis. However, if $q < 0$, the MF energy is minimized by a p-dependent order parameter, denoted as $\tau_{AF} = \frac{1}{\sqrt{2}}(\sqrt{1+\tilde{p}}\ 0\ \sqrt{1-\tilde{p}})$, where $\tilde{p} \equiv \frac{p}{nc_1}$. Here, it is essential to note that $\langle F_z\rangle = \tilde{p}$, which implies that τ_{AF} is defined for $-1 \le \tilde{p} \le 1$. Beyond this interval, the order parameter exhibits ferromagnetic behavior. The main focus of this thesis is on this $\tilde{p}$-dependent τ_{AF} to analyze the impact of non-zero magnetization $\tilde{p}$ on spinor droplets.

The order parameter τ_{AF} gives $\langle F_z^2\rangle = 1$, $\langle F_z\rangle = \tilde{p}$, and $\langle\mathbf{F}\rangle = \tilde{p}\hat{e}_z$ and the resulting MF and BMF energies are (See Section 3.3.2 for the derivation):

$$\frac{E_{MF}}{V} = (q - \tilde{p}p)n + \frac{(c_0 + c_1\tilde{p}^2)n^2}{2} \tag{3.39}$$

$$\begin{aligned}\frac{E_{BMF}}{V} &= \frac{8\sqrt{2}}{15}\alpha(c_1 n)^{5/2} I_0(\tilde{q},\beta) \\ &+ \frac{8\sqrt{2}}{15}\alpha\left((c_0+c_1)n\right)^{5/2}\left[I_+(\kappa) + I_-(\kappa)\right],\end{aligned} \tag{3.40}$$

where $\tilde{q} = \frac{q}{nc_1}$, $I_\pm = \frac{(1\pm\kappa)^{5/2}}{4\sqrt{2}}$, $\kappa \equiv \sqrt{1 - \frac{4\beta^2 c_0 c_1}{(c_0+c_1)^2}}$, $\beta = \sqrt{1-\tilde{p}^2}$ and $I_0(\tilde{q},\beta)$ is

approximately (See Section 3.3.3):

$$I_0(\tilde{q},\beta) \approx \frac{15\pi\beta^2}{32\sqrt{2}}\left[\sqrt{-\tilde{q}+1} - \frac{\beta^2}{32}\frac{1}{(-\tilde{q}+1)^{3/2}}\right]. \tag{3.41}$$

The results in [64] are obtained when $\tilde{p}=0$ and $\tau_{AF} = 1/\sqrt{2}\,(1\;0\;1)$.

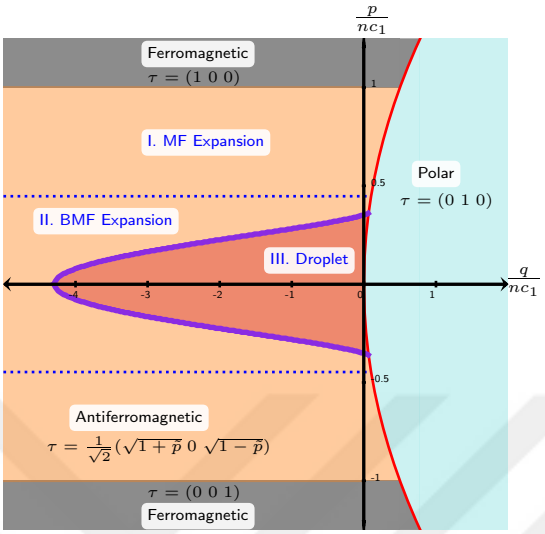

Figure 3.8: The phase diagram of mechanical stability for the spin-1 droplet is presented concerning the quadratic Zeeman energy q/nc_1 and the linear Zeeman energy p/nc_1. The orange region in the diagram corresponds to the antiferromagnetic order. Outside the dashed blue lines, particularly when $|\tilde{p}| > 0.44$, the mean-field (MF) interaction is repulsive. Conversely, inside the dashed lines, where $|\tilde{p}| < 0.44$, the MF interaction becomes attractive. This occurs for a specific ratio of $c_1/c_0 = -5$, with c_0 being negative. The boundary of the droplet phase is represented by a solid purple line, indicating the region where the gas can be stabilized by beyond-mean-field (BMF) fluctuations. Three distinct regions are identifiable: In Region I, the repulsive MF interaction leads to gas expansion. In Region II, even though the MF energy is attractive, the BMF repulsion is relatively strong, causing expansion. In Region III, the MF attraction is stabilized by the repulsive BMF energy, resulting in a stable droplet phase.The total particle number in the system is $\tilde{N} = 500$.

Note that when $\tilde{p} = 0$, the MF interaction is attractive if $c_0 < 0$. Furthermore, the MF energy decreases in magnitude as polarization $|\tilde{p}|$ increases. Interestingly, if $\tilde{p} > \sqrt{|c_0|/c_1}$, it becomes repulsive, which causes the gas to expand above a critical level $\tilde{p}_c$ shown with dotted lines in Fig. 3.8.

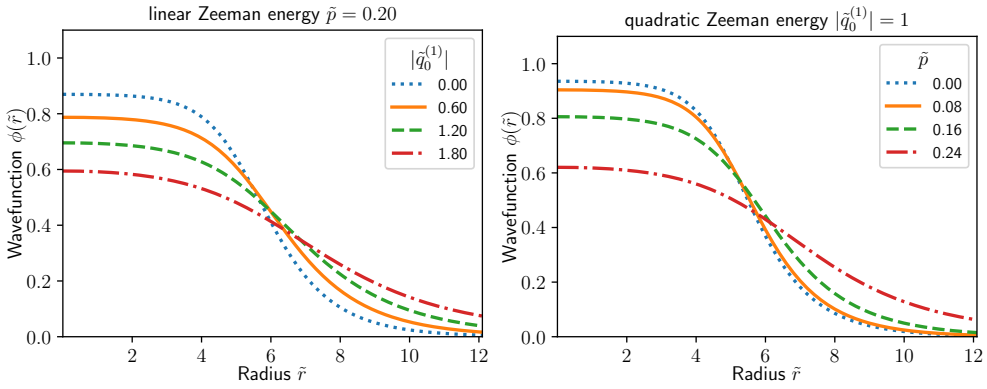

Figure 3.9: The ground state wavefunctions of the spin-1 condensate in the antiferromagnetic (AF) phase are displayed for various combinations of the quadratic Zeeman energy $\tilde{q}_0^{(1)}$ and linear Zeeman energy $\tilde{p}$. The total particle number is fixed at $\tilde{N} = 500$, and the ratio c_1/c_0 is set to -5 with c_0 being negative. On the left plot, the wavefunctions are illustrated for a constant value of $\tilde{p} = 0.2$ while varying $\tilde{q}_0^{(1)}$. Above a critical value $\tilde{q}_c$, the formation of a self-bound droplet becomes unfeasible. On the right plot, the wavefunctions are shown for $|\tilde{q}_0^{(1)}| = 1$ with different values of $\tilde{p}$. Similarly, above a critical value $\tilde{p}_c$, the droplet is no longer self-trapped. Both plots clearly demonstrate how changes in the quadratic and linear Zeeman energies can significantly influence the formation and stability of the self-bound droplet in the spin-1 condensate within the antiferromagnetic phase.

In the region where the mean-field (MF) interaction is attractive, i.e., $\tilde{p} < \sqrt{|c_0|/c_1}$, the contribution of the BMF energy becomes repulsive due to the positive value of c_1. This repulsive BMF energy plays a crucial role in stabilizing the gas. Specifically, the stabilization is achieved through the hard modes represented by the I_+ and I_0 dispersion, while the soft mode I_- containing imaginary parts can be ignored, similar to the approach in the previous section 3.2.2.

3.3.2 Bogoliubov Theory of Spin-1 Gas

The Hamiltonian in (3.38) reduces to quadratic form with the Bogoliubov approximation [23]:

$$\begin{aligned}\hat{H}_{eff} = \quad & \frac{Vn^2}{2}(c_0 + c_1\langle\mathbf{F}\rangle^2) + qN\langle F_z^2\rangle - pN\langle F_z\rangle \\ & + \sum_{\mathbf{k}\neq\mathbf{0}} \Big\{ \left[\epsilon_{\mathbf{k}} - nc_1\langle\mathbf{F}\rangle^2 + qm^2 - q\langle F_z^2\rangle\right] \hat{a}^\dagger_{\mathbf{k},m}\hat{a}_{\mathbf{k},m} \\ & + nc_1\langle\mathbf{F}\rangle\cdot\mathbf{F}_{mm'}\hat{a}^\dagger_{\mathbf{k},m}\hat{a}_{\mathbf{k},m'} \\ & + \frac{nc_0}{2}(2\hat{D}^\dagger_{\mathbf{k}}\hat{D}_{\mathbf{k}} + \hat{D}_{\mathbf{k}}\hat{D}_{-\mathbf{k}} + \hat{D}^\dagger_{\mathbf{k}}\hat{D}^\dagger_{-\mathbf{k}}) \\ & + \frac{nc_1}{2}(2\hat{\mathbf{F}}^\dagger_{\mathbf{k}}\hat{\mathbf{F}}_{\mathbf{k}} + \hat{\mathbf{F}}_{\mathbf{k}}\hat{\mathbf{F}}_{-\mathbf{k}} + \hat{\mathbf{F}}^\dagger_{\mathbf{k}}\hat{\mathbf{F}}^\dagger_{-\mathbf{k}})\Big\}, \end{aligned} \tag{3.42}$$

where $\epsilon_{\mathbf{k}} = \hbar^2\mathbf{k}^2/2M$ is the free particle dispersion, $\langle\mathbf{F}\rangle \equiv \sum_{m,m'}\mathbf{F}_{mm'}\tau^*_m\tau_{m'}$ is the expectation value of the spin-1 order parameter, $\hat{D}_{\mathbf{k}} \equiv \sum_m \tau^*_m\hat{a}_{\mathbf{k},m}$ and $\hat{\mathbf{F}}_{\mathbf{k}} \equiv \sum_{m,m'}\mathbf{F}_{mm'}\tau^*_m\hat{a}_{\mathbf{k},m'}$ are the density and spin fluctuation operators, N_0 is the number of particles in the $\mathbf{k} = 0$ state, τ is the ground state order parameter in the spin-1 manifold.

The MF energy of spin-1 BEC obtained from (3.42) is [23]

$$\frac{E_{\mathrm{MF}}}{V} = \quad \frac{n^2}{2}(c_0 + c_1\langle\mathbf{F}\rangle^2) + qn\langle F_z^2\rangle - pn\langle F_z\rangle, \tag{3.43}$$

while the rest of the terms form the quantum fluctuations.

The order parameter τ_{AF} gives $\langle F_z^2\rangle = 1$, $\langle F_z\rangle = \tilde{p}$, and $\langle\mathbf{F}\rangle = \tilde{p}\hat{e}_z$ and the resulting quadratic Hamiltonian is:

$$\begin{aligned}\hat{H} \quad & = E_0^{AF} + \sum_{\mathbf{k}\neq 0}\Bigg\{ (\epsilon_{\mathbf{k}} - q + c_1 n)\,\hat{a}^\dagger_{\mathbf{k},0}\hat{a}_{\mathbf{k},0} \\ + \quad & \frac{c_1 n\beta}{2}\left(\hat{a}^\dagger_{\mathbf{k},0}\hat{a}^\dagger_{-\mathbf{k},0} + \hat{a}_{\mathbf{k},0}\hat{a}_{-\mathbf{k},0}\right) \\ + \quad & \sum_{m=\pm 1}\left[\epsilon_{\mathbf{k}} + \frac{(c_0+c_1)n(1+m\tilde{p})}{2}\right]\hat{a}^\dagger_{\mathbf{k},m}\hat{a}_{\mathbf{k},m} \\ + \quad & \sum_{m=\pm 1}\left[\frac{(c_0+c_1)n(1+m\tilde{p})}{4}\right]\left(\hat{a}^\dagger_{\mathbf{k},m}\hat{a}^\dagger_{-\mathbf{k},m} + \hat{a}_{\mathbf{k},m}\hat{a}_{-\mathbf{k},m}\right) \\ + \quad & \frac{(c_0-c_1)n\beta}{4}\Big(2\hat{a}^\dagger_{\mathbf{k},-1}\hat{a}_{\mathbf{k},1} + \hat{a}^\dagger_{\mathbf{k},-1}\hat{a}^\dagger_{-\mathbf{k},1} + \hat{a}^\dagger_{\mathbf{k},1}\hat{a}^\dagger_{-\mathbf{k},-1} \\ + \quad & 2\hat{a}^\dagger_{\mathbf{k},1}\hat{a}_{\mathbf{k},-1} + \hat{a}_{\mathbf{k},-1}\hat{a}_{-\mathbf{k},1} + \hat{a}_{\mathbf{k},1}\hat{a}_{-\mathbf{k},-1}\Big)\Bigg\}, \end{aligned} \tag{3.44}$$

where $\beta = \sqrt{1-\tilde{p}^2}$, and E_0^{AF} is the MF energy:

$$\frac{E_0^{AF}}{V} = (q - \tilde{p}p)n + \frac{(c_0 + c_1\tilde{p}^2)n^2}{2}. \tag{3.45}$$

The diagonalization of the quadratic Hamiltonian in (3.44) yields three distinct Bogoliubov modes [21]:

$$\begin{aligned} E_{k,\pm 1} &= \sqrt{\epsilon_{\mathbf{k}}[\epsilon_{\mathbf{k}} + (c_0 + c_1)n(1 \pm \kappa)]} \\ E_{k,0} &= \sqrt{(\epsilon_{\mathbf{k}} - q + (1-\beta)c_1 n)\,(\epsilon_{\mathbf{k}} - q + (1+\beta)c_1 n)}, \end{aligned} \tag{3.46}$$

where $\kappa \equiv \sqrt{1 - \frac{4\beta^2 c_0 c_1}{(c_0+c_1)^2}}$. We reexpress the MF energy density functional to renormalize the diverging BMF energy:

$$\frac{(c_0 + c_1\tilde{p}^2)n^2}{2} = \frac{[\tilde{p}^2(c_0+c_1) + (1-\tilde{p}^2)c_0]n^2}{2}. \tag{3.47}$$

Then, replace the coupling constants c_0 and $c_0 + c_1$ in (3.47) with the second-order corrected coupling constants $\bar{c}_0$ and $\bar{c}_0 + \bar{c}_1$ (See Appendix of Ref. [23]):

$$\bar{c}_0 = c_0 + \frac{(c_0^2 + 2c_1^2)}{V} \sum_{\mathbf{k}\neq 0} \frac{1}{2\epsilon_{\mathbf{k}}}, \tag{3.48}$$

$$\bar{c}_0 + \bar{c}_1 = (c_0 + c_1) + \frac{(c_0 + c_1)^2}{V} \sum_{\mathbf{k}\neq 0} \frac{1}{2\epsilon_{\mathbf{k}}}. \tag{3.49}$$

Subsequently, we partition the total renormalization energy into three distinct modes to prevent divergence in each mode individually. The BMF energies become:

$$\begin{aligned} E_{BMF,\pm 1} = \frac{1}{2}\sum_{\mathbf{k}\neq 0} \Bigg\{ & E_{k,\pm 1} - \left(\epsilon_{\mathbf{k}} + \frac{(c_0+c_1)(1\pm\tilde{p})n}{2}\right) \\ & + \frac{(\kappa^2+1)(c_0+c_1)^2 n^2}{4\epsilon_{\mathbf{k}}} \Bigg\}, \end{aligned} \tag{3.50}$$

$$E_{BMF,0} = \frac{1}{2}\sum_{\mathbf{k}\neq 0} \left\{ E_{k,0} - (\epsilon_{\mathbf{k}} - \tilde{q} + c_1 n) + \frac{\beta^2 (c_1 n)^2}{2\epsilon_{\mathbf{k}}} \right\}, \tag{3.51}$$

where $\tilde{q} = \frac{q}{nc_1}$. Then, the total BMF energy density functional for the AF order:

$$\begin{aligned} \frac{E_{BMF}^{AF}}{V} &= \frac{8\sqrt{2}}{15}\alpha (c_1 n)^{5/2} I_0(\tilde{q}, \beta) \\ &+ \frac{8\sqrt{2}}{15}\alpha \left((c_0+c_1)n\right)^{5/2} [I_+(\kappa) + I_-(\kappa)], \end{aligned} \tag{3.52}$$

where $I_\pm = \frac{(1\pm\kappa)^{5/2}}{4\sqrt{2}}$ and $I_0(\tilde{q}, \beta)$ can be approximated as (See Appendix 3.3.3):

$$I_0(\tilde{q}, \beta) \approx \frac{15\pi\beta^2}{32\sqrt{2}} \left[\sqrt{-\tilde{q}+1} - \frac{\beta^2}{32} \frac{1}{(-\tilde{q}+1)^{3/2}} \right]. \tag{3.53}$$

3.3.3 Analytical approximation for $I_0(\tilde{q}, \beta)$

The BMF energy for $E_{k,0}$ mode is determined by the following integral:

$$I_0(\tilde{q}, \beta) = \frac{15}{8\sqrt{2}} \int_0^\infty dx\, x^2 \times \left[\sqrt{(x^2 - \tilde{q} + 1)^2 - \beta^2} - (x^2 - \tilde{q} + 1) + \frac{\beta^2}{2x^2} \right], \tag{3.54}$$

where $\epsilon_{\mathbf{k}} \equiv c_1 n x^2$ substitution is applied.

We change the variable $y \equiv x^2 - \tilde{q} + 1$ in the integral (3.54) and expand $\sqrt{1 - \beta^2/y^2}$ in Taylor series up to the second order in the range $x \geq 0$ and $\tilde{q} \leq 0$. It yields:

$$I_0(\tilde{q}, \beta) \quad = -\frac{15\beta^2}{16\sqrt{2}} \int_0^\infty dx \left(\frac{(\tilde{q} - 1)}{x^2 - \tilde{q} + 1} + \frac{\beta^2 x^2}{4(x^2 - \tilde{q} + 1)^3} \right). \tag{3.55}$$

Each term above can be calculated to give:

$$I_0(\tilde{q}, \beta) \approx \frac{15\pi\beta^2}{32\sqrt{2}} \left[\sqrt{-\tilde{q} + 1} - \frac{\beta^2}{32} \frac{1}{(-\tilde{q} + 1)^{3/2}} \right]. \tag{3.56}$$

Including higher order terms in the expansion of $\sqrt{1 - \beta^2/y^2}$ enhances accuracy, but our numerical analysis confirms that the second-order expansion is satisfactory, providing less than one percent error for all $\tilde{q}$ values.

3.3.4 Polarized AF Spin-1 Droplet

For the parameter regime where $c_0 < 0$ and $c_1 > 0$, we determine the pressure of the gas using the thermodynamic identity $P = -\partial E/\partial V$, where the total energy is composed of E_{MF}, E^+_{BMF}, and E^0_{BMF}. This results in the following expression for the pressure:

$$P = \left(\frac{c_0 + \tilde{p}^2 c_1}{2} \right) n^2 + \frac{4\sqrt{2}}{15} \alpha (c_1 n)^{5/2}\, h(\tilde{q}, \beta), \tag{3.57}$$

where $h(\tilde{q}, \beta) = 3I_0(\tilde{q}, \beta) + 3\left(c_0/c_1 + 1\right)^{5/2} I_+(\kappa) - 2\tilde{q} I_0'(\tilde{q}, \beta)$. Here, prime on I_0 denotes the partial derivative with respect to $\tilde{q}$. The equilibrium density for the infinite homogeneous droplet can be calculated by $P = 0$ condition:

$$n_0 = \frac{225}{128} \frac{(c_0 + \tilde{p}^2 c_1)^2}{c_1^5\, h^2(\tilde{q}_0, \beta)}, \tag{3.58}$$

where $\tilde{q}_0 = \frac{q}{n_0 c_1}$. n_0 corresponds to the equilibrium density result obtained in Ref. [64] for the case of zero magnetization ($\tilde{p} = 0$). By taking the limit $q \to 0$, we determine a density scale $n_0^{(1)} = \frac{25|c_0|^2}{512\alpha^2|c_1|^5}$, which we utilize to express the dimensionless modified GPE. Since $h(\tilde{q}, \beta)$ is a monotonically increasing function of $\tilde{q}$, the equilibrium density decreases with an increase in the quadratic Zeeman energy $\tilde{q}$. As $\tilde{q}$ becomes larger, stronger BMF fluctuations occur, and the system can stabilize at lower densities.

We use again the locked-in approximation $\Psi(\mathbf{r}) = \psi(\mathbf{r})\tau^{AF}$ where the order parameter $\tau^{AF} = 1/\sqrt{2}\left(\sqrt{1+\tilde{p}}\ 0\ \sqrt{1-\tilde{p}}\right)$ and write the energy functional

$$\begin{aligned} \mathcal{E} \quad & [\psi^*, \psi] = \frac{\hbar^2}{2M}|\nabla\psi|^2 \\ + \quad & (q - \tilde{p}p)\,|\psi|^2 + \left(\frac{c_0 + c_1\tilde{p}^2}{2}\right)|\psi|^4 \\ + \quad & \frac{8\sqrt{2}}{15}\alpha\left[(c_1 n)^{5/2} I_0(\tilde{q}, \beta) + ((c_0 + c_1)n)^{5/2}\, I_+(\kappa)\right]|\psi|^5. \end{aligned} \tag{3.59}$$

Using $\psi(\mathbf{r}) = \sqrt{n_0^{(1)}}\phi(\mathbf{r})$, we minimize the total energy $E = \int d^3\mathbf{r}\mathcal{E}[\psi^*, \psi] - \mu N$ with the total number of particles $N = \int d^3\mathbf{r}|\psi|^2$ which yields the modified GPE

$$\begin{aligned} \tilde{\mu}\phi \quad = \quad & -\frac{1}{2}\tilde{\nabla}^2\phi \\ + \quad & \left\{-3\left(1 + \frac{c_1}{c_0}\tilde{p}^2\right)|\phi|^2 + \frac{5}{4}I_0\left(\frac{\tilde{q}_0^{(1)}}{|\phi|^2}, \beta\right)|\phi|^3\right. \\ + \quad & \left.\frac{5}{4}\left(\frac{c_0}{c_1} + 1\right)^{5/2} I_+(\kappa)|\phi|^3 - \frac{\tilde{q}_0^{(1)}}{2}I_0'\left(\frac{\tilde{q}_0^{(1)}}{|\phi|^2}, \beta\right)|\phi|\right\}\phi, \end{aligned} \tag{3.60}$$

where $\tilde{q}_0^{(1)} = \frac{q}{n_0^{(1)} c_1}$, $\tilde{\mathbf{r}} = \mathbf{r}/\xi$, $\xi = \sqrt{\frac{6\hbar^2}{M|c_0|n_0^{(1)}}}$ is the coherence length of the droplet. In the limit $\tilde{p} \to 0$, we recover the GPE of the unpolarized AF gas $\tau^{AF} = 1/\sqrt{2}(1\ 0\ 1)$ with $I_+(\kappa) \to \left(\frac{c_1}{c_0 + c_1}\right)^{5/2}$. The droplet phase is expected up to a critical $|\tilde{q}| \approx 4.4$ for $\tilde{N} \approx 500$ and $c_1/c_0 = -5$ [64].

When the absolute value of $\tilde{p}$ is greater than or equal to approximately 0.45 (represented by the blue dashed line in Fig. 3.8), the mean-field (MF) interaction becomes repulsive. As a result, the gas undergoes an expansion, and further corrections provided by BMF fluctuations contribute to this repulsion. Conversely, when the absolute value of $\tilde{p}$ is less than $\sqrt{|c_0|/c_1}$, the MF term drives a density collapse, while the BMF interactions still remain effectively repulsive. In general, the effect of $\tilde{p}$ is more obvi-

ous in the MF terms compared to the BMF corrections. On the other hand, the effect of $|\tilde{q}|$ is relatively small in the MF interactions but strengthens the BMF fluctuations for a given value of $\tilde{p}$.

In Fig. 3.9, we present the droplet wavefunctions obtained from the numerical solution of the modified Gross-Pitaevskii equation (GPE). The right panel shows the wavefunctions for $|\tilde{q}_0^{(1)}| = 1$ while varying $\tilde{p}$, and the left panel shows the wavefunctions for $\tilde{p} = 0.2$ while varying $|\tilde{q}_0^{(1)}|$.

When the magnetization $\tilde{p}$ is fixed, a larger value of $|\tilde{q}_0^{(1)}|$ results in a stronger repulsive effect from the BMF energy, leading to an increase in the droplet radius. For $\tilde{p} = 0.2$, once $|\tilde{q}_c| \approx 2.2$, the gas is unable to form a droplet. On the other hand, when $|\tilde{q}_0^{(1)}|$ is fixed, a higher magnetization $\tilde{p}$ leads to both reduced MF attraction and decreased BMF repulsion. As the polarization changes the MF attraction at a higher rate compared to the BMF repulsion, the critical value of $|\tilde{q}_c|$ becomes lower with increasing $\tilde{p}$. When $\tilde{p} > \tilde{p}_c \approx 0.3$ for $|\tilde{q}_0^{(1)}| = 1$, even a small BMF repulsion is enough to cause gas expansion, as the MF attraction becomes significantly weaker. Consequently, beyond this critical level of $\tilde{p}_c$, the gas cannot form a bound droplet.

We determine the critical levels for each combination of $\tilde{q}_0^{(1)}$ and $\tilde{p}$ within the relevant parameter region for $c_1/c_0 = -5$ and represent the droplet phase boundary in Fig. 3.8 using a solid red curve.

3.3.5 Discussion of experimental realization and Conclusion

Although experimentally realized spinor Bose-Einstein condensates (BECs) thus far are mechanically stable with $c_0 > 0$, future cold atom settings may enable tuning of the spinor BEC scattering lengths using theoretically proposed optical Feshbach resonances [53, 54]. For instance, considering an atom with scattering lengths $a_0 = -50a_B$ in the spin-0 channel and $a_2 = 20a_B$ in the spin-1 channel, with Land'e factor $g_L = 1/2$ ($s = 1/2, l = 0, I = 3/2$), we obtain $c_1/c_0 = -5$ with $c_0 < 0$. In the absence of linear and quadratic Zeeman energies, a spinor droplet with a density of $8.3 \times 10^{16}\ cm^{-3}$ and a radius of $0.6\ \mu m$ can be formed with a total particle number of approximately $N \approx 130,000$. This droplet remains self-bound until the critical

level of quadratic Zeeman energy $q \approx 680\ kHz$. For an initial magnetization per particle of $\tilde{p} = 0.2$, the gas remains stable until the quadratic Zeeman energy exceeds $320\ kHz$, resulting in a central density of approximately $2.1 \times 10^{16}\ cm^{-3}$ and a radius of $0.95\ \mu m$.

In conclusion, Rabi-coupled Bose mixtures and spinor gases exhibit several similarities: (i) BMF energies are dependent on the Rabi-frequency or quadratic Zeeman energy, (ii) introducing a non-zero Rabi-frequency or quadratic Zeeman energy causes one of the Bogoliubov modes to become gapped, and (iii) the polarization and effective mean-field energy can be significantly altered using detuning or linear Zeeman energy. As a result, droplet formation and its properties are highly influenced by the linear and quadratic Zeeman energies in spinor gases and the Rabi-frequency and detuning in Bose mixtures.

CHAPTER 4

VORTEX LATTICES IN BOSE MIXTURE DROPLETS

Quantum droplets in the Bose mixture exhibit a delicate equilibrium that crucially relies on quantum fluctuations to stabilize the mean-field tendency toward collapse. Most research on droplets has focused on scenarios with weak or no trapping, where the condensate is in the self-trapped droplet states with liquid-like, flat-density profiles. However, the weakly trapped droplets respond to rotation by exciting center-of-mass motion or splitting instability. In our thesis, we explore the opposite limit of weak external confinement, where the external potential prevents splitting and center-of-mass excitation. In this regime, we discover that a rapidly rotating quantum droplet with a triangular vortex lattice is formed. The overall density profile closely follows the Thomas-Fermi analytical result, which is obtained by solving a cubic equation. Interestingly, rapidly rotating droplets exhibit three significant differences compared to repulsive Bose-Einstein condensates (BECs) with vortex lattices. First, the vortex core size in droplets changes rapidly at finite density, a feature that is visible in the numerically obtained density profiles. We find that the vortex core size aligns well with an analytical estimate of the coherence length for droplets. Second, the change in the density profile leads to a slight but observable distortion in the lattice, consistent with the distortion expected from nonuniform superfluid density. Finally, unlike repulsive BECs, which rapidly expand as the rotation frequency approaches the trapping frequency, rapidly rotating droplets experience only a fractional change in their size. This behavior can also allow for the creation of clouds with a low filling factor, which can serve as a means to probe strongly correlated bosonic states.

4.1 Introduction

Rotating a Bose-Einstein condensate (BEC) gives rise to novel non-classical effects, due to the irrotational nature of superfluid flow in the absence of density singularities [7, 8]. The angular momentum in a phase-coherent BEC is carried by quantized vortices, forming a regular lattice that mimics solid body rotation. In experiments with single-component repulsive BECs, a triangular lattice of singly quantized vortices was observed when the BEC was rotated in an isotropic harmonic trap [25, 75, 76]. The dependence of vortex core size, vortex density, and condensate radius on the rotation frequency and superfluid density for rotating repulsive BECs has been studied theoretically in both the Thomas-Fermi (TF) and the lowest Landau level (LLL) regimes [77]. In contrast, BECs of attractively interacting atoms are only metastable under harmonic confinement, and they carry angular momentum through center-of-mass (COM) rotation instead of vortices [78].

Researchers have extensively investigated vortex lattices also in two-component Bose-Einstein condensate (BEC) mixtures with varying intracomponent interactions g_{11} and g_{22}, as well as intercomponent interaction g_{12} [15, 16, 26, 77]. Depending on the strength of the repulsive intercomponent interaction $g_{12} > 0$, the mixture can exhibit coincident or displaced lattices with triangular, square, or rectangular symmetries. For attractive intercomponent interactions $g_{12} < 0$ and mechanically stable Bose mixtures with $|g_{12}| < \sqrt{g_{11}g_{22}}$, both components coincide and form a triangular lattice [15]. However, the mean-field (MF) treatment of the Bose mixture predicts that the condensate is unstable toward collapse for $g_{12} < 0$ and $|g_{12}| < \sqrt{g_{11}g_{22}}$ [8]. Nonetheless, if the mixture is confined by a harmonic trap, it can be metastable for a small number of particles.

The quantum fluctuations can intervene and prevent the predicted mean-field collapse. In Bose mixture systems, quantum droplets represent self-trapped phases that remain mechanically stable even without external confinement [1]. The effective attractive MF) interaction is countered by repulsive beyond mean-field (BMF) fluctuations. Specifically, when $g_{12} \lesssim -\sqrt{g_{11}g_{22}}$, the overall attractive MF energy, proportional to $-\delta g n^2$ (where $\delta g = |g_{12}| - \sqrt{g_{11}g_{22}}$ and n is the condensate density), is relatively weak and can be stabilized by the BMF energy, which scales as $g_{BMF}n^{5/2}$. In cases

with large particle numbers N, the interaction energy dominates the ground state, resulting in an equilibrium density profile that resembles an incompressible liquid with a constant density [1]. However, for smaller N, the droplet can still self-stabilize, but the ground state exhibits a smoothly decaying density profile. Importantly, there exists a critical particle number below which the kinetic energy cost becomes too substantial for the droplet to maintain its stability, and expand the gas to infinity if it is not confined or trapped.

The quantum droplet exhibits characteristics of both attractively and repulsively interacting condensates due to the interplay between mean-field and fluctuation energies. Consequently, the response of a quantum droplet to rotation is not straightforward, and a new length scale becomes relevant to account for the balance between these energies. Previous investigations of this phenomenon have mainly focused on weakly trapped condensates. In weak external confinement, angular momentum is primarily carried by center-of-mass (COM) rotation for the droplets with liquid-like flat-density profiles [79, 80]. This allows the droplet to conserve the ground-state interaction energy by preserving the flat-top density profile. However, this physical reasoning also leads to splitting instability under density perturbation, causing the droplet to break into smaller fragments [81–84]. This instability has been observed in simulations for both two-dimensional (2D) and three-dimensional (3D) rotating quantum droplets [81, 82]. However, vortices can be locally stable within unconfined flat-top droplets if phase-imprinted or when the external confinement is adiabatically removed [81–83]. Even weak confinement can help avoid splitting instability and make vortex states stable. Recent predictions indicate that a rotating droplet under harmonic confinement exhibits a combination of COM rotation and vortex states [79, 80].

The existing literature on quantum droplets primarily focuses on their self-trapping behavior, and the external confinement is mostly considered as irrelevant. In this thesis, we aim to classify the physical regimes of trapped droplets by investigating the relevant energy scales in the problem. The interplay between the strengths of potential and interaction energies, along with the balance between the free equilibrium density and particle number, determines the significance of the confining potential in the rotating droplet scenario. We propose that a strongly confined droplet can be driven into a rapidly rotating regime, leading to the formation of a large vortex

lattice. To explore this phenomenon, we investigate rapidly rotating droplets in the strongly confined Thomas-Fermi (TF) regime using numerical and approximate analytical methods. Our numerical findings reveal that the confined droplet exhibits a triangular vortex lattice under rapid rotation. The strong confinement ensures that the splitting instability is avoided, even when the rotation frequency is close to the trap frequency. The density profile of the vortex lattice closely follows the TF profile, featuring a convex peak at the center and a rapid fall near the TF radius. As the rotation frequency approaches the trapping frequency $\tilde{\Omega} \to 1$, the effective confinement weakens, and the density profile of the vortex lattice converges to that of a flat-top droplet. Notably, in contrast to the diverging size of rapidly rotating repulsive Bose-Einstein condensates (BECs) [85, 86], the strongly confined TF droplet converges to a finite radius as $\tilde{\Omega} \to 1$. Hence, the physics of self-trapping plays a crucial role in the rapid rotation limit.

Our numerical simulations indicate that the vortex core sizes near the center and the edge of the droplet exhibit noticeable differences. To describe the density dependence of the core size, we develop an approximate analytical formula. In repulsive Bose-Einstein condensates (BECs), the vortex cores scale as $\zeta \propto 1/\sqrt{n_0}$, where n_0 is the condensate density. However, for the strongly confined Thomas-Fermi (TF) droplet, we find that the core size follows $\zeta \propto \frac{1}{\sqrt{n_0}\sqrt{n_0^{1/2}-n_c^{1/2}}}$, where n_c is approximately equal to the equilibrium density of the unconfined droplet. The existence of a new pole in the denominator at a finite density leads to a visible variation in the core size across different regions of the vortex lattice. Additionally, we calculate the deviation of the vortex lattice from a perfect triangular lattice, which remains observable and in agreement with numerical results. We propose that rapidly rotating droplets offer an opportunity to explore Bose-Einstein condensates where the number of particles are in the order of the number of vortices. While the Gross-Pitaevskii (GP) equation and our assumptions about the local energy of fluctuations are expected to break down in this limit, we observe that the strongly correlated regime may be approached through rapidly rotating droplets.

The chapter is organized as follows: In Section 4.2, we examine the different regimes of the problem and outline the treatment of mixture droplets using the effective GP equation. Section 4.3 discusses the TF solution for the strongly confined droplet and

presents the numerical results of the GP equation. In Section 4.5, we derive a formula for the vortex core size and compare it with the numerical solution. We also discuss the corrections to the uniform triangular lattice. Section 4.6 discusses the possibility of achieving a vortex lattice with a low filling factor. Finally, in Section 4.7, we explore the experimental parameters required to observe the suggested phenomena and outline potential avenues for future research.

4.2 Length scales and parameter regimes

We consider a two-component Bose condensate with weak interactions and identical masses m for both components. The interactions are characterized by intra- and intercomponent s-wave scattering lengths a_{11}, a_{22}, and a_{12}, respectively. For simplicity, we assume that the intracomponent repulsive interactions are equal, i.e., $a_{11} = a_{22} = a > 0$, making the two components fully symmetric. The intercomponent interaction is taken to be attractive, with $a_{12} < -a$, resulting in a slightly attractive mean-field (MF) interaction. Consequently, the effectively repulsive beyond mean-field (BMF) energy becomes significant, playing a crucial role in the total interaction energy and mechanical stability of the condensate [1].

To simplify the problem further, we exploit the symmetry between the components and the attractive interspecies interaction, setting $\Psi_1(\mathbf{r}) = \Psi_2(\mathbf{r})$ [1]. Additionally, we assume that the density gradient within the condensate is sufficiently low to justify the use of the local density approximation (LDA) [1, 2, 87]. The droplet is confined radially with an angular frequency $\omega_\perp$ and is tightly confined along the z-axis with an angular frequency ω_z. The total energy of the mixture is:

$$\begin{aligned} E &= \int dV \Bigg\{ \frac{\hbar^2}{2m}|\nabla\Psi|^2 + \frac{1}{2}mw_z^2z^2|\Psi|^2 + \frac{1}{2}mw_\perp^2r^2|\Psi|^2 \\ &\quad + \frac{(1-\alpha_s)g}{4}|\Psi|^4 + \frac{8\sqrt{2}}{15\sqrt{\pi}}(1+\alpha_s)^{5/2}ga^{3/2}|\Psi|^5 \Bigg\}, \end{aligned} \tag{4.1}$$

where position vector $\mathbf{r} = (x, y)$, scattering length ratio $\alpha_s = \frac{|a_{12}|}{a}$ and coupling constant $g = \frac{4\pi\hbar^2 a}{m}$. The MF and BMF energies are represented by the first and second terms in the second line of Eq. (4.1), respectively. It is important to highlight that the effective MF energy becomes attractive when the parameter α_s exceeds 1

slightly. In experimental setups, the scattering length α_s can be conveniently adjusted through the use of an appropriate Feshbach resonance.

The simplest geometry that allows for vortex topological excitations in a Bose condensate is a two-dimensional configuration, rather than a three-dimensional one. In this setup, we assume strong confinement along the third dimension and integrate the energy functional over the z-axis. Use a Gaussian wavefunction $\phi_0(z) = \frac{1}{(\pi a_z)^{1/4}} e^{\frac{-z^2}{2a_z^2}}$, with $a_z = \sqrt{\frac{\hbar}{m\omega_z}}$. Thus, the condensate wavefunction takes the form $\Psi(\mathbf{r}, z) = \psi(\mathbf{r})\phi_0(z)$. Although tight confinement along the third direction might appear to contradict the local density approximation (LDA) assumption, recent research [88, 89] has demonstrated that the transition from three-dimensional to two-dimensional behavior is smooth.

The integrated expression of the local energy functional shares qualitative similarities with the strictly two-dimensional LDA functional [82, 83]. Both the two-dimensional energy expressions for the mean-field and Lee-Huang-Yang (LHY) energies, $\propto |\Psi|^4 \ln \frac{|\Psi|^2}{\sqrt{e}}$, as well as the integrated form provided above exhibit a shallow minimum below zero, followed by a rapid increase after becoming positive. Integrating out the z-axis is also expected to provide a better quantitative agreement for typical experimental confinement scenarios. In our thesis, we consider the energy functional in the rotating frame with a fixed particle number N. To make the problem dimensionless, we use the scale of the radial harmonic oscillator $\omega_\perp$. The extended GP equation becomes:

$$\begin{aligned} \tilde{\mu}\tilde{\psi} &= -\frac{1}{2}(\tilde{\nabla} - \tilde{\mathbf{\Omega}} \times \tilde{\mathbf{r}})^2\tilde{\psi} + \frac{1}{2}\tilde{r}^2\left(1 - \tilde{\Omega}^2\right)\tilde{\psi} \\ &+ \frac{\gamma_{int}}{2}\left[(1-\alpha_s)|\tilde{\psi}|^2 + \overline{\beta}_{LHY}(1+\alpha_s)^{5/2}|\tilde{\psi}|^3\right]\tilde{\psi}, \end{aligned} \tag{4.2}$$

where $\tilde{\mathbf{r}} = \mathbf{r}/a_\perp$, $\tilde{\nabla} = a_\perp\nabla$, $\tilde{\psi} = a_\perp\psi$, $\tilde{\Omega} = \frac{\Omega}{\omega_\perp}$. The interaction parameters are $\gamma_{int} \equiv 2\sqrt{2\pi}\frac{a}{a_z}$ and $\overline{\beta}_{LHY} \equiv \frac{16\sqrt{2}}{3\sqrt{5}\pi^{3/4}}\frac{a^{3/2}}{a_z^{1/2}a_\perp}$, where $a_\perp = \sqrt{\frac{\hbar}{m\omega_\perp}}$.

Let's consider the relationship between physical length scales and the dimensionless quantities derived earlier. In the strictly two-dimensional problem with component symmetry, we have three important physical length scales: the oscillator length $a_\perp$, the inter-component and intra-component scattering lengths a_{12} and a, respectively. The total particle number in two components, N, is another parameter that determines the physical regime. The oscillator length $a_\perp$ represents the length scale at which the

kinetic and potential energy reach equilibrium, providing the typical feature size for single-particle wavefunctions in the trap. Scaling all lengths with $a_\perp$ naturally yields a dimensionless scale of approximately 1, where the kinetic energy due to bending of the wavefunction becomes relevant. Thus, clouds that are large on this scale have negligible kinetic energy.

The confinement along the z-axis introduces another length scale, a_z, which allows independent control of the effective two-dimensional interaction, giving rise to the dimensionless parameter $\gamma_{int} \sim a/a_z$. The ratio of inter-to-intracomponent interaction $\alpha_s = |a_{12}|/a$ determines how attractive the mean-field interaction is, and it must be above 1 for droplet formation, but it will be chosen to ensure that the droplet remains dilute. Lastly, the dimensionless parameter $\overline{\beta}_{LHY}$ measures the importance of the LHY contribution compared to the mean-field energy.

Note that the parameters α_s, $\overline{\beta}_{LHY}$, and γ_{int} depend on s-wave scattering and oscillator lengths. Each parameter can be independently tuned in an experiment. Although the GP equation presented earlier depends on only two combinations of γ_{int}, α_s, and $\overline{\beta}_{LHY}$, we choose to use all three independently. This choice allows us to scale the total interaction energy and LHY energy through γ_{int} and $\overline{\beta}_{LHY}$, respectively, providing more flexibility in experimental control.

There are four terms in the energy functional. The potential and MF terms prefer a smaller cloud radius, while the kinetic energy and BMF terms prefer to increase the cloud size. A balance between these two effects determines the equilibrium state of the droplet. By considering various combinations of these contributions, we can identify different regimes. The most straightforward scenario is when interactions are negligible, and the kinetic energy and trap potential dominate, resulting in a harmonic oscillator ground state with a size of approximately $a_\perp$.

Another important regime is just the opposite where interactions are dominant over both the kinetic and potential energy. Consider the GP equation (4.2) without any kinetic or potential terms:

$$\tilde{\mu}\tilde{\psi} = \frac{\gamma_{int}}{2}\left[(1-\alpha_s)|\tilde{\psi}|^2 + \beta_{LHY}|\tilde{\psi}|^3\right]\tilde{\psi}, \tag{4.3}$$

where $\beta_{LHY} = \overline{\beta}_{LHY}(1+\alpha_s)^{5/2}$. The density n_{min} that minimizes the chemical

potential can be found by minimizing the argument of the right-hand side (RHS) of (4.3) with respect to $|\tilde{\psi}|$:

$$n_{min} = \frac{4(\alpha_s - 1)^2}{9\beta_{LHY}^2}. \tag{4.4}$$

Here n_{min} is the density of a large self-trapped droplet. If kinetic energy is negligible in the equilibrium we define the droplet to be a TF droplet.

The flat-top Thomas-Fermi (TF) density profile of a droplet can be altered in two ways: either through the kinetic energy or the confinement energy. When the kinetic energy is not negligible compared to the interaction energy, the wavefunction gradient exerts an effective repulsive force on the condensate. Consequently, the flat-top profile is replaced with a Gaussian profile, resulting in what we call the "Weak droplet regime." In this regime, the droplet is still self-trapped, but the density profile deviates from the minimum density due to the influence of kinetic energy.

On the other hand, let's consider the effect of confinement on a droplet that is large enough to be described by the Thomas-Fermi approximation. When the trapping potential becomes significant, the particles are squeezed toward the center of the droplet to minimize the confinement energy. This leads to a density profile with a convex peak at the center and a rapid fall near the surface. We refer to this scenario, where kinetic energy is negligible but potential energy causes a significant curvature in the equilibrium density, as the "Strongly Confined Thomas-Fermi Regime" (further details can be found in Section 4.3). This regime is eventually realized for all parameters when the number of particles is large enough.

To quantify the regimes, assume a constant density droplet with $\tilde{\psi}(\tilde{r}) = \sqrt{n_{min}}\theta(R_{TF} - \tilde{r})$, where $\theta(\tilde{r})$ is the step function. For N particles uniformly filling a circle of radius R, the energies would scale as

$$\begin{aligned} E_k &\sim N/R^2, \\ E_p &\sim NR^2, \\ E_{MF} &\sim (N/R^2)N, \\ E_{LHY} &\sim (N/R^2)^{3/2}N. \end{aligned} \tag{4.5}$$

However, the balance between the MF and BMF terms creates a new length scale and corresponding density n_{min}. Thus the radius and the particle number are not

independent. Thus, $R_{TF} = \frac{3\beta_{LHY}}{2\sqrt{\pi}(\alpha_s-1)}\sqrt{N}$ is the Thomas-Fermi (TF) radius of the flat-top droplet. Using this ansatz, the energy scales in (4.1) become:

$$E_{int} = \frac{-7}{135}\frac{\gamma_{int}|\alpha_s-1|^3}{\beta_{LHY}^2}N, \tag{4.6}$$

$$E_p = \frac{9}{16\pi}\frac{\beta_{LHY}^2}{|\alpha_s-1|^2}N^2, \tag{4.7}$$

$$E_k = \frac{2\pi}{9}\frac{|\alpha_s-1|^2}{\beta_{LHY}^2}, \tag{4.8}$$

where $E_{int} = E_{MF} + E_{BMF}$ is the total interaction, $E_k \approx \frac{N}{2R_{TF}^2}$ is the kinetic, and $E_p = \frac{1}{2}\int d^2\tilde{\mathbf{r}}\tilde{r}^2|\tilde{\psi}|^2$ is the potential energy. For the TF regime, the total interaction energy must be much greater than the kinetic energy:

$$\frac{|E_{int}|}{E_k} = \frac{7}{30\pi}\gamma_{int}|\alpha_s-1|N \gg 1. \tag{4.9}$$

For strong confinement, the potential energy must be comparable with the interaction energy:

$$\frac{|E_{int}|}{E_p} = \frac{112\pi}{1215}\frac{\gamma_{int}|\alpha_s-1|^5}{\beta_{LHY}^4}\frac{1}{N} \lesssim 1. \tag{4.10}$$

By independently scaling the interaction energy, γ_{int} allows us to drive the system into the weakly confined Thomas-Fermi (TF) regime by increasing $\gamma_{int} \propto a/a_z$. On the other hand, the strongly confined TF regime can always be achieved by increasing the particle number N, regardless of the other parameters. This is because the potential (4.7) and interaction energies (4.6) scale with N^2 and N, respectively, while the kinetic energy (4.8) has a slower dependence on N.

The condition (4.9) for the TF regime is independent of β_{LHY}, as both the interaction (4.6) and kinetic (4.8) energies scale with β_{LHY} by the same order in the two-dimensional TF regime. The parameter inequalities corresponding to different regimes are summarized in Table 4.1.

4.3 Strongly Confined Thomas-Fermi Regime

Rotating a weakly confined droplet is expected to result in center-of-mass (COM) motion. In such a case, the interaction energy is minimized by conserving the density profile, and all the angular momentum is carried by the rotation of the shifted

Table 4.1: The rotating quantum droplet under confinement can be classified into four different regimes. We use the scales obtained by the energy ratios in (4.9) and (4.10) to quantify the regimes.

	Strongly Confined	Weakly Confined
TF Droplet	$\gamma_{int}\lvert\alpha_s-1\rvert N \gg 1$ $\frac{\gamma_{int}\lvert\alpha_s-1\rvert^5}{\beta_{LHY}^4}\frac{1}{N} \lesssim 1$	$\gamma_{int}\lvert\alpha_s-1\rvert N \gg 1$ $\frac{\gamma_{int}\lvert\alpha_s-1\rvert^5}{\beta_{LHY}^4}\frac{1}{N} \gg 1$
Weak Droplet	$\gamma_{int}\lvert\alpha_s-1\rvert N \approx 1$ $\frac{\gamma_{int}\lvert\alpha_s-1\rvert^5}{\beta_{LHY}^4}\frac{1}{N} \lesssim 1$	$\gamma_{int}\lvert\alpha_s-1\rvert N \approx 1$ $\frac{\gamma_{int}\lvert\alpha_s-1\rvert^5}{\beta_{LHY}^4}\frac{1}{N} \gg 1$

COM [79, 80]. Furthermore, the flat-top density profile of the droplet can experience splitting instability in the absence of sufficient confinement [81, 82], where the droplet can break into smaller fragments under a density perturbation. This splitting can be prevented by introducing a sufficient energy cost through strong confinement. Therefore, we can expect vortex lattices to form in a strongly confined droplet under rotation. Additionally, the density profile of the strongly confined TF droplet is significantly different from the flat-top profile, ensuring that the vortex lattices remain stable even in the rapid rotation limit. For these reasons, we focus on studying the rotating droplet in the strongly confined TF regime, particularly considering the coarse-grained density profile as a function of the rotation frequency $\tilde{\Omega}$.

In the case of a regular vortex lattice formation, the kinetic energy of the rotating condensate is nearly equal to the energy of a solid body rotating with the velocity $\mathbf{\Omega} \times \mathbf{r}$. As a result, the Gross-Pitaevskii (GP) equation that gives the envelope of the coarse-grained density profile can be obtained by neglecting the first term in the equation (4.2):

$$\tilde{\mu}\tilde{\psi} - \frac{1}{2}\tilde{r}^2\left(1-\tilde{\Omega}^2\right)\tilde{\psi} = \frac{\gamma_{int}}{2}\left[(1-\alpha_s)|\tilde{\psi}|^2 + \beta_{LHY}|\tilde{\psi}|^3\right]\tilde{\psi}. \tag{4.11}$$

In this scenario, rotation primarily influences the droplet's density profile through the centrifugal effect. The confining potential is renormalized and weakened by a factor of $(1-\tilde{\Omega}^2)$. In the weakly confined regime, the solutions of (4.11) exhibit a nearly flat-top density profile. However, in the case of strong potential, the particles are expected to be gathered around the trap's center.

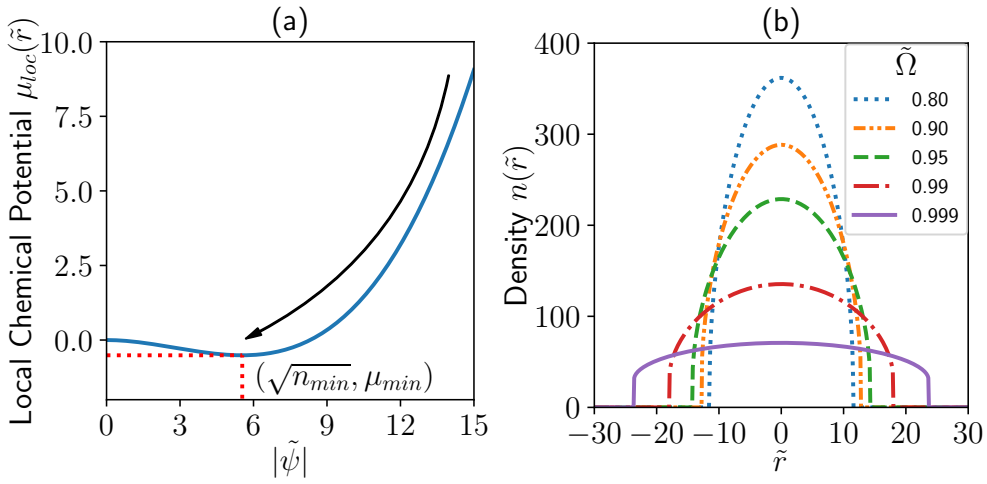

Figure 4.1: (a) The local chemical potential $\mu_{loc}(\tilde{r}) = \tilde{\mu} - \frac{1}{2}\tilde{r}^2\left(1 - \tilde{\Omega}^2\right)$ in (4.11) vs. $|\tilde{\psi}|$ (Blue line). Since $\alpha_s > 1$ and β_{LHY} is positive, μ_{loc} shows a local negative minimum at $|\tilde{\psi}| = \sqrt{n_{min}}$, then monotonically increase with $|\tilde{\psi}|$. The solution to (4.11) for $\tilde{\mu} > \tilde{\mu}_{min}$ can be found by evaluating $\mu_{loc}(\tilde{r})$ for different $\tilde{r}$, along the curved arrow. The density jumps to 0 when the local chemical potential is equal to the minimum value μ_{min}. (b) The analytical solutions of the GP equation (4.11) of the rotating Bose mixture droplets in the strongly confined TF regime for various $\tilde{\Omega}$. The parameters are $\alpha_s = 1.05$, $\beta_{LHY} = 6 \times 10^{-3}$, $\gamma_{int} = 1$, $N = 10^5$. The convexity due to the strong confinement flattens and approaches the flat-top profile as $\tilde{\Omega} \to 1$.

In this regime, we can understand the density profile by examining the local chemical potential as we move outward from the center of the trap. Consider the local chemical potential, μ_{loc}, given by (4.11), as a function of $|\tilde{\psi}|$. Since $\alpha_s > 1$ and $\beta_{LHY} > 0$, μ_{loc} has a negative minimum at $|\tilde{\psi}| = \sqrt{n_{min}}$, then it becomes positive and rapidly increases, as depicted in Fig.(4.1).

Consider the solution to (4.11) for a given chemical potential $\tilde{\mu} > \tilde{\mu}min$, where $\tilde{\mu}min$ represents the chemical potential when the density is n_{min}. At the center of the trap, $\tilde{r} = 0$, the magnitude of $|\tilde{\psi}|$ is at its maximum value. As $\tilde{r}$ increases, the magnitude of $|\tilde{\psi}|$ follows the path indicated by the curved arrow in Fig. (4.1)(a). When the radial position $\tilde{r} = R_0$ is reached, such that $|\tilde{\psi}(R_0)| = \sqrt{n_{min}}$, the local chemical potential $\tilde{\mu} - \frac{1}{2}\tilde{r}^2\left(1 - \tilde{\Omega}^2\right)$ reaches its minimum, causing $|\tilde{\psi}(\tilde{r})|$ to abruptly fall to zero for $\tilde{r} > R_0$. As a result, a convex density profile with a rapid decrease in density at the level of n_{min} is obtained. Figure (4.1)(b) shows solutions to (4.11) for different

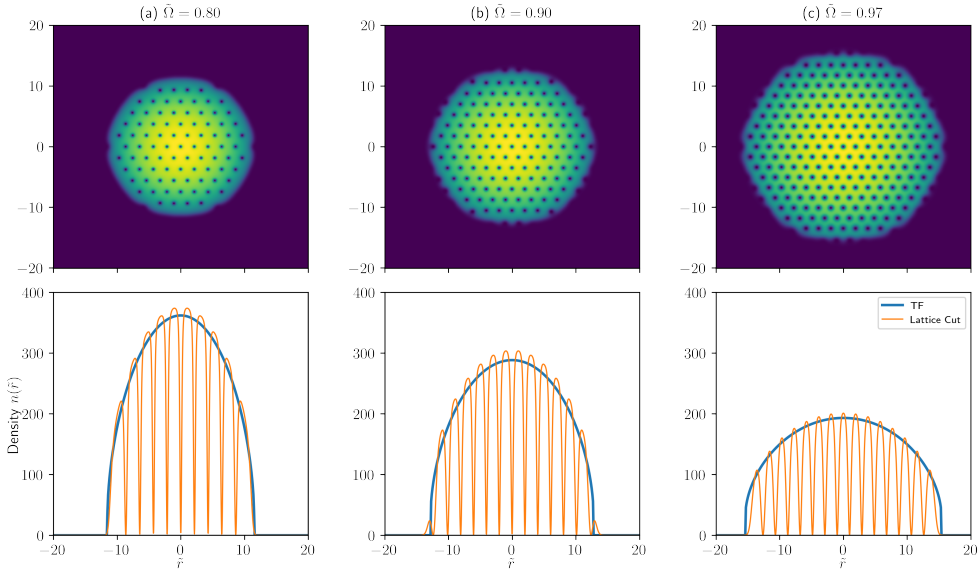

Figure 4.2: The numerical solutions of the GP equation (4.2) of the rotating Bose mixture droplets for the parameters $\alpha_s = 1.05$, $\beta_{LHY} = 1 \times 10^{-3}$, $\gamma_{int} = 2$, $N = 10^5$, and (a) $\tilde{\Omega} = 0.80$,(b) $\tilde{\Omega} = 0.90$,(c) $\tilde{\Omega} = 0.97$. (upper panel) 2-D density profiles of the vortex lattices, (lower panel) the density profile of the vortex lattices along the x-axis (orange lines), and the rotating TF solution of the GP equation (4.11) (blue lines).

rotation levels $\tilde{\Omega}$. As $\tilde{\Omega} \to 1$, the cloud becomes flatter.

We conducted numerical simulations of the GP equation (4.2) for rotating Bose mixture droplets in the strongly confined Thomas-Fermi regime, focusing on rapidly rotating frequencies $\tilde{\Omega} > 0.5$. The parameters used are $\alpha_s = 1.05$, $\beta_{LHY} = 1 \times 10^{-3}$, $\gamma_{int} = 2$, and $N = 1 \times 10^5$. The results obtained for $\tilde{\Omega} = 0.80, 0.90, 0.97$ are displayed in Fig.(4.2), showing that triangular vortex lattices are formed in the strongly confined droplet in the rapid rotation limit.

We ensured the convergence of our numerical results by using different initial wavefunctions (random, Gaussian, and Jacobi-theta). All led to almost identical density profiles and locally triangular vortex lattices with occasional dislocation defects. We chose the Jacobi-theta function initial condition as it resulted in rapid convergence without dislocations and minimized total energy.

The results show that the density profiles of the cloud containing vortex lattices closely follow the solutions of the TF equation (4.11) (solid lines). The peak den-

sity at the center decreases, and the overall profile flattens as the rotation frequency is increased. The inclusion of kinetic energy makes only a small change in the overall density profile, with the most significant change being the smoother fall at the edge of the cloud.

One noteworthy difference between the rotating droplets and the vortex lattices seen in repulsive BEC experiments is the functional form of the coarse-grained density profile. While the TF profile for an ordinary BEC remains an inverted parabola and its radius increases with increasing rotation, the droplet exhibits a finite density jump at the surface, and the functional form smoothly changes from a high curvature profile to a flat profile with increasing density. Note that the cloud radius for the rotations $\tilde{\Omega} = 0.8$ and 0.97 are not significantly different. More remarkably, as $\tilde{\Omega} \to 1$, the cloud radius limits to the size of the non-rotating TF droplet R_{TF}.

Another significant difference is observed in the radius of the droplet. In the rapidly rotating limit, the droplet radius converges to a finite value, R_{TF}, whereas the condensate radius diverges for repulsive BECs in either the Thomas-Fermi or lowest Landau level regimes. There, the radius scales with: $R(\tilde{\Omega})/R(0) = (1-\tilde{\Omega}^2)^{-3/10}$ and $R(\tilde{\Omega})/R(0) = (1-\tilde{\Omega})^{-1/4}$, respectively [77]. We calculate the TF droplet radius for various $\tilde{\Omega}$ by solving (4.11). We also find the radius of the rotating droplets from the numerical solutions of 2D GP equation (4.2). We show the results in Fig.(4.3). The difference in the cloud sizes is a consequence of the self-trapping property of the droplets. The rotation weakens the trapping potential for repulsive BECs, leading to their expansion without confinement, and thus, their condensate size diverges as the rotation frequency approaches one. In contrast, the droplet can stabilize itself without any trap, and as a result, the droplet radius remains much smaller than the BEC cloud radius even in the extremely rapid rotating limit.

The smaller change in droplet size with rotation suggests that the rapid rotation limit could be more accessible in experiments, as imperfections in the harmonic trap become less problematic. In typical rotating BEC experiments, imperfections near the trap's center limit the upper rotation frequencies attainable and dissipate angular momentum as the cloud radius increases. However, the small size change of the droplets under rotation may prevent these effects and pave the way to reaching the rapid rota-

tion limit.

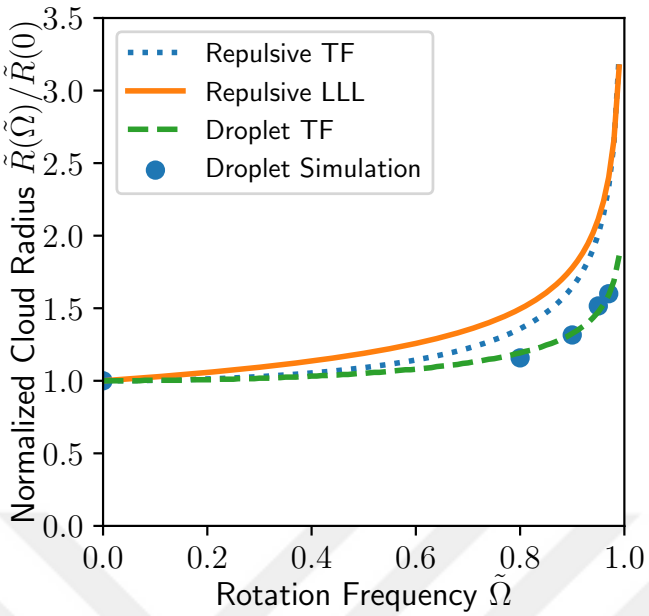

Figure 4.3: The comparison of the radius of the condensates for the rotation frequency $\tilde{\Omega} \in [0, 1]$: Repulsive BEC in TF regime (dotted), Repulsive BEC in LLL regime (solid), and Droplet in the TF regime (dashed). The scattered data present the radius of the simulation results. The droplet radius converges to a finite value as $\tilde{\Omega} \to 1$, contrary to the diverging behavior of the repulsive BECs.

4.4 Analytical Solution of the Cubic TF Equation

By applying the change of variables $t = x + \frac{b}{3a}$, the cubic equation $ax^3 + bx^2 + cx + d = 0$ can be transformed into the depressed form $t^3 + pt + q = 0$. The corresponding values for p and q are given by $p = \frac{3ac - b^2}{3a^2}$ and $q = \frac{2b^3 - 9abc + 27a^2d}{27a^3}$, respectively. In this form, the real solution to the cubic equation can be found using trigonometric methods. Now, let's consider the GP equation (4.11) for the strongly confined TF droplet, which can also be expressed as a cubic equation but with the coefficient c being zero. By applying the change of variables $t = |\tilde{\psi}| + \frac{1 - \alpha_s}{\beta_{LHY}}$, the cubic equation takes the form:

$$|\tilde{\psi}(\tilde{r} \leq R_{TF})| = \frac{2(\alpha_s - 1)}{3\beta_{LHY}} \times \left\{ \frac{1}{2} + \cos\left[\frac{1}{3} \arccos\left(1 + \frac{27\beta_{LHY}^2 \mu_{loc}(\tilde{r})}{\gamma_{int}(\alpha_s - 1)^3} \right) \right] \right\}. \tag{4.12}$$

Here the local chemical potential is denoted as $\mu_{loc}(\tilde{r})$, and it is defined as $\mu - \frac{\tilde{r}^2}{2}(1 - \tilde{\Omega}^2)$. Here, μ represents the chemical potential, and $\tilde{r}$ is a spatial variable.

The term R_{TF} refers to the Thomas-Fermi (TF) radius of the strongly confined TF droplet, which is determined at the point where $|\tilde{\psi}(\tilde{R}_{TF})| = \sqrt{n_{min}}$. To calculate R_{TF}, we identify the location where the density falls rapidly, specifically using the condition $|\tilde{\psi}(\tilde{R}_{TF})| = \frac{2(\alpha_s - 1)}{3\beta_{LHY}}$:

$$\begin{aligned} R_{TF} &= \sqrt{\left(\mu + \frac{2\gamma_{int}(\alpha_s - 1)^3}{27\beta_{LHY}^2} \right) \frac{2}{1 - \tilde{\Omega}^2}} \\ &= \sqrt{\frac{2(\mu - \mu_{min})}{1 - \tilde{\Omega}^2}}, \end{aligned} \tag{4.13}$$

where the chemical potential of the flat-top droplet is given by $\mu_{min} = -\frac{2\gamma_{int}(\alpha_s - 1)^3}{27\beta_{LHY}^2}$. When we consider the limit $\tilde{\Omega} \to 1$, the external trap is effectively removed due to the centrifugal effect, causing the droplet to approach the flat-top profile. As a result, the divergence of the droplet radius is prevented, and we find that $\lim_{\tilde{\Omega} \to 1} \mu = \mu_{min}$. In fact, in this limit, the droplet radius should recover the flat-top radius, given by $R_{TF} = \frac{3\beta_{LHY}}{2\sqrt{\pi}(\alpha_s - 1)}\sqrt{N}$.

4.5 Properties of the Vortex Lattice

In the numerical results presented in Fig. (4.2), it is evident that the vortex core sizes exhibit visible differences between the center and the edge of the droplet. This variation is emphasized in Fig. (4.4). This stands in contrast to the nearly uniform core size observed in the vortex lattices of repulsive Bose-Einstein condensates (BECs) [35]. To gain insights into the underlying cause for this core size change in the rapidly rotating TF droplet, we explore different approaches to studying the core size.

Specifically, we investigate a condensate with a limiting uniform density n_0 in proximity to an impenetrable surface. To determine the healing length of the condensate,

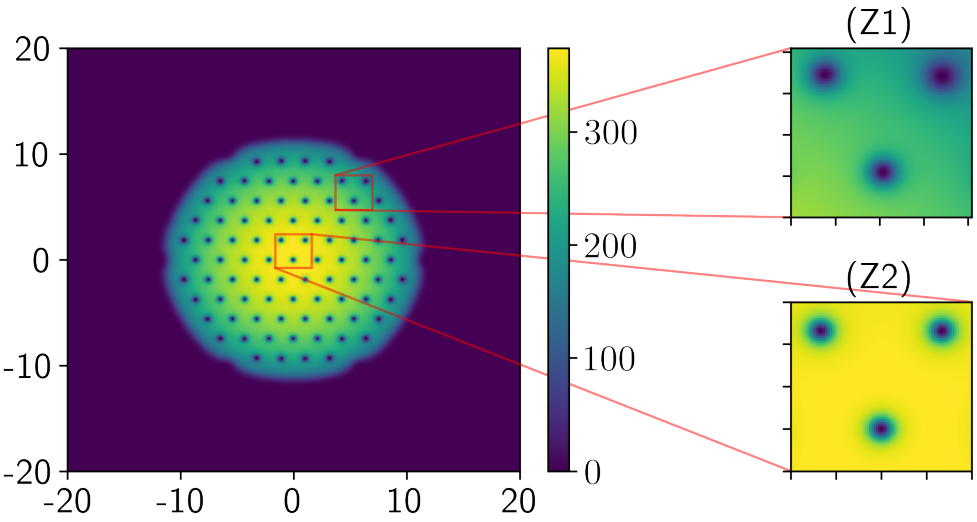

Figure 4.4: Density profile of the vortex lattice with $\tilde{\Omega} = 0.8$ in Fig.4.2(a). The insets show the 2D zooms of equal areas in the vortex lattice near the edge (Z1) and the center (Z2) of the droplet. The core size is larger, and the vortex unit cell area decreases near the edge.

we solve the equation:

$$\frac{1}{2}\tilde{\nabla}^2\tilde{\psi} = (1-\alpha_s)\left(|\tilde{\psi}|^2 - n_0\right)\tilde{\psi} + \bar{\beta}_{LHY}\left(|\tilde{\psi}|^3 - n_0^{3/2}\right)\tilde{\psi}, \tag{4.14}$$

This equation is derived by substituting the equilibrium density chemical potential $\tilde{\mu} = (1-\alpha_s)n_0 + \beta_{LHY}n_0^{3/2}$ into equation (4.3). We investigate the density dependence of the core size using three different approaches and compare their results with the numerical solutions shown in Fig.(4.2).

Firstly, we numerically solve equation (4.14) in one dimension by replacing $\tilde{\nabla}^2\tilde{\psi} \equiv \frac{\partial^2\tilde{\psi}}{\partial\tilde{x}^2}$. Secondly, we numerically solve the equation in two dimensions using $\tilde{\nabla}^2\tilde{\psi} \equiv \frac{1}{\tilde{r}}\frac{\partial}{\partial\tilde{r}}\left(\tilde{r}\frac{\partial\tilde{\psi}}{\partial\tilde{r}}\right) - \frac{\tilde{\psi}}{\tilde{r}^2}$.Finally, we derive an analytical formula for the coherence length ζ as follows.

While examining the healing length equation (4.14) in one dimension, we discover a constant of motion for different $\tilde{x}$ by multiplying both sides of the equation by $\frac{\partial\tilde{\psi}}{\partial\tilde{x}}$.

Then, (4.14) becomes:

$$\frac{1}{2}\frac{\partial}{\partial\tilde{x}}\left(\left(\frac{\partial\tilde{\psi}}{\partial\tilde{x}}\right)^2\right) = \frac{\partial V}{\partial|\tilde{\psi}|}\frac{\partial\tilde{\psi}}{\partial\tilde{x}}$$

$$V[|\tilde{\psi}|] = (1-\alpha_s)\left(\frac{|\tilde{\psi}|^4}{2} - n_0|\tilde{\psi}|^2\right)$$

$$+ \quad \beta_{LHY}\left(\frac{2|\tilde{\psi}|^5}{5} - n_0^{3/2}|\tilde{\psi}|^2\right). \tag{4.15}$$

Hence, $\frac{1}{2}\left(\frac{\partial\tilde{\psi}}{\partial\tilde{x}}\right)^2 - V[|\tilde{\psi}|]$ is a constant of the differential equation, assuming $\tilde{\psi}(\tilde{r}) >= 0$ for any $\tilde{r} \in \mathcal{R}^+$. We evalulate this constant for the limits $\tilde{x} \to 0$ and $\tilde{x} \to \infty$, where $\lim_{\tilde{x}\to\infty}\tilde{\psi} = \sqrt{n_0}$, which provides the healing length scale of the condensate $\zeta \approx \sqrt{n_0}/\left(\frac{\partial\psi}{\partial\tilde{x}}\right)_{\tilde{x}\to 0}$:

$$\zeta = \frac{1}{\sqrt{\frac{3\gamma_{int}\beta_{LHY}}{5}n_0\left(n_0^{1/2} - n_c^{1/2}\right)}}, \tag{4.16}$$

where $n_c = \frac{25(\alpha_s-1)^2}{36\bar{\beta}_{LHY}^2}$ is close to the flat-top density scale n_{min}. This approximation fails for densities n_0 below n_c, which signals the splitting instability. In Fig.(4.5), we present a comparison of the core size estimates obtained through three approaches with the numerical simulations from Fig.(4.2)(a). The core size of the vortices is plotted for different radial distances. Both the numerical and analytical results for the core size align well with the actual simulation data. Notably, the core size at the center of the droplet is smaller compared to the surface of the cloud due to the decrease in condensate density near the edge.

The core size dependence on the density of the TF droplets differs significantly from that of repulsive Bose-Einstein condensates (BECs). In rapidly rotating repulsive BECs in the TF regime, the core size scales as $\zeta \propto \sqrt{\frac{\tilde{\Omega}}{2gn_0}}$ [77], with the TF density profile being an inverse-parabola. On the other hand, for the TF droplet, the core size scales as $\zeta \propto \frac{1}{\sqrt{n_0}\sqrt{n_0^{1/2}-n_c^{1/2}}}$ as given by equation (4.16), and the density remains finite (n_{min}) near the surface. The presence of the density scale n_c in the denominator leads to a higher sensitivity of the core size to density changes in the condensate. Additionally, the finite density near the surface makes the vortices near the edge more visible in comparison to the surface of the inverse-parabola profile. Therefore, we anticipate that the differences in the vortex cores at the center and near the surface of

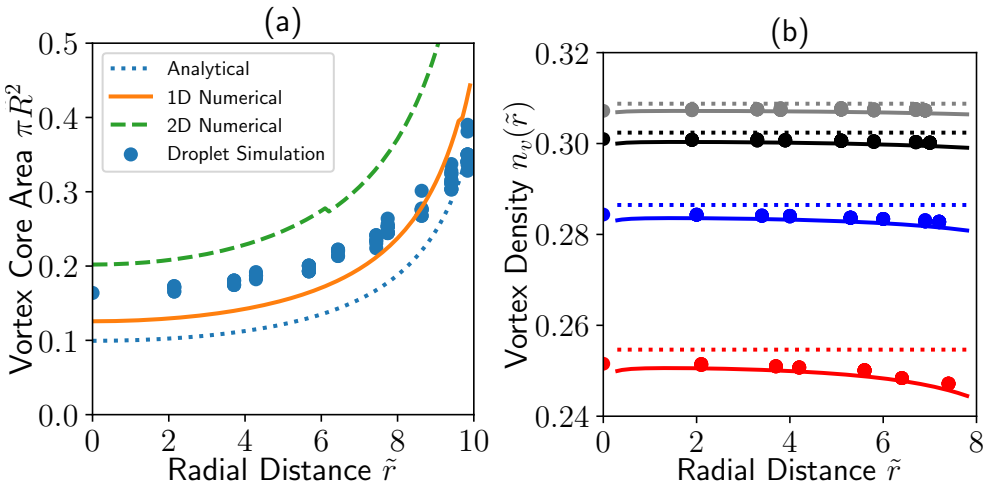

Figure 4.5: (a) The vortex core area estimates by numerical solutions of 1-D (solid line) and 2-D (dashed line) healing length equation (4.14), analytical approximation (4.16) (dotted line) and the simulation data for (filled points) $\tilde{\Omega} = 0.8$. The density levels n_0 for the numerical and analytical solutions to (4.14) and (4.16) are taken from the strongly confined TF droplet equation (4.11). The difference in the core size along the TF droplet is more tractable than the repulsive BECs. (b) The vortex density of the rotating TF droplet calculated up to the first order in (4.17) for $\tilde{\Omega} = 0.80$ (gray), $\tilde{\Omega} = 0.90$ (black), $\tilde{\Omega} = 0.95$ (blue), and $\tilde{\Omega} = 0.97$ (red). The dotted lines represent the uniform vortex densities $n_{v0} = \tilde{\Omega}/\pi$. The scattered data shows the vortex density computed on the simulation data of Fig. 4.2, whereas the solid lines are the solutions to (4.17). The vortex density closely follows the uniform limit with an agreement on the corrections.

the condensate should be more observable for the TF droplets compared to repulsive BECs.

The presence of spatial inhomogeneity in the superfluid density causes deviations from the vortex density of an infinitely homogeneous lattice, given by $n_{v0} = \frac{\Omega m}{\hbar\pi}$ [90]. Although these deviations are generally small, they reflect the density profile of the cloud. We utilized image processing tools to numerically calculate the local change in the lattice constant of the triangular lattice and observed such deviations.

We further calculated the change in the vortex density using the approach of Ref.[90]:

$$n_v(\tilde{r}) = \frac{\tilde{\Omega}}{\pi} + \frac{1}{8\pi}\tilde{\nabla}\cdot\left\{\frac{1}{n(\tilde{r})}\tilde{\nabla}\left[n(\tilde{r})\ln\left(\frac{e}{\pi\zeta^2(\tilde{r})n_v(\tilde{r})}\right)\right\}\right]. \tag{4.17}$$

In the expression (4.17), $n_v(\tilde{\Omega})$ represents the vortex density, $n(\tilde{r})$ denotes the condensate density, and $\zeta(\tilde{r})$ corresponds to the coherence length. The first term in the equation represents the uniform vortex density n_{v0} in dimensionless form, while the second term calculates the corrections to n_{v0}, which correspond to deviations from uniformity in the condensate density.

To numerically solve equation (4.17), it is necessary to find expressions for the superfluid density $n(\tilde{r})$ and the coherence length $\zeta(\tilde{r})$. To obtain corrections to the vortex density of the strongly confined Thomas-Fermi (TF) droplet, we utilize the analytical solution (4.13) to the GP equation (4.11) as the superfluid density $n(\tilde{r})$. The corresponding coherence length $\zeta(\tilde{r})$ is computed using the analytical approximation (4.16), where the limiting density n_0 is again replaced by the same superfluid density $n(\tilde{r})$. We then solve equation (4.17) up to the first order to obtain the vortex density $n_v(\tilde{r})$.

By comparing these results with the vortex density profile obtained from the actual simulation data in Fig.(4.2) for different rotation frequencies $\tilde{\Omega} = 0.80, 0.90, 0.95, 0.97$, we can validate the accuracy of the approach. The comparison is shown in Fig.(4.5)(b).

The deviations from the uniform vortex density arise from the gradient of the superfluid density. It is worth noting that the TF density profile becomes smoother as the rotation rate $\tilde{\Omega}$ increases. Consequently, the deviations from the uniform vortex density are more pronounced for lower rotation rates. Moreover, these deviations become even more significant toward the edge of the droplet due to the convex profile with a rapid fall-off at the edge. However, as the rotation rate approaches $\tilde{\Omega} \to 1$, the density profile tends to assume a flat-top shape, and the vortex density approaches the uniform vortex density throughout the condensate. Consequently, for rapid rotation rates, a nearly perfect vortex triangular lattice is expected to be observed, in contrast to the radially distorted vortex lattice observed in repulsive TF Bose-Einstein condensates under an isotropic harmonic trap [90].

4.6 Vortex Lattices with Low Filling Factors

There exists a theoretical correspondence between rotating Bose condensates and two-dimensional electron gases under strong magnetic fields [91, 92]. This analogy has the potential to enable the realization of quantum Hall physics in rotating Bose condensates under harmonic traps, including the exploration of strongly correlated phases. However, achieving the correlated regime for rotating ultracold gases remains an experimental challenge, as described below. As a result, researchers have proposed various methods to achieve strongly correlated phases in ultracold atomic gases [93], such as modified harmonic potentials [86, 94, 95], optically dressed states [96, 97], and tight-binding optical lattices [98, 99]. Recently, fractional quantum Hall states have been experimentally realized in ultracold Bose gases in driven optical lattices [100], marking the first demonstration of this effect outside of electronic systems.

In the case of rotating repulsive Bose-Einstein condensates under an isotropic harmonic trap, increasing the rotation frequency $\tilde{\Omega}$ effectively reduces the confining potential $\propto (1-\tilde{\Omega}^2)$. Additionally, as $\tilde{\Omega}$ increases, the condensate is driven into the mean-field Landau level (LLL) regime, where the intervortex spacing becomes comparable to the vortex core size. In this regime, the explicit expression for the cloud size is given by $R_0 = \left(\frac{8Nad_\perp^4}{Z(1-\tilde{\Omega})}\right)^{1/4}$ [77], where Z is the confining length along the z-axis. It is important to note that R_0 expands excessively as $\tilde{\Omega} \to 1$. Another crucial length scale is the interparticle distance, which is simply determined by the condensate density n. As the interparticle distance becomes comparable to the intervortex spacing, quantum fluctuations of the particles become significant, leading to a failure of the Gross-Pitaevskii mean-field approach [92]. This ratio is characterized by the filling factor $\nu = \frac{N}{N_v}$, where N_v and N are the numbers of vortices and particles, respectively. For low values of ν (approximately $\nu \approx 6-10$), the quantum fluctuations induce stronger correlations among the particles, driving the system into strongly correlated phases. Therefore, achieving low filling factor values is crucial in ultracold atom research. For the mean-field LLL state of the confined repulsive BEC,

the number of vortices and the corresponding filling factor are given by [77, 92]:

$$N_v \approx \frac{R_0^2}{d_\perp^2} \approx \sqrt{\frac{8Na}{Z(1-\tilde{\Omega})}}, \tag{4.18}$$

$$\nu \equiv \frac{N}{N_v} = \sqrt{\frac{Z(1-\tilde{\Omega})N}{8a}}. \tag{4.19}$$

To achieve a low filling factor of $\nu \sim 5$, typical values of $Z/a \approx 100$ and $N \approx 1000$ require a rotation frequency of $\tilde{\Omega} > 0.99$. However, operating at such high values of $\tilde{\Omega}$ results in excessive expansion of the cloud size due to the effective cancellation of the confining trap. This expansion makes the experiments impractical due to the large size of the system. Interestingly, the strongly confined Thomas-Fermi (TF) droplets exhibit only fractional expansion under rotation, which presents an opportunity to achieve low filling factors in a more manageable experimental setting.

So far, our focus has primarily been on the fractional change in the droplet size under rotation. However, the competing interactions in the droplets also allow for highly controllable equilibrium densities n_{min}. As the rotating droplet approaches a flat-top density around $n_{min} = \frac{4(\alpha_s-1)^2}{9\beta_{LHY}^2}$, while the approximate vortex density is around $n_{v0} = \frac{\tilde{\Omega}}{\pi}$, we can assume that the radius of the rotating droplet is close to the flat-top TF radius $R_{TF} = \frac{3\beta_{LHY}}{2\sqrt{\pi}(\alpha_s-1)}\sqrt{N}$. With these considerations, the filling factor of the rotating droplet $\nu = \frac{N}{N_v}$ becomes:

$$\frac{N}{N_v} = \frac{N}{\pi R_{TF}^2 n_v} = \frac{\pi 4(\alpha_s-1)^2}{9\beta_{LHY}^2} = \frac{\pi n_{min}}{\tilde{\Omega}}, \tag{4.20}$$

Therefore, achieving low filling factor levels can be accomplished by reducing the minimum density of the droplet, denoted as n_{min}. Let's consider the parameters $N = 500$, $\alpha_s = 1.25$, $\beta_{LHY} = 0.02$, and $\gamma_{int} = 20$, which are theoretically predicted to result in a strongly confined Thomas-Fermi (TF) droplet with $n_{min} \approx 1.2$ and $R_{TF} = 11.5$. With a rotation frequency of $\tilde{\Omega} = 0.99$, the filling factor is expected to be close to $\nu \approx 3.8$. We obtained the numerical solution of the Gross-Pitaevskii equation (4.2) for the given parameters. The 2D density profile of the vortex lattice and its cross-section along the x-axis are presented in Fig.(4.6)(a) and (b), respectively. In this case, there are approximately 80 vortices in the droplet consisting of 500 particles, leading to a filling factor of $\nu \approx 6.25$. Even better results can be achieved by adjusting the related parameters accordingly. The discrepancy between the numerical result

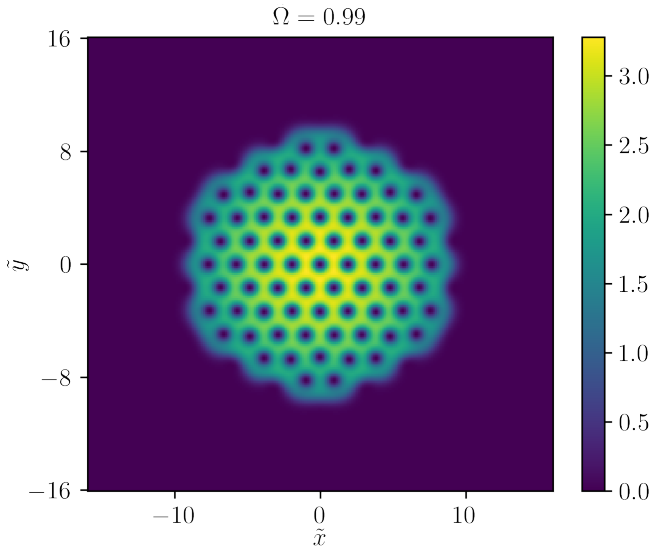

Figure 4.6: The vortex lattice of a rotating strongly confined droplet with a low filling factor. There are approximately 80 vortices for particle number $N = 500$, i.e. $\nu \approx 6.25$. The parameters are $\alpha_s = 1.25$, $\beta_{LHY} = 0.025$, $\gamma_{int} = 20$, and $\tilde{\Omega} = 0.99$. The color bar indicates the condensate density.

and the theoretical expectation is attributed to the fact that the density profile is not perfectly flat-top for this specific parameter choice. Interesting questions that require further research are whether the low filling factor implies the LLL regime or rotating quantum droplet can be driven into the LLL regime at all. The key to the obtained results is the stabilization of the condensate by the LHY fluctuations. Whether this stabilization mechanism still exists in the LLL regime should be considered. The traditional condition for the LLL regime is $\mu \approx gn_0 \ll 2\hbar\omega_\perp$. However, the chemical potential of the self-trapped droplets is negative. Hence the conditions to drive the droplet into the LLL regime should also be reconsidered. Moreover, we do not know how the vortex core changes or whether vortex lattices are stable as the density profile of the rotating droplet strictly converges the flat-top shape. Since the rotating flat-top droplet lacks splitting instability, this regime requires careful examination.

4.7 Discussion of experimental realization and Conclusion

Now we discuss the experimental feasibility of realizing vortex lattices in Bose mixture droplets. Several research groups have already experimentally realized Bose mixture droplets without any trap [3, 32, 33, 101]. Additionally, theoretical investigations of vortices and vortex lattices in dipolar droplets have been conducted using similar assumptions as presented in this part of the thesis, employing local density approximation (LDA) treatment of the mean-field (MF) and Lee-Huang-Yang (LHY) terms [102–107]. Furthermore, experimental observations of vortex lattices have been reported in rotating dipolar droplets [108, 109]. The extended Gross-Pitaevskii (GP) approach used in this study has shown excellent agreement between numerical estimates and experimental results [108, 109].

Key parameters governing the different regimes of the problem are $\alpha_s = \frac{|a_{12}|}{a}$, $\gamma_{int} \equiv 2\sqrt{2\pi}\frac{a}{a_z}$, and $\beta_{LHY} \equiv \frac{16\sqrt{2}}{3\sqrt{5}\pi^{3/4}}\frac{a^{3/2}}{a_z^{1/2}a_\perp}$. To achieve results close to the parameter choices in this thesis ($\alpha_s = 1.05$, $\beta_{LHY} = 10^{-3}$, $\gamma = 2$), researchers may consider a Bose mixture of ^{39}K atoms in states $|1,0\rangle$ and $|1,-1\rangle$ with a total particle number of $N = 10^5$. The scattering lengths are $a = 60a_0$ and $a_{12} = 63a_0$, where a_0 is the Bohr radius. The radial and vertical trap frequencies are $\omega_\perp/2\pi = 1.3kHz$ and $\omega_z/2\pi = 4MHz$, leading to trap length scales of $a_z \approx 8nm$ and $a_\perp \approx 450nm$. These conditions result in a rotating droplet size of $4.5 - 6.8\mu m$ for $\tilde{\Omega} \sim 0.80 - 0.97$. For $\tilde{\Omega} = 0.8$, the core radius at the center is expected to be around $90nm$, and near the edge, it should be approximately $125nm$. It's important to note that these specific parameter choices are merely illustrative, and similar phenomena can be observed in a much wider parameter regime.

In summary, the thesis presents a compact vortex lattice for the strongly confined TF droplet under rotation, where the condensate size does not diverge as $\tilde{\Omega} \to 1$ due to the self-trapping property of the droplet. This contrasts with the diverging size observed in rotating repulsive BECs, potentially providing greater experimental feasibility to reach rapidly rotating limits. Additionally, it is possible to engineer lattices with much lower filling factors by tuning the droplet flat-top density. Moreover, the core sizes along the condensate exhibit noticeable differences and can be described analytically. Future research directions could explore the possibility of driving the droplet into the

LLL regime and investigating strongly correlated phases in droplets with low filling factors.

CHAPTER 5

JACOBI-THETA FORMALISM OF BOSE MIXTURE DROPLET

In Section 1.4, we derived and normalized the vortex lattice density profile functions using the Jacob-Theta formalism for both single vortex and two vortices per unit cell. Furthermore, the square root of the density profile is also calculated for both cases to ensure that the LHY energy integrals can also be obtained through a similar formalism. Here we use the derived formalism to calculate the total energy of the binary mixture droplet, including the kinetic, MF, and LHY energies.

The Hamiltonian of the binary mixture droplet rotating along the $z-$axis with the angular frequency Ω and confined along the $z-$axis and radial plane with the trapping frequencies ω_z and $\omega_\perp$, respectively, is given in the rotating frame as:

$$\begin{aligned}\hat{K} &= \hat{H}-\mu\hat{N}=\int d^3\vec{x}\psi^*(\vec{x})\left[\frac{\left(-i\hbar\nabla-M\Omega\hat{e}_z\times\vec{r}\right)^2}{2M}+\frac{1}{2}M\left(\omega_\perp^2-\Omega^2\right)r^2\right.\\ &\qquad\left.+\frac{1}{2}Mw_z^2z^2-\mu(z)\right]\psi(\vec{x})\\ &\quad+g\frac{1-\alpha}{4}\int d^3\vec{x}|\psi(\vec{x})|^4+\frac{8\sqrt{2}}{15\sqrt{\pi}}(\alpha+1)^{5/2}ga^{3/2}\int d^3\vec{x}|\psi(\vec{x})|^5, \qquad (5.1)\end{aligned}$$

where $\psi(\vec{x})=\phi_0(z)\phi(\vec{r})$, and $\alpha=|g_{12}|/g$. Here $\phi_0(z)$ is the ground state wavefunction of the harmonic oscillator confining along the $z-$axis. α is a crucial parameter to tune the MF energy into the attractive regime, in which the droplet phase is observed for $\alpha\gtrsim 1$. The first and second sums in the last line of Eq.(5.1) correspond to MF and LHY energies, respectively. We implicitly assume that the different components of the mixture are in phase so that a scalar field is sufficient to express their behavior.

In the rapidly rotating limit, $\phi(\vec{r})$ function can expressed in terms of the Jacobi-Theta functions, and the resulting functions for the density and its square roots are (See

Section. 1.4):

$$
\begin{aligned}
|\phi(\vec{r})|^2 &= \frac{1}{\pi\sigma^2}\sum_{\vec{K}}\tilde{g}_{\vec{K}}e^{i\vec{K}\vec{r}}e^{-r^2/\sigma^2}, \\
|\phi(\vec{r})| &= \frac{1}{\sqrt{\pi\sigma^2}}\sum_{\vec{K}}\tilde{h}_{\vec{K}}e^{i\vec{K}\vec{r}}e^{-r^2/2\sigma^2},
\end{aligned}
\tag{5.2}
$$

where

$$
\tilde{g}_{\vec{K}} = (-1)^{m_1+m_2+m_1m_2}e^{-\pi/2v\left[(m_1v)^2+(m_2-um_1)^2\right]}. \tag{5.3}
$$

The ground state of the harmonic oscillator with the length scale $a_z = \sqrt{\hbar/m\omega_z}$ is:

$$
\phi_0(z) = \frac{1}{\left(\pi a_z^2\right)^{1/4}}e^{-z^2/2a_z^2}. \tag{5.4}
$$

Now let us consider the single particle, MF, and LHY energy of the system for single and two vortices per unit cell configurations.

5.1 Single particle energy in the Lowest Landau Level

The single particle part of the Hamiltonian can be separated into the radial plane and vertical axis. Since tight confinement is assumed along $z-$axis, the contribution to the single particle energy is the ground state energy of the 1-dimensional harmonic oscillator $\hbar\omega_z/2$. In the radial plane, the single particle energy is:

$$
E_s = \int d^2\vec{r}\phi^*(\vec{r})\hat{h}_0\phi(\vec{r}),
$$

where

$$
\hat{h}_0 = \frac{\left(-i\hbar\nabla - M\Omega\hat{e}_z\times\vec{r}\right)^2}{2M} + \frac{1}{2}M\left(\omega_\perp^2 - \Omega^2\right)r^2.
$$

The particle in the LLL state has the wavefunction:

$$
\phi(\vec{r}) = \sum_{m=0}^{\infty} c_m u_{0,m}(\vec{r}), \tag{5.5}
$$

where

$$
\hat{h}_0 u_{0,m} = \hbar\left(\omega_\perp - \Omega\right)m u_{0,m}, \tag{5.6}
$$

where

$$u_{0,m}(\vec{r}) = \frac{1}{a_\perp \sqrt{2\pi m!}} \left(\frac{x+iy}{a_\perp}\right)^m e^{-\frac{x^2+y^2}{2a_\perp^2}}. \tag{5.7}$$

The single-particle energy E_s becomes:

$$\begin{aligned} E_s &= \frac{\hbar\omega_z}{2} + \int d^2\vec{r} \left(\sum_{m'=0}^{\infty} c^*_{m'} u^*_{0,m'}\right) \left(\sum_{m=0}^{\infty} c_m \hat{h}_0 u_{0,m}\right) \\ &= \frac{\hbar\omega_z}{2} + \hbar\left(w_\perp - \Omega\right) \sum_m m \left|c_m\right|^2 + \hbar w_\perp. \end{aligned} \tag{5.8}$$

To express the single particle energy in terms of the physical quantities, consider the expected size of the condensate:

$$\begin{aligned} \langle r^2 \rangle &= \sum_{m,m'} c^*_m c_m \int d^2\vec{r} u_{0,m} u^*_{0,m'} r^2 \\ &= \sum_{m,m'} c^*_{m'} c_m \int d^2\vec{r} a_\perp \sqrt{m+1} u_{0,m+1} a_\perp \sqrt{m'+1} u_{0,m'+1} \\ &= a_\perp^2 \sum_m \left|c_m\right|^2 (m+1), \end{aligned} \tag{5.9}$$

where $r^2 = (x+iy)(x-iy)$ is used. Therefore,

$$\sum \left|c_m\right| m^2 = \frac{\langle r^2 \rangle}{a_\perp^2} - 1. \tag{5.10}$$

The energy becomes:

$$E_s = \hbar\left(\omega_\perp - \Omega\right) \frac{\langle r^2 \rangle}{a_\perp^2} + \hbar\Omega + \frac{\hbar\omega_z}{2}. \tag{5.11}$$

Note that we did not have to use any specific form of the density profile. The only assumption to reach the same conclusion is that all the particles occupy either of the LLL states. Whichever distribution among the states would yield the same amount of kinetic energy.

5.2 MF and LHY energy: Single vortex per unit cell

The MF energy of the rotating droplet is:

$$\begin{aligned} E_{MF} &= \frac{g}{4}(1-\alpha) \int d^3\vec{x} |\psi(\vec{x})|^4 \\ &= \frac{g}{4}(1-\alpha) \int_{-\infty}^{\infty} dz \left|\phi_0(z)\right|^4 \int d^2\vec{r} |\phi(\vec{r})|^4. \end{aligned} \tag{5.12}$$

Here the first integral is $\int_{-\infty}^{\infty} dz\,|\phi_0(z)|^4 = \frac{1}{\sqrt{2\pi a_z^2}}$. The second integral can be calculated as:

$$\begin{aligned}\int d^2\vec{r}|\phi(\vec{r})|^4 &= \frac{1}{(\pi\sigma^2)^2}\sum_{\vec{K},\vec{K}'}\tilde{g}_{\vec{K}}\tilde{g}_{\vec{K}'}\underbrace{\int d^2\vec{r}e^{i\left(\vec{K}+\vec{K}'\right)\vec{r}}e^{-2r^2/\sigma^2}}_{=\frac{\pi\sigma^2}{2}e^{-\frac{|\vec{K}+\vec{K}'|^2\sigma^2}{8}}} \\ &= \frac{1}{2\,(\pi\sigma^2)}\sum_{\vec{K},\vec{K}'}\tilde{g}_{\vec{K}}\tilde{g}_{\vec{K}'}e^{-\frac{|\vec{K}+\vec{K}'|^2\sigma^2}{8}}. \end{aligned} \tag{5.13}$$

We can ignore the terms in the sum not satisfying the criteria $|\vec{K}+\vec{K}'| = 0$. Therefore, MF energy can be approximated as:

$$E_{MF} = \frac{1}{2\,(\pi\sigma^2)}\frac{g}{4}(1-\alpha)\frac{1}{\sqrt{2\pi a_z^2}}\sum_{\vec{K}}\tilde{g}_{\vec{K}}^2. \tag{5.14}$$

We calculate the LHY energy in a similar manner:

$$E_{LHY} = g\frac{8\sqrt{2}}{15\sqrt{\pi}}(\alpha+1)^{5/2}a^{3/2}\int d^3\vec{x}|\psi(\vec{x})|^5, \tag{5.15}$$

where $\int d^3\vec{x}|\psi(\vec{x})|^5 = \int_{-\infty}^{\infty} dz\,|\phi_0(z)|^5 \int d^2\vec{r}|\phi(\vec{r})|^5$. Here

$$\int_{-\infty}^{\infty} dz\,|\phi_0(z)|^5 = \sqrt{\frac{2}{5}}\frac{1}{\left(\pi a_z^2\right)^{3/4}}, \tag{5.16}$$

and

$$\begin{aligned}\int d^2\vec{r}|\phi(\vec{r})|^5 &= \int d^2\vec{r}|\phi(\vec{r})|^2|\phi(\vec{r})|^2|\phi(\vec{r})| \\ &= \frac{1}{\left(\pi\sigma^2\right)^{5/2}}\sum_{\vec{K},\vec{K}',\vec{K}''}\tilde{g}_K\tilde{g}_{K'}\tilde{h}_{K''}\int d^2\vec{r}e^{-5r^2/2\sigma^2}e^{i\left(\vec{K}+\vec{K}'+\vec{K}''\right)\vec{r}} \\ &= \frac{2}{5\left(\pi\sigma^2\right)^{3/2}}\sum_{\vec{K},\vec{K}',\vec{K}''}\tilde{g}_K\tilde{g}_{K'}\tilde{h}_{K''}e^{\frac{-|\vec{K}+\vec{K}'+\vec{K}''|^2\sigma^2}{10}} \\ &\approx \frac{2}{5\left(\pi\sigma^2\right)^{3/2}}\sum_{\vec{K},\vec{K}'}\tilde{g}_K\tilde{h}_{K'}\tilde{g}_{K+K'}. \end{aligned} \tag{5.17}$$

Therefore, the LHY energy is:

$$E_{LHY} = \frac{32}{75\sqrt{5}\pi^{5/4}}\frac{ga^{3/2}}{a_z^{3/2}\left(\pi\sigma^2\right)^{3/2}}(\alpha+1)^{5/2}\sum_{\vec{K},\vec{K}'}\tilde{g}_K\tilde{h}_{K'}\tilde{g}_{K+K'}. \tag{5.18}$$

5.3 MF and LHY energy: Two vortices per unit cell

The calculations of the MF and LHY energies can also be extended to the vortex lattices with two vortices per unit cell. In this case, the functions $|\phi_2(\vec{r})|^2$ and $|\phi_2(\vec{r})|$ that define vortex lattice profile are calculated in Section 1.4:

$$|\phi_2(\vec{r})|^2 = \frac{e^{-r^2/\sigma^2}}{\pi\sigma^2} \sum_{\vec{K},\vec{K}'} \hat{g}_K \hat{g}_{K'} e^{i\vec{K}\vec{r}} e^{-i\vec{K}'(\vec{r}-\Delta\vec{r})}, \tag{5.19}$$

where

$$\hat{g}_{\vec{K}} = \frac{g_{\vec{K}}}{\left(\sum_{\vec{K}''} g_{\vec{K}''}^2 e^{-i\vec{K}''\cdot\Delta\vec{r}}\right)^{1/2}}. \tag{5.20}$$

$$|\phi_2(\vec{r})| = \frac{e^{-r^2/2\sigma^2}}{\sqrt{\pi\sigma^2}} \sum_{\vec{K},\vec{K}'} \hat{h}_{\vec{K}} \hat{h}_{\hat{K}'} e^{i\vec{K}\vec{r}} e^{i\vec{K}'(\vec{r}-\Delta\vec{r})}, \tag{5.21}$$

where

$$\hat{h}_k = \tilde{h}_k \frac{1}{\left(\sum_{\vec{K}} \left(\frac{g_k}{g_0}\right)^2 e^{-i\vec{K}\vec{r}}\right)^{1/4}}. \tag{5.22}$$

MF energy in (5.12) can be calculated with the same formalism, but by replacing the single vortex per unit cell function $|\phi(\vec{r})|^2$ with the two vortices per unit cell function $|\phi_2(\vec{r})|^2$ in (5.19):

$$\int d^2\vec{r}|\phi_2(\vec{r})|^4 = \frac{1}{(\pi\sigma^2)^2} \sum_{\substack{\vec{K},\vec{K}',\\ \vec{K}'',\vec{K}'''}} \tilde{g}_{\vec{K}}\tilde{g}_{\vec{K}'}\tilde{g}_{\vec{K}''}\tilde{g}_{\vec{K}'''} e^{-i(\vec{K}'+\vec{K}''')\Delta\vec{r}} \times \underbrace{\int d^2\vec{r} e^{i\left(\vec{K}+\vec{K}'+\vec{K}''+\vec{K}'''\right)\vec{r}} e^{-2r^2/\sigma^2}}_{=\frac{\pi\sigma^2}{2} e^{-\frac{\left|\vec{K}+\vec{K}'+\vec{K}''+\vec{K}'''\right|^2\sigma^2}{8}}}. \tag{5.23}$$

Use the same approximation in which only the terms with $\left|\vec{K}+\vec{K}'+\vec{K}''+\vec{K}'''\right| = 0$ significantly contributes to the summation, since $\pi\sigma^2 \gg v_c$. The integral becomes:

$$\int d^2\vec{r}|\phi_2(\vec{r})|^4 = \frac{1}{2\left(\pi\sigma^2\right)} \sum_{\vec{K},\vec{K}',\vec{K}''} \tilde{g}_{\vec{K}}\tilde{g}_{\vec{K}'}\tilde{g}_{\vec{K}''}\tilde{g}_{\vec{K}+\vec{K}'+\vec{K}''} e^{+i(\vec{K}+\vec{K}'')\Delta\vec{r}}. \tag{5.24}$$

Therefore, the MF energy is:

$$E_{MF} = \frac{1}{8\sqrt{2\pi}} \frac{(1-\alpha)g}{a_z\left(\pi\sigma^2\right)} \sum_{\vec{K},\vec{K}',\vec{K}''} \tilde{g}_{\vec{K}}\tilde{g}_{\vec{K}'}\tilde{g}_{\vec{K}''}\tilde{g}_{\vec{K}+\vec{K}'+\vec{K}''} e^{+i(\vec{K}+\vec{K}'')\Delta\vec{r}}. \tag{5.25}$$

Let us now calculate the LHY energy $\propto |\phi_2(\vec{r})|^2$:

$$\int d^2\vec{r}|\phi_2(\vec{r})|^5 = \frac{1}{\left(\pi\sigma^2\right)^{5/2}} \sum_{\substack{\vec{K},\vec{K}',\vec{K}'',\\ \vec{K}''',\vec{K}^{(4)},\vec{K}^{(5)}}} \tilde{g}_{\vec{K}}\tilde{g}_{\vec{K}'}\tilde{g}_{\vec{K}''}\tilde{g}_{\vec{K}'''}\tilde{h}_{\vec{K}^{(4)}}\tilde{h}_{\vec{K}^{(5)}} \times e^{-i(\vec{K}'+\vec{K}'''+\vec{K}^{(5)})\Delta\vec{r}} \underbrace{\int d^2\vec{r}e^{i\vec{F}\vec{r}}e^{-5r^2/2\sigma^2}}_{=\frac{2\pi\sigma^2}{5}e^{-\frac{|\vec{F}|^2\sigma^2}{10}}}, \quad (5.26)$$

where $\vec{F} = \vec{K} + \vec{K}' + \vec{K}'' + \vec{K}''' + \vec{K}^{(4)} + \vec{K}^{(5)}$. Approximate the summation by considering only the contributions with the constraint $|\vec{F}| = 0$:

$$\int d^2\vec{r}|\phi_2(\vec{r})|^5 = \frac{2}{\left(5\pi\sigma^2\right)^{3/2}} \sum_{\substack{\vec{K},\vec{K}',\vec{K}'',\\ \vec{K}''',\vec{K}^{(4)}}} \Bigg[\tilde{g}_{\vec{K}}\tilde{g}_{\vec{K}'} \quad \tilde{g}_{\vec{K}''}\tilde{g}_{(\vec{K}+\vec{K}'+\vec{K}''+\vec{K}'''+\vec{K}^{(4)})}\tilde{h}_{\vec{K}'''}\tilde{h}_{\vec{K}^{(4)}} e^{+i(\vec{K}+\vec{K}''+\vec{K}''')\Delta\vec{r}}\Bigg]. \quad (5.27)$$

The LHY energy becomes

$$\begin{aligned} E_{LHY} &= \frac{32}{75\sqrt{5}\pi^{5/4}}\frac{ga^{3/2}}{a_z^{3/2}}\frac{(\alpha+1)^{5/2}}{\left(\pi\sigma^2\right)^{3/2}} \quad (5.28)\\ &\times \sum_{\substack{\vec{K},\vec{K}',\vec{K}'',\\ \vec{K}''',\vec{K}^{(4)}}} \Bigg[\tilde{g}_{\vec{K}}\tilde{g}_{\vec{K}'}\tilde{g}_{\vec{K}''}\tilde{g}_{(\vec{K}+\vec{K}'+\vec{K}''+\vec{K}'''+\vec{K}^{(4)})}\tilde{h}_{\vec{K}'''}\tilde{h}_{\vec{K}^{(4)}} e^{+i(\vec{K}+\vec{K}''+\vec{K}''')\Delta\vec{r}}\Bigg]. \end{aligned}$$

CHAPTER 6

CONCLUSION

In summary, the weakly interacting Bose condensates are traditionally stabilized by external means such as magnetic or optical traps. The equilibrium properties and the dynamics of the condensates are generally studied by the mean-field Gross-Pitaevskii approach. The beyond mean-field fluctuations are considered minor quantitative corrections. However, the quantum droplets exhibit self-stabilized phases, in which the beyond mean-field fluctuations play a central role in stabilizing the attractive mean-field interaction. The droplet phases are experimentally realized for binary mixture and dipolar condensates. The theoretical approach to studying the droplet phases is the microscopic Bogoliubov theory and the extended Gross-Pitaevskii equation obtained through the local density approximation. In this thesis, we apply the Bogoliubov theory to discuss whether the spin-1 condensates can exhibit the quantum droplet phase.

Spin-1 condensates consist of spin-1 atoms distributed among the different hyperfine states and allow for the spin exchange processes. They are rotationally symmetric in the absence of external magnetic fields. It is assumed that the dipolar relaxation time scale is long with respect to the binary collision time scales so that the longitudinal magnetization of the condensate is conserved. The interactions between the atoms are modeled by the contact potential. Only the even total spin channels are allowed due to the symmetry considerations of the two-body wavefunction of the colliding pair. These properties of the condensate lead us to characterize the interaction Hamiltonian by two independent parameters: density and spin coupling constants. Since the interaction energy depends on the spin properties, various magnetic phases can be observed throughout the condensate such as ferromagnetic, polar, etc.

We find that the droplet phase is not possible for the ferromagnetic phase, in which the spin-1 condensate acts as a single component weakly interacting Bose gas. However, the polar and antiferromagnetic order parameters provide the necessary parameter regime to obtain attractive mean-field and repulsive Lee-Huang-Yang energies. Interestingly, the Lee-Huang-Yang energy is quadratic Zeeman energy dependent in both magnetic orders. Therefore, one can tune the droplet properties by playing with an external parameter. Furthermore, we realize an analogy between the Rabi-coupled binary mixture and spin-1 condensates. The quantum fluctuations are tunable through external means and the mean-field energy can be profoundly altered by polarizing the condensate. We derive the phase diagram of mechanical stability in the parameter planes of linear p and quadratic q Zeeman energies, and detuning δ and Rabi-frequency ω_R for spin-1 and Rabi-coupled mixture condensates, respectively.

Finally, we study how the quantum droplets respond to the rotation. The major challenge in rotating the repulsive Bose condensates is the excessive largening of the condensate size at the rapid rotation limit. The centrifugal effect due to the rotation effectively weakens the trapping potential. Therefore, the repulsive condensate expands excessively as the rotation frequency approaches the trapping frequency. We find that the change in the confined droplet size at the rapid rotation limit is only fractional due to the self-trapping property of the condensate. We numerically find that the triangular vortex lattices can be formed in the strongly confined quantum droplet and the course-grained density profile of the lattice closely follows the analytical solution of the Gross-Pitaevskii equation for the droplet in the strongly confined Thomas-Fermi regime.

We derive an approximate analytical formula for the core size in the same regime. We find that the differences in the core size through the droplet are more tractable than the repulsive condensates since the droplet density profile shows a finite value at the edge and a rapid fall. We also extract the vortex density distribution through the droplet and compare it to estimates that calculate the vortex density for a given inhomogeneous superfluid density profile. We find that the spatial periodicity through the vortex lattice approaches the perfect lattice, as the droplet density approaches the flat-top profile in the rapid rotation limit.

REFERENCES

References

[1]D. S. Petrov, "Quantum mechanical stabilization of a collapsing Bose-Bose mixture", Phys. Rev. Lett. **115**, 155302 (2015).

[2]F. Wächtler and L. Santos, "Ground-state properties and elementary excitations of quantum droplets in dipolar Bose-Einstein condensates", Phys. Rev. A **94**, 043618 (2016).

[3]C. R. Cabrera, L. Tanzi, J. Sanz, B. Naylor, P. Thomas, P. Cheiney, and L. Tarruell, "Quantum liquid droplets in a mixture of Bose-Einstein condensates", Science **359**, 301–304 (2018).

[4]I. Ferrier-Barbut, H. Kadau, M. Schmitt, M. Wenzel, and T. Pfau, "Observation of quantum droplets in a strongly dipolar Bose gas", Phys. Rev. Lett. **116**, 215301 (2016).

[5]F. Dalfovo, S. Giorgini, L. P. Pitaevskii, and S. Stringari, "Theory of Bose-Einstein condensation in trapped gases", Rev. Mod. Phys. **71**, 463–512 (1999).

[6]L. D. Landau and E. M. Lifshitz, *Statistical physics: volume 5*, Vol. 5 (Elsevier, 2013).

[7]L. Pitaevskii and S. Stringari, *Bose-Einstein condensation and superfluidity*, Vol. 164 (Oxford University PressOxford, Jan. 2016).

[8]C. J. Pethick and H. Smith, *Bose–Einstein condensation in dilute gases* (Cambridge University Press, Sept. 2008).

[9]M. Inguscio and L. Fallani, *Atomic physics: precise measurements and ultracold matter* (OUP Oxford, 2013).

[10]A. Griffin, "Conserving and gapless approximations for an inhomogeneous bose gas at finite temperatures", Physical Review B **53**, 9341 (1996).

[11]A. L. Fetter and J. D. Walecka, *Quantum theory of many-particle systems* (Courier Corporation, 2012).

[12]N. Bogoliubov, “On the theory of superfluidity”, J. Phys **11**, 23 (1947).

[13]J. O. Andersen, “Theory of the weakly interacting bose gas”, Rev. Mod. Phys. **76**, 599–639 (2004).

[14]N. Navon, S. Piatecki, K. Günter, B. Rem, T. C. Nguyen, F. Chevy, W. Krauth, and C. Salomon, “Dynamics and thermodynamics of the low-temperature strongly interacting Bose gas”, Phys. Rev. Lett. **107**, 135301 (2011).

[15]K. Kasamatsu, M. Tsubota, and M. Ueda, “Vortices in multicomponent Bose-Einstein condensates”, International Journal of Modern Physics B **19**, 1835–1904 (2005).

[16]E. J. Mueller and T.-L. Ho, “Two-component Bose-Einstein condensates with a large number of vortices”, Phys. Rev. Lett. **88**, 180403 (2002).

[17]I. Bloch, J. Dalibard, and W. Zwerger, “Many-body physics with ultracold gases”, Rev. Mod. Phys. **80**, 885–964 (2008).

[18]C. Chin, R. Grimm, P. Julienne, and E. Tiesinga, “Feshbach resonances in ultracold gases”, Rev. Mod. Phys. **82**, 1225–1286 (2010).

[19]A. Eckardt, C. Weiss, and M. Holthaus, “Ground-state energy and depletions for a dilute binary Bose gas”, Physical Review A **70**, 043615 (2004).

[20]K. Murata, H. Saito, and M. Ueda, “Broken-axisymmetry phase of a spin-1 ferromagnetic bose-einstein condensate”, Phys. Rev. A **75**, 013607 (2007).

[21]Y. Kawaguchi and M. Ueda, “Spinor Bose–Einstein condensates”, Phys. Rep. **520**, 253–381 (2012).

[22]D. M. Stamper-Kurn and M. Ueda, “Spinor Bose gases: Symmetries, magnetism, and quantum dynamics”, Rev. Mod. Phys. **85**, 1191–1244 (2013).

[23]S. Uchino, M. Kobayashi, and M. Ueda, “Bogoliubov theory and Lee-Huang-Yang corrections in spin-1 and spin-2 Bose-Einstein condensates in the presence of the quadratic Zeeman effect”, Phys. Rev. A **81**, 063632 (2010).

[24]J. J. Sakurai and E. D. Commins, *Modern quantum mechanics, revised edition*, 1995.

[25]J. R. Abo-Shaeer, C. Raman, J. M. Vogels, and W. Ketterle, “Observation of vortex lattices in Bose-Einstein condensates”, Science **292**, 476–479 (2001).

[26]T.-L. Ho, “Bose-Einstein condensates with large number of vortices”, Phys. Rev. Lett. **87**, 060403 (2001).

[27]K. F. Riley, M. P. Hobson, and S. J. Bence, *Mathematical methods for physics and engineering*, 1999.

[28]H. Hu and X.-J. Liu, "Consistent theory of self-bound quantum droplets with bosonic pairing", Phys. Rev. Lett. **125**, 195302 (2020).

[29]Q. Gu and L. Yin, "Phonon stability and sound velocity of quantum droplets in a boson mixture", Phys. Rev. B **102**, 220503 (2020).

[30]G. Ferioli, G. Semeghini, L. Masi, G. Giusti, G. Modugno, M. Inguscio, A. Gallemı, A. Recati, and M. Fattori, "Collisions of self-bound quantum droplets", Phys. Rev. Lett. **122**, 090401 (2019).

[31]P. Cheiney, C. R. Cabrera, J. Sanz, B. Naylor, L. Tanzi, and L. Tarruell, "Bright soliton to quantum droplet transition in a mixture of Bose-Einstein condensates", Phys. Rev. Lett. **120**, 135301 (2018).

[32]T. G. Skov, M. G. Skou, N. B. Jørgensen, and J. J. Arlt, "Observation of a Lee-Huang-Yang fluid", Phys. Rev. Lett. **126**, 230404 (2021).

[33]G. Semeghini, G. Ferioli, L. Masi, C. Mazzinghi, L. Wolswijk, F. Minardi, M. Modugno, G. Modugno, M. Inguscio, and M. Fattori, "Self-bound quantum droplets of atomic mixtures in free space", Phys. Rev. Lett. **120**, 235301 (2018).

[34]Z. Guo, F. Jia, L. Li, Y. Ma, J. M. Hutson, X. Cui, and D. Wang, "Lee-Huang-Yang effects in the ultracold mixture of $^{23}\mathrm{Na}$ and $^{87}\mathrm{Rb}$ with attractive interspecies interactions", Phys. Rev. Res. **3**, 033247 (2021).

[35]M.-O. Mewes, M. R. Andrews, N. J. van Druten, D. M. Kurn, D. S. Durfee, C. G. Townsend, and W. Ketterle, "Collective excitations of a Bose-Einstein condensate in a magnetic trap", Phys. Rev. Lett. **77**, 988–991 (1996).

[36]F. Gerbier, J. H. Thywissen, S. Richard, M. Hugbart, P. Bouyer, and A. Aspect, "Experimental study of the thermodynamics of an interacting trapped Bose-Einstein condensed gas", Phys. Rev. A **70**, 013607 (2004).

[37]C. Mordini, D. Trypogeorgos, A. Farolfi, L. Wolswijk, S. Stringari, G. Lamporesi, and G. Ferrari, "Measurement of the canonical equation of state of a weakly interacting 3D Bose gas", Phys. Rev. Lett. **125**, 150404 (2020).

[38]R. P. Smith, R. L. D. Campbell, N. Tammuz, and Z. Hadzibabic, "Effects of interactions on the critical temperature of a trapped Bose gas", Phys. Rev. Lett. **106**, 250403 (2011).

[39]S. B. Papp, J. M. Pino, R. J. Wild, S. Ronen, C. E. Wieman, D. S. Jin, and E. A. Cornell, "Bragg spectroscopy of a strongly interacting ^{85}Rb Bose-Einstein condensate", Phys. Rev. Lett. **101**, 135301 (2008).

[40]S. L. Cornish, S. T. Thompson, and C. E. Wieman, "Formation of bright matter-wave solitons during the collapse of attractive Bose-Einstein condensates", Phys. Rev. Lett. **96**, 170401 (2006).

[41]K. E. Wilson, A. Guttridge, J. Segal, and S. L. Cornish, "Quantum degenerate mixtures of Cs and Yb", Phys. Rev. A **103**, 033306 (2021).

[42]M. Schmitt, M. Wenzel, F. Böttcher, I. Ferrier-Barbut, and T. Pfau, "Self-bound droplets of a dilute magnetic quantum liquid", Nature **539**, 259–262 (2016).

[43]P. Zin, M. Pylak, and M. Gajda, "Revisiting a stability problem of two-component quantum droplets", Phys. Rev. A **103**, 013312 (2021).

[44]M. Ota and G. Astrakharchik, "Beyond Lee-Huang-Yang description of self-bound Bose mixtures", SciPost Physics **9**, 20 (2020).

[45]P. Naidon and D. S. Petrov, "Mixed bubbles in Bose}-{Bose mixtures", Phys. Rev. Lett. **126**, 115301 (2021).

[46]J. Sánchez-Baena, J. Boronat, and F. Mazzanti, "Supersolid striped droplets in a Raman spin-orbit-coupled system", Phys. Rev. A **102**, 053308 (2020).

[47]Y. Ma, C. Peng, and X. Cui, "Borromean droplet in three-component ultracold Bose gases", Phys. Rev. Lett. **127** (2021).

[48]J. C. Smith, D. Baillie, and P. B. Blakie, "Quantum droplet states of a binary magnetic gas", Phys. Rev. Lett. **126**, 025302 (2021).

[49]R. N. Bisset, L. A. P. Ardila, and L. Santos, "Quantum droplets of dipolar mixtures", Phys. Rev. Lett. **126**, 025301 (2021).

[50]J. Stenger, S. Inouye, D. M. Stamper-Kurn, H.-J. Miesner, A. P. Chikkatur, and W. Ketterle, "Spin domains in ground-state Bose-Einstein condensates", Nature **396**, 345–348 (1998).

[51]M.-S. Chang, C. D. Hamley, M. D. Barrett, J. A. Sauer, K. M. Fortier, W. Zhang, L. You, and M. S. Chapman, "Observation of spinor dynamics in optically trapped ^{87}Rb Bose-Einstein condensates", Phys. Rev. Lett. **92**, 140403 (2004).

[52]H. Schmaljohann, M. Erhard, J. Kronjäger, M. Kottke, S. van Staa, L. Cacciapuoti, J. J. Arlt, K. Bongs, and K. Sengstock, "Dynamics of $F = 2$ spinor Bose-Einstein condensates", Phys. Rev. Lett. **92**, 040402 (2004).

[53]T. L. Nicholson, S. Blatt, B. J. Bloom, J. R. Williams, J. W. Thomsen, J. Ye, and P. S. Julienne, "Optical Feshbach resonances: Field-dressed theory and comparison with experiments", Phys. Rev. A **92**, 022709 (2015).

[54]O. Thomas, C. Lippe, T. Eichert, and H. Ott, "Experimental realization of a Rydberg optical Feshbach resonance in a quantum many-body system", Nat. Commun. **9**, 1–6 (2018).

[55]T. Kuwamoto, K. Araki, T. Eno, and T. Hirano, "Magnetic field dependence of the dynamics of ^{87}Rb spin-2 Bose-Einstein condensates", Phys. Rev. A **69**, 063604 (2004).

[56]A. Black, E. Gomez, L. Turner, S. Jung, and P. Lett, "Spinor dynamics in an antiferromagnetic spin-1 condensate", Phys. Rev. Lett. **99**, 070403 (2007).

[57]E. Aybar and M. Ö. Oktel, "Temperature-dependent density profiles of dipolar droplets", Phys. Rev. A **99**, 013620 (2019).

[58]Y. V. Kartashov, G. E. Astrakharchik, B. A. Malomed, and L. Torner, "Frontiers in multidimensional self-trapping of nonlinear fields and matter", Nature Reviews Physics **1**, 185–197 (2019).

[59]F. Böttcher, J.-N. Schmidt, J. Hertkorn, K. S. H. Ng, S. D. Graham, M. Guo, T. Langen, and T. Pfau, "New states of matter with fine-tuned interactions: Quantum droplets and dipolar supersolids", Rep. Prog. Phys. **84**, 012403 (2020).

[60]T. A. Yoğurt, "Quantum droplets", GitHub repository (2023).

[61]J. Mur-Petit, M. Guilleumas, A. Polls, A. Sanpera, M. Lewenstein, K. Bongs, and K. Sengstock, "Dynamics of $F = 1$ ^{87}Rb condensates at finite temperatures", Phys. Rev. A **73**, 013629 (2006).

[62]J. Guzman, G.-B. Jo, A. N. Wenz, K. W. Murch, C. K. Thomas, and D. M. Stamper-Kurn, "Long-time-scale dynamics of spin textures in a degenerate F=1 ^{87}Rb spinor Bose gas", Phys. Rev. A **84**, 063625 (2011).

[63]S. Huh, K. Kim, K. Kwon, and J.-y. Choi, "Observation of a strongly ferromagnetic spinor Bose-Einstein condensate", Phys. Rev. Res. **2**, 033471 (2020).

[64]T. A. Yoğurt, A. Keleş, and M. Ö. Oktel, "Spinor boson droplets stabilized by spin fluctuations", Phys. Rev. A **105**, 043309 (2022).

[65]A. Macia, J. Sánchez-Baena, J. Boronat, and F. Mazzanti, "Droplets of trapped quantum dipolar bosons", Phys. Rev. Lett. **117**, 205301 (2016).

[66]D. Baillie, R. M. Wilson, R. N. Bisset, and P. B. Blakie, "Self-bound dipolar droplet: A localized matter wave in free space", Phys. Rev. A **94**, 021602 (2016).

[67]A. Cappellaro, T. Macrı, G. F. Bertacco, and L. Salasnich, "Equation of state and self-bound droplet in Rabi-coupled Bose mixtures", Sci. Rep. **7**, 1–9 (2017).

[68]F. Böttcher, M. Wenzel, J.-N. Schmidt, M. Guo, T. Langen, I. Ferrier-Barbut, T. Pfau, R. Bombın, J. Sánchez-Baena, J. Boronat, et al., "Dilute dipolar quantum droplets beyond the extended Gross-Pitaevskii equation", Physical Review Research **1**, 033088 (2019).

[69]R. Ołdziejewski and K. Jachymski, "Properties of strongly dipolar Bose gases beyond the Born approximation", Physical Review A **94**, 063638 (2016).

[70]Y. Wang, L. Guo, S. Yi, and T. Shi, "Theory for self-bound states of dipolar Bose-Einstein condensates", Physical Review Research **2**, 043074 (2020).

[71]E. Chiquillo, "Low-dimensional self-bound quantum Rabi-coupled bosonic droplets", Phys. Rev. A **99**, 051601 (2019).

[72]L. Lavoine, A. Hammond, A. Recati, D. S. Petrov, and T. Bourdel, "Beyond-mean-field effects in Rabi-coupled two-component Bose-Einstein condensate", Phys. Rev. Lett. **127**, 203402 (2021).

[73]A. Hammond, L. Lavoine, and T. Bourdel, "Tunable three-body interactions in driven two-component Bose-Einstein condensates", Phys. Rev. Lett. **128**, 083401 (2022).

[74]M. Abad and A. Recati, "A study of coherently coupled two-component Bose-Einstein condensates", The European Physical Journal D **67**, 1–11 (2013).

[75]K. W. Madison, F. Chevy, W. Wohlleben, and J. Dalibard, "Vortex formation in a stirred Bose-Einstein condensate", Phys. Rev. Lett. **84**, 806–809 (2000).

[76]M. R. Matthews, B. P. Anderson, P. C. Haljan, D. S. Hall, C. E. Wieman, and E. A. Cornell, "Vortices in a Bose-Einstein condensate", Phys. Rev. Lett. **83**, 2498–2501 (1999).

[77]A. L. Fetter, "Rotating trapped Bose-Einstein condensates", Rev. Mod. Phys. **81**, 647–691 (2009).

[78]G. M. Kavoulakis, A. D. Jackson, and G. Baym, "Rotating Bose-Einstein condensates with attractive interactions", Phys. Rev. A **70**, 043603 (2004).

[79]S. Nikolaou, G. Kavoulakis, and M. Ogren, "Novel superfluid states in rotating quantum droplets confined in a harmonic potential", preprint arXiv:2305.09422 (2023).

[80]P. Examilioti and G. Kavoulakis, "Ground state and rotational properties of two-dimensional self-bound quantum droplets", Journal of Physics B: Atomic, Molecular and Optical Physics **53**, 175301 (2020).

[81]Y. Li, Z. Chen, Z. Luo, C. Huang, H. Tan, W. Pang, and B. A. Malomed, "Two-dimensional vortex quantum droplets", Phys. Rev. A **98**, 063602 (2018).

[82]Y. V. Kartashov, B. A. Malomed, L. Tarruell, and L. Torner, "Three-dimensional droplets of swirling superfluids", Phys. Rev. A **98**, 013612 (2018).

[83]M. N. Tengstrand, P. Stürmer, E. Ö. Karabulut, and S. M. Reimann, "Rotating binary Bose-Einstein condensates and vortex clusters in quantum droplets", Phys. Rev. Lett. **123**, 160405 (2019).

[84]S. R. Otajonov, E. N. Tsoy, and F. K. Abdullaev, "Variational approximation for two-dimensional quantum droplets", Phys. Rev. E **102**, 062217 (2020).

[85]V. Schweikhard, I. Coddington, P. Engels, V. P. Mogendorff, and E. A. Cornell, "Rapidly rotating Bose-Einstein condensates in and near the lowest Landau level", Phys. Rev. Lett. **92**, 040404 (2004).

[86]V. Bretin, S. Stock, Y. Seurin, and J. Dalibard, "Fast rotation of a Bose-Einstein condensate", Phys. Rev. Lett. **92**, 050403 (2004).

[87]F. Ancilotto, M. Barranco, M. Guilleumas, and M. Pi, "Self-bound ultradilute Bose mixtures within local density approximation", Phys. Rev. A **98**, 053623 (2018).

[88]T. Ilg, J. Kumlin, L. Santos, D. S. Petrov, and H. P. Büchler, "Dimensional crossover for the beyond-mean-field correction in Bose gases", Phys. Rev. A **98**, 051604 (2018).

[89]P. Zin, M. Pylak, and M. Gajda, "Self-consistent description of Bose-Bose droplets: harmonically trapped quasi-two-dimensional droplets", Phys. Rev. A **106**, 013320 (2022).

[90]D. E. Sheehy and L. Radzihovsky, "Vortex lattice inhomogeneity in spatially inhomogeneous superfluids", Phys. Rev. A **70**, 051602 (2004).

[91]S. Viefers, "Quantum Hall physics in rotating Bose-Einstein condensates", Journal of Physics: Condensed Matter **20**, 123202 (2008).

[92]N. R. Cooper, "Rapidly rotating atomic gases", Advances in Physics **57**, 539–616 (2008).

[93]N. Cooper, "Fractional quantum Hall states of bosons: properties and prospects for experimental realization", in *Fractional quantum Hall effects: new developments* (World Scientific, 2020), pp. 487–521.

[94]R. J. Fletcher, A. Shaffer, C. C. Wilson, P. B. Patel, Z. Yan, V. Crépel, B. Mukherjee, and M. W. Zwierlein, "Geometric squeezing into the lowest Landau level", Science **372**, 1318–1322 (2021).

[95]B. Mukherjee, A. Shaffer, P. B. Patel, Z. Yan, C. C. Wilson, V. Crépel, R. J. Fletcher, and M. Zwierlein, "Crystallization of bosonic quantum Hall states in a rotating quantum gas", Nature **601**, 58–62 (2022).

[96]N. R. Cooper and J. Dalibard, "Reaching fractional quantum Hall states with optical flux lattices", Physical review letters **110**, 185301 (2013).

[97]A. Eckardt, "Colloquium: atomic quantum gases in periodically driven optical lattices", Rev. Mod. Phys. **89**, 011004 (2017).

[98]A. S. Sørensen, E. Demler, and M. D. Lukin, "Fractional quantum Hall states of atoms in optical lattices", Phys. Rev. Lett. **94**, 086803 (2005).

[99]M. Hafezi, A. S. Sørensen, E. Demler, and M. D. Lukin, "Fractional quantum Hall effect in optical lattices", Phys. Rev. A **76**, 023613 (2007).

[100]J. Léonard, S. Kim, J. Kwan, P. Segura, F. Grusdt, C. Repellin, N. Goldman, and M. Greiner, "Realization of a fractional quantum Hall state with ultracold atoms", Nature, 1–5 (2023).

[101]C. D'Errico, A. Burchianti, M. Prevedelli, L. Salasnich, F. Ancilotto, M. Modugno, F. Minardi, and C. Fort, "Observation of quantum droplets in a heteronuclear bosonic mixture", Phys. Rev. Res. **1**, 033155 (2019).

[102]A. Cidrim, F. E. A. dos Santos, E. A. L. Henn, and T. Macrı, "Vortices in self-bound dipolar droplets", Phys. Rev. A **98**, 023618 (2018).

[103]S. B. Prasad, T. Bland, B. C. Mulkerin, N. G. Parker, and A. M. Martin, "Vortex lattice formation in dipolar Bose-Einstein condensates via rotation of the polarization", Phys. Rev. A **100**, 023625 (2019).

[104]A. Gallemı, S. M. Roccuzzo, S. Stringari, and A. Recati, "Quantized vortices in dipolar supersolid Bose-Einstein condensed gases", Phys. Rev. A **102**, 023322 (2020).

[105]F. Ancilotto, M. Barranco, M. Pi, and L. Reatto, "Vortex properties in the extended supersolid phase of dipolar Bose-Einstein condensates", Phys. Rev. A **103**, 033314 (2021).

[106]A. Gallemı and L. Santos, "Superfluid properties of a honeycomb dipolar supersolid", Phys. Rev. A **106**, 063301 (2022).

[107]T. Bland, E. Poli, C. Politi, L. Klaus, M. A. Norcia, F. Ferlaino, L. Santos, and R. N. Bisset, "Two-dimensional supersolid formation in dipolar condensates", Phys. Rev. Lett. **128**, 195302 (2022).

[108]L. Klaus, T. Bland, E. Poli, C. Politi, G. Lamporesi, E. Casotti, R. N. Bisset, M. J. Mark, and F. Ferlaino, "Observation of vortices and vortex stripes in a dipolar condensate", Nature Physics **18**, 1453–1458 (2022).

[109]T. Bland, G. Lamporesi, M. J. Mark, and F. Ferlaino, "Vortices in dipolar Bose-Einstein condensates", arXiv preprint arXiv:2303.13263 (2023).

CURRICULUM VITAE

PERSONAL INFORMATION

Surname, Name: Yoğurt, Taha Alper
Nationality: Turkish (TC)

EDUCATION

Degree	Institution	Year of Graduation
B.S.	Bilkent University Electronics Engineering	2012
High School	Ankara Fen Lisesi	2007

PROFESSIONAL EXPERIENCE

Year	Place	Enrollment
February 2016- Ongoing	METU, Physics	Research Assistant
November 2013-February 2016	ASELSAN Inc.	System Test Engineer

PUBLICATIONS

International Publications

[1] Yoğurt, T. A., U. Tanyeri, A. Keleş, and M. Ö. Oktel, "Vortex lattices in strongly confined quantum droplets", Submitted to PRA, Jul. 2023. [Online]. Available: https://doi.org/10.48550/arXiv.2308.02704.

[2] Yoğurt, T. A., A. Keleş, and M. Ö. Oktel, "Polarized rabi-coupled and spinor

boson droplets", Phys. Rev. A, vol. 107, p. 023 322, 2 Feb. 2023. [Online]. Available: https://link.aps.org/doi/10.1103/PhysRevA.107.023322.

[3] Yoğurt, T. A., A. Keleş, and M. Ö. Oktel, "Spinor boson droplets stabilized by spin fluctuations", Phys. Rev. A, vol. 105, p. 043 309, 4 Apr. 2022. [Online]. Available: https://link.aps.org/doi/10.1103/PhysRevA.105.043309.